CALIFORNIA INSTITUTE OF TECHNOLOGY

EARTHQUAKE ENGINEERING RESEARCH LABORATORY

NONLINEAR ANALYSIS OF PACOIMA DAM WITH SPATIALLY NONUNIFORM GROUND MOTION

THESIS BY

STEVEN W. ALVES

REPORT NO. EERL 2004-11

PASADENA, CALIFORNIA
OCTOBER 2004

(DEFENDED OCTOBER 7, 2004)

Nonlinear Analysis of Pacoima Dam with Spatially Nonuniform Ground Motion

Thesis by

Steven W. Alves

In Partial Fulfillment of the Requirements

for the Degree of

Doctor of Philosophy

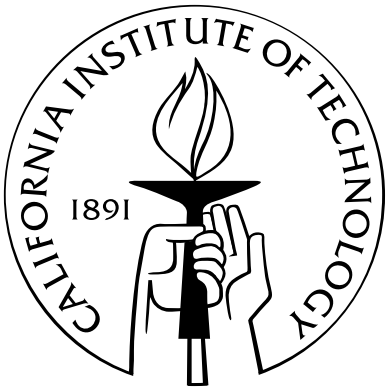

California Institute of Technology

Pasadena, California

2005

(Defended October 7, 2004)

Acknowledgements

I would like to thank my advisor, John Hall. He has always been available, and he has provided valuable guidance throughout my time at Caltech.

Zee Duron, my HMC advisor, helped me find direction in my academic career, and still provides advice whenever I need it. He also provided the shaker for my experiment and much appreciated help. Thanks to all of my fellow students, and Raul, for taking time to help me shake the dam. Also, thanks to James Beck who was always willing to provide consultations regarding MODE-ID.

Thanks to the California Strong Motion Instrumentation Program for providing funding during the project.

The support of my parents and my family and my friends has been very important and much appreciated during my time at Caltech.

Thanks to Matt, Steve, Julie and all of the Civil Engineering students for sharing this Caltech experience and providing support when I needed it.

Abstract

Spatially uniform ground motion is an assumption that has often been made for structural analysis of arch dams. However, it has been recognized for many years that the ground motion in a canyon during an earthquake is amplified at the top of the canyon relative to the base. Pacoima Dam has been strongly shaken by the 1971 San Fernando earthquake and the 1994 Northridge earthquake. The acceleration records from both of these events demonstrate the spatial nonuniformity of the ground motion, but the amount and quality of the data made it difficult to study in detail. An opportunity to do so arose on January 13, 2001, when a relatively small magnitude 4.3 earthquake was recorded by an upgraded accelerometer array at Pacoima Dam.

Frequency-dependent topographic amplification is apparent at locations along both abutments at 80% height of the dam relative to the base. Also, the ground motion is delayed at the abutment locations compared to the base. The delays are consistent with seismic waves traveling upward along the canyon, and the waves appear to be dispersive since the delays are frequency-dependent. Both of these effects are quantified in this thesis by several approaches that involve varying degrees of approximation. A method for generating nonuniform ground motion from a single 3-component ground motion specified for one location in the canyon, e.g., at the base, is developed using transfer functions that quantify the amplification and phase delay. The method is demonstrated for the 2001 earthquake and the Northridge earthquake with several variations in the transfer functions.

The 2001 earthquake records were also used for system identification. These results do not agree with results from a forced vibration experiment, which indicate a stiffer system. The earthquake must induce nonlinear vibrations, even though the ex-

citation is quite small. This observation has implications for applications of structural health monitoring.

The generated nonuniform ground motions are supplied as input to a finite element model. The results indicate that the method for generating nonuniform input produces ground motion that yields reasonable modeled responses, but there is some evidence that the time delays may be larger for stronger ground motion. Comparisons of the responses from ground motions generated with various implementations of amplification and time delays were made. For modeling purposes, accuracy of the amplification appears to be more important than the delays, which can be dealt with using a simpler approximation. The nonuniform input produces a response that is substantially different than the response produced by uniform input. The major difference is that while the pseudostatic response is a rigid body motion for uniform input, it causes deformation of the dam, mostly close to the abutments, for nonuniform input. In order to refine the proposed method for generating nonuniform ground motion, more data is required from Pacoima Dam and other structures with instrumentation coverage along the abutments.

Contents

List of Figures

List of Tables

Chapter 1

Introduction

Seismic analyses of arch dams have traditionally been done with the assumption that the input ground motion is uniform along the abutments. However, it has been known for many years that the seismic ground motion in a canyon is spatially nonuniform to a significant degree. It is important to understand the nature of the input seismic ground motion to an arch dam, so realistic dynamic analyses can be performed for the purpose of safety assessment of existing and future dams. The ground motion from earthquakes has been observed to be amplified at the top of the canyon relative to the base, and assuming that the seismic motion arrives at the dam as upward propagating waves, the ground motion will arrive at the crest of the dam after it arrives at the base. An earthquake occurred on January 13, 2001, that was recorded by an accelerometer array at Pacoima Dam. This data presented an opportunity to study the nonuniformity in the ground motion along the abutments of an arch dam.

Pacoima Dam is a concrete arch dam located in the San Gabriel Mountains in Los Angeles County that was completed in 1928 (Hall, 1988; Morrison Knudsen, 1994; EERI, 1995). The dam is about 113 meters from base to crest and the crest is about 180 meters long. The dam varies in thickness from about 3 meters at the crest to 30 meters at the base. A concrete thrust block supports the dam at the south abutment, which is referred to as the left abutment. The thrust block meets the dam at a contraction joint that is a little less than 20 meters high. This joint is one of the eleven contraction joints in the dam. The joints have beveled keys that are 30 cm deep. There is a spillway tunnel in the rock just to the south of the left abutment

that is about 20 meters below the crest of the dam. Two different views of Pacoima Dam are shown in Figure 1.1.

On February 9, 1971, Pacoima Dam was shaken by the magnitude 6.6 San Fernando earthquake, which had an epicenter about 8 km north of the dam and a focal depth of about 9 km. The water surface was 45 meters below the crest at this time. An accelerometer site was located on a ridge on the left abutment about 15 meters above the dam crest. Peak accelerations of 1.25g horizontal and 0.7g vertical were recorded at this site (Hall, 1988). The large recorded accelerations above the dam are an indication of amplification caused by the topography of the canyon and ridge. During the earthquake, a section of the upper left abutment rock moved slightly away from the dam and an area just downstream of that section moved more than 20 cm. The contraction joint at the thrust block opened almost 1 cm and a crack formed in the thrust block. Repairs were made to close the joint and the crack, and thirty-five post-tensioned steel tendons were installed to stabilize the upper left abutment rock in 1976 (Morrison Knudsen, 1994).

(a) View of right abutment

(b) View of left abutment

Figure 1.1: Pacoima Dam

In 1977, an extensive array of accelerometers was installed at Pacoima Dam. The locations of the 17 accelerometers on the dam and along the abutments are shown in Figure 1.2. The 3-component accelerometer on the ridge above the left abutment was left in place, and another 3-component accelerometer was placed downstream of the dam in the base of the canyon (Hall, 1988). These accelerometers were in place on January 17, 1994, when the magnitude 6.7 Northridge earthquake occurred with an epicenter about 18 km southwest of the dam and a focal depth of about 19 km. The water surface was 40 meters below the crest during the earthquake. The peak accelerations at the downstream site and on the ridge above the left abutment were 0.4g and 1.6g, respectively (Darragh et al., 1994a; 1994b). Most of the recordings in the 17-channel array could not be processed and digitized due to large amplitudes and high frequencies. Sections of the records are missing and two channels did not record at all. However, peak accelerations recorded were 0.5g at the base of the dam and 2.0g along the abutments near the crest. The variation of the ground motion in the canyon is demonstrated by these records from the Northridge earthquake.

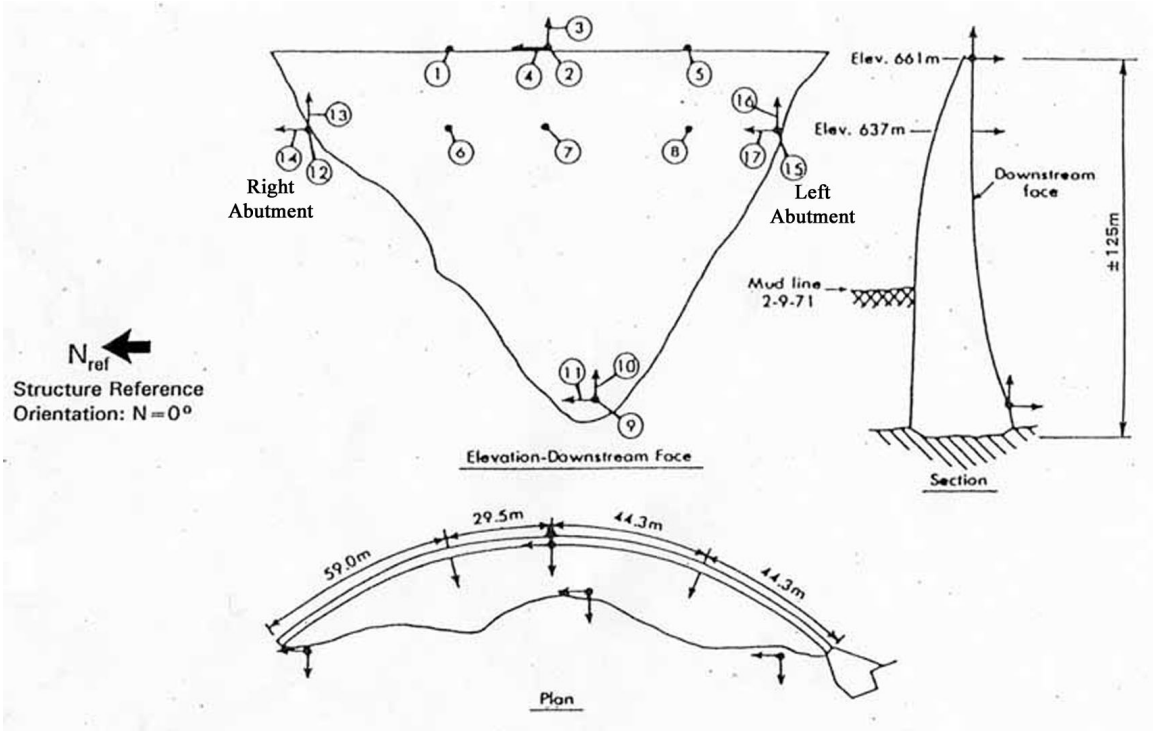

Figure 1.2: Locations of the 17 accelerometers at Pacoima Dam (CSMIP, 2001a)

The damage sustained in 1994 was even more severe than in 1971 (Morrison Knudsen, 1994; EERI, 1995). The rock mass downstream of the thrust block slid almost 50 cm, but the steel tendons kept the rock mass adjacent to the thrust block from sliding as much. That part of the upper left abutment only slid about 3 cm, but that movement opened the joint between the dam and the thrust block 5 cm at the crest, decreasing to about 0.5 cm at the bottom of the joint. The rest of the contraction joints were closed after the earthquake, but there was evidence that the joints had opened and closed during the earthquake. A crack extended from the open joint diagonally through the thrust block into the abutment. There were also several cracks in the left-most block of the dam arch adjacent to the thrust block. Horizontal lift joints also opened in this area and an offset of about 1 cm to 1.5 cm was observed at the lift joint about 15 meters below the crest. The top portion had moved downstream relative to the bottom. There was no significant damage observed at the right abutment. Repairs were made to the dam and measures were taken to stabilize rocks on the left abutment. The accelerometer array was also repaired and upgraded.

On January 13, 2001, a magnitude 4.3 earthquake occurred with an epicenter about 6 km south of Pacoima Dam and a depth of about 9 km. The water level was about 41 meters below the crest during this event. The ground motion recorded by the 17-channel array exhibited significant spatial nonuniformity. The peak accelerations were 0.02g at the base of the dam and 0.10g along the abutments near the crest (CSMIP, 2001a). The characteristics of the ground motion nonuniformity during the 2001 earthquake are studied in Chapter 2, and a method for generating nonuniform ground motion from a single 3-component record is developed and demonstrated for the 2001 earthquake and the Northridge earthquake in Chapter 3.

A system identification study was done using the acceleration records from the 2001 earthquake, and a forced vibration experiment was done in 2002 to compare the measured and identified modal properties. Two dominant, closely spaced modes are found from both the earthquake records and the forced vibration experiment, but the frequencies differ. This is discussed in Chapters 4, 5 and 6. A finite element model

was constructed and calibrated considering the results from the system identification studies. This model was used for dynamic analyses with spatially nonuniform ground motion of the 2001 earthquake and the Northridge earthquake. The proposed method for generating nonuniform ground motion is evaluated through these finite element analyses, and the responses to nonuniform input and uniform input are compared to assess the importance of modeling with nonuniform ground motion. The model and the results of the analyses are described in Chapters 7, 8 and 10. In Chapter 9, there is a discussion of how much foundation-structure interaction is accounted for in the system identification, which is investigated using output from the finite element analysis of the 2001 earthquake.

Chapter 2

January 13, 2001 Earthquake Records

The 17-channel accelerometer array located on the downstream face of Pacoima Dam is shown in Figure 1.2. Channels 1–8 are on the dam body: six of these channels are oriented radially, one channel is tangential, and one channel is vertical. Channels 9–17 are located at three stations near the dam-foundation rock interface. At each station, one channel is oriented in the east-west (stream) direction, one is vertical, and one is north-south (cross-stream). Channels 9–11 are located at the base of the dam. It should be noted that channel 9 and channel 11 are actually positioned as radial and tangential, respectively, but at the base location those directions are very near to east-west and north-south so they are assumed to be equivalent. Channels 12–14 are located at the north abutment (referred to as the right abutment) at about 80% height of the dam. Channels 15–17 are located at the south abutment (referred to as the left abutment) at about 80% height, where the dam and the thrust block meet. Positive directions for each channel are shown in Figure 1.2.

2.1 Recorded Motion

The processed acceleration recorded at Pacoima Dam on January 13, 2001, during the magnitude 4.3 earthquake is plotted in Figure 2.1. The velocity and displacement computed from the acceleration records are plotted in Figures 2.2 and 2.3, respectively. The figures only show the 8-second period in which the strongest motion was

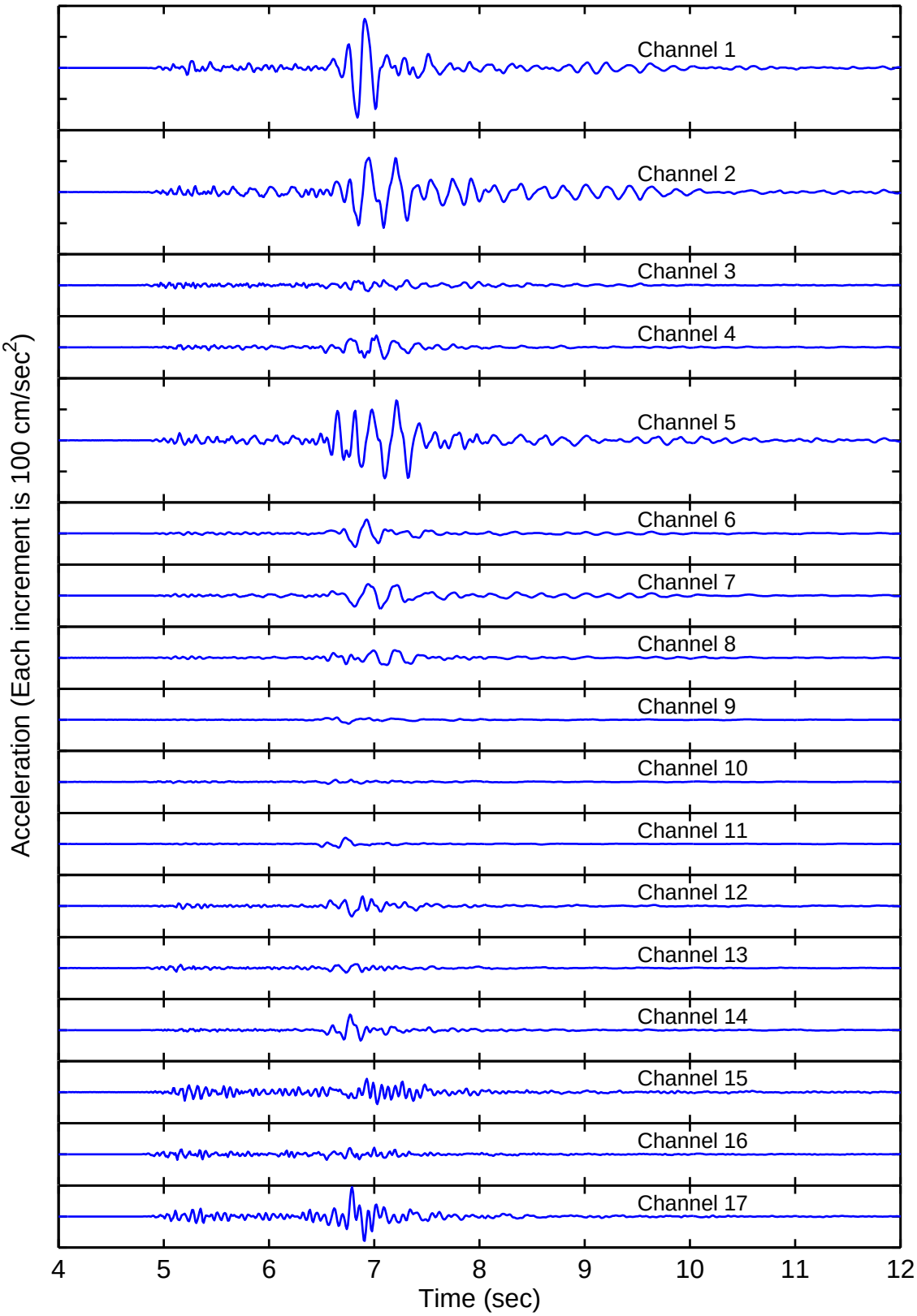

Figure 2.1: Acceleration recorded on January 13, 2001

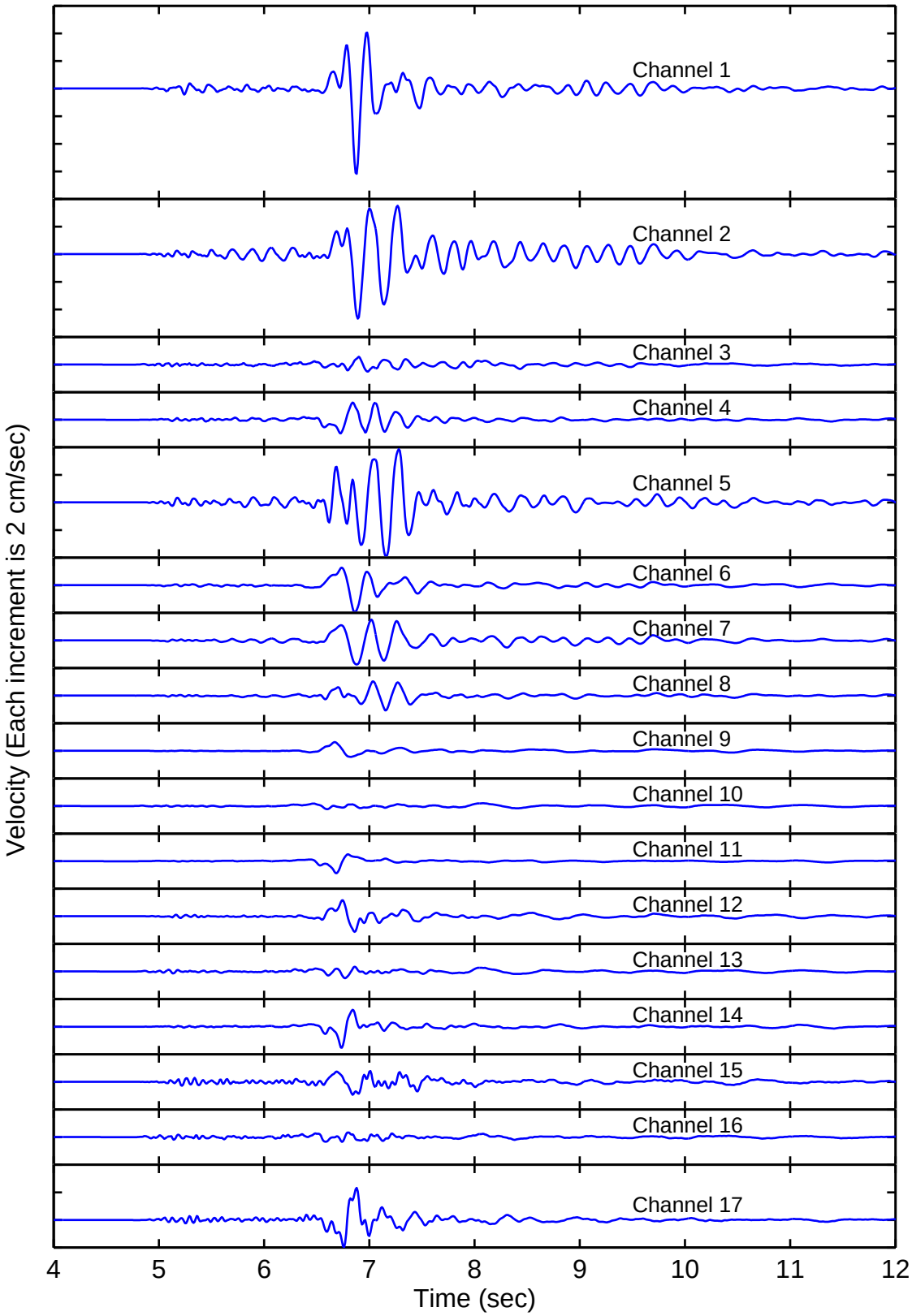

Figure 2.2: Velocity computed from acceleration recorded on January 13, 2001

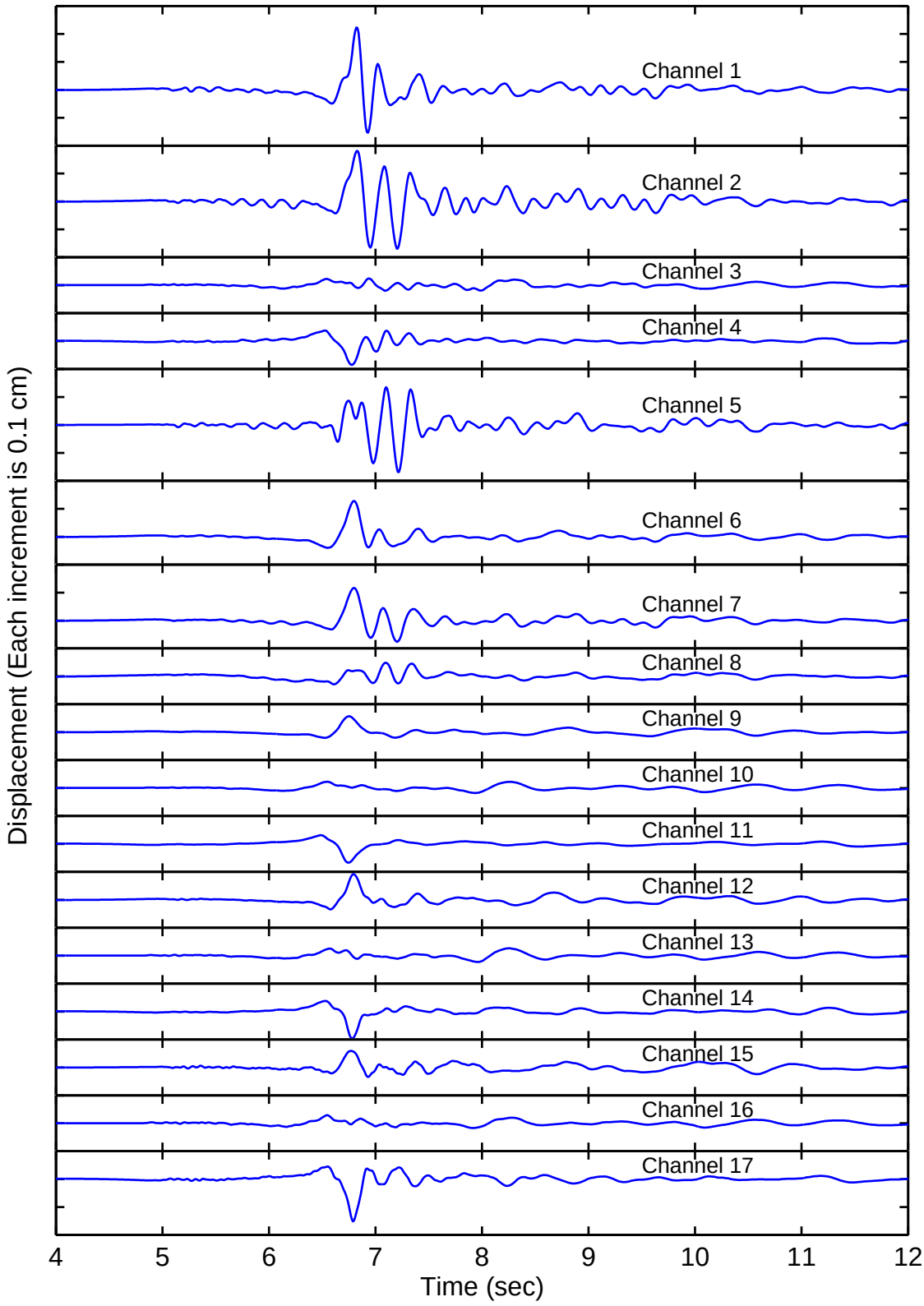

Figure 2.3: Displacement computed from acceleration recorded on January 13, 2001

Channel	Location/Orientation	Acceleration	Velocity	Displacement
1	crest at north third point/radial	−0.16g	−6.2 cm/sec	0.22 cm
2	center crest/radial	−0.12g	−4.7 cm/sec	0.18 cm
3	center crest/up	−0.02g	0.6 cm/sec	0.02 cm
4	center crest/tangential	0.04g	1.3 cm/sec	−0.09 cm
5	crest at south quarter point/radial	0.13g	−3.9 cm/sec	−0.17 cm
6	80% height at north third point/radial	0.05g	−2.0 cm/sec	0.13 cm
7	80% height at center/radial	−0.04g	−1.7 cm/sec	0.12 cm
8	80% height at south quarter point/radial	0.02g	−1.1 cm/sec	0.05 cm
9	base/west	−0.01g	0.6 cm/sec	0.06 cm
10	base/up	0.01g	−0.2 cm/sec	0.02 cm
11	base/north	0.02g	−0.9 cm/sec	−0.07 cm
12	right abutment/west	−0.03g	1.2 cm/sec	0.09 cm
13	right abutment/up	−0.01g	−0.5 cm/sec	0.03 cm
14	right abutment/north	0.05g	−1.5 cm/sec	−0.10 cm
15	left abutment/west	0.04g	−0.9 cm/sec	0.06 cm
16	left abutment/up	0.02g	−0.3 cm/sec	0.03 cm
17	left abutment/north	0.10g	2.3 cm/sec	−0.15 cm

Table 2.1: Peak values of acceleration, velocity and displacement observed at each of the 17 channels on January 13, 2001

recorded. CSMIP Report OSMS 01–02 shows 20 seconds of the processed records (CSMIP, 2001a). Peak values of acceleration, velocity and displacement are listed in Table 2.1 for each channel. The highest acceleration, velocity and displacement observed on the dam are 0.16g, 6.2 cm/sec and 0.22 cm, respectively. The highest acceleration, velocity and displacement observed at the dam-foundation interface are 0.10g, 2.3 cm/sec and 0.15 cm, respectively. Since the accelerometer array had been upgraded and the level of shaking is much lower than it was during the 1994 Northridge earthquake, the acceleration records show none of the off-scale high frequency motions that characterized the Northridge accelerograms, which are presented in Section 3.3.

2.2 Spatially Nonuniform Ground Motion along the Abutments

2.2.1 Topographic Amplification

The recorded motions from the 2001 earthquake on the right and left abutments at about 80% height of the dam are of higher amplitude than those at the base. This topographic amplification is represented as a function of frequency in Figure 2.4 as ratios of response spectral displacement (SD) computed from the respective components of the abutment and base motions.

$$Amp_{n,m}(\omega) = \frac{SD_n(\omega)}{SD_m(\omega)} \tag{2.1}$$

where ω is frequency, n is an abutment channel number and m is a base channel number ($n = 12, \ldots, 17$ and $m = 9, 10, 11$). Both zero percent and five percent damped spectral displacement ratios are shown. Pseudo-velocity response spectra (PSV) and pseudo-acceleration response spectra (PSA) ratios yield identical results. Spectral displacement ratios were used instead of the transfer functions between Fourier amplitude spectra, because computing the spectral displacement is basically a smoothing operation. Therefore, the frequency-dependent amplification factors are relatively smooth. The amplification computed from Fourier amplitude transfer functions is shown in Figure 2.5 to illustrate the difference.

$$Amp_{n,m}(\omega) = \left| \frac{A_n(\omega)}{A_m(\omega)} \right| \tag{2.2}$$

where $A_k(\omega)$ is the Fourier spectrum for $a_k(t)$, the acceleration recorded by channel k. Fourier spectra of velocity and displacement also yield similar results, which, theoretically, should be identical. It would be difficult to determine a reasonable general amplification factor from the Fourier spectra result.

It is clear from Figure 2.4 that using 5% damped spectral displacement to compute the amplification gives a smoother result than using 0% damped spectral dis-

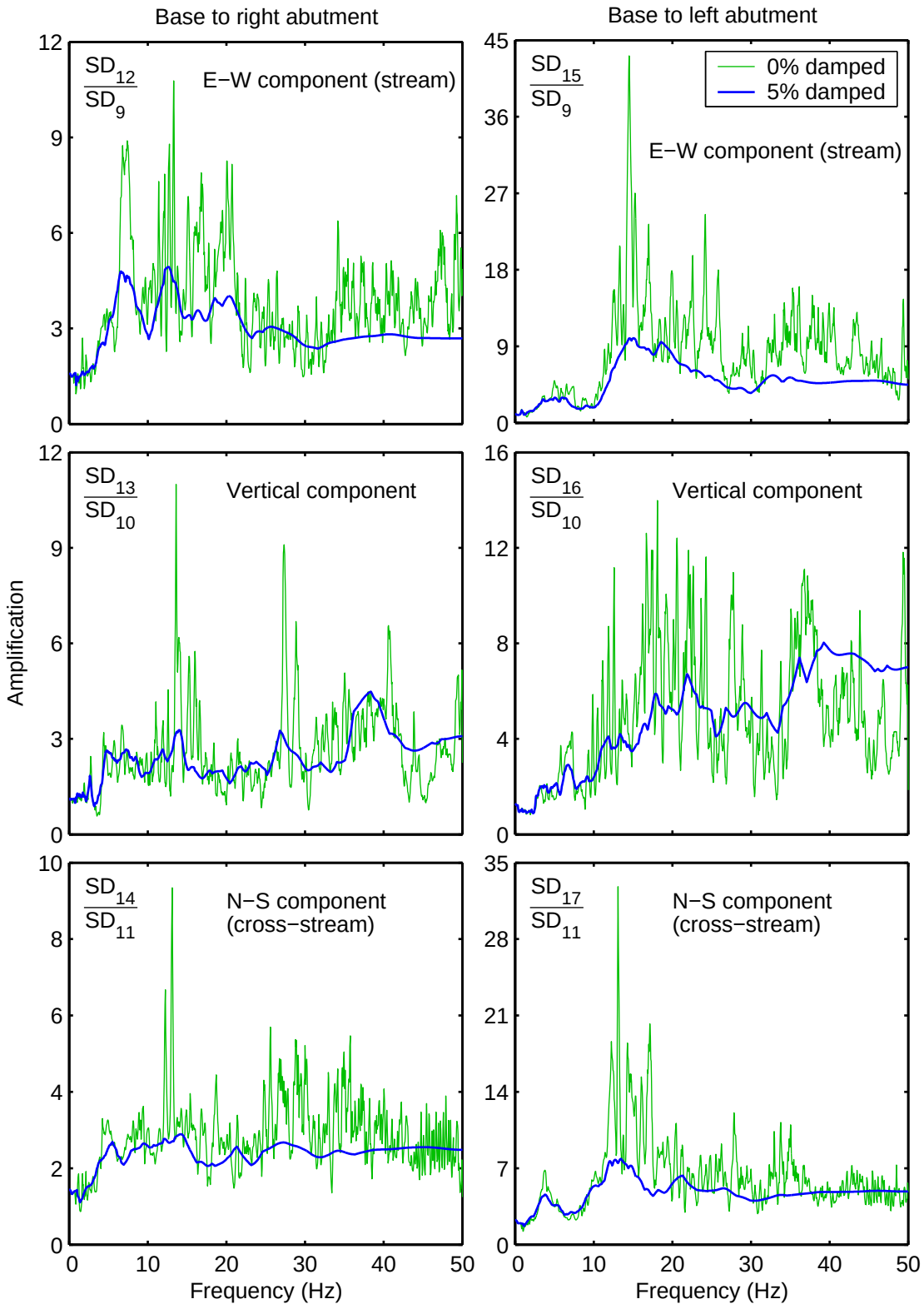

Figure 2.4: Amplification on the abutments of Pacoima Dam referenced to motion at the base of the dam in terms of ratios of spectral displacement (0% and 5% damped)

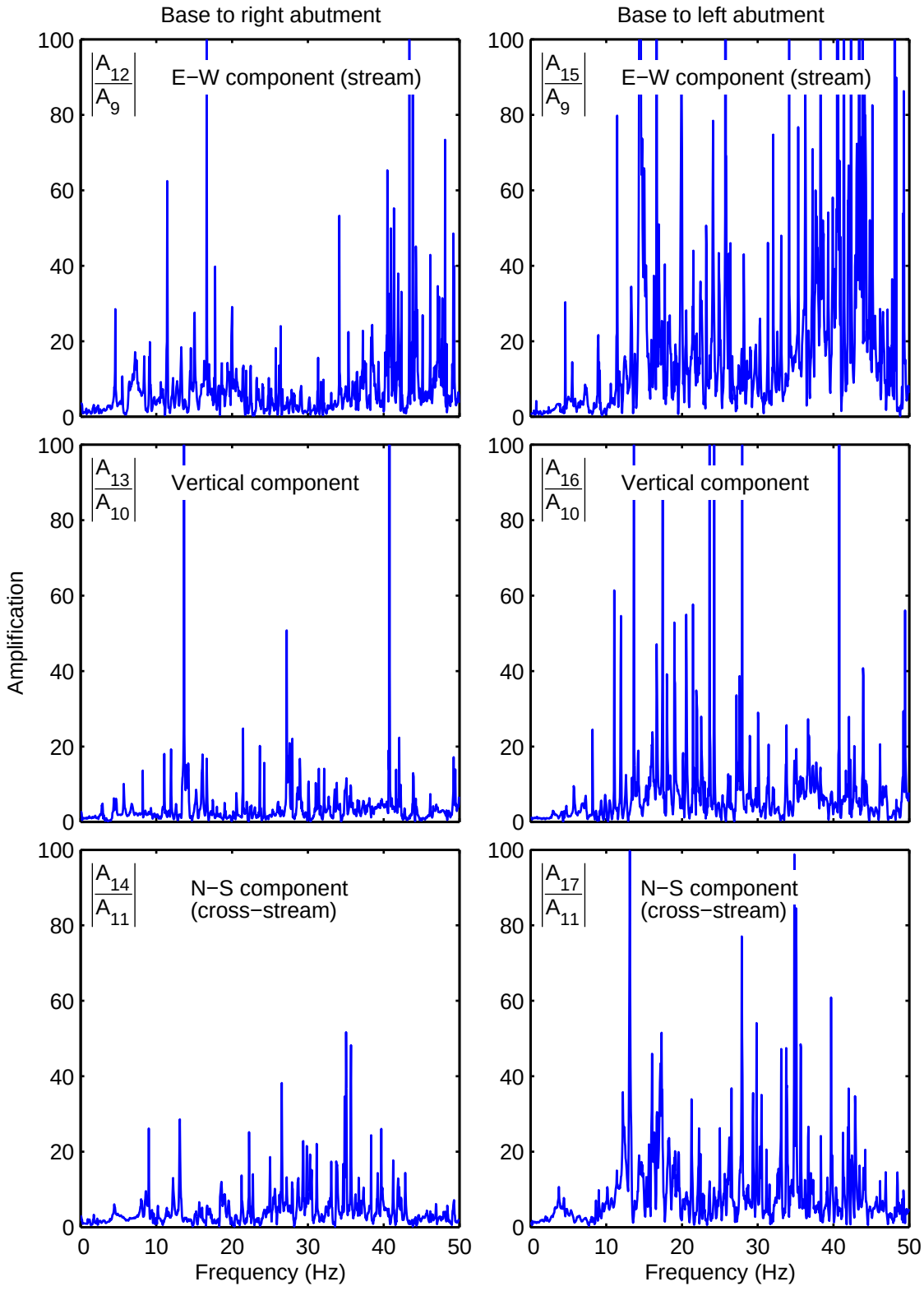

Figure 2.5: Amplification on the abutments of Pacoima Dam referenced to motion at the base of the dam in terms of Fourier amplitude transfer functions

placement. It is also apparent that 0% damped spectral displacement ratios yield amplification functions that are generally larger than 5% damped spectral displacement ratios, particularly at frequencies above 10 Hz. The smoother functions would be preferred for using as general amplification to be applied to a general record, since the less smooth amplification is more event specific. This is even more apparent with the Fourier transfer functions in Figure 2.5. However, the smoothness of the amplification function is not the only consideration. The function should also be an accurate characterization of the magnitude of the physical amplification caused by the topography, meaning that the smooth functions should not underestimate the overall amplification.

If data were available from several earthquakes, perhaps a better way to compute the site amplification would involve averaging 0% damped spectral displacement ratios over the different earthquakes. In lieu of this, the 5% damped spectral displacement ratios are believed to be a good approximation of the topographic amplification, at least for the purposes of modeling the structural response of Pacoima Dam. It is expected that a significant portion of the response of Pacoima Dam is at frequencies below 10 Hz. It will be shown in Chapter 4 that the first two natural frequencies of the dam are close to 5 Hz. For the most part, the 5% damped spectral displacement ratios do not significantly underestimate the 0% damped spectral displacement ratios below 10 Hz, with one exception around 7 Hz for the stream component of the base to right abutment amplification.

Below 10 Hz, the average overall amplification is around 2 to 4 at both abutments for all three components. The vertical components are amplified relatively less than the horizontal components. The stream component is amplified more on the right abutment than the left abutment, and the cross-stream component is amplified more on the left abutment than the right abutment. As the frequency gets closer to 0 Hz the amplification gets smaller; and at frequencies above 10 Hz, the amplification gets larger at the left abutment, which is where damage occurred in previous earthquakes.

Mickey et al. (1974) investigated the topographic amplification at Pacoima Dam during eight aftershocks of the 1971 San Fernando earthquake. The amplification was

measured between a station on the left abutment ridge above the dam crest, adjacent to the strong-motion accelerometer that was in place during the San Fernando earthquake, and a free-field site at the base of the canyon downstream from the dam. The aftershocks ranged in magnitude M_L from 2.7 to 3.7 with epicentral distances from Pacoima Dam varying between 4.5 km and 30 km, so the ground motion was probably smaller than the motion recorded on January 13, 2001. The overall average amplification observed in 1971 was significantly smaller than the 2001 amplification, but the abutment station in 1971 was actually at a higher elevation in the canyon. Thus, larger amplification would have been expected in 1971 if the process is linear, since larger motion was observed at the upper left abutment station compared to the 80% height abutment station (channels 15–17) in January 2001 (CSMIP, 2001b). Reimer (1973) also investigated the amplification between the same sites for three different aftershocks to the San Fernando earthquake with magnitudes between 2.0 and 3.3 and epicentral distances from Pacoima Dam between 5 km and 15 km. The results are difficult to compare, but it appears as though the amplification is larger than was observed from the other eight aftershocks and closer to the observed January 2001 amplification. Thus, the evidence is not conclusive, but the topographic amplification may be ground motion amplitude-dependent. If that is the case, the amplification for an earthquake the size of the Northridge earthquake would be larger than the amplification observed from smaller events like the San Fernando earthquake aftershocks and the 2001 earthquake. However, lacking additional data, the amplification observed from the 2001 earthquake records is taken to adequately approximate the amplification for larger earthquakes.

2.2.2 Seismic Wave Travel Time

Another aspect of the nonuniformity in the input ground motion is the time delay of wave arrivals between the base of the dam and points higher along the abutments. The incident seismic waves will actually be reflected, so the situation is more complicated and determining a time delay is a simplification. However, if the reflected motion is

much smaller than the incident motion, then computing time delays between arrivals can characterize the motion well. If seismic waves were non-dispersive, the time delay would be a frequency-independent quantity. For non-dispersive waves, the time delay between two records can be characterized by determining the value of time shift for which the cross-correlation of the records is maximized. The cross-correlation between an abutment acceleration ($a_n(t)$) and a base acceleration ($a_m(t)$) is defined by

$$C_{n,m}(\tau) = \int_0^T a_n(t+\tau)a_m(t)\,\mathrm{d}t\,, \quad -T < \tau < T \tag{2.3}$$

where T is the duration of the records, which was taken as 20 seconds for the January 2001 records. The time delay between channel n and channel m is defined as

$$\tau_{n,m} = \{\tau : C_{n,m}(\tau) \text{ is maximized}\} \tag{2.4}$$

A positive time delay indicates that the abutment record lags behind the base record. The time delays computed in this manner are listed in Table 2.2 for respective components of the motions from the base station to the two abutment stations. These delays were computed using the recorded accelerations, but the velocities or displacements may also be used. If the time delay was a frequency-independent quantity, acceleration, velocity and displacement correlations should yield the same delays. However, the velocity and displacement computed delays are smaller, indicating that the delay is shorter for lower frequency waves.

Obtaining frequency-dependent delays by taking the phase from the transfer functions between Fourier spectra and dividing by the frequency is not a viable option,

	E-W (stream)	Vertical	N-S (cross-stream)
Base to right abutment	$\tau_{12,9} = 0.050$ sec	$\tau_{13,10} = 0.024$ sec	$\tau_{14,11} = 0.048$ sec
Base to left abutment	$\tau_{15,9} = 0.040$ sec	$\tau_{16,10} = -0.008$ sec	$\tau_{17,11} = 0.066$ sec

Table 2.2: Time delays computed from the base to the abutment stations for each component of the January 13, 2001 earthquake acceleration records (lag is positive)

since the relative phase is not a unique quantity. Therefore, another method to compute time delay that allows for dispersive waves was devised. The displacement responses of a 5% damped single degree of freedom oscillator to the two records of interest are computed. Then the cross-correlation is computed between the two responses and the maximum is determined to yield the time delay between the records at the undamped natural frequency of the oscillator. This is repeated for each frequency. The 5% damped displacement response to an acceleration $a(t)$ is computed from

$$d_{5\%}(t) = \frac{1}{\omega_d} \int_0^t a(\tau) e^{-0.05\omega_u(t-\tau)} \sin \omega_d (t-\tau) \, \mathrm{d}\tau \tag{2.5}$$

where ω_u is the undamped natural frequency and ω_d is the damped natural frequency. The results of this method are shown in Figure 2.6 with the constant delays given in Table 2.2 included for comparison. The time delay was determined by only considering the values of the cross-correlation between -0.1 seconds and 0.1 seconds, because the delays computed directly from cross-correlation of the records indicate that the frequency-dependent delays should lie within this range. Any larger delays computed for a frequency are considered to be an anomaly. However, even with this constraint, discontinuities appear in the computed time delays. The figure includes lines labeled actual and modified. The actual lines are direct results of the method described, and the modified lines were simply adjusted in the discontinuous sections to obtain continuous time delay functions. The approach is approximate but it is believed that the continuous delays are more realistic. The frequency dependence is apparent, but the delays are fairly constant at frequencies above 5 Hz. At high frequencies, the time delays are consistent with those computed by directly cross-correlating the accelerations, and at lower frequencies the delays are generally smaller.

The abutment accelerations in the horizontal directions lag the base accelerations by times ranging from 40 to 66 milliseconds. These delays are a significant fraction of the fundamental period of the dam, which is about 200 milliseconds. Time delays for the vertical component are less. Assuming that the seismic waves are vertically incident body waves, the vertical component should record predominantly compression

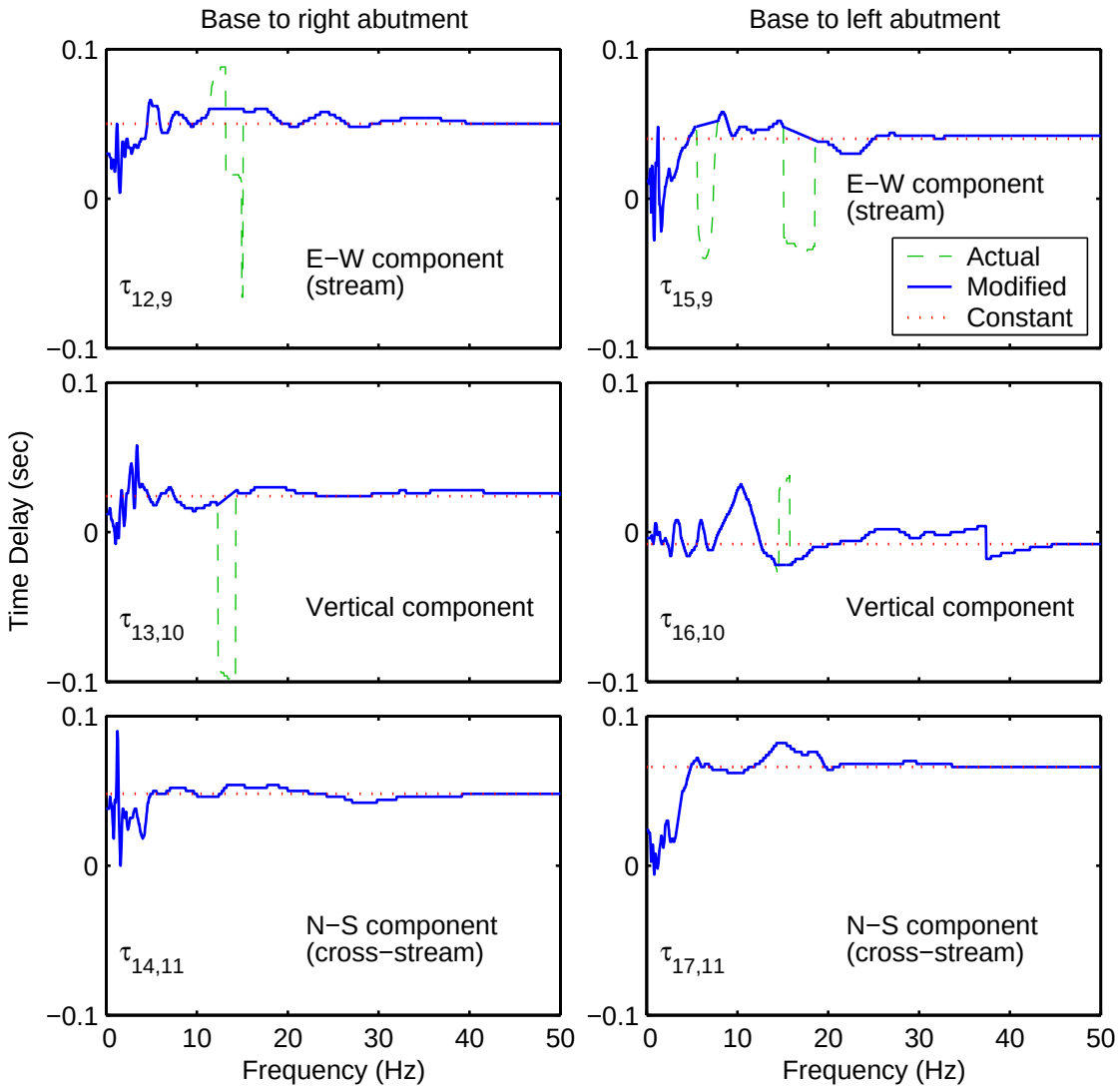

Figure 2.6: Frequency-dependent time delays on the abutments of Pacoima Dam referenced to motion at the base of the dam computed by cross-correlating the displacement responses of 5% damped SDOF's, modified delays are adjusted from the actual delays to be continuous (they coincide otherwise) and constant delays computed by cross-correlating the accelerations are shown for comparison (lag is positive)

waves which travel faster than shear waves. So, shorter vertical component delays may be reasonable. However, the records in Figures 2.1, 2.2 and 2.3 appear to show that the strongest motion in the vertical components (channels 13 and 16) arrives in synchrony with the shear wave arrivals in the horizontal components, and the vertical component at the left abutment actually leads the vertical component at the base. So, the problem is, in reality, more complicated and the vertical component delays

are difficult to interpret, especially at the left abutment. Perhaps, the relatively small amount of vertical motion makes accurate calculations difficult because of noise.

A long-range goal of collecting ground motion data at the base and sides of canyons, as at Pacoima Dam, is to develop rules for prescribing nonuniform seismic input in safety assessment analyses of dams. Based on the data presented here, one could propose that time delay be a function of elevation and shear wave speed in the rock to account for the travel time of seismic waves. For Pacoima Dam, there is about an 83 meter elevation difference between the base and abutment recording stations, and a shear wave velocity for rock of 1130 to 2350 m/sec can be assumed, which is based on a range of previously determined rock properties (Woodward-Lundgren, 1971) and assuming a unit weight of rock of 25.9 kN/m^3 (165.0 lb/ft^3). Using these properties and assuming an upward propagating shear wave result in a time delay between 35 and 74 milliseconds, which includes the range found for the horizontal components of ground acceleration (Table 2.2). The cause of the shorter delays for the vertical motion is not completely understood, so collecting more data is necessary to determine whether there is a physical reason for the smaller vertical component delays. The frequency dependence giving shorter delays at low frequency can also be included, but more data is also necessary to understand the physical basis for the dispersion. Based on data presented in Section 2.2.1, one could also propose that topographic amplification be a function of frequency and elevation in the canyon, with additional dependence on the side of the canyon at which the input is prescribed.

Rules for topographic amplification and time delay could be applied to components of a reference motion to generate a suite of motions around a canyon. This is demonstrated in Chapter 3 by generating ground motions at the locations corresponding to channels 12–17 from the base accelerations (channels 9–11) recorded during the January 2001 and Northridge earthquakes. Theoretically, the reference motion could be located anywhere in the canyon, but the base is a convenient location. From the base of the canyon, the motion along the abutments would be amplified and delayed in time. Producing the reference motion would require a different procedure than the current standard used to produce a uniform motion to be applied to the dam.

2.3 Foundation-Structure Interaction

For the purposes of modeling the response of Pacoima Dam to recorded earthquake ground motion, as will be described in subsequent chapters, the motion is assumed to be free-field. However, the recorded ground motion is not free-field since the dam is present when the recordings are made. Therefore, it would be desirable to have some quantification of the degree to which the foundation-structure interaction affects the recorded motion at the base and abutments of the dam. The Fourier amplitude spectra of the seventeen acceleration records from January 13, 2001, are shown in Figure 2.7. Only frequencies between 0 Hz and 10 Hz are shown to focus on the first two natural frequencies of the system, which are shown to be near 5 Hz in Chapter 4.

Generally, channels 1–8 are dominated by response between 3 Hz and 6 Hz, while channels 9–17 have more spread out frequency contributions. The channels on the dam (1–8) have a response that is dominated by frequencies near 5 Hz, while the response at the base and abutments of the dam (channels 9–17) is not dominated by frequency content around 5 Hz. However, this does not necessarily mean that the presence of the dam has an insignificant affect on the ground motion, especially on the abutments (channels 12–17) where frequency content near 5 Hz is significant for some components, although it does not dominate as much as it does in channels 1–8.

Bell and Davidson (1996) concluded from the 1994 Northridge earthquake records that while the base records may be a reasonable approximation of the base free-field motion, the records on the abutments showed significant contribution from foundation-structure interaction. That conclusion was made based on a larger earthquake with significant nonlinear response, but it appears as though it may also apply to smaller earthquakes. However, in this study, the motion recorded at the base and abutment locations will be assumed to adequately approximate free-field motion. Further study could investigate the impact of this assumption by attempting to use deconvolution to obtain a free-field estimate from the recorded motion.

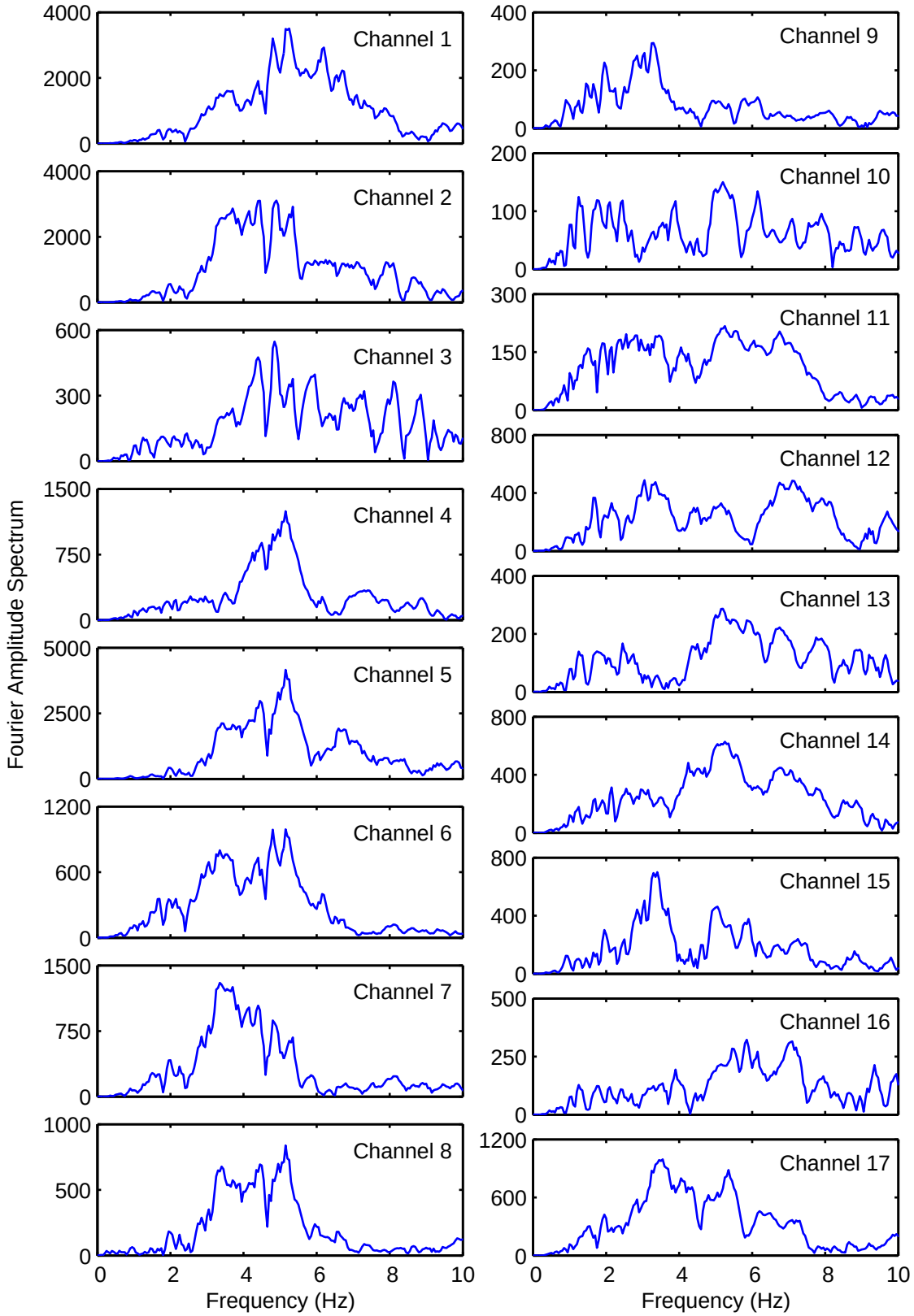

Figure 2.7: Fourier amplitude spectra of the January 13, 2001 acceleration records

Chapter 3

Generation of Abutment Records

The analysis of the earthquake records obtained on January 13, 2001, makes it possible to generate abutment records corresponding to channels 12–17 at Pacoima Dam from reference accelerations recorded at the base of the dam (channels 9–11) for use in structural analyses that account for nonuniform input ground motion. The approach can be tested by comparing records generated from the January 13, 2001 base records to the actual recordings made on the abutments. Also, the abutment records from the 1994 Northridge earthquake that were unable to be digitized can be re-created. These records are, of course, an approximation and the method assumes that the topographic amplification and seismic wave travel times are not significantly dependent on the amplitude of the ground motion. The basic approach could be generalized to generate nonuniform ground motions for analysis of any structure situated in a canyon.

3.1 Method for Generating Records

In Chapter 2, the abutment records were compared to the base records for the January 2001 earthquake. Two basic quantities came out of this comparison: amplification and time delay. These quantities can be used to create abutment records at the locations of channels 12–17 (80% height of the dam) from records obtained at the base of the dam where channels 9–11 are located. This is accomplished in the frequency domain. The amplification is the amplitude of the transfer function between a base record and an abutment record; and the negative of the time delay multiplied by the frequency gives

the phase of the transfer function. The Fourier transform of an abutment acceleration $A_n(\omega)$ generated from the Fourier transform of a base acceleration $A_m(\omega)$ is given by

$$A_n(\omega) = Amp_{n,m}(\omega)\, e^{-i\,\omega\,\tau_{n,m}(\omega)}\, A_m(\omega) \tag{3.1}$$

where $Amp_{n,m}(\omega)$ is the amplification function, $\tau_{n,m}(\omega)$ is the time delay function and ω is frequency. The phase of the transfer function is represented by $-\omega\,\tau_{n,m}(\omega)$.

3.1.1 Amplification

Various amplification functions were used to generate different sets of ground motion for comparison. Both the 5% damped and 0% damped spectral displacement ratios shown in Figure 2.4 were used, and the Fourier amplitude transfer functions shown in Figure 2.5 were also used to illustrate how the impulsive nature of these functions is not suitable for generating realistic earthquake records. A set of piecewise linear functions was also formulated in an attempt to simulate the generality of smooth functions that might be attained if amplification functions could be averaged over several different events. The piecewise linear functions are approximations of the spectral displacement ratios. The piecewise linear approximations are shown in Figure 3.1 with the 5% damped spectral displacement ratios shown for reference.

3.1.2 Time Delay

Similarly, various relative phase functions were used to incorporate time delays into the abutment records. The modified time delays shown in Figure 2.6, which will be referred to as the frequency-dependent time delays, were converted to relative phase as in Equation 3.1. Constant time delays were also used and converted to relative phase in the same way. The constant delays give linear phase functions. The time delays given in Table 2.2 were used, and a simpler set of constant time delays was also used in hopes of determining the importance of using different delays for each component at a location. For this purpose, constant delays of 0.048 seconds and 0.054 seconds were applied to all three components on the right and left abutments,

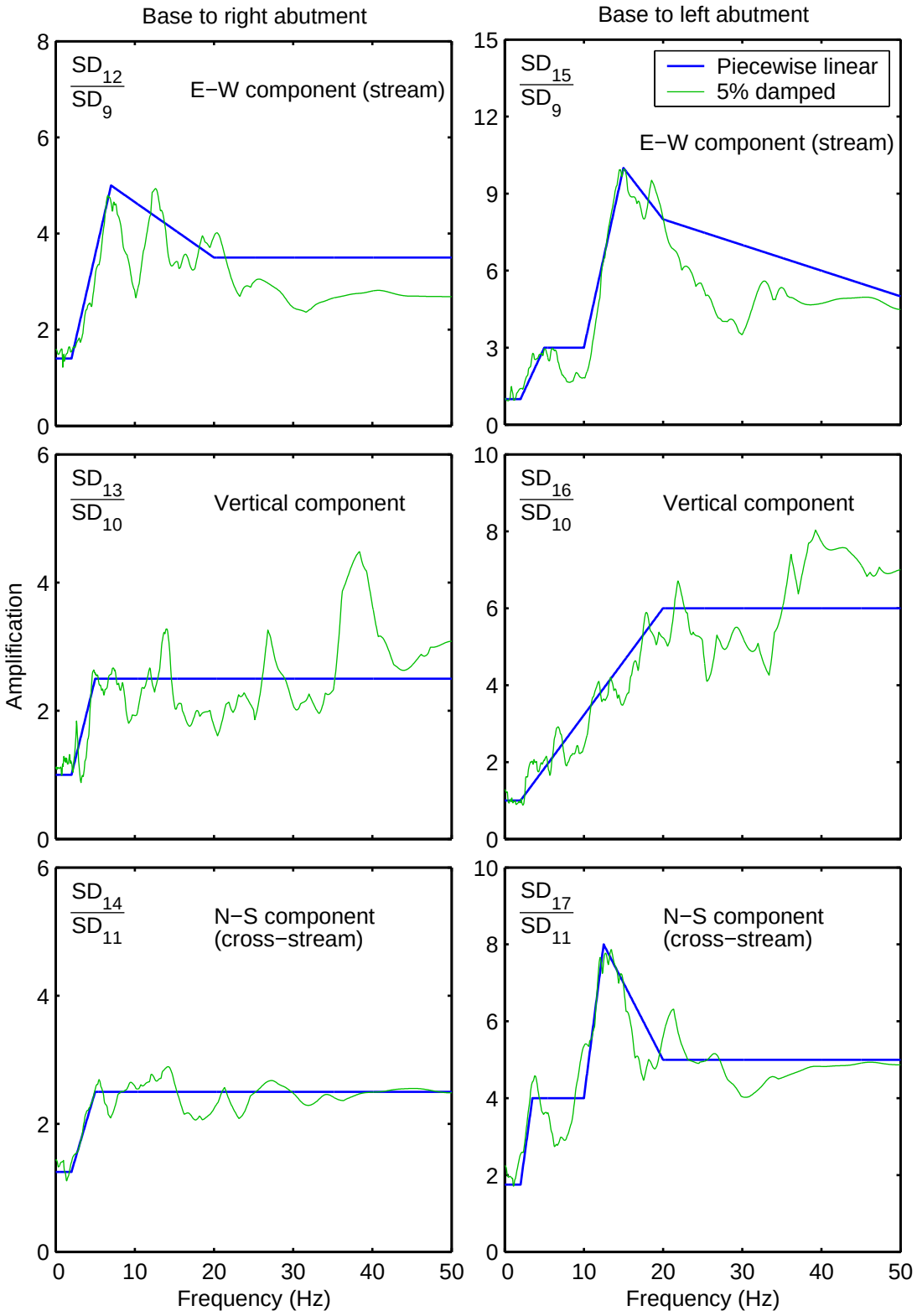

Figure 3.1: Piecewise linear amplification approximated from 5% damped spectral displacement ratios of abutment and base records from January 13, 2001

respectively. These values are approximately the averages of the horizontal component delays at the respective locations given in Table 2.2. These delays will be referred to as the constant, component-independent time delays and the other constant delays will be referred to as the constant, component-dependent time delays. Lastly, the actual phase of the Fourier transfer functions from the January 2001 records was used. Time delay cannot be computed from the Fourier phase because it is not unique; and like the Fourier amplitude, the phase is event specific. However, records were generated with the actual relative phase for comparison to the other approaches. The relative phases computed from the frequency-dependent time delays and the Fourier transfer functions are shown in Figure 3.2.

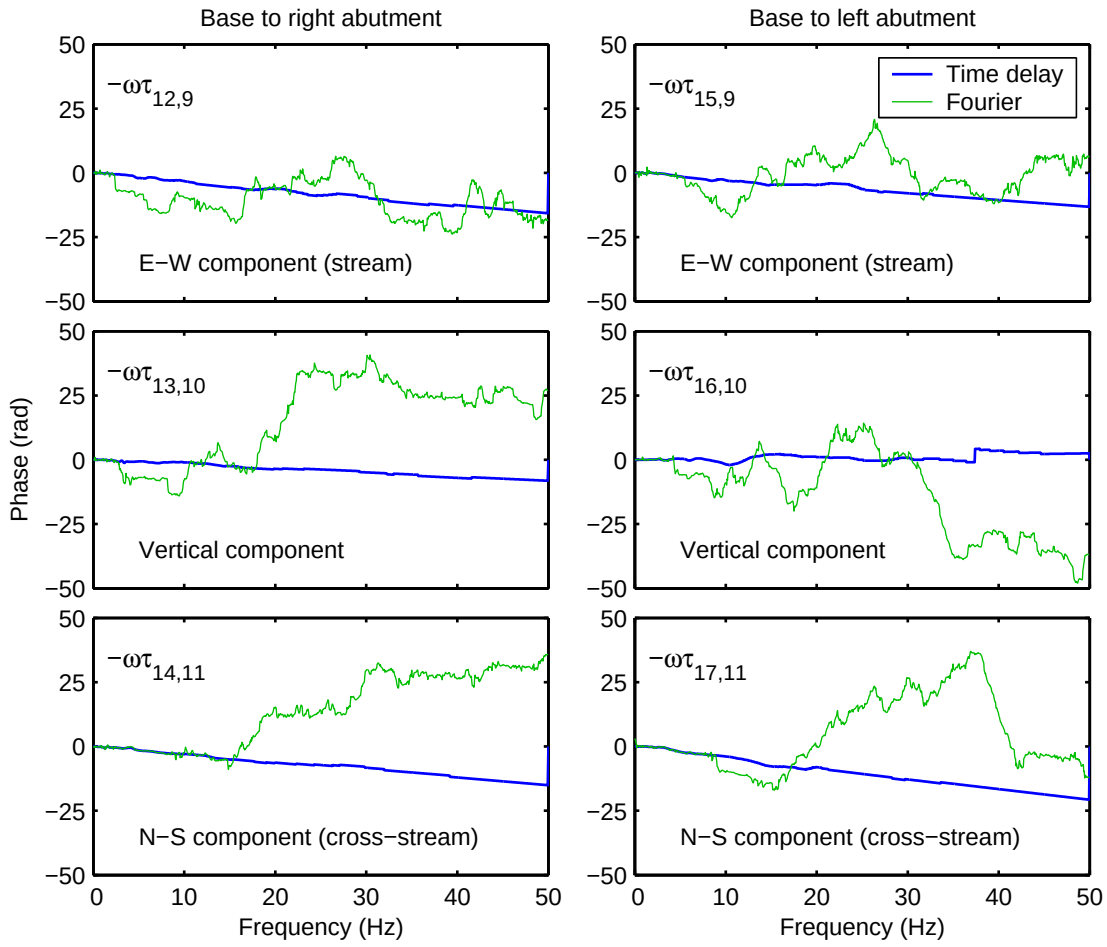

Figure 3.2: Relative phase of abutment and base records from January 13, 2001, computed from the time delays found by cross-correlating displacement responses of 5% damped SDOF's and directly from the phase of the Fourier transfer functions

3.2 Records Generated for the January 13, 2001 Earthquake

The described method was used to generate abutment records from the January 13, 2001 base records to compare to the actual abutment records. These generated ground motions can then be used as input to the finite element model and the dam response can be compared to the modeled response with the actual records, which is described in Chapter 8. This comparison was done as a way to assess the appropriateness of the generated records for structural analyses.

Since the amplification and time delay were each implemented four different ways, there are sixteen ways to generate the abutment records. All sixteen combinations are listed in Table 3.1. Only examples that illustrate significant differences are presented here. Note that method 16 actually re-creates the January 2001 records exactly, since the transfer functions were obtained from the January 2001 records.

The abutment accelerations generated with the piecewise linear amplification and the Fourier transfer function phase (method 4) are compared to 6 seconds of the actual records in Figure 3.3, and the accelerations generated with the Fourier amplitude transfer functions and the frequency-dependent time delays (method 13) are compared to the actual records in Figure 3.4. Method 4 uses approximate amplification and the exact relative phase from the January 2001 records and method 13 uses the exact amplification and approximate relative phase computed from the time delays determined by cross-correlating the displacement responses of 5% damped SDOF's. First, notice that the approximate amplification with exact phase (Figure 3.3) generates accelerations that match the actual records fairly well, but there is some underestimation of the actual records in a few of the channels, particularly channel 15 around 7 to 7.5 seconds. Nevertheless, the piecewise linear functions give a good approximate amplification to obtain the abutment acceleration records. Also, notice that the actual amplification with the approximate phase (Figure 3.4) generates acceleration records that are quite similar to the actual recordings except for a little underestimation at channel 15 around 7.25 seconds, so the frequency-dependent time delays yield a good

Method	Amplification/Phase
1	Piecewise linear approximation/ Frequency-dependent time delay
2	Piecewise linear approximation/ Constant, component-dependent time delay
3	Piecewise linear approximation/ Constant, component-independent time delay
4	Piecewise linear approximation/ Fourier transfer function phase
5	5% damped spectral displacement ratios/ Frequency-dependent time delay
6	5% damped spectral displacement ratios/ Constant, component-dependent time delay
7	5% damped spectral displacement ratios/ Constant, component-independent time delay
8	5% damped spectral displacement ratios/ Fourier transfer function phase
9	0% damped spectral displacement ratios/ Frequency-dependent time delay
10	0% damped spectral displacement ratios/ Constant, component-dependent time delay
11	0% damped spectral displacement ratios/ Constant, component-independent time delay
12	0% damped spectral displacement ratios/ Fourier transfer function phase
13	Fourier amplitude transfer functions/ Frequency-dependent time delay
14	Fourier amplitude transfer functions/ Constant, component-dependent time delay
15	Fourier amplitude transfer functions/ Constant, component-independent time delay
16	Fourier amplitude transfer functions/ Fourier transfer function phase

Table 3.1: List of the abutment record generation methods

approximation to the relative phase.

When both the approximate amplification and approximate relative phase are used to generate the records, the match with the actual records is still good. The abutment accelerations generated with the piecewise linear amplification and the frequency-dependent time delays (method 1) are compared to the actual records in

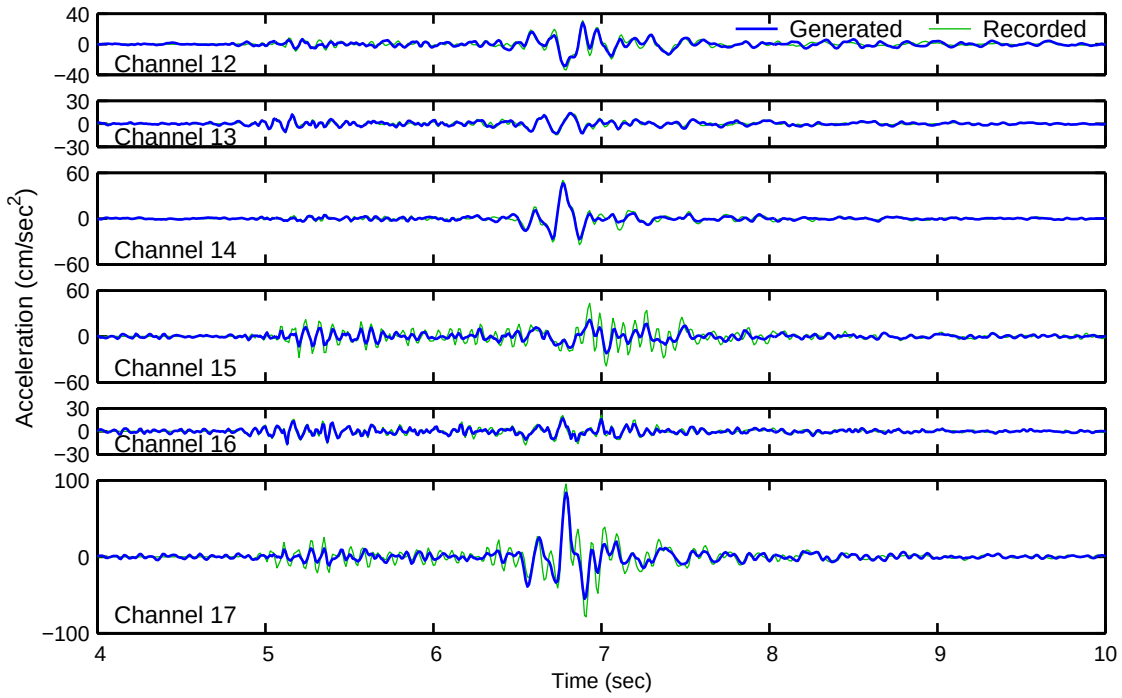

Figure 3.3: Abutment accelerations generated from the January 13, 2001 base records by method 4 compared to the actual records

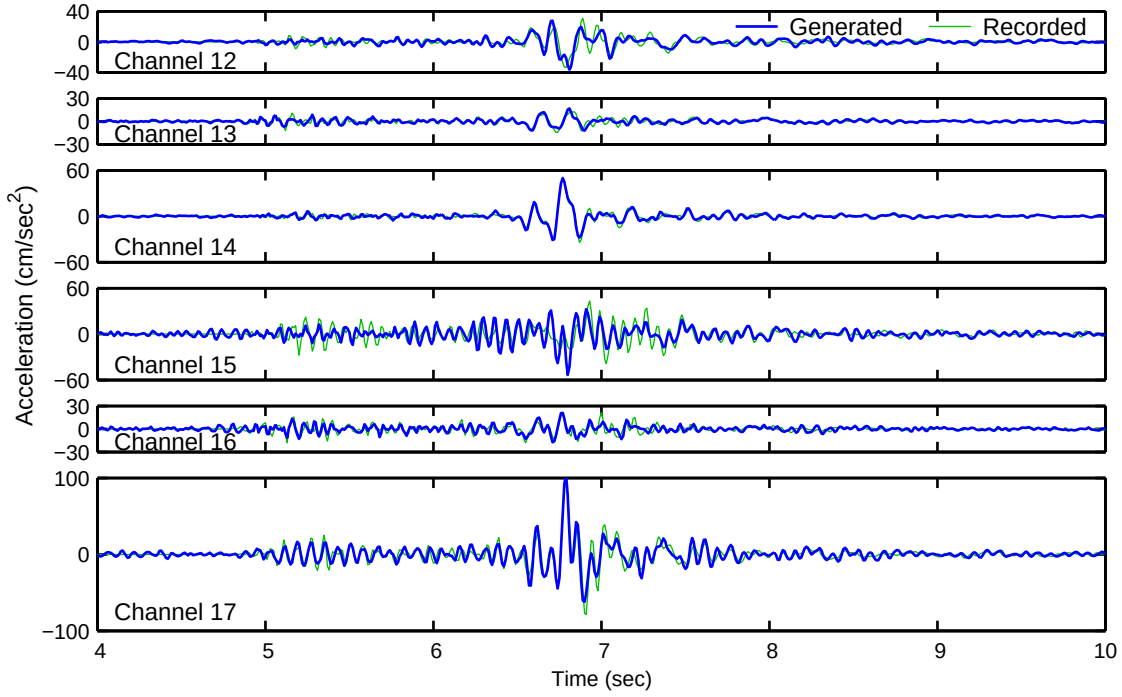

Figure 3.4: Abutment accelerations generated from the January 13, 2001 base records by method 13 compared to the actual records

Figure 3.5. The discrepancies from the actual accelerations that appear in methods 4 and 13 are basically combined in method 1. Figure 3.6 shows that the abutment displacements integrated from the accelerations generated by method 1 match the actual recorded displacements even better than the accelerations match, because the piecewise linear functions agree best with the actual amplification at low frequencies.

The effect of using the constant, component-dependent time delays instead of the frequency-dependent time delays (both with the piecewise linear amplification) is shown in Figures 3.7 and 3.8. The accelerations are well synchronized between the two methods and differences are not significant, in general. So, the constant, component-dependent time delays (method 2) yield similar accelerations to those obtained with frequency-dependent time delays (method 1), and hence they agree fairly well with the recorded accelerations. However, greater difference is illustrated in the displacements. The lower frequency delays are not smaller for the constant delays like they are for the frequency-dependent delays, so the pulses arrive later (except for channel 16, which has a negative delay). This is particularly apparent at channel 17. So, the method 2 displacements do not have the same level of agreement with the actual records as the method 2 accelerations.

If the constant, component-independent time delays are used with the piecewise linear amplification (method 3), the exact same records are generated as from method 2 except they are shifted in time because the delays are different. The agreement of the accelerations generated by method 3 with the actual recorded accelerations is shown in Figure 3.9. The horizontal component agreement is still fairly good, but the vertical component (channels 13 and 16) agreement is not since the vertical delays in the actual records are smaller than the average values used for the component-independent delays. The question is whether this difference is important for modeling purposes since the vertical motions are smaller and may not be as important to the response of Pacoima Dam as horizontal motions.

Generating the abutment records with 5% damped spectral displacement ratios (method 5) and 0% damped spectral displacement ratios (method 9) as the amplification with frequency-dependent time delays yield similar results to each other.

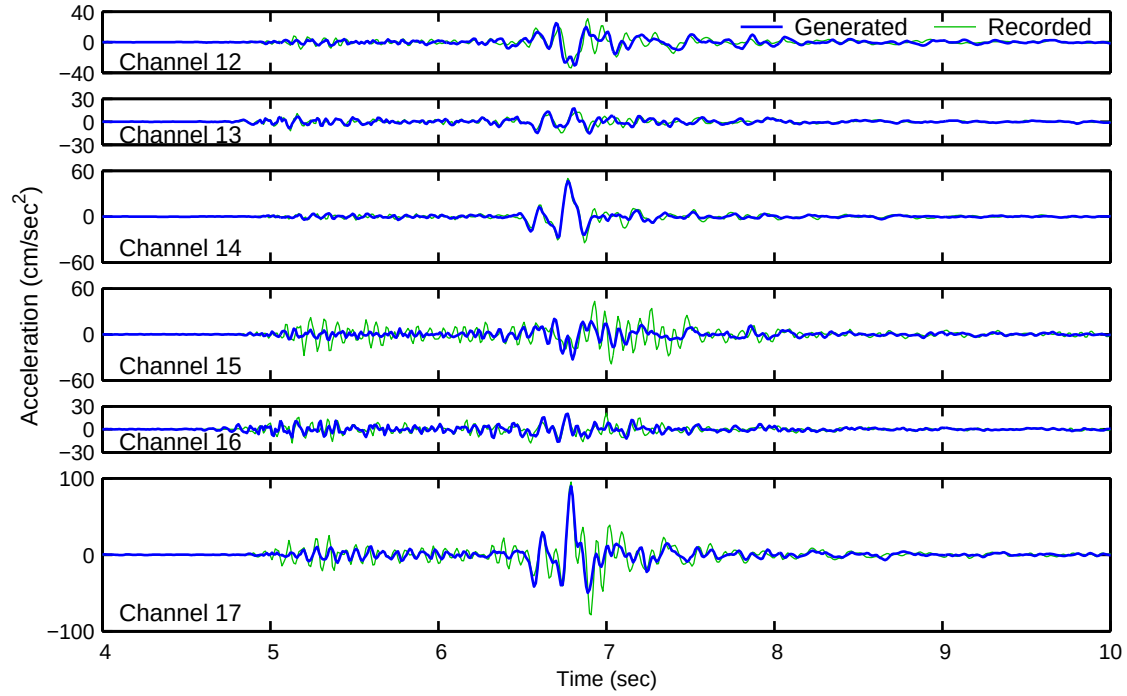

Figure 3.5: Abutment accelerations generated from the January 13, 2001 base records by method 1 compared to the actual records

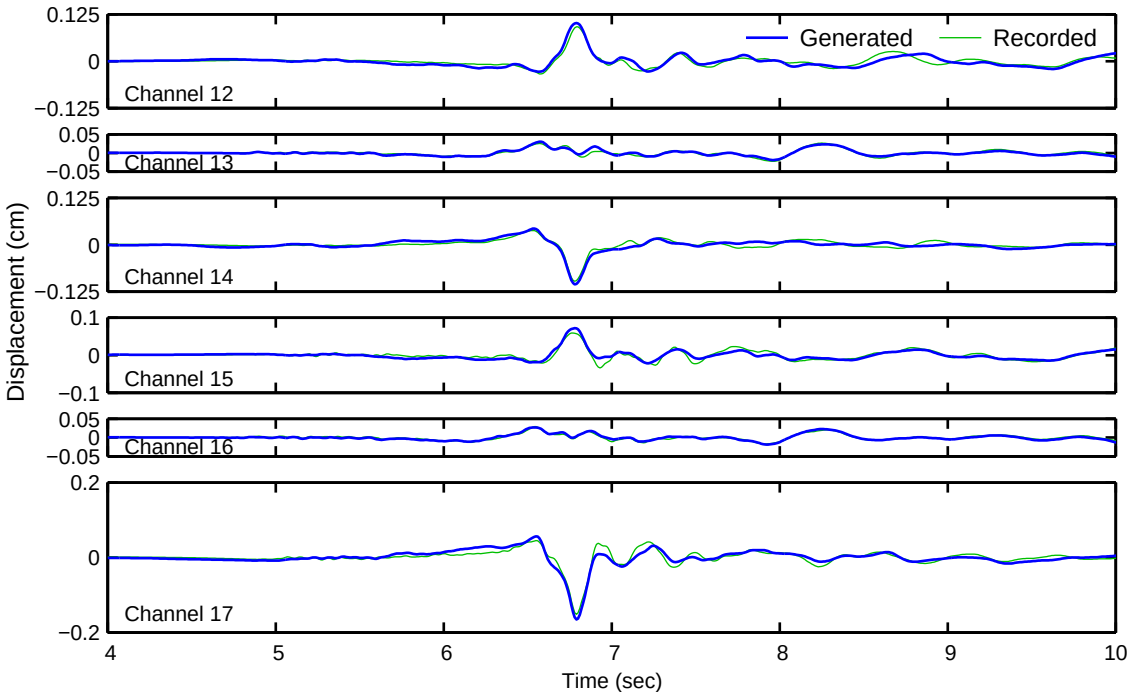

Figure 3.6: Abutment displacements generated from the January 13, 2001 base records by method 1 compared to the actual records

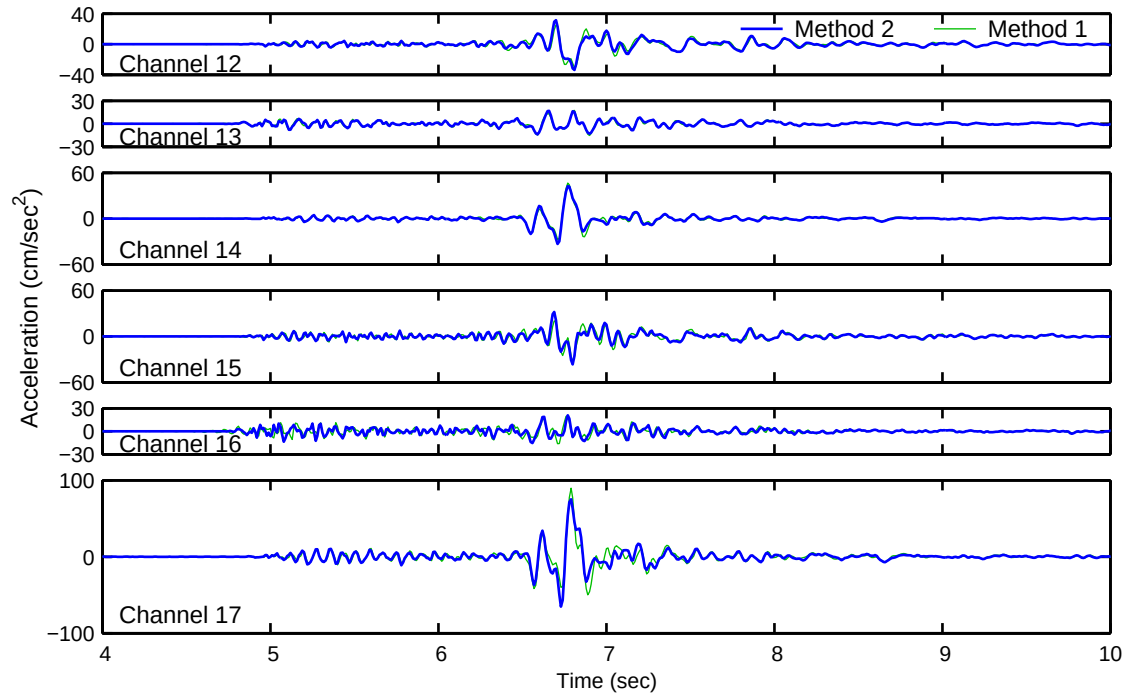

Figure 3.7: Abutment accelerations generated from the January 13, 2001 base records by method 2 compared to method 1

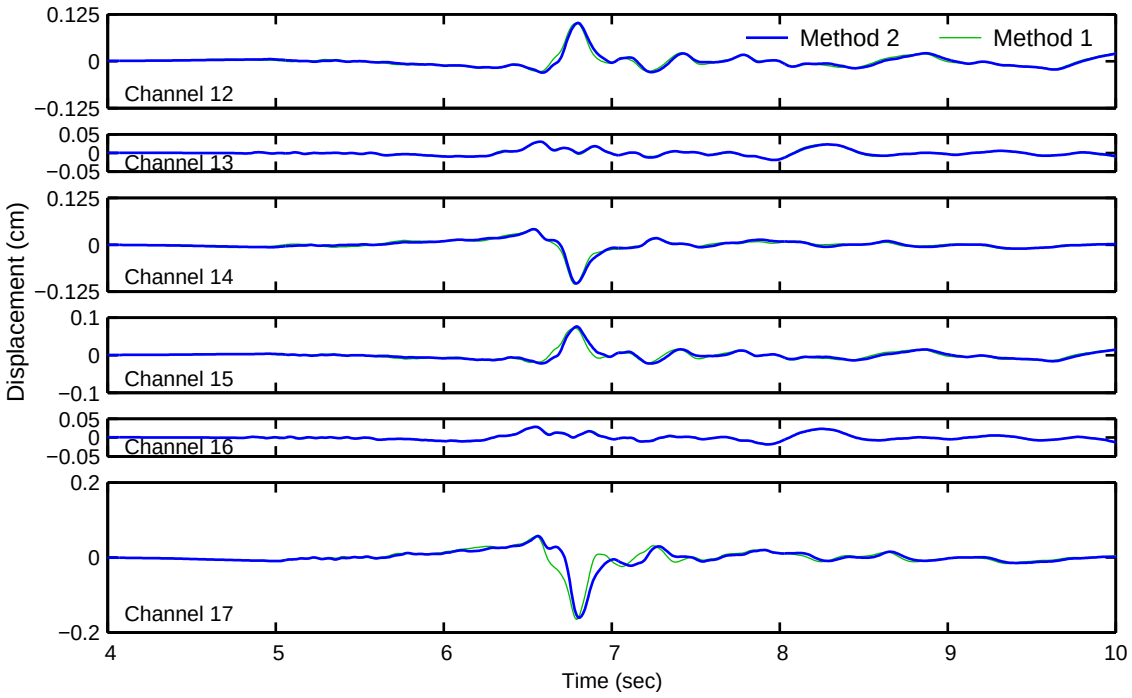

Figure 3.8: Abutment displacements generated from the January 13, 2001 base records by method 2 compared to method 1

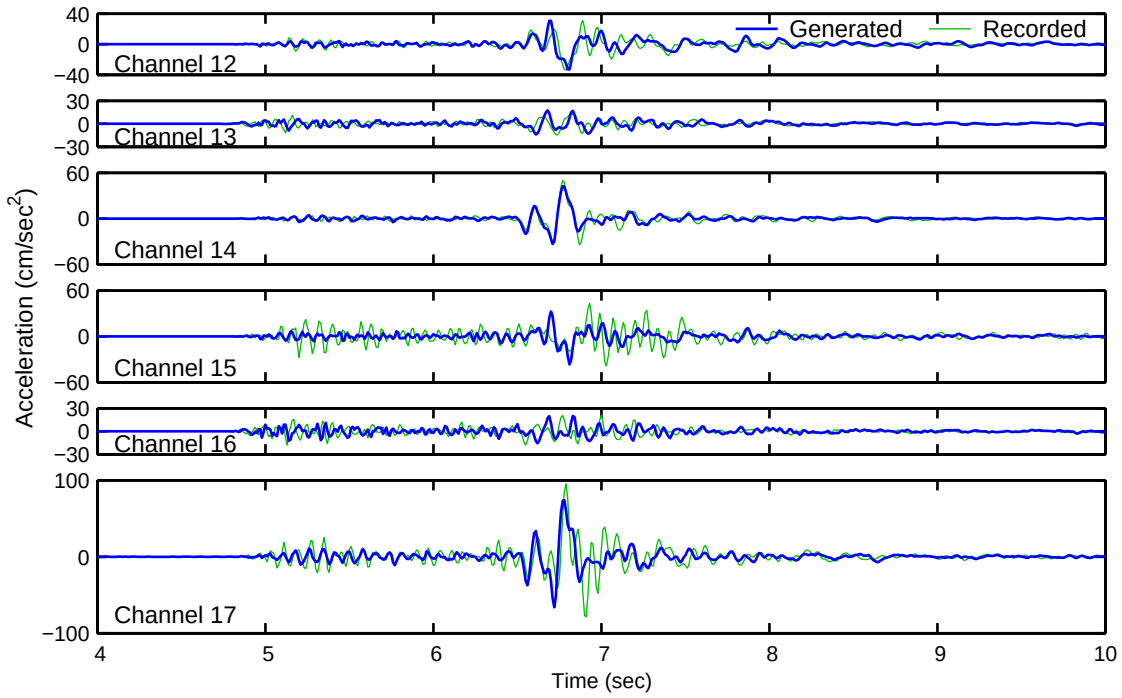

Figure 3.9: Abutment accelerations generated from the January 13, 2001 base records by method 3 compared to the actual records

However, as expected, the smoother 5% damped spectral ratios give abutment accelerations that are more similar to the records generated with the piecewise linear amplification (method 1), and the 0% damped spectral ratios generate records that are more similar to those generated with the Fourier amplitude transfer functions (method 13). The good agreement between these respective sets of records is shown in Figures 3.10 and 3.11.

All four amplification functions generate records that are fairly good approximations of the actual recordings. The more impulsive Fourier amplitude transfer functions do the best job, but they are specific to the January 2001 earthquake so the smoother estimates may be more desirable for a general event. The same is true for the relative phase functions. The Fourier transfer function phase does the best job of reproducing the records, but the frequency-dependent approximation that is based on the physical quantity of time delay is probably a better option for an arbitrary ground motion. The constant, component-dependent time delays yield similar accelerations to the frequency-dependent delays, but the smaller displacement delays

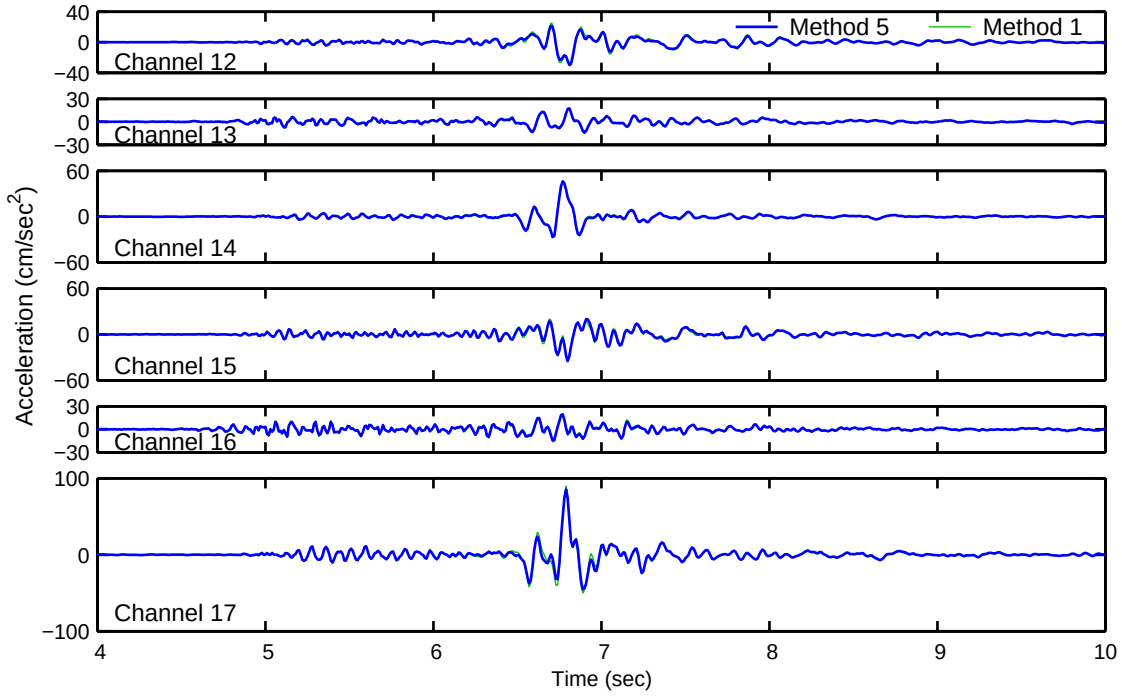

Figure 3.10: Abutment accelerations generated from the January 13, 2001 base records by method 5 compared to method 1

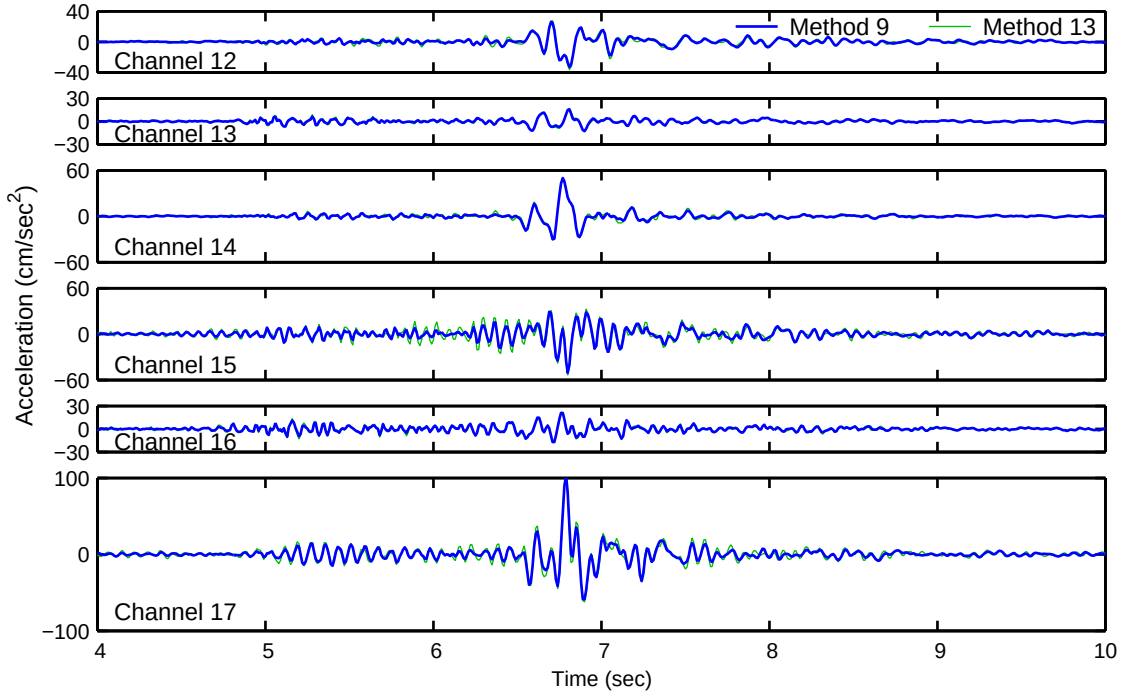

Figure 3.11: Abutment accelerations generated from the January 13, 2001 base records by method 9 compared to method 13

are not captured; and the constant, component-independent delays do not account for the smaller vertical component delays. However, the constant time delays may still be adequate for response modeling purposes.

3.3 Records Generated for the Northridge Earthquake

Before discussing the abutment records (channels 12–17) generated to replace the undigitized Northridge earthquake records, the partial recordings should be presented. The partial acceleration records (channels 1–6, 12, 13 and 15–17) and the complete processed acceleration records (channels 8–11) are shown in Figure 3.12. Channels 7 and 14 failed to record at all during the Northridge earthquake. The velocity and displacement of channels 8–11 obtained by CSMIP are shown in Figures 3.13 and 3.14, respectively. CSMIP Report OSMS 95–05 presents the partial records (CSMIP, 1995) and CSMIP Report OSMS 94–15A presents the complete processed records (CSMIP, 1994). The ground motion recorded during the Northridge earthquake is, of course, significantly larger than the motion recorded on January 13, 2001; and the Northridge accelerations contain some very high frequency spikes that must be associated with some nonlinear impact behavior that did not occur in January 2001.

Since channels 9–11 were completely digitized, the abutment records can be re-created using the same generation methods previously described without any modification. These generated motions can be compared to the partial abutment records except for channel 14. However, the period of strongest motion cannot be compared with the exception of channel 12, which was almost completely captured.

If the Fourier amplitude transfer functions from the January 2001 earthquake records are used as amplification to generate abutment records for the Northridge earthquake, then the generated records do not re-create realistic Northridge accelerations very well. To illustrate this, the channel 12 and channel 15 accelerations generated using the Fourier transfer function amplitude and phase (method 16) are

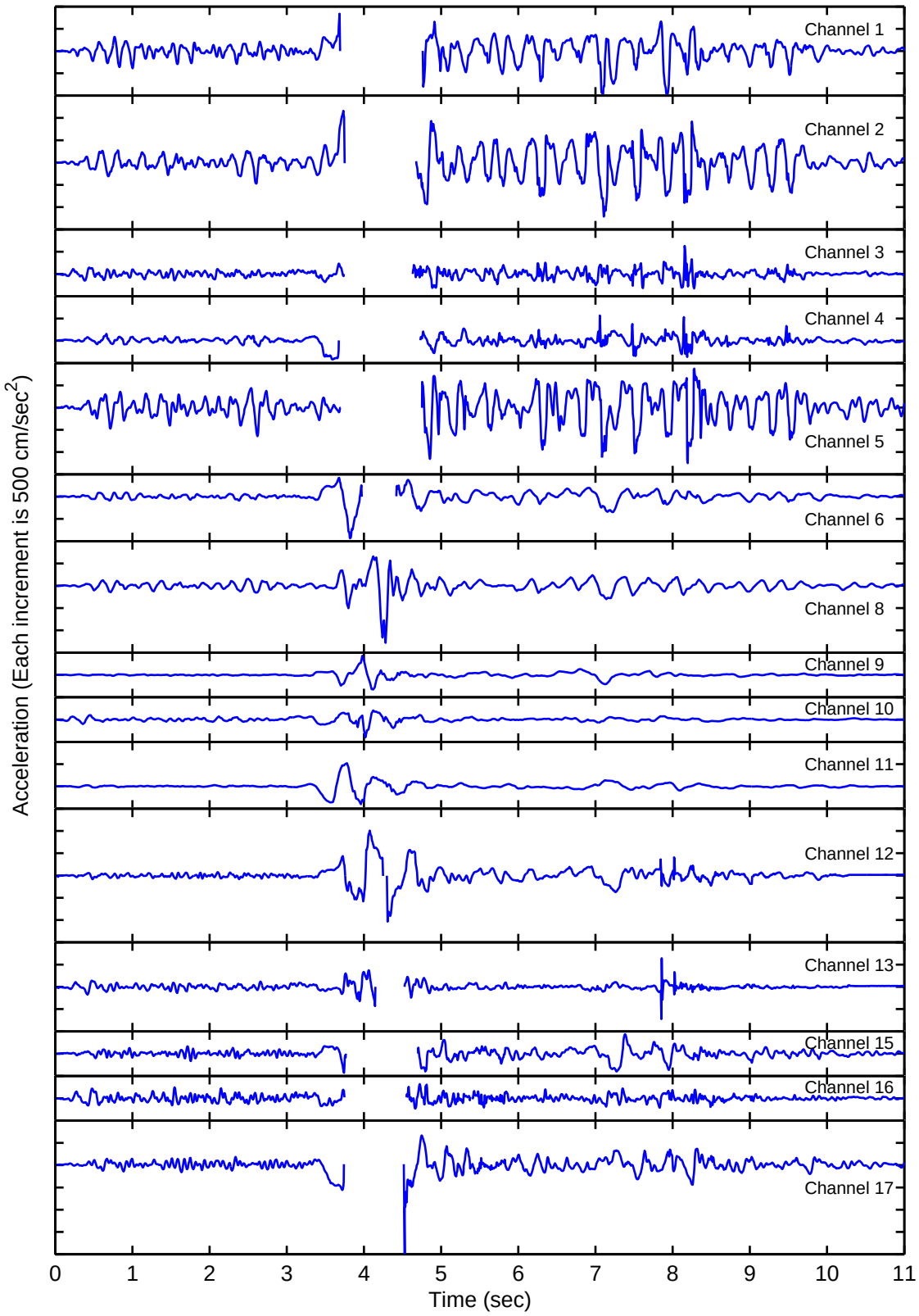

Figure 3.12: Acceleration recorded during the Northridge earthquake

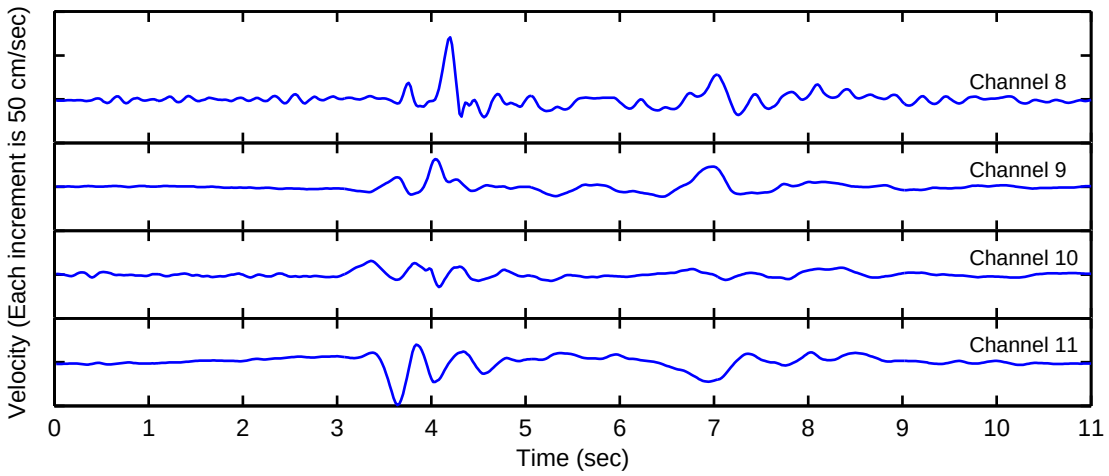

Figure 3.13: Velocity computed from acceleration recorded at channels 8–11 during the Northridge earthquake

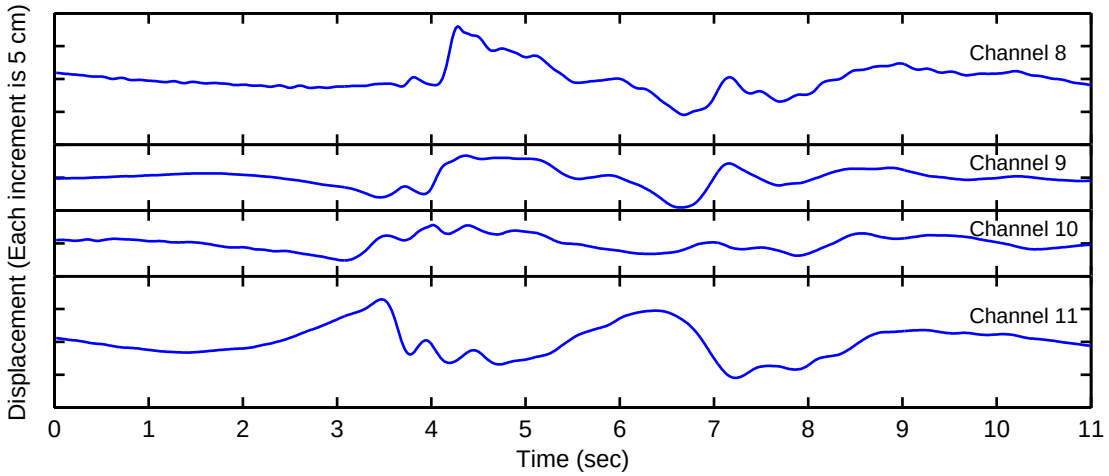

Figure 3.14: Displacement computed from acceleration recorded at channels 8–11 during the Northridge earthquake

compared to the partial abutment records in Figure 3.15. The oscillations are too large at the beginning and end of the records. This is particularly noticeable in the last 6 seconds of channel 12, and channel 15 has too much contribution at a high frequency throughout the record. The problem is that certain frequencies are overly amplified because of very large peaks in the amplification function that are only present because these frequencies were absent in the January 2001 base records, not because they were significant in the 2001 abutment records. This is not a problem when re-creating the January 2001 abutment records, since the same input base

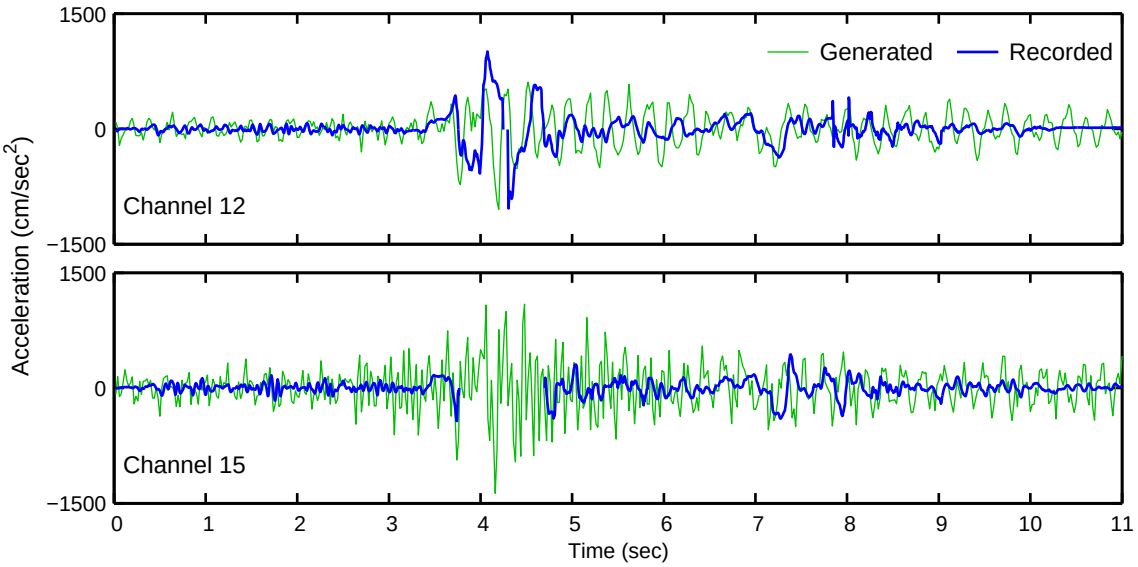

Figure 3.15: Channel 12 and channel 15 accelerations generated from the Northridge earthquake channel 9 record by method 16 compared to the actual partial records

records are used. Therefore, as has been previously stated, smoother approximate amplification functions are more appropriate to generate general earthquake records.

The difference between using the actual phase from the transfer functions and the approximate frequency-dependent phase to generate records is noticeable but not particularly significant. The channel 12 displacement computed using the piecewise linear amplification and Fourier transfer function phase (method 4) is compared to the displacement computed using the piecewise linear amplification and frequency-dependent time delay (method 1) in Figure 3.16. There is a significant displacement

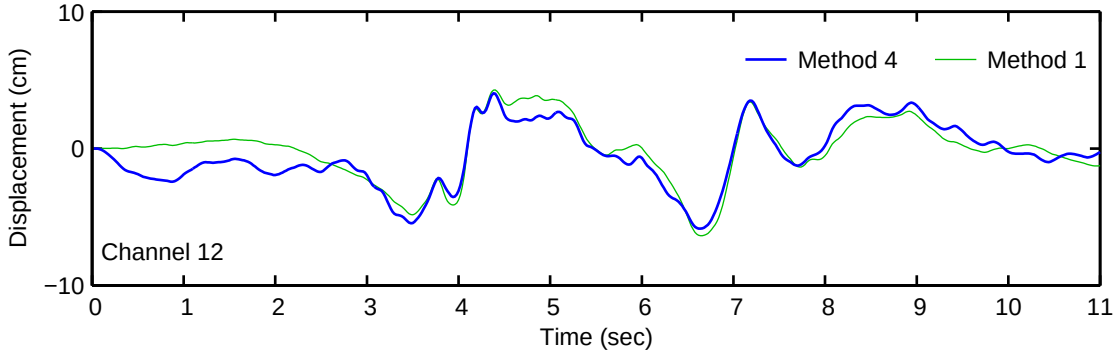

Figure 3.16: Channel 12 displacement generated from the Northridge earthquake channel 9 record by method 4 compared to method 1

that occurs less than a quarter of a second into the record generated with the Fourier phase, which may not be realistic since the strong acceleration does not arrive for a few seconds. Regardless of whether the Fourier phase produces a realistic displacement, the approximate frequency-dependent phase is preferable, since the relative phase should not be event specific.

The abutment records generated with the smoother amplification functions and the frequency-dependent time delays generally produce more realistic records that agree better with the partial records. The records generated with the piecewise linear amplification and frequency-dependent delays (method 1) are shown in Figure 3.17 compared to the partial records. Generally, the generated records are a little smaller

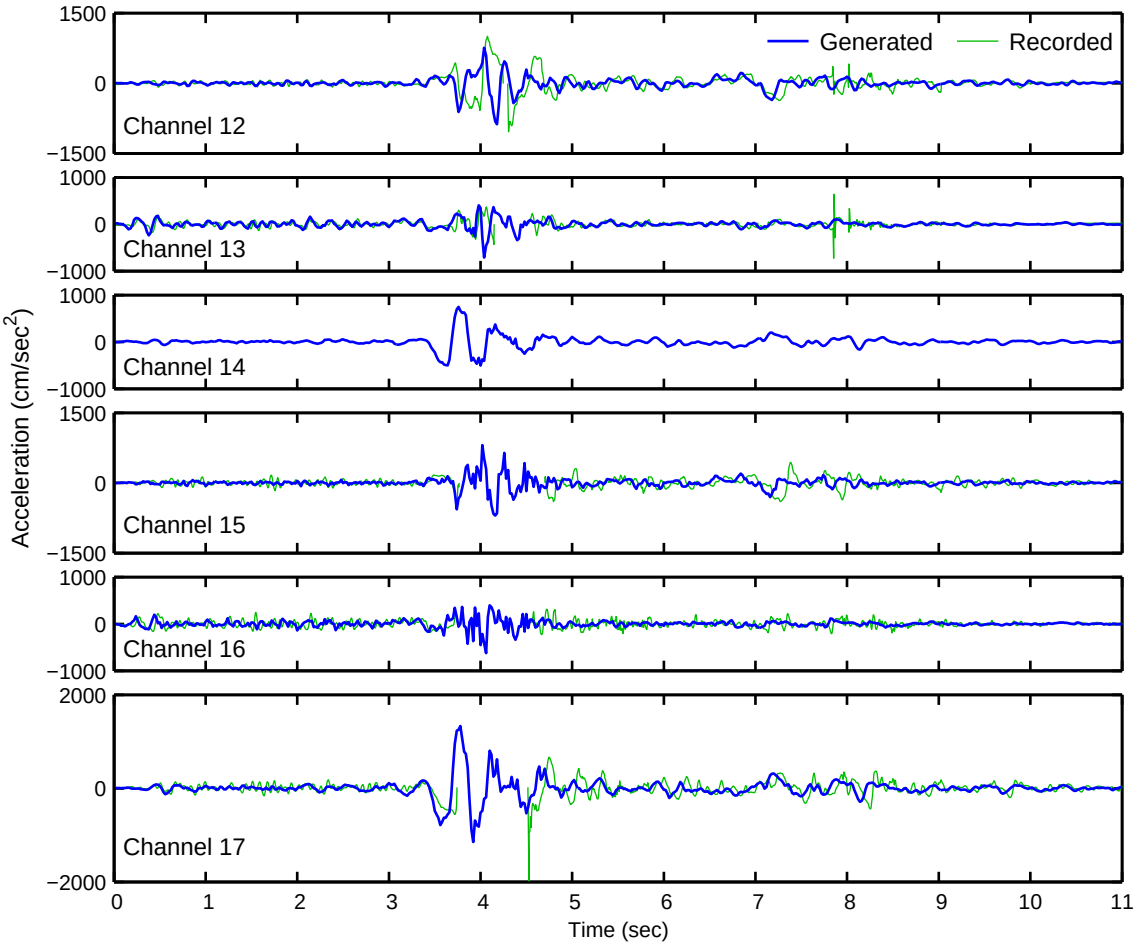

Figure 3.17: Abutment accelerations generated from the Northridge earthquake base records by method 1 compared to the actual partial records

than the actual recordings after 5 seconds on the left abutment (channels 15–17). The generated left abutment motions lack some higher frequency oscillation that is present in the partial records. Channels 12 and 13 agree better after 5 seconds. However, the agreement with the strong motion that was digitized at channel 12 is not very good. The generated strong motion is a little small and it is not in-phase with the partial record. Using the 5% damped spectral displacements for amplification (method 5) does not improve the agreement since the generated accelerations are very similar to those generated by method 1. The accelerations generated by method 5 are compared to the partial recordings in Figure 3.18. With the 0% damped spectral displacements (method 9), the left abutment accelerations are generated with more

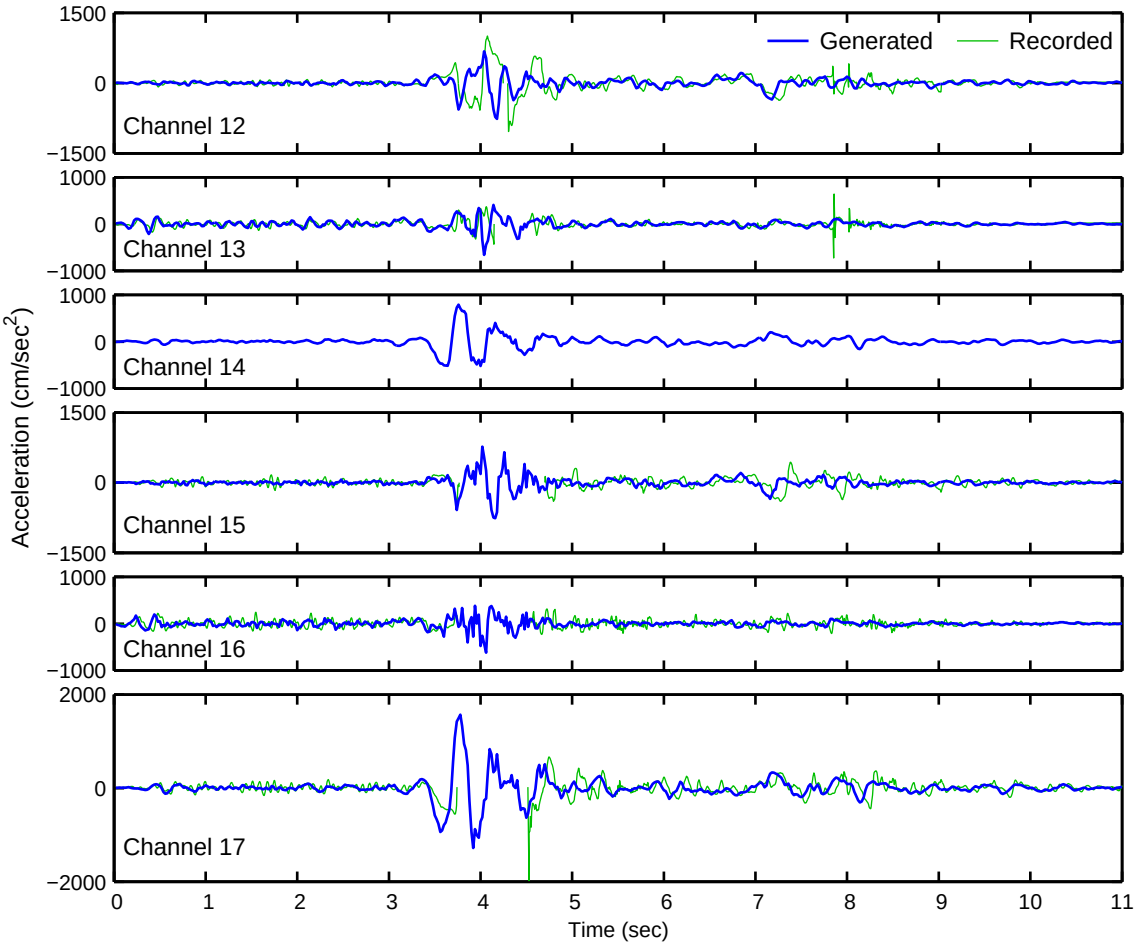

Figure 3.18: Abutment accelerations generated from the Northridge earthquake base records by method 5 compared to the actual partial records

high frequency content but the channel 12 acceleration is very similar to that from method 1. The accelerations generated by method 9 are compared to the partial recordings in Figure 3.19. Also, the displacements generated by methods 1 and 9 are plotted in Figure 3.20 to simply show the generated displacements and to illustrate that the displacements created with different amplification functions are very similar.

Another thing to notice from the accelerations generated using the frequency-dependent time delays is that, often the generated records seem to lead the partial recordings in time. This may indicate that the time delays are actually ground motion amplitude-dependent. With larger motion the foundation rock may actually soften, meaning that the wave speeds in the rock would decrease. This would explain the

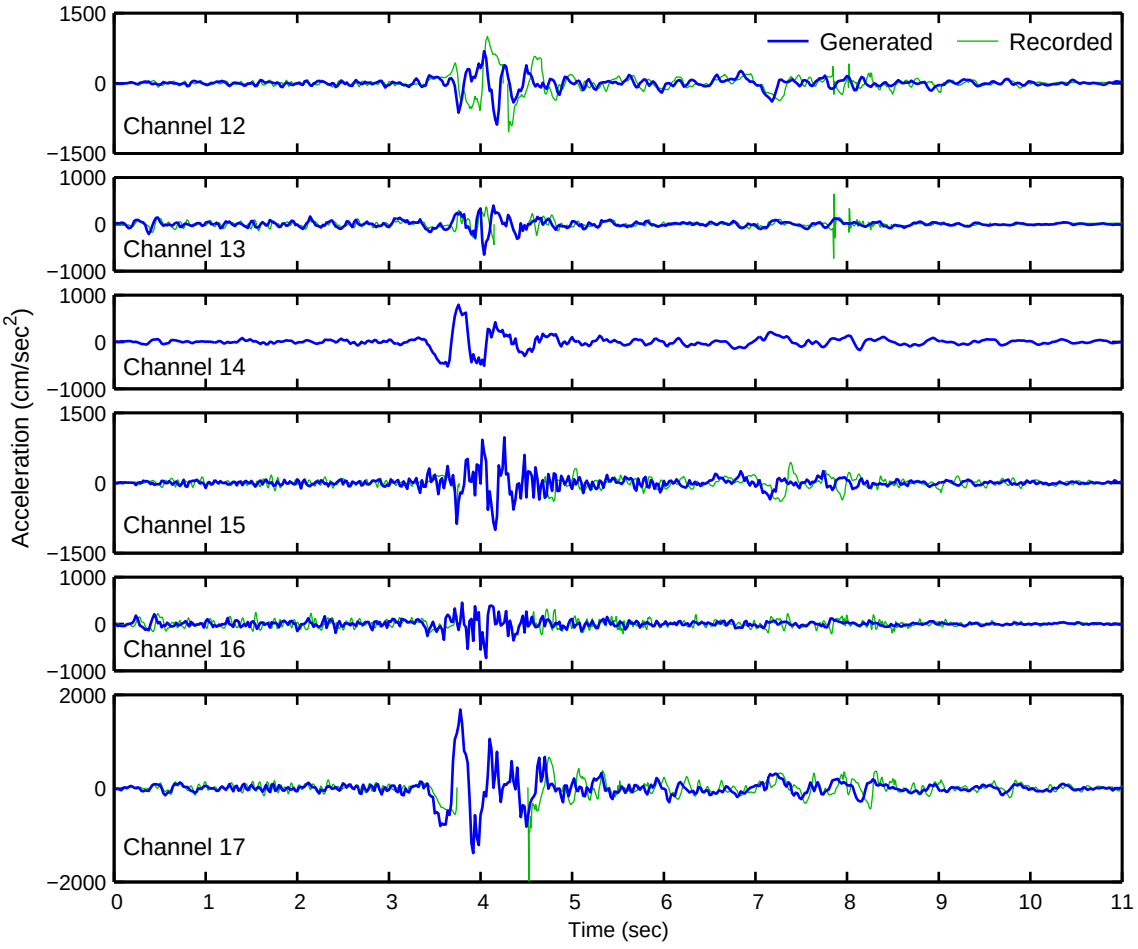

Figure 3.19: Abutment accelerations generated from the Northridge earthquake base records by method 9 compared to the actual partial records

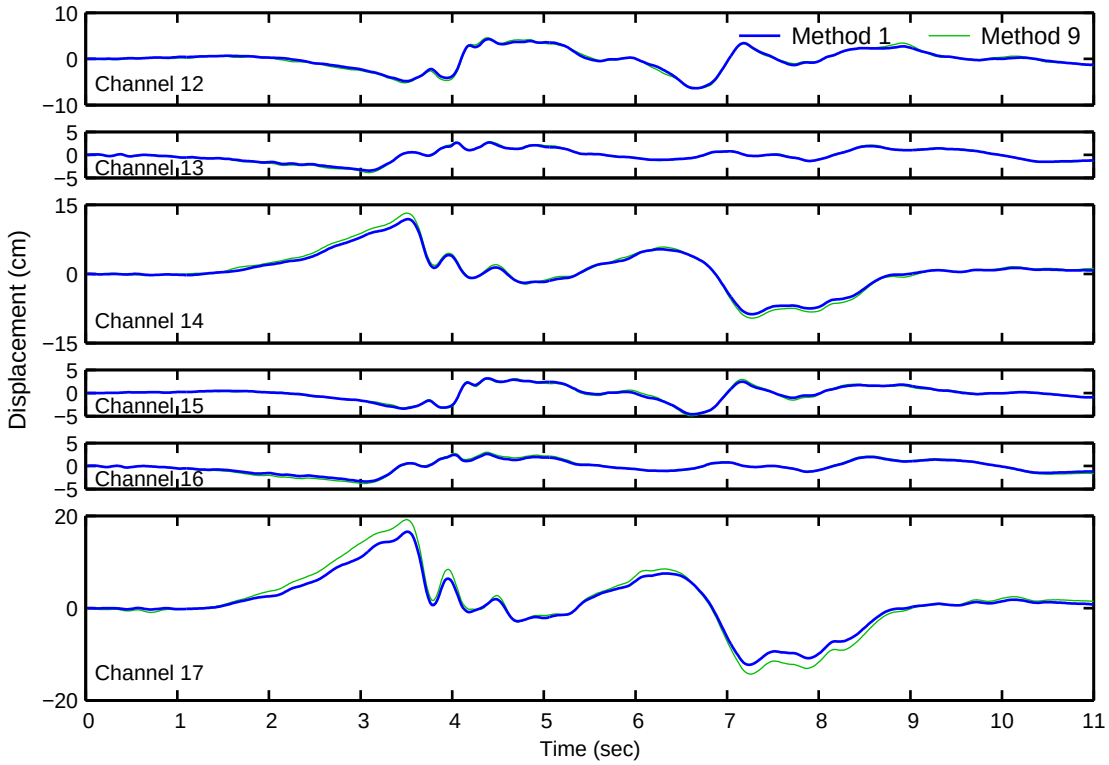

Figure 3.20: Abutment displacements generated from the Northridge earthquake base records by method 1 compared to method 9

need for larger time delays for a larger earthquake. In order to test this, another set of records was generated with the piecewise linear amplification and frequency-dependent time delays (method 1) with the generated abutment records simply shifted 0.05 seconds later. This set of generated abutment accelerations is compared to the partial records in Figure 3.21. The synchronization is better for many of the significant characteristics of the records, but the strong motion section of channel 12 still has a significant mismatch. Another observation is that channel 16 is better synchronized with this positive delay. This indicates that channel 16 leading channel 10 in the January 2001 records is an anomaly, as expected, probably resulting from the small amplitude of the vertical motion.

Unlike the accelerations generated from the January 2001 base records, the accelerations generated using the constant, component-dependent time delays are not all synchronized with the accelerations generated with the frequency-dependent delays. The cross-stream records have a rather low frequency oscillation (below 5 Hz) that

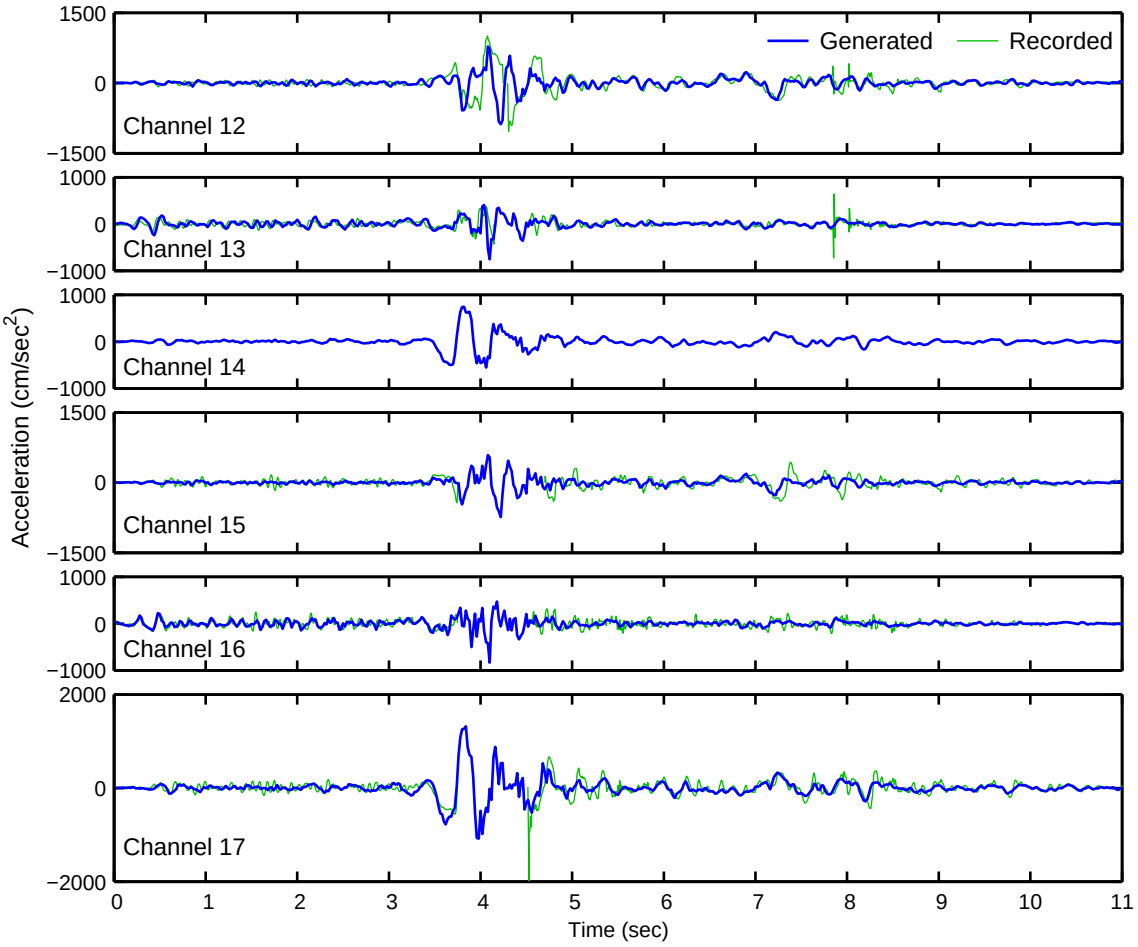

Figure 3.21: Abutment accelerations generated from the Northridge earthquake base records by method 1 and delayed 0.05 sec compared to the actual partial records

dominates. Since the frequency-dependent time delays are smaller at low frequencies, the constant time delay generates cross-stream accelerations that are more delayed. This is most apparent in channel 17. Figure 3.22 shows the accelerations generated with the piecewise linear amplification and constant, component-dependent delays (method 2) compared to the partial records. Notice that the initial negative pulse in channel 17 is synchronized better with the partial record than it is with the frequency-dependent delay in Figure 3.17. However, while the difference is noticeable, it is really quite insignificant.

The constant, component-independent delays only produce accelerations that are shifted in time from the component-dependent delays. The horizontal components

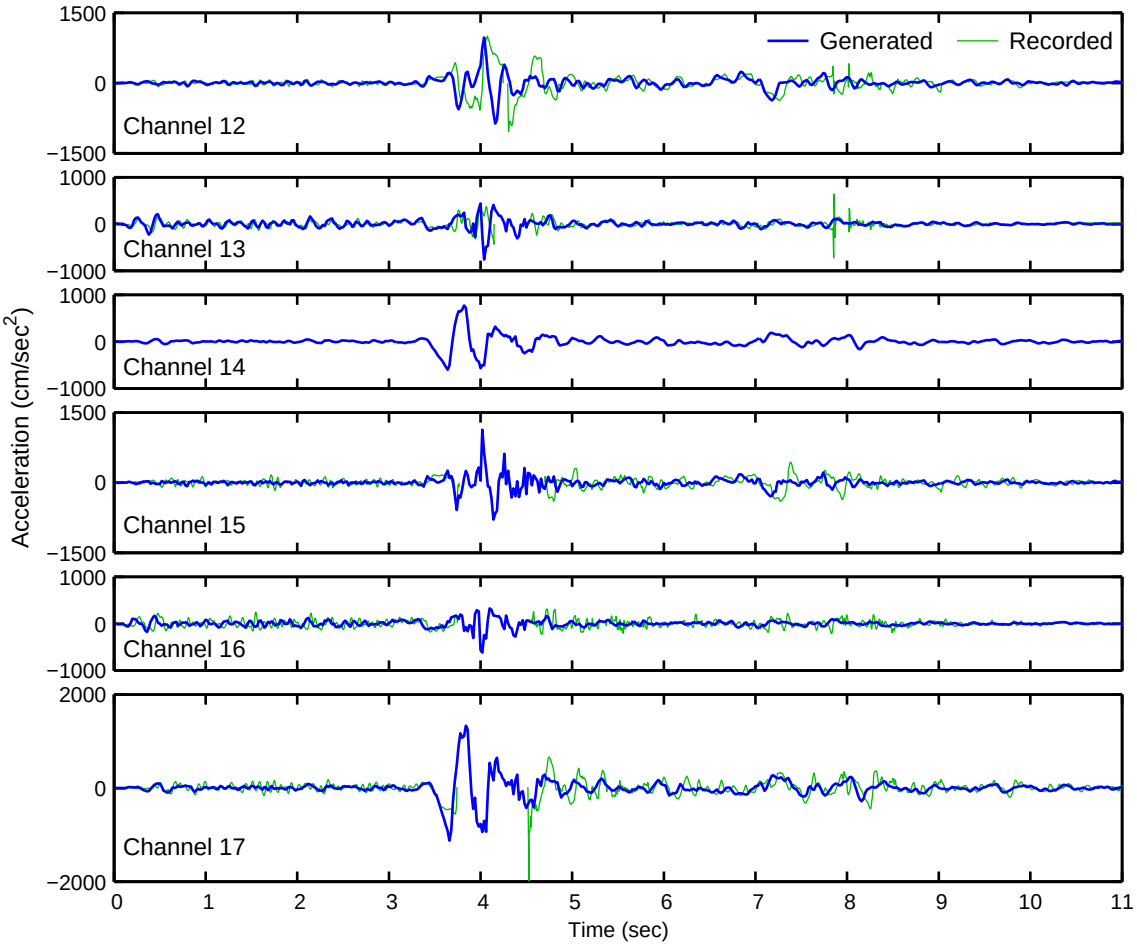

Figure 3.22: Abutment accelerations generated from the Northridge earthquake base records by method 2 compared to the actual partial records

are only slightly affected. However, the vertical components are affected more significantly because the component-independent delays are larger. The vertical accelerations generated with the constant, component-independent delays and piecewise linear amplification (method 3) are compared to the partial records in Figure 3.23. The vertical accelerations are better synchronized with the larger delays, so perhaps using component-independent delays is actually more realistic.

So, it is unclear whether the time delays should be larger for higher amplitude ground motion due to slower wave speeds in the rock, which was tested with the extra 0.05-second delay, or whether the improved synchronization was for other reasons; because using constant time delays and ignoring smaller vertical component delays to

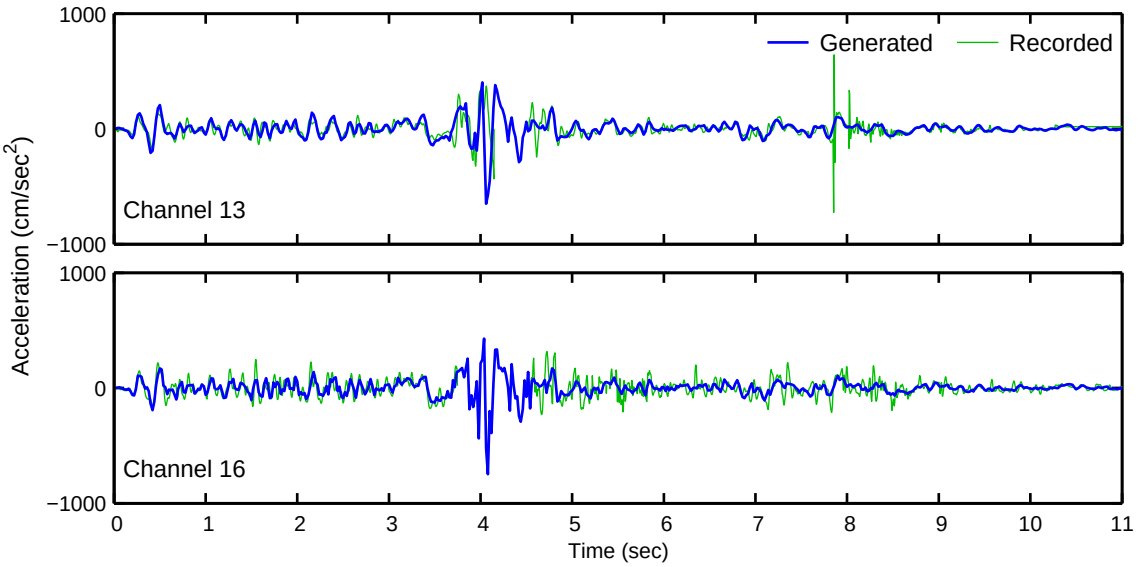

Figure 3.23: Vertical abutment accelerations generated from the Northridge earthquake channel 10 record by method 3 compared to the actual partial records

generate records also produces better synchronization. Study of more data would be necessary to determine with any certainty whether softening of the foundation during a large earthquake causes the time delays between abutment locations to increase. However, it does seem like a physically reasonable occurrence. It is also not clear whether the degree of the topographic amplification is ground motion amplitude-dependent as was discussed in Section 2.2.1, since most of the strongest motion was not digitized during the Northridge earthquake. However, the possible affect does not appear to be extremely significant. The abutment records generated with the approximate piecewise linear amplification and the approximate types of time delays do appear to re-create the partial Northridge abutment motions reasonably well. Thus, methods 1, 2 or 3 should produce nonuniform motion that is a good representation of actual ground motion, even though the methods are approximate. An approximate approach is preferred since the generation method should apply to any ground motion provided for a single location in a canyon. Method 1 is considered as the base case for generating Northridge earthquake ground motion to be used in dynamic structural analyses as discussed in Chapter 10.

Chapter 4

System Identification

A system identification study of Pacoima Dam using earthquake records was performed using a program developed by James Beck called MODE-ID. Documentation on MODE-ID can be found in Beck and Jennings (1980) and Werner et al. (1987). System identification provides modal properties that are important for understanding the vibrational characteristics of the dam and can be used to calibrate a finite element model. The complete January 13, 2001 earthquake records and the partial Northridge earthquake records were analyzed.

4.1 MODE-ID

The program models a structure as a linear system with classical normal modes excited by ground motion that can be spatially nonuniform. No structural model is needed. The modal parameters are estimated by nonlinear least-squares matching of the modeled response to the measured response. Measured acceleration time histories are supplied as input to the model and as the measured output to match. The output error function that is minimized by an optimization procedure is given by

$$J(\theta) = \sum_{i=1}^{NR} \int_{T_i}^{T_f} [\ddot{w}_i(t) - \ddot{y}_i(t;\theta)]^2 \, \mathrm{d}t \tag{4.1}$$

where $\ddot{w}_i$ and $\ddot{y}_i$ are the measured and modeled acceleration, respectively, at the ith output response degree of freedom, NR is the number of output response degrees of

freedom, $[T_i, T_f]$ is the time interval of the records to be matched and θ represents a vector of the modal parameters being estimated. The modal parameters estimated are the natural frequencies, damping, shapes and participation factors for each mode. A pseudostatic matrix can also be estimated. The pseudostatic matrix estimated by MODE-ID consists of rows corresponding to the output response degrees of freedom and columns corresponding to the input degrees of freedom. Each entry in the matrix can be interpreted as the static displacement at a response degree of freedom if one of the input degrees of freedom is displaced a unit amount while the others are held fixed.

For Pacoima Dam, channels 1–8 are supplied as output accelerations and channels 9–17 are supplied as input accelerations. While MODE-ID can estimate the entries in the pseudostatic matrix, including 72 free parameters in excess of the other modal parameters gives MODE-ID too many parameters to fit. An option is also available in MODE-ID that allows for the pseudostatic matrix to be input and held fixed throughout the optimization routine. The matrix was calculated using the finite element model that will be described in Chapter 7. For this purpose, the nine input channels were assumed to entirely characterize the input to the dam, meaning that all of the degrees of freedom in the finite element model along the dam-foundation interface were displaced by amounts based solely on unit displacements at each of the nine input channels. The pseudostatic matrix obtained is

$$\begin{bmatrix}
-0.024 & 0.198 & -0.424 & 0.917 & 0.062 & 0.392 & 0.047 & -0.260 & -0.309 \\
0.032 & 0.598 & -0.182 & 0.598 & -0.251 & 0.856 & 0.368 & -0.348 & -0.733 \\
-0.045 & 0.626 & 0.020 & 0.021 & 0.252 & -0.044 & 0.023 & 0.122 & 0.024 \\
-0.016 & 0.141 & 0.361 & 0.088 & -0.374 & 0.440 & -0.013 & 0.233 & 0.197 \\
-0.066 & 0.408 & 0.405 & 0.069 & -0.359 & 0.512 & 0.928 & -0.048 & -0.551 \\
0.167 & 0.081 & -0.237 & 0.725 & 0.024 & 0.072 & 0.048 & -0.105 & -0.177 \\
0.215 & 0.278 & -0.106 & 0.489 & -0.115 & 0.532 & 0.294 & -0.162 & -0.485 \\
0.160 & 0.175 & 0.254 & 0.071 & -0.158 & 0.320 & 0.699 & -0.017 & -0.208
\end{bmatrix}$$

The eight rows correspond to output channels 1–8 and the nine columns correspond to input channels 9–17, for example, the entry in row 2, column 4 is the displacement at channel 2 due to a unit displacement at channel 12 with channels 9–11 and 13–17 held fixed.

Theoretically, MODE-ID estimates the vibrational properties of a system with motion prevented at the locations of the input degrees of freedom. In the case where the input degrees of freedom may not completely characterize the input, it is not clear how much foundation-structure interaction is included in the identified system. For Pacoima Dam, the input is only sampled at three locations, so it is reasonable to assume that there is still a significant contribution from the foundation of the dam in the identified properties. However, the Pacoima Dam system in which all degrees of freedom along the dam-foundation interface are free to move would be less stiff to some degree than the system that is identified by MODE-ID. The significance of this is investigated in Chapter 9 using the output from the finite element model subjected to the January 2001 earthquake records.

4.2 January 13, 2001 Earthquake

The January 13, 2001 earthquake was small, so the response is likely to have been linear. The modal parameters identified from the January 2001 records can be used to calibrate the finite element model employed in Chapters 7–10. The primary purpose of this model is to be used for dynamic earthquake analyses. The finite element model is calibrated in its linear state and then nonlinearity can be captured by the dam model as described in Chapter 7. Accelerations from channels 9–17 are input to the MODE-ID model and accelerations from channels 1–8 are used as the output that the MODE-ID model attempts to match. The abutment channels (12–17) are not included in the output of the system, because the topographic effects on the abutments will be included in the finite element model by nonuniform ground motion input along the abutments of the dam.

4.2.1 Full Length Records

The Pacoima Dam system was identified using 20 seconds of the January 2001 accelerations as input and output. The 20-second duration starts at 3 seconds into the record since the ground motion does not become significant until after 4 seconds due to a buffer stored before the instruments were triggered. The pseudostatic matrix given in Section 4.1 is input to MODE-ID and held fixed. A 2-mode model is identified with natural frequencies of 4.73 Hz and 5.06 Hz with damping of 6.2% and 6.6% of critical, respectively. The 4.73 Hz mode has a symmetric shape and the 5.06 Hz mode has a mostly antisymmetric shape. The shapes estimated by MODE-ID for only the horizontal crest level stations (channels 1, 2, 4 and 5) are shown in plan view in Figure 4.1 with the undeformed crest shown for reference. The thrust block is not included. The modes are not perfectly symmetric and antisymmetric since the dam itself is not a symmetric structure, but the modes will be referred to as symmetric and antisymmetric.

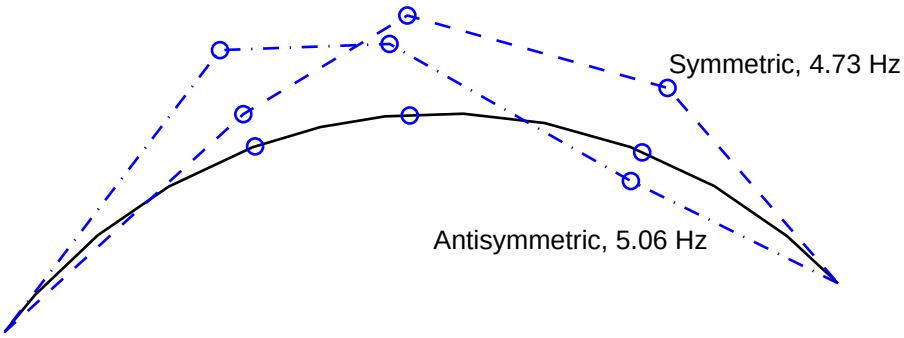

Figure 4.1: Symmetric and antisymmetric mode shapes estimated by MODE-ID (The open circles are the locations of the crest level stations.)

The output computed by MODE-ID for the 2-mode model to best fit the records is compared to the recorded accelerations over a 6-second interval in Figure 4.2. The fit is good, but if a third mode is included the fit is even better. Allowing MODE-ID to have more parameters leads to a better fit, but the question is whether the third mode is realistic. With a 3-mode model, the first two natural frequencies identified are 4.83 Hz and 5.06 Hz with damping of 6.2% and 7.3%, respectively. These modes are consistent with the 2-mode model and the shapes for the symmetric (4.83 Hz)

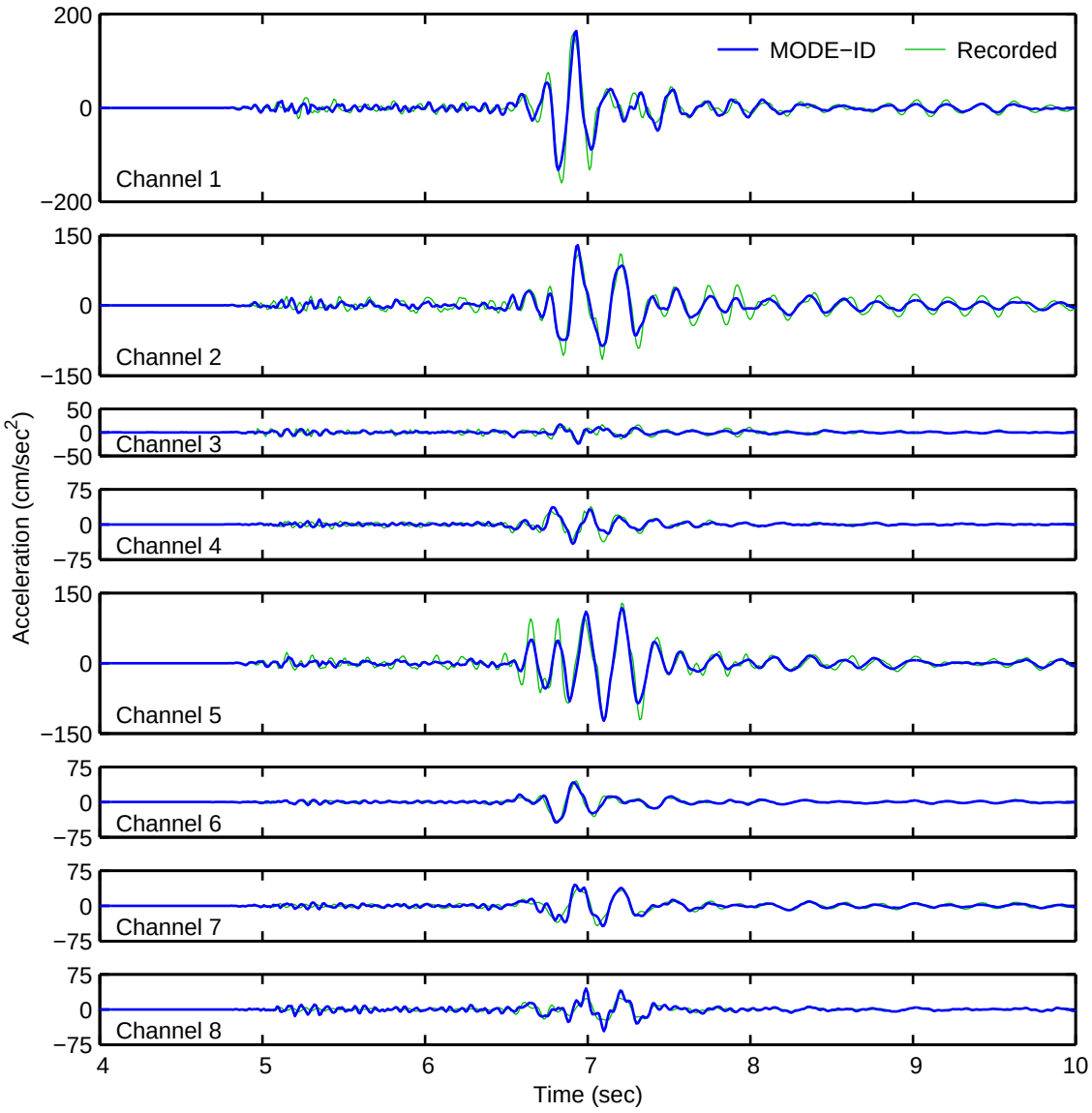

Figure 4.2: Best fit output accelerations (channels 1–8) computed by MODE-ID for the 2-mode model compared to the recorded accelerations

and antisymmetric (5.06 Hz) modes are similar to those shown in Figure 4.1. The third identified mode has a natural frequency of 6.75 Hz with 21.9% damping and it appears to be a higher order cantilever mode. The large damping for this mode indicates that it may not be realistic or at least not significant in the response of the dam. Therefore, only the first two modes will be used in Chapter 7 to calibrate the finite element model.

Results from forced vibration tests previously performed on Pacoima Dam can

be compared to the results of the MODE-ID system identification study. Tests were performed in April 1980 where the first symmetric and first antisymmetric modes were found at 5.45 Hz and 5.60 Hz, respectively (ANCO Engineers, 1982). These frequencies are significantly higher than those estimated by MODE-ID. The water level was 23 meters below the crest during the 1980 tests, which is 18 meters above the level during the January 2001 earthquake. If the reservoir had been at the lower 2001 level during the 1980 tests, then the frequencies determined by the forced vibration experiment would have been even higher. Modal damping estimated from the 1980 test results by the half-power method was 7.3% (symmetric) and 9.8% (antisymmetric) which also exceeds the MODE-ID estimates, but the data from the tests were of a quality that made it difficult to determine damping accurately (Hall, 1988).

Another forced vibration experiment was also done on Pacoima Dam in July 1971, shortly after the 1971 San Fernando earthquake (Reimer, 1973). The results from these tests indicate a symmetric mode at 5.10 Hz and an antisymmetric mode at 5.56 Hz. No information on damping was reported. The reservoir was empty during these tests. The lower frequencies compared to the 1980 results are likely a result of damage to the left abutment that had not yet been repaired. Thus, the system had been repaired and stiffened before the 1980 tests. The Northridge earthquake did occur between the 1980 tests and the January 2001 earthquake, and the left abutment rock was again damaged. Assuming that the response of Pacoima Dam to the January 2001 earthquake is linear, to explain the lower frequencies estimated by MODE-ID the damage would have needed to be more severe than in 1971 and left unrepaired. However, repairs were, in fact, made after the Northridge earthquake. To investigate this issue further, additional forced vibration tests were performed on Pacoima Dam and are discussed in Chapter 5.

4.2.2 Windowed Records

Short windows of the accelerations were used as input and output to MODE-ID in order to determine whether the modal properties of Pacoima Dam varied during the

duration of the January 2001 earthquake. Overlapping 4-second windows ranging between 4 seconds and 22 seconds into the record were used. The windows were overlapped so that there was a window centered every second from 6 seconds to 20 seconds into the record. A 2-mode model was identified for each window with the same pseudostatic matrix given in Section 4.1. The modes are generally estimated with symmetric and antisymmetric shapes. The variation in the natural frequencies for the two modes is shown in Figure 4.3, where the frequency is plotted for the time at the center of the window.

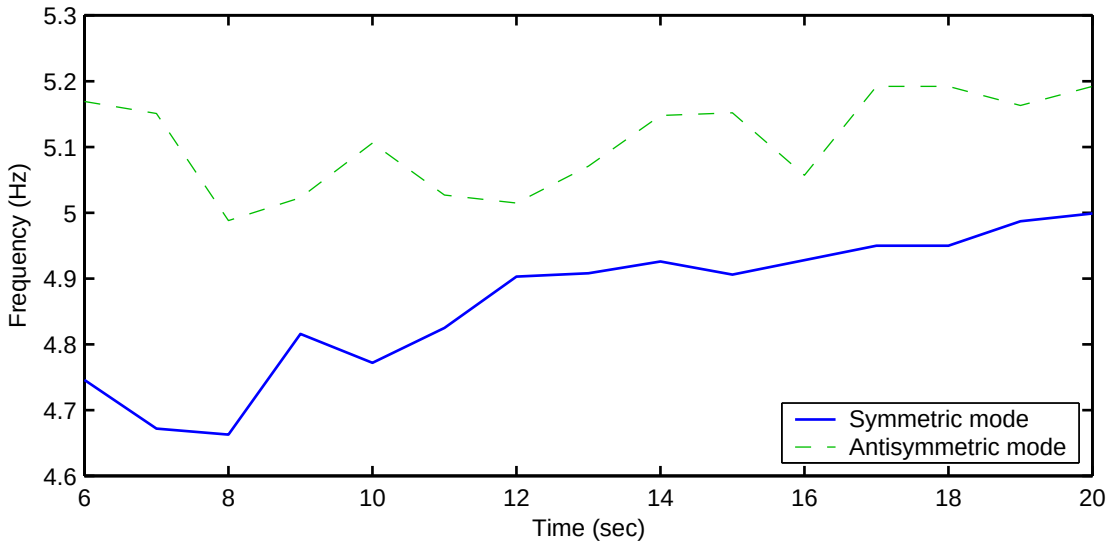

Figure 4.3: Natural frequency variation in time of the symmetric and antisymmetric modes of Pacoima Dam estimated by MODE-ID using 4-second windows of the January 13, 2001 earthquake records

The symmetric mode frequency increases noticeably as the amplitude of the motion decreases at the end of the records. The antisymmetric mode frequency also increases slightly as the record progresses. This may indicate that the response of Pacoima Dam to the January 13, 2001 earthquake was actually somewhat nonlinear, since the stiffness appears to increase as the motion gets smaller. The total variation in the natural frequencies may not be thought to be that large when the error associated with the short window duration is considered, but the increasing trend is probably real. Notice that the natural frequencies at the end of the records are still significantly smaller than the values obtained from forced vibration. There is also a

general decreasing trend in the damping as the record progresses which is consistent with the observed nonlinearity in natural frequency. The damping starts as high as about 8% and falls to as low as about 1% at the end of the records. Despite the variation in modal properties caused by an unknown source of nonlinearity, the finite element model will be calibrated using the modal parameters estimated by MODE-ID using the entire 20-second duration since the variation is not very large and the accuracy with the short windows is not expected to be as good.

4.2.3 Testing MODE-ID

MODE-ID has previously been used to identify the modal properties of building and bridge systems, but not dam systems. Unlike a building, a dam is subjected to nonuniform input ground motion; and unlike a bridge, which can be subjected to nonuniform motion, a dam is in continuous contact with the foundation. In order to assess the ability of MODE-ID to identify a dam system, the modal parameters of a preliminary linear finite element model were identified using the output time histories from the model subjected to the January 2001 earthquake input. For the test, the foundation of the model was rigid, so there would be no problem interpreting how much foundation-structure interaction was included in the identified system.

The finite element model was designed to have the two fundamental modes at 5.06 Hz (antisymmetric) and 5.12 Hz (symmetric), with Rayleigh damping chosen to give approximately 6% damping for both modes. The recorded accelerations at channels 9–17 were supplied as input to the finite element model, and 9 seconds of the accelerations at locations consistent with channels 1–8 and channels 9–17 were computed by the finite element model and supplied to MODE-ID as output and input, respectively. Since the foundation is rigid, the computed accelerations at channels 9–17 supplied to MODE-ID are the same as the recorded accelerations supplied as input to the finite element model. The pseudostatic matrix was slightly different than the one given in Section 4.1 since the model is different. MODE-ID identified a system with the first two modes at 5.14 Hz (symmetric) and 5.19 Hz (antisymmetric) with

6.8% and 6.6% damping, respectively. The order of the modes is switched, but the MODE-ID estimation is good considering the extreme closeness of the modes. These two modes were actually identified as part of a 3-mode model, since inclusion of a third mode at higher frequency was required to fit the simulated output. This was due to high frequency content in the input motion on the left abutment that was transmitted to the dam body in the finite element model. This content does not show up in the actual records on the dam, and so appears to be a localized effect not captured by the finite element model.

The ability of MODE-ID was also tested with uniform input ground motion supplied to the finite element model. The three components of acceleration chosen were channels 9–11 from the January 2001 earthquake. Only these three records were supplied as input to MODE-ID and the output corresponding to channels 1–8 were again supplied from the finite element model. With uniform input ground motion, MODE-ID identifies a model with modes at 5.06 Hz (antisymmetric) and 5.12 Hz (symmetric) with 6.2% and 5.7% damping, respectively. Only a 2-mode model was required to find these modes. The modal parameters are more accurately estimated with uniform motion, but the estimates are not significantly worse with nonuniform motion. Therefore, it was concluded that MODE-ID has the capability to obtain reasonably good estimates of the modal parameters of a dam system with a rigid foundation and nonuniform input ground motion.

4.3 Northridge Earthquake

System identification of Pacoima Dam can also be performed with the Northridge earthquake acceleration records using MODE-ID. However, the dam response to the earthquake was likely nonlinear, so identification was done with short windows in time of the records. The behavior of the structure is approximated as linear over the time window and the change in modal properties can be tracked. Windowing is also necessary since several of the records are missing portions during the middle of the earthquake (see Figure 3.12). The pseudostatic matrix given in Section 4.1 needs to

be modified since channels 7 and 14 did not record. The seventh row and the sixth column are removed since those channels cannot be used in the identification.

Using a window over the first 3.2 seconds of the earthquake, before the arrival of the shear wave pulse, a 2-mode model can be identified with natural frequencies of 4.8 Hz and 5.2 Hz with damping of 10% and 8%, respectively. The modes are not distinctly symmetric or antisymmetric, but the 4.8 Hz mode can be interpreted as symmetric and the 5.2 Hz mode appears to have an antisymmetric character. These two natural frequencies are close to the frequencies determined for the modes found with the January 2001 earthquake accelerations, but the damping determined with the Northridge records is higher. The variance in damping is probably due to inaccuracy in the estimates, especially because the 3.2-second window does not provide much information to match. However, the consistent natural frequencies indicate that the system had vibrational properties before the shear wave arrival during the Northridge earthquake that are similar to those during the January 2001 earthquake.

After the arrival of the shear wave, three 2-second non-overlapping windows between 4.8 seconds and 10.8 seconds were used to identify the system. Due to the necessary short duration of the windows, the nonlinear nature of the response and the fact that the modes are closely spaced, the identified modal parameters are probably not very accurate, in particular the damping and mode shape values. However, the measure-of-fit in MODE-ID is most sensitive to natural frequency (Beck and Jennings, 1980), so the frequencies are the most trusted quantities. The natural frequencies tend to have decreased from the earlier values to about 4 Hz on average. These results seem to indicate that the system is softer after the arrival of the shear wave pulse than it was before, which is consistent with the expectation of nonlinear behavior during the strong shaking and the observation of damage. Bell and Davidson (1996) had similar findings from the Northridge records: before the shear wave arrival, modes described as symmetric and antisymmetric were found with natural frequencies of 4.8 Hz and 5.4 Hz, respectively; and after the shear wave, the symmetric and antisymmetric modes decreased to 3.8 Hz and 4.7 Hz; with modal damping typically found in the 6% to 9% range.

Chapter 5

Forced Vibration Experiment

A forced vibration field experiment was performed at Pacoima Dam to investigate uncertainties in the modal parameters as determined by MODE-ID. These uncertainties arose from inconsistency with previous forced vibration results. The goals of the experiment were simply to determine the natural frequencies and damping of the first two modes and distinguish between symmetric and antisymmetric shapes, as well as identifying the natural frequencies of higher modes. Additionally, the relative amplitude of motion on the abutments compared to the crest was recorded.

5.1 Experimental Setup

The testing was carried out over one week in July/August 2002 (two days to setup, two days to acquire data, and one day to clean up). During the testing, the water level was about 36 meters below the crest of the dam, 5 meters higher than during the 2001 earthquake. An eccentric mass shaker that exerts a unidirectional, sinusoidal force that is proportional to excitation frequency squared was used to generate the input (Figure 5.1(a)). The shaker was placed near the center of the crest on the upstream side. Frequency sweeps were conducted from 2.5 Hz to 11.0 Hz for shaking in both the stream and cross-stream directions. The shaker force ranged from 2.72 kN (0.61 kips) at 2.5 Hz to 52.75 kN (11.86 kips) at 11.0 Hz.

Kinemetrics SS-1 Ranger seismometers were used to measure the motion at five locations in two perpendicular, horizontal directions. Two Rangers are shown in

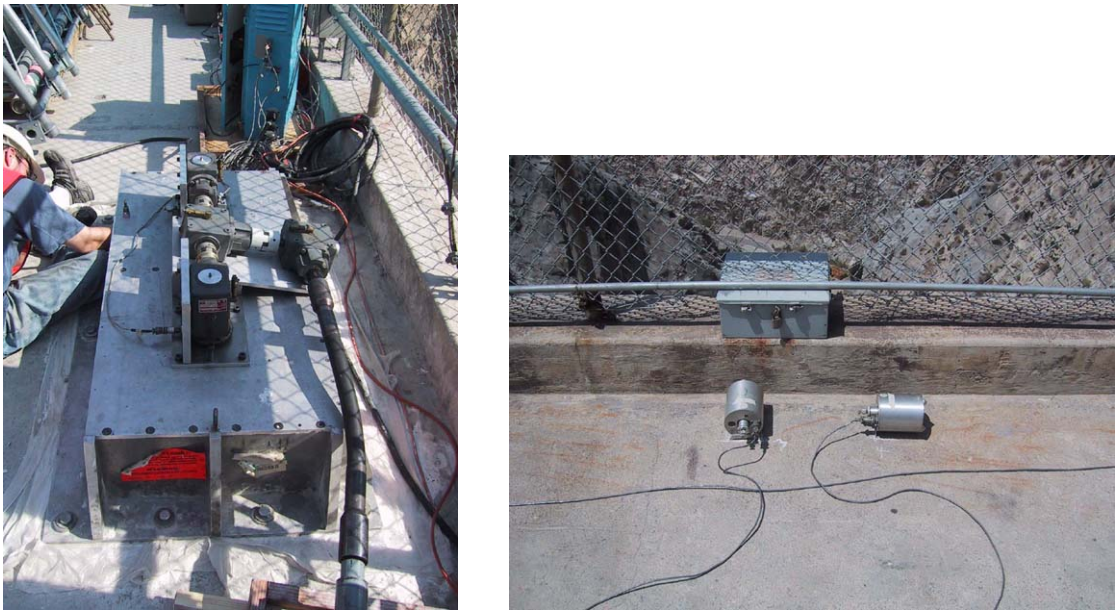

(a) Eccentric mass shaker (b) Two Kinemetrics SS-1 Ranger seismometers

Figure 5.1: Experimental equipment

Figure 5.1(b). The Rangers have a response proportional to velocity at frequencies above their natural frequency, which is approximately 1 Hz. The Rangers were placed near the existing accelerometers at the three crest locations on the downstream side (center C, right third R, left quarter L), oriented radially and tangentially, and at the two locations along the right and left abutments about 24 meters below the crest, oriented east-west and north-south. The channels are numbered 1fv through 10fv as shown in Figure 5.2. Notice that the numbering is different than for the accelerometer array. Location C was situated about 1.2 meters north of the existing accelerometers near the center of the crest and the orientations of channels 1fv and 2fv at location C were estimated to be N86E and S04E, respectively, which are essentially stream and cross-stream. (N86E is 86° to the east away from the north and S04E is 4° to the east away from the south, so N86E is essentially to the east and S04E is essentially to the south.) Channels 7fv and 8fv were actually located on a steel platform adjacent to the accelerometers because no suitable rock location was available.

The shaker was placed about 2.6 meters northeast of Ranger location C. Direc-

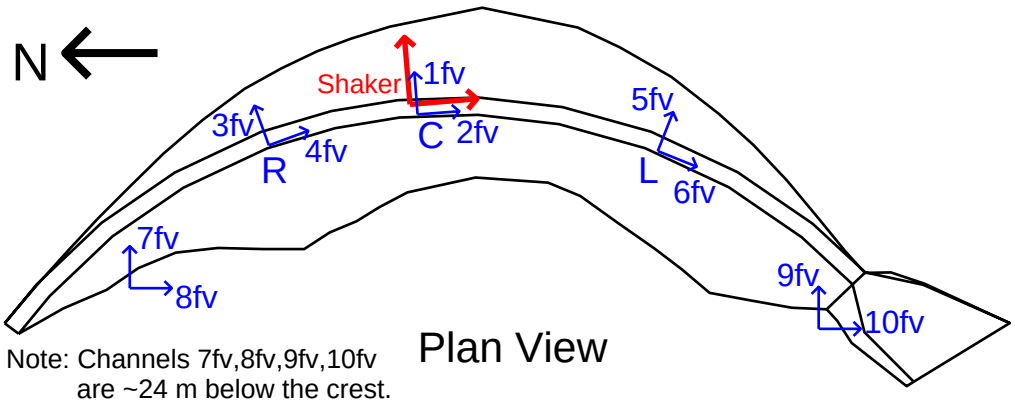

Figure 5.2: Locations of the Rangers and the shaker with orientations

tions of shaking were radial and tangential at this point, about N85E and S05E, respectively, which are also essentially stream and cross-stream (Figure 5.2). A complete set of data from the forced vibration testing, amplitude and phase plots from each Ranger for both directions of shaking over the entire range of the frequency sweeps, is presented in Appendix A. Much larger responses are produced when the dam is shaken in the N85E direction (stream) as compared to the S05E direction (cross-stream). However, even the highest radial velocities recorded on the crest for the N85E shaking are less than 1% as large as radial velocities recorded on the crest during the January 2001 earthquake.

5.2 Modal Isolation

5.2.1 Rotation of Shaking and Recording Directions

For a perfectly symmetric dam with the shaker at the centerline, shaking in the stream direction excites only symmetric modes and shaking in the cross-stream direction excites only antisymmetric modes. This is because the motion of the dam centerline is in the stream direction for a symmetric mode and cross-stream for an antisymmetric mode. At Pacoima Dam, due to the lack of sufficient symmetry, the directions of motion at location C for the first symmetric mode and the first antisymmetric mode were both primarily in the stream direction. As a result, there is

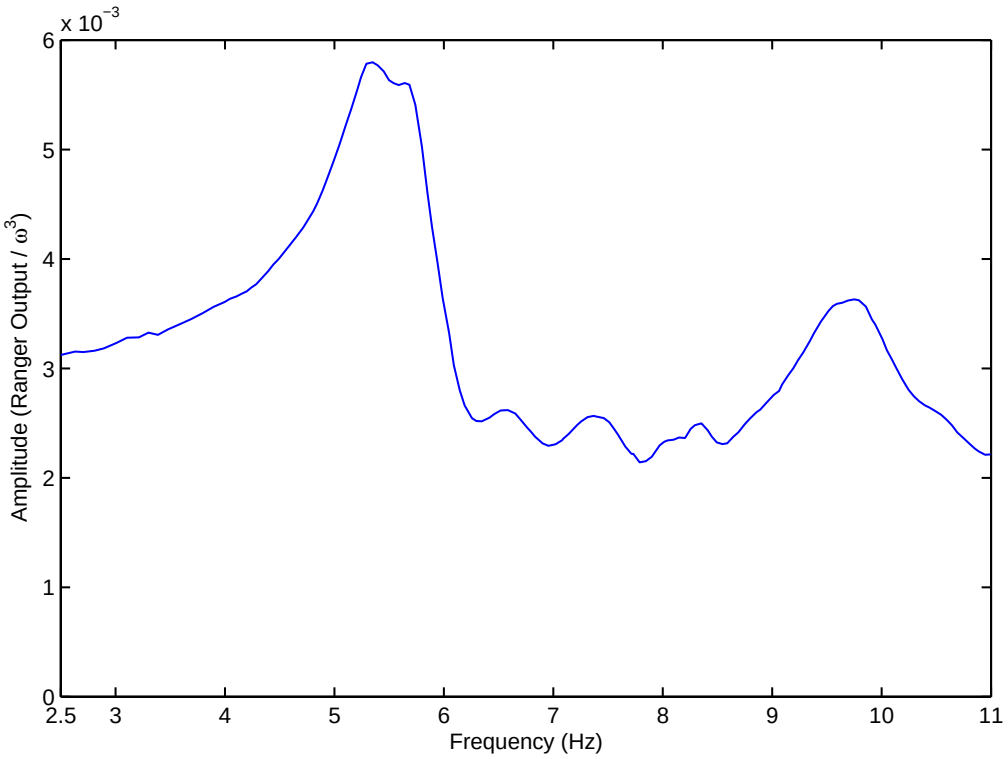

Figure 5.3: Frequency response curve for channel 1fv from the N85E shaking test

considerable interference between the two modes for both directions of shaking, and this makes the determination of natural frequencies and damping difficult. Figure 5.3 shows the interfering resonances of the symmetric and antisymmetric modes between 5 Hz and 6 Hz in the amplitude of the channel 1fv response from the N85E shake. The quantity plotted in the figure is the amplitude of the Ranger output divided by frequency cubed and is proportional to the displacement of the dam per unit shaker force. All frequency response curves in this chapter and in Appendix A have been plotted similarly.

One technique to eliminate interference between two modes is to align the direction of shaking perpendicular to the motion of one of the modes, which should eliminate the response of that mode, thus isolating the other one (Duron and Hall, 1986). For the Pacoima Dam data, this was done mathematically by combining the results of the two shaking directions vectorially. The symmetric mode was eliminated in this way. However, the procedure was less successful in eliminating the antisymmetric

mode, so it was modified by including a perpendicular force component with its phase shifted by 90°. This method should be capable of eliminating a mode with motion that is elliptical at a point, which could be an effect of non-classical modes. As a further enhancement, the pair of Ranger data channels at locations C, R and L were also combined vectorially in order to maximize the peak of the mode being isolated. The resultant Ranger output with amplitude A and phase θ measured in a direction rotated clockwise from radial by an angle α with shaking in a direction rotated clockwise from N85E (stream) by an angle β and an elliptical shape with the minor axis a factor of C as large as the major axis is given by

$$\begin{aligned} A\sin(\omega t+\theta) &= [R_S\sin(\omega t+\phi_{RS})\cos\alpha + T_S\sin(\omega t+\phi_{TS})\sin\alpha]\cos\beta \\ &+ [R_X\sin(\omega t+\phi_{RX})\cos\alpha + T_X\sin(\omega t+\phi_{TX})\sin\alpha]\sin\beta \\ &+ C\,[R_S\sin(\omega t+\phi_{RS}+\gamma)\cos\alpha + T_S\sin(\omega t+\phi_{TS}+\gamma)\sin\alpha]\cos(\beta+\frac{\pi}{2}) \\ &+ C\,[R_X\sin(\omega t+\phi_{RX}+\gamma)\cos\alpha + T_X\sin(\omega t+\phi_{TX}+\gamma)\sin\alpha]\sin(\beta+\frac{\pi}{2}) \end{aligned} \tag{5.1}$$

where ω is the excitation frequency, R_S and T_S are the measured radial and tangential amplitudes for the N85E (stream) shaking, R_X and T_X are the measured radial and tangential amplitudes for the S05E (cross-stream) shaking, ϕ_{RS} and ϕ_{TS} are the measured radial and tangential phases for the stream shaking, ϕ_{RX} and ϕ_{TX} are the measured radial and tangential phases for the cross-stream shaking, C is between 0 and 1 ($C = 0$ gives a unidirectional force) and γ gives the 90° phase shift of the perpendicular force component in order to get an elliptical force ($\gamma = \frac{\pi}{2}$ or $\gamma = -\frac{\pi}{2}$ for counterclockwise or clockwise rotation, respectively).

It was found that unidirectional shaking along S01E eliminated the symmetric mode in the vicinity of the resonating antisymmetric mode. To eliminate the antisymmetric mode, best results were achieved with a shaking force at S21E combined with a 90° phase shifted and perpendicular force component 15% as large with counterclockwise rotation, although even this modified procedure does not appear to completely eliminate the antisymmetric mode from the vicinity of the symmetric mode resonance.

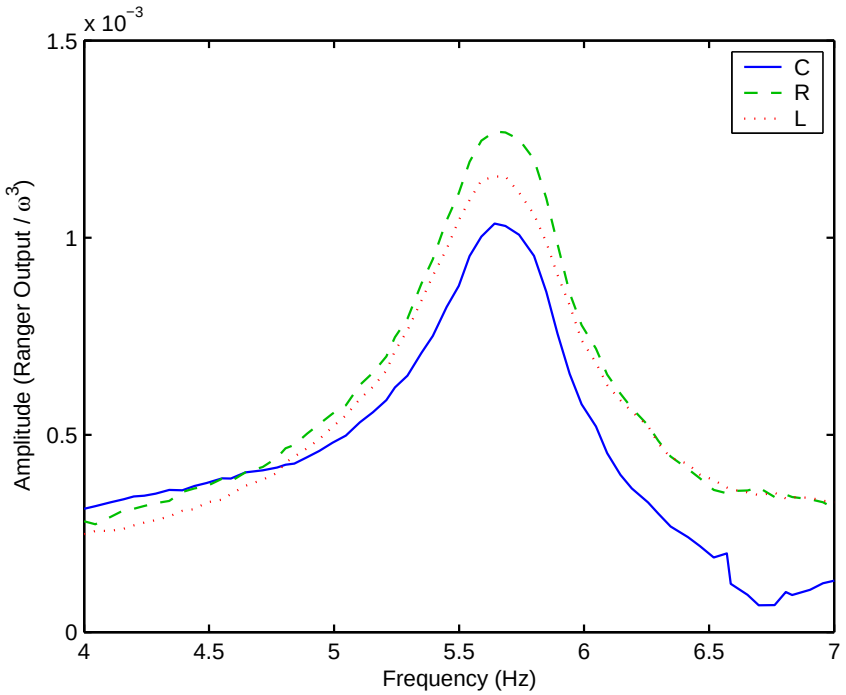

Figure 5.4: Frequency response curves on the crest at locations C, R and L for the antisymmetric mode

Results of the modal isolation attempt are shown in Figure 5.4 for the antisymmetric mode and Figure 5.5 for the symmetric mode. Motions at locations C, R and L are included in each figure. Because the shaker force has been rotated significantly from N85E, the response amplitudes are reduced 70% or more from those shown in Figure 5.3 for the N85E shake. From Figure 5.4, the resonant frequency of the antisymmetric mode is found to be around 5.65 Hz to 5.70 Hz with damping between 4.5% and 5.5% of critical, which was determined by the half-power method. As shown in Figure 5.5, the resonant frequency of the symmetric mode is between 5.30 Hz and 5.45 Hz depending on the location. The variation in natural frequency is probably a result of the antisymmetric mode not being completely eliminated. The damping for the symmetric mode estimated by the half-power method appears to be affected by the remaining presence of the antisymmetric mode, particularly at location C. The damping estimated from locations R and L is around 5.5% to 7.0% of critical.

The determined directions of motion and the phase shifts relative to location C at locations C, R and L for the first symmetric and first antisymmetric modes are

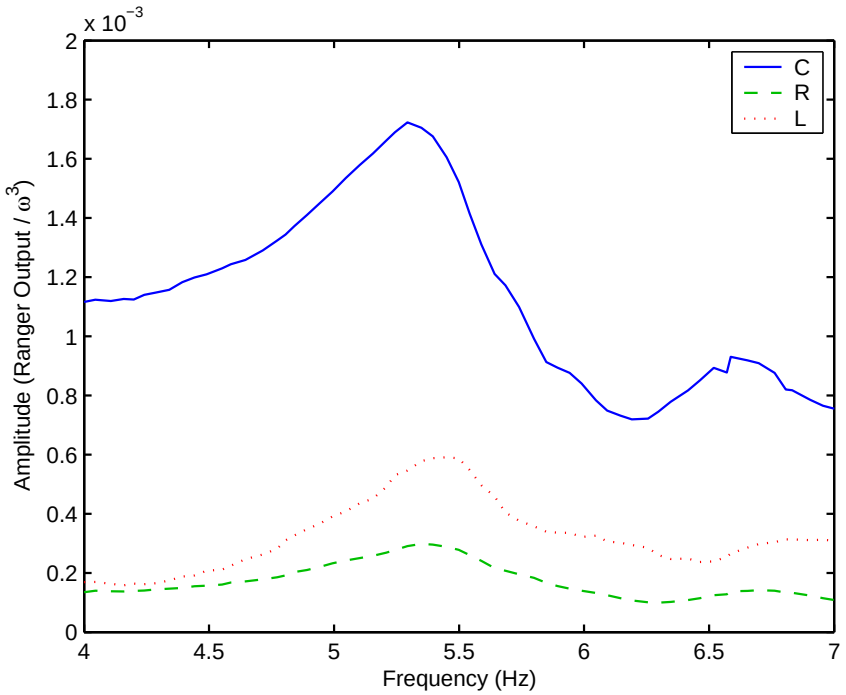

Figure 5.5: Frequency response curves on the crest at locations C, R and L for the symmetric mode

shown in Table 5.1. A negative relative phase indicates that the location lags behind the reference. It should be noted that the phase shifts for locations R and L are not particularly close to the values of 0° or 180° expected for classical modes. The measured mode shapes are plotted in Figure 5.6 using the amplitudes determined from Figures 5.4 and 5.5 and the directions given in Table 5.1. While there are some noticeable differences, the shapes have a basically similar character to those estimated by MODE-ID (Figure 4.1). At location C, the S87E direction of motion for the symmetric mode is 4° away from being perpendicular to the S01E shaking force orientation used to eliminate the symmetric mode; and the N63E direction of motion for the antisymmetric mode is 6° away from being perpendicular to the S21E shaking force orientation used to eliminate the antisymmetric mode. These differences could represent small errors in alignment of the shaker and Rangers, or be due to some modal interference still present, or they could result from some variation in motion of the dam that occurs over the 2.6 meter distance separating the shaker and location C.

Location	Symmetric Mode		Antisymmetric Mode	
	Direction	Phase	Direction	Phase
C	S87E	0.0°	N63E	0.0°
R	S29E	-21.08°	N64E	-23.47°
L	S87E	-23.85°	S59E	144.35°

Table 5.1: Direction of motion and relative phase for locations on the crest for the symmetric and antisymmetric modes

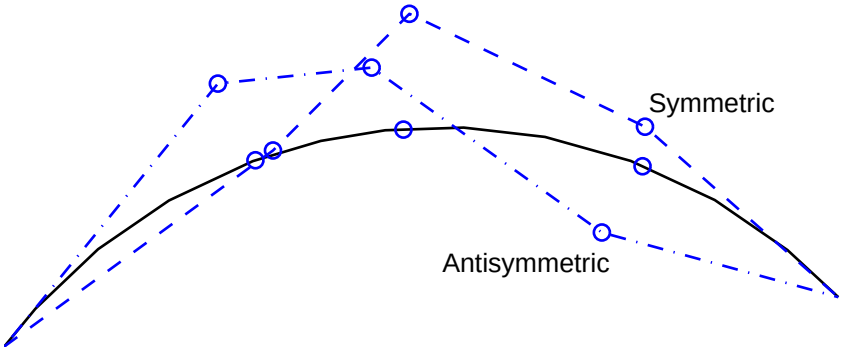

Figure 5.6: Symmetric and antisymmetric mode shapes determined from forced vibration testing (The open circles are the locations of the crest level Rangers.)

5.2.2 Check for Reciprocity

If the shaker and location C are close enough together so that the motion of the dam is essentially the same at both locations, then, by the reciprocal theorem, the motion at location C in some direction D1 due to a shaker force in the perpendicular direction D2 should be the same as the motion at location C in direction D2 due to the same shaker force applied in direction D1. These two responses at location C, computed with D1 at S05E and D2 at N85E, the original shaking directions, are shown in Figure 5.7. There is a small difference between the two responses, perhaps implying that the motion of the dam is not the same at the shaker and location C for the frequency range examined. However, since the difference is not large when compared to the level of motion for the N85E shake (see Figure 5.3 and Appendix A), the slight discrepancies in the directions to isolate the modes mentioned in the previous section could be due to small errors in alignment or a small amount of modal interference.

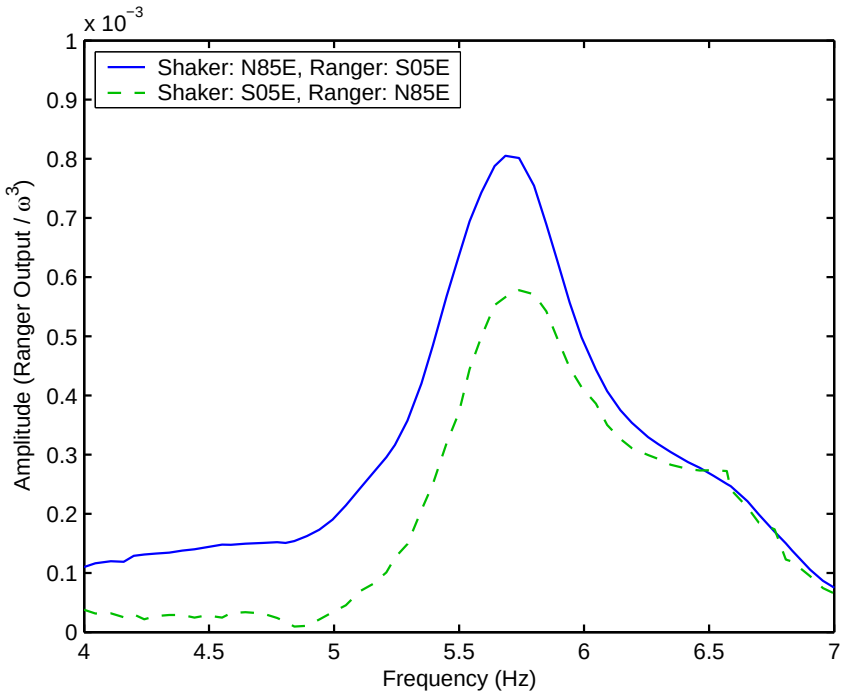

Figure 5.7: Frequency response curves at location C in the S05E and N85E directions due to shaking forces in the N85E and S05E directions, respectively

5.2.3 Summation of Channel 3fv and Channel 5fv Recordings

In order to obtain more accurate estimates for the modal parameters another approach was used to isolate the symmetric and antisymmetric modes, based on the premise that for channels 3fv and 5fv (radial at locations R and L) the symmetric mode should be in-phase and the antisymmetric mode should be out-of-phase. Using the N85E shake, varying amounts of the two radial responses were added until the antisymmetric mode disappeared as much as possible, and varying amounts of the two responses were subtracted until the symmetric mode disappeared as much as possible. In order to isolate the symmetric mode, the channel 5fv recordings were multiplied by 1.5 and added to the channel 3fv recordings; and to isolate the antisymmetric mode, the channel 5fv recordings were multiplied by 0.1 and subtracted from the channel 3fv recordings. The relative amounts of response combined to isolate the modes are fairly consistent with the mode shapes shown in Figure 5.6. A factor closer to 1.1 instead of 1.5 would have made more sense based on the antisymmetric mode shape, but the

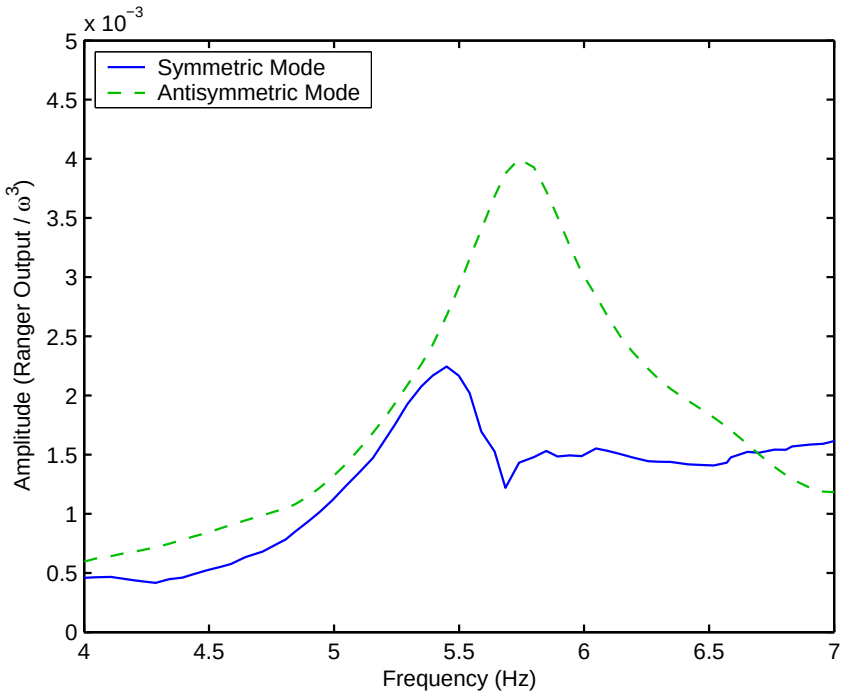

Figure 5.8: Frequency response curves computed by combining channels 3fv and 5fv for N85E shaking to isolate the symmetric and antisymmetric modes

discrepancy is not very significant considering the possible sources of error. Results are presented in Figure 5.8 from which values of natural frequency and damping were determined as 5.45 Hz and 4.0% for the symmetric mode and 5.75 Hz and 5.0% for the antisymmetric mode. Considering the results from both attempts to isolate the modes, estimates for the modal parameters are given in Table 5.2.

Mode	Natural Frequency	Damping
Symmetric	5.35 Hz $< f_n <$ 5.45 Hz	$4.0\% < \zeta < 7.0\%$
Antisymmetric	5.65 Hz $< f_n <$ 5.75 Hz	$4.5\% < \zeta < 5.5\%$

Table 5.2: Estimated modal parameters

5.3 Higher Modes and Abutment Recordings

The most pronounced higher mode resonance appears in Figure 5.3 at about 9.8 Hz. There are probably other lower modes as indicated by the several smaller peaks at intermediate frequencies, although the lowest of the peaks at about 6.5 Hz seems too

close to the first symmetric and antisymmetric resonances to be a mode of the dam. No further investigation of higher modes was performed in this study.

Motions at the abutment locations were much smaller than those on the dam, as would be expected. The largest abutment motions occur for the N85E shake near the resonant frequencies for the first symmetric and antisymmetric modes and sometimes at higher frequencies (see Appendix A). The peak amplitudes are about 5% of the maximum responses shown in Figure 5.3. When the dam is isolated in the symmetric mode, the amplitude of motion at the right and left abutment locations is 4.3% and 5.6%, respectively, as large as the motion at location C; and when the dam is isolated in the antisymmetric mode, the right and left abutment locations move 7.4% and 8.9%, respectively, as much as location C. The motion of the abutments for the symmetric mode is mostly in the north-south direction, and the abutments move mostly east-west for the antisymmetric mode.

Chapter 6

Variation of Modal Properties

Several attempts have been made to identify the modal properties of Pacoima Dam since the San Fernando earthquake in 1971. Forced vibration tests were performed in July 1971 (Reimer, 1973), April 1980 (ANCO Engineers, 1982) and July/August 2002 by the author; and earthquake recordings from the 1994 Northridge earthquake and the earthquake on January 13, 2001, were employed in a system identification study using the computer program MODE-ID. In all cases, two fundamental modes were identified with symmetric and antisymmetric shapes, and the symmetric mode has the lower frequency than the antisymmetric mode. However, the natural frequencies and damping of the identified modes vary. The response of Pacoima Dam to the Northridge earthquake was significantly nonlinear since damage was observed after the event (Morrison Knudsen, 1994; EERI, 1995). Therefore, the stiffness and damping of the dam system should be different for the Northridge earthquake, but the forced vibration tests and the January 2001 earthquake are all assumed to have induced a linear response from Pacoima Dam. The variations in the modal parameters for the excitations that are assumed to induce linear vibrations are shown in Table 6.1, with the water level for each event included. The reservoir level is an important factor since the added mass of the water can affect the properties of the dam system.

The variation in the modal damping is not very significant considering the difficulty associated with estimating the damping for closely spaced modes and the fact that the quality of the 1980 data was not good for estimating damping, but the frequency variations do indicate a significant variation in the stiffness of the dam sys-

Excitation	Date	Water Level Below Crest	Symmetric Mode Frequency (Damping)	Antisymmetric Mode Frequency (Damping)
Forced Vibration	July 1971	Empty	5.10 Hz (-)	5.56 Hz (-)
Forced Vibration	April 1980	23 meters	5.45 Hz (7.3%)	5.60 Hz (9.8%)
Earthquake	Jan 2001	41 meters	4.73 Hz–4.83 Hz (6.2%)	5.06 Hz (6.6%–7.3%)
Forced Vibration	Jul/Aug 2002	36 meters	5.35 Hz–5.45 Hz (4.0%–7.0%)	5.65 Hz–5.75 Hz (4.5%–5.5%)

Table 6.1: Natural frequencies and damping of the first symmetric and antisymmetric modes of Pacoima Dam identified by various system identification studies

tem. The difference in stiffness between the 1971 tests and the 1980 tests would be even larger if the reservoir had contained water in 1971 since the added mass would decrease the frequencies even more, but the stiffness increase between the 1971 tests and the 1980 tests can already be satisfactorily explained. Damage occurred at the left abutment during the San Fernando earthquake and it was repaired after the 1971 tests but before 1980. It is reasonable that stiffening the left abutment would increase the symmetric mode frequency more than the antisymmetric mode frequency since the symmetric mode has a thrusting component that should be more affected by the stiffer left abutment than the motion of the antisymmetric mode.

The natural frequencies from the 1980 tests and the 2002 tests are comparable, but notice that the reservoir was 13 meters deeper in 1980. So that might explain why the antisymmetric mode frequency was a little lower in 1980. However, the fact that the symmetric mode frequency was not lower when the reservoir was deeper in 1980 might indicate that the dam system, without considering the reservoir contribution, had lost some stiffness by 2002. This likely happened during the Northridge earthquake when the left abutment was again damaged. The repairs after the Northridge earthquake may not have completely returned the dam to its pre-earthquake stiffness.

The natural frequencies determined from the 2002 tests are significantly higher than the frequencies identified from the 2001 earthquake records by MODE-ID. However, there was no damage observed after the January 2001 earthquake and no repairs were made that would have stiffened the system. The reservoir was only 5 meters

deeper in 2002 than it was in 2001, which should not significantly alter the system. The water level was lower during the 2001 earthquake, anyway, and a higher water level would be needed to explain lower frequencies. The response of the dam to the forced vibration is about two orders of magnitude smaller than to the 2001 earthquake. Therefore, the response to the forced vibration tests is probably linear while the 2001 earthquake must have produced some source of nonlinearity in the response of Pacoima Dam that caused the stiffness to be reduced, but did not lead to any permanent damage. This is contrary to the initial assumption that the response of Pacoima Dam to the January 2001 earthquake was linear. The stiffness drop associated with the decrease in natural frequencies of both modes is about 21.5%. This decrease is quite large even though the 2001 earthquake only induced small amplitude motions of Pacoima Dam (peak acceleration, velocity and displacement on the crest of only 0.16g, 6.2 cm/sec and 0.22 cm).

One factor considered as a possible cause of the natural frequency decrease during the 2001 earthquake was temperature. While the 2001 earthquake occurred during the winter, the forced vibration experiments were done during the warmer spring and summer months. The colder temperature may have caused the concrete to contract enough to open the contraction joints slightly and decrease the overall stiffness of the dam when the earthquake occurred. However, as will be discussed in Chapter 7, this was found to be unlikely based on a comparison of GPS and temperature data from the dam site with the response of the finite element model subjected to temperature fluctuations. The nonlinearity in the 2001 earthquake response is not believed to be in the dam concrete. The likely explanation for the nonlinearity is softening of the foundation, particularly at the upper left abutment. The left abutment has been damaged and repaired in both the San Fernando and Northridge earthquakes. While damage was not observed after the January 2001 earthquake, perhaps the fractured rock loses stiffness when subjected to even low-level earthquake excitation, but stiffness was not permanently reduced because the rock was not permanently displaced. Perhaps, seismic waves traveling through the foundation induce this behavior more easily than sinusoidal forcing on the crest of the dam, but the difference may simply

be that the forced vibration generates much smaller ground motion that is not strong enough to excite the foundation rock significantly. However, this will have to remain as speculation.

Chapter 7

SCADA Finite Element Model

A finite element model of Pacoima Dam was constructed using SCADA, a nonlinear finite element analysis program for analyzing arch dams developed by John Hall. Documentation on SCADA can be found in Hall (1996). Modifications were made to the original program to accommodate nonuniform ground motion input. The model was calibrated to approximately match modal properties determined from system identification.

7.1 SCADA

Smeared Crack Arch Dam Analysis (SCADA) is a finite element analysis program for modeling concrete arch dams. The dam mesh is made up of 4-node shell elements. Nonlinear behavior is modeled in the shell elements in the form of contraction joints and cracks in the dam concrete. These contact nonlinearities are modeled by the smeared crack method. This method includes opening, closing and sliding nonlinearities through conditions on the shell element stresses at the integration points. The smeared crack method does not model the discrete interface behavior of joints and cracks, but the approach is computationally efficient and still gives useful results. Contraction joints are in a vertical plane of the elements parallel to the radial direction and are assumed to have zero tensile strength, which is conservative since a grouted joint would have some tensile strength. Cracks can form in the horizontal plane of the elements and cracking initially occurs when the stress in the cantilever

direction exceeds a prescribed tensile strength. SCADA can also operate in a linear mode without joints or cracks. The dam mesh geometry is updated to follow the computed deflections of the nodes. Nonlinearity in the system is limited to the dam elements. The foundation of the dam is modeled using elastic variable-node solid elements with mass omitted and the reservoir is modeled using linear 8-node water elements. The water is modeled by the Laplace equation with the dynamic water pressure as the unknown and water compressibility is neglected. The foundation and reservoir only interact with the dam. There is no reservoir-foundation interaction.

SCADA can perform four different components of a static analysis: construction, temperature change, water level change and grouting. In a construction step, a set of dam elements is assembled into the mesh with their gravity loads. In a temperature step, the dam elements are subjected to a temperature change that varies linearly between integration points. In a water level step, the elements are subjected to a change in hydrostatic pressure. The water mesh is not used in the static analysis since only hydrostatic forces are present. Gaps can develop in the dam elements during the static analysis by opening of joints and cracks. A grouting step simulates the closing of the gaps by filling with material.

For the dynamic analysis, nonuniform earthquake ground motions are applied in three components at each node of the dam-foundation interface. The input motions are free-field, i.e., that which would occur at the interface were the dam not present. The ground motions are also applied to the floor and sides of the reservoir. Rayleigh damping is employed using the stiffness and mass matrices of the dam mesh and the stiffness matrix of the foundation mesh to construct a proportional damping matrix. The formulation described in Hall (1996) has been modified to accommodate nonuniform input. The earthquake is represented by a set of forces that, if applied to the foundation nodes at the interface with the dam mesh absent, would produce the desired free-field motions. For nonuniform motion, these forces are computed from the product of the foundation stiffness matrix and the nonuniform input displacement added to the product of the foundation damping matrix and the nonuniform input velocity. These forces are applied to the nodes at the interface with both the dam

and foundation meshes present. The resulting dam motions are absolute rather than relative to the uniform free-field motion used in the original version of SCADA. The water is excited by the accelerations of the reservoir floor and sides as in the original SCADA, except that the input accelerations can be nonuniform. The water loads are modified by removing the nodal "forces" to the water mesh arising from rigid accelerations of the dam face, since the output is no longer relative to uniform input.

7.2 Nonuniform Ground Motion

In the program, nonuniform ground motion is required to be specified for every node of the dam-foundation interface. However, the ground motions from the earthquakes (actual records and those generated as in Chapter 3) are only available at three locations along the interface. Therefore, the ground motions at every node along the interface need to be interpolated from these three locations. Ground motions along the north side of the canyon are interpolated from the right abutment (channels 12–14) and base (channels 9–11), and ground motions along the south side of the canyon are interpolated from the left abutment (channels 15–17) and base (channels 9–11). Each component of motion is dealt with separately and the interpolation weights are simply based on nodal elevation, so nodal motions above the abutment recording stations and below the base recording station are actually extrapolated. The interpolation is done using the ground accelerations.

In order to account for frequency-dependent time delay in the ground motion, the interpolation process is carried out in the frequency domain. The accelerations are converted to the frequency domain by the Fourier transform. Then the abutment motions are phase shifted to be synchronized with the base motions. This is accomplished using a set of input relative phase functions. For the actual January 13, 2001 records and ground motions generated with frequency-dependent time delays, the relative phase functions are those computed by cross-correlating the displacement responses of 5% damped single degree of freedom oscillators to the January 2001 earthquake records as explained in Chapters 2 and 3. These functions are shown in Figure 3.2.

For ground motions generated from constant time delays, the linear relative phase functions that are associated with the constant delays are used. Once synchronized, the nodal ground motions are interpolated directly based on nodal elevation. This is identical to interpolating the synchronized motions in the time domain. The interpolated ground motions are still synchronized, so phase shifts, interpolated from the input relative phase functions, are introduced to the ground motions to give larger delays at increasing elevation along the abutments. The entire interpolation process in the frequency domain is summarized by

$$A_{node}(\omega) = \left[\frac{y - y_m}{y_n - y_m} A_n(\omega)\, e^{i\,\omega\,\tau_{n,m}(\omega)} + \frac{y_n - y}{y_n - y_m} A_m(\omega) \right] e^{-i\,\frac{y - y_m}{y_n - y_m}\,\omega\,\tau_{n,m}(\omega)} \qquad (7.1)$$

where $A_{node}(\omega)$ is the Fourier transform of the interpolated nodal acceleration, $A_n(\omega)$ and $A_m(\omega)$ are the Fourier transforms of an abutment acceleration (channel n) and a base acceleration (channel m), respectively, with coincident directions, $-\omega\,\tau_{n,m}(\omega)$ represents the relative phase function, y_n and y_m are the elevations of channel n and channel m, respectively, and y is the elevation of the node.

After the nodal ground accelerations are converted back to the time domain by the inverse Fourier transform, the nodal ground velocities and displacements can be obtained through integration. This process yields free-field ground motion input consisting of three components of acceleration, velocity and displacement at each node of the dam mesh along the dam-foundation interface that can be supplied to SCADA. The velocities and displacements are used to compute the forces applied at the dam-foundation interface, and the accelerations are used for the excitation of the water.

7.3 Finite Element Meshes

The finite element mesh generated for Pacoima Dam is shown in Figure 7.1. The elements modeling the thrust block on the left abutment are highlighted. In the figure, the dam is shown as if one is looking from downstream at an elevated vantage.

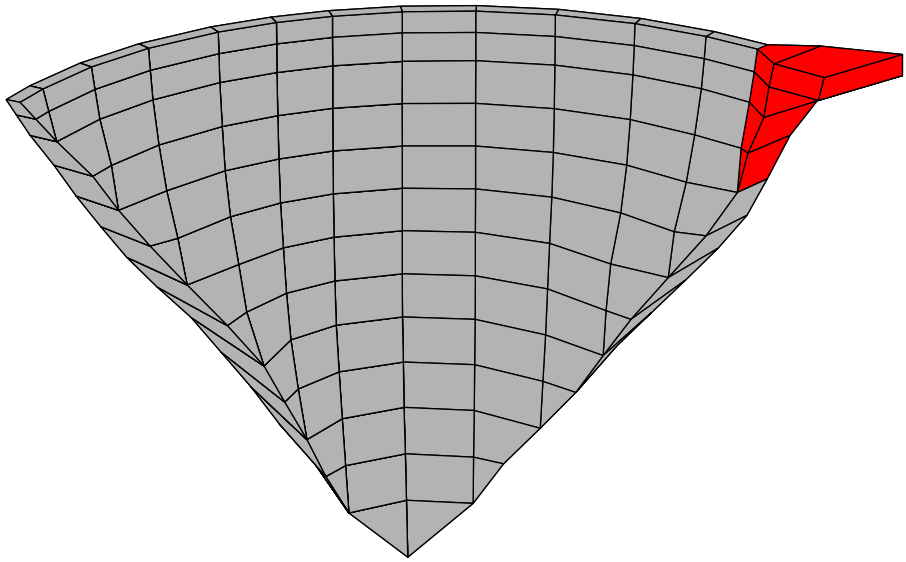

Figure 7.1: Finite element mesh of Pacoima Dam with the thrust block on the left abutment highlighted (viewed from downstream at an elevated vantage)

Note that when viewing from downstream, the left abutment is actually to the right of the dam. The dam is modeled using 110 elements and 124 nodes. The thrust block is modeled as part of the dam using 6 elements.

The meshes generated for the reservoir and foundation are shown with the dam mesh in Figure 7.2, again viewed from downstream and above. The three meshes are separated for clarity. The reservoir is modeled by 1320 elements and 1612 nodes. The upstream direction of the reservoir is rotated by 20°, as seen in Figure 7.2, to follow the initial topography of the canyon upstream of the dam. The reservoir mesh extends about 675 feet upstream or about 180% of the dam height. The foundation is modeled by 728 elements and 1080 nodes. The foundation extends 500 feet away from the dam and 240 feet upstream and downstream of the dam at the dam-foundation interface. To approximate the topography immediately extending away from the dam crest, the foundation slopes up 50° over horizontal above the right abutment and extends horizontally away from the left abutment.

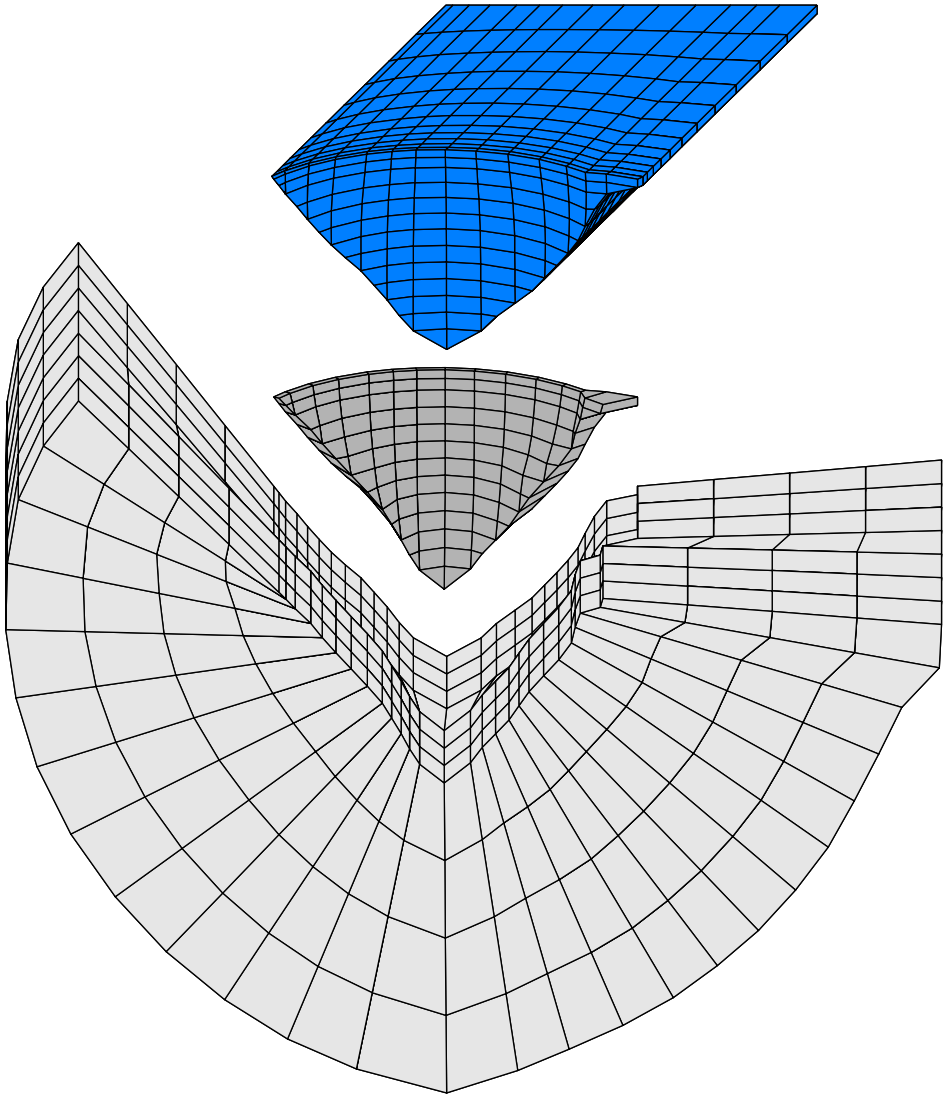

Figure 7.2: Finite element meshes of Pacoima Dam, the reservoir and the foundation (viewed from downstream at an elevated vantage)

7.4 Calibration

7.4.1 Forced Vibration Properties

Material properties for the finite element model were chosen to calibrate the model to match modal frequencies determined from the 2002 forced vibration experiment. The calibration is done using a linear SCADA model. The elastic moduli for the dam concrete and foundation rock were chosen as 28.1 GPa (4080 ksi) and 13.9 GPa

(2020 ksi), respectively. Poisson's ratios for the concrete and rock were set to 0.20 and 0.25, respectively. The unit weight of concrete was set to 22.3 kN/m^3 (142 lb/ft^3) and the unit weight of water is 9.8 kN/m^3 (62.4 lb/ft^3). The pressure degrees of freedom of the reservoir mesh were fixed down to an elevation of 38 meters below the crest to set the water level close to the level it was at during the 2002 tests, 36 meters below the crest. The natural frequencies for the fundamental symmetric and antisymmetric modes of this model are 5.46 Hz and 5.68 Hz, respectively. These frequencies are close to those determined from the 2002 forced vibration testing given in Chapter 5 (5.35 Hz–5.45 Hz and 5.65 Hz–5.75 Hz). The mode shapes on the crest associated with these frequencies are shown in Figure 7.3 with the undeformed crest shown for reference. The thrust block is not included in the shapes. The antisymmetric shape is similar to the shape determined from the 2002 forced vibration experiment shown in Figure 5.6. The symmetric shapes do not agree as well, but the differences may be due to the difficulty associated with isolating the symmetric mode in the forced vibration data. The model has three more modes under 10 Hz at frequencies of 8.03 Hz, 8.62 Hz and 9.95 Hz.

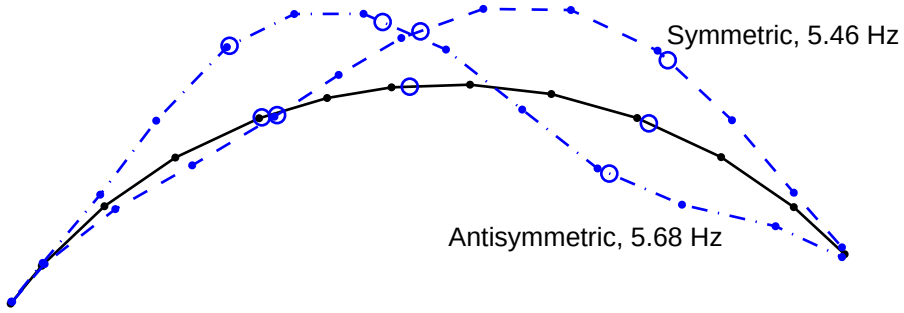

Figure 7.3: Symmetric and antisymmetric mode shapes computed from the linear SCADA model calibrated to the 2002 forced vibration modal frequencies (The open circles are the locations of the crest level stations and the dots are the locations of the nodes on the crest.)

The amplitudes of the mode shapes at the points on the abutments corresponding to the locations of the Rangers during the 2002 tests can also be determined as another way to test the validity of the model. The amplitudes on the abutments relative to the amplitude at the center of the crest computed from the model are somewhat larger for

the symmetric mode and smaller for the antisymmetric mode compared to the same quantities determined from the forced vibration tests. The directions of the motion are not consistent, either. However, the amplitude of the motion on the abutments is small, so the differences are not significant for the calibration of the model. The amplitudes on the abutments relative to the amplitude at the center of the crest are compared between the 2002 tests and the model in Table 7.1.

	Symmetric Mode		Antisymmetric Mode	
	Right Abutment	Left Abutment	Right Abutment	Left Abutment
2002 Tests	4.3%	5.6%	7.4%	8.9%
Model	7.1%	10.8%	5.4%	3.3%

Table 7.1: Amplitude of abutment motion relative to the amplitude of motion at the center of the crest from the 2002 forced vibration tests and computed from the SCADA model calibrated to the forced vibration modal frequencies

7.4.2 Earthquake Properties

In order to use the SCADA model for earthquake analyses, it is calibrated to approximate the modal parameters determined from the MODE-ID results using the January 2001 earthquake records. Since the mechanism that causes the decrease in stiffness compared to forced vibration results is not known, the concrete and rock stiffnesses are both decreased 22% from the forced vibration calibrated stiffnesses. The scaled elastic moduli used for the dam and foundation are 21.9 GPa (3180 ksi) and 10.9 GPa (1575 ksi), respectively. The concrete modulus is in the typical range for dam concrete and it is in the range determined from field data; and it is more realistic than the value used to calibrate to the forced vibration properties, which is higher than expected for typical concrete. The rock modulus is within a rather large range of field data (Woodward-Lundgren, 1971). It corresponds to a shear wave velocity of about 1280 m/sec. The other material properties were left unchanged from the forced vibration calibrated model: Poisson's ratios equal to 0.20 and 0.25 for the dam and foundation, respectively, a unit weight of concrete equal to 22.3 kN/m^3 (142 lb/ft^3) and a unit weight of water equal to 9.8 kN/m^3 (62.4 lb/ft^3). The water level was

again set to 38 meters below the crest, since the water was about 41 meters below the crest during the 2001 earthquake. The fundamental symmetric and antisymmetric mode frequencies for this model are 4.82 Hz and 5.02 Hz, respectively. These are close to the values estimated by MODE-ID (4.73 Hz–4.83 Hz and 5.06 Hz) as discussed in Chapter 4. The computed mode shapes on the crest for the first two modes are shown in Figure 7.4 with the undeformed crest shown for reference. Notice that the mode shapes are identical to the shapes of the forced vibration calibrated model in Figure 7.3. The shapes are not identical to the shapes estimated by MODE-ID shown in Figure 4.1, but the differences are not significant.

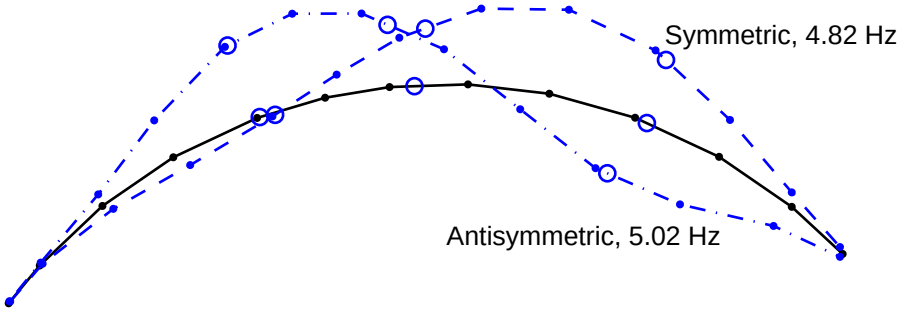

Figure 7.4: Symmetric and antisymmetric mode shapes computed from the linear SCADA model calibrated to the MODE-ID estimated modal frequencies using the 2001 earthquake records (The open circles are the locations of the crest level stations and the dots are the locations of the nodes on the crest.)

For nonlinear behavior, the tensile strength of the concrete for horizontal cracking is set to 3.79 MPa (550 psi), which is a typical value for concrete. The strength is not reduced to account for the presence of lift joints in the dam that might facilitate cracking. Joints are present in the dam in all columns of elements, except for the thrust block elements and the two elements furthest to the north at the right abutment. This gives the dam model eleven joints which is consistent with Pacoima Dam. Lateral sliding between the joints is not allowed in the model since Pacoima Dam has keys in the joints, but vertical sliding between the joints and sliding in the cracks is permitted.

Stiffness and mass proportional damping is specified to give modal damping of about 6.8% and 7.0% for the symmetric and antisymmetric modes, respectively. These

values are close to the values estimated by MODE-ID using the 2001 earthquake records (6.2% and 6.6%–7.3%). The damping is mostly stiffness proportional so that it is large at higher frequencies in an attempt to reduce the high frequency response near the left abutment discussed in Section 4.2.3.

7.5 Temperature Fluctuations

On September 1, 1995, Pacoima Dam was instrumented with continuously operating GPS receivers. Data obtained through July 26, 1998, have been analyzed (Behr et al., 1998). The relative displacement of a point near the center of the crest in the east-west (stream) direction referenced to a point on the thrust block was compared to average regional temperature as measured in Burbank, California, which is about 20 km south of Pacoima Dam. An oscillatory displacement with peak-to-peak amplitude of 17±2 mm was observed with an approximately annual period. This period correlates well with seasonal temperature variations. The center of the crest of the dam moves eastward (upstream) during warm summer months and westward (downstream) during cooler winter months. The average daily temperature varied over a range of approximately 28°F during the course of a year. The peak displacement of the crest was determined to lag behind the peak temperature by 35 days. Correlation of the crest displacement to higher frequency temperature variations and other effects, e.g., changes in reservoir level, were less apparent.

The SCADA model response can be compared to these results using successive temperature steps in a static analysis. The models that are calibrated to the 2002 forced vibration modal properties and the 2001 earthquake modal properties yield very similar results for this analysis when joints are included, since the stiffness of the system is the only property that is different. The results are identical for linear analysis. The earthquake calibrated model is discussed here, since that model is the one used for further analyses. The reservoir level is set to 47 meters below the crest, which is about the average level during the period the GPS and temperature data were analyzed. The coefficient of thermal expansion for the model is $5.5\text{x}10^{-6}/°\text{F}$.

The reference temperature is 66°F and the temperature cycles between 52°F and 80°F. Temperature changes are applied uniformly throughout the dam, even on the upstream face below the water level. This is a simplification that does not account for heat conduction and water temperature, so the 35 day lag between peak temperature and peak displacement cannot be modeled. However, the peak-to-peak annual displacement can be compared to the measurements.

With joints included in the model, the agreement with the observed results is not good. When heated to 80°F, the center of the crest displaces about 7 mm eastward (upstream) relative to a point on the thrust block, which is consistent with the measurements. However, when cooled to 52°F, the center of the crest also displaces slightly eastward (upstream) relative to a point on the thrust block. The crest is not moving downstream when the dam is cooled because the joints are opening instead. Without joints in the model, the agreement is much better. The center of the crest displaces eastward (upstream) when heated and westward (downstream) when cooled, and the peak-to-peak relative displacement is about 14 mm. The modeled results, both with and without joints, are shown in Figure 7.5.

This analysis indicates that the contraction joints of the dam are closed throughout the course of the year. Therefore, temperature variations are not the cause of the stiffness reduction observed in the dam system during the January 2001 earthquake compared to forced vibration results. This also means that Pacoima Dam is in a different initial state than the nonlinear SCADA model predicts. Grout in the contraction joints may supply sufficient tensile strength to prevent the joints from opening, or perhaps, creep of the concrete over time has caused the dam to be in a more compressed state that requires larger tensile stresses to pull the joints open. Notice also that the largest peak-to-peak displacements recorded on the crest during the January 13, 2001 earthquake (about 4 mm) are actually smaller than the displacements induced by thermal variations. This may actually indicate that the linear SCADA model without joints is the better model for analyzing Pacoima Dam excited by the 2001 earthquake.

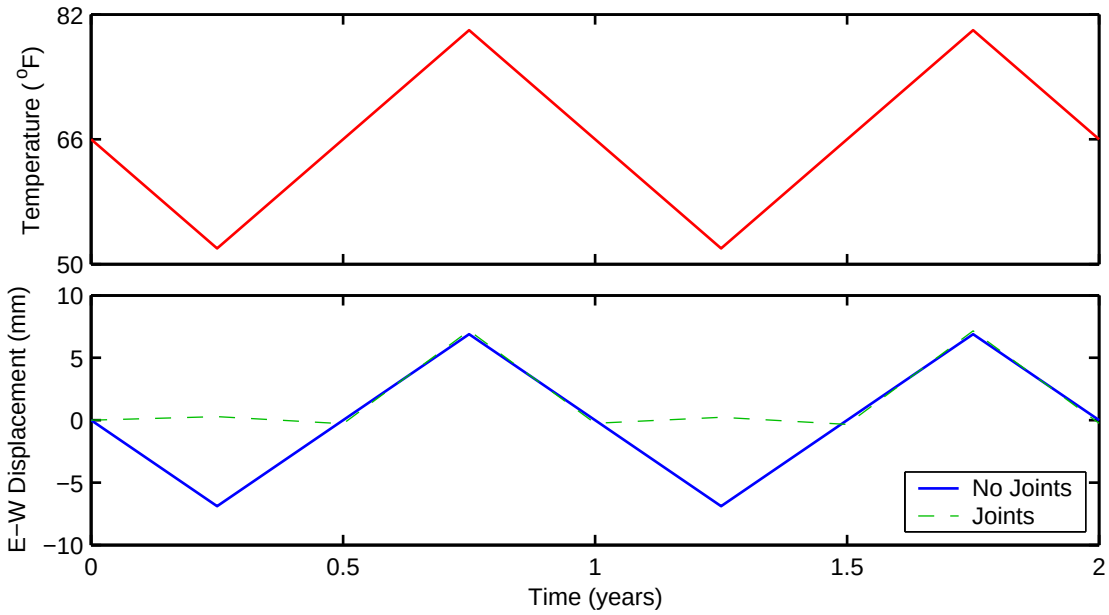

Figure 7.5: East-west displacement (eastward is positive) at the center of the crest relative to a point on the thrust block computed from the SCADA model, with and without joints, subjected to temperature changes simulating two years of seasonal variations

7.6 Damaged Model

An attempt was made to simulate the damage sustained by the Pacoima Dam system during the San Fernando earthquake, since the damage had not been repaired before the 1971 forced vibration tests done by Reimer (1973). The SCADA model calibrated to match the 2002 forced vibration results was modified in three ways. First, the reservoir was removed since Reimer's tests were performed without water present. This actually has the effect of increasing the natural frequencies of the system. The other two modifications simulate damage at the left abutment and thrust block. Thirty elements of the foundation at the left abutment were softened to have an elastic modulus of 2.8 GPa (400 ksi) to simulate the effect of fractured rock. The foundation was softened down to a level 47 meters below the crest at the dam-foundation interface. The softened elements are shown with the dam mesh in Figure 7.6. This is a reasonable depth to soften the foundation. After the 1971 forced vibration tests, post-tensioned steel tendons were planned to be installed to about

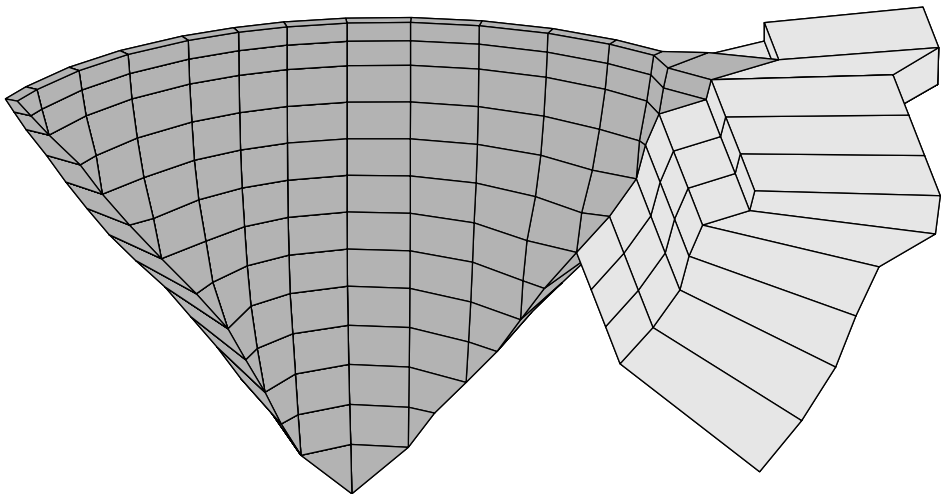

Figure 7.6: Finite element meshes of Pacoima Dam and the softened region of the foundation at the left abutment (viewed from downstream at an elevated vantage)

this depth and holes for consolidation grouting were drilled to about 35 meters deep to strengthen the rock (International Engineering Co., 1972). The final modification to the model was to disconnect the elements between the dam and the thrust block to a level about 20 meters below the crest. This was accomplished by adding three extra nodes to the dam mesh at the same coordinates as the upper three nodes connecting the dam and thrust block, and connecting the thrust block elements to these nodes instead. This simulates the open joint between the dam and the thrust block. This is done differently than opening one of the joints within the dam elements, because the linear stiffness, which does not include the joints in the model, is used to compute the natural frequencies and mode shapes.

With this model, natural frequencies for the symmetric and antisymmetric modes are computed at 5.18 Hz and 5.50 Hz, respectively. These compare reasonably well to the frequencies determined in 1971 (5.10 Hz and 5.56 Hz). The mode shapes associated with these two modes are shown in Figure 7.7 with the undeformed crest shown for reference. Notice that the movement at the left abutment is less constrained because of the open joint. This damaged model is probably a reasonable simulation of the damage to the left abutment that occurred during the San Fernando earthquake, as well as the Northridge earthquake. Damage to the rock cannot occur dynamically in

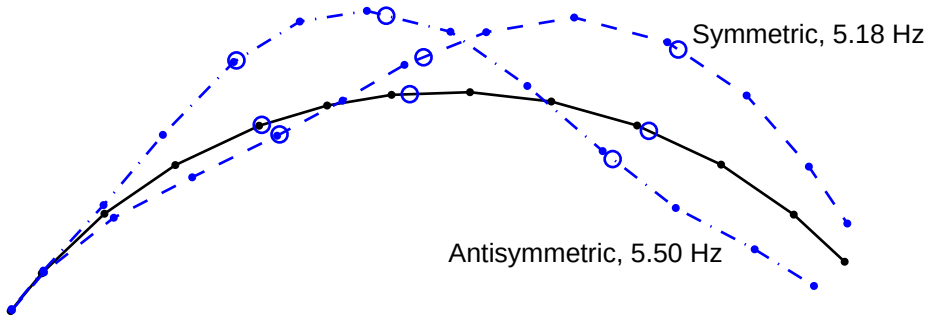

Figure 7.7: Symmetric and antisymmetric mode shapes computed from the linear SCADA model modified to simulate damage with no reservoir, a softened region of foundation and an open joint (The open circles are the locations of the crest level stations and the dots are the locations of the nodes on the crest.)

SCADA since the foundation is modeled elastically. Therefore, both the undamaged and damaged models will be subjected to the generated Northridge earthquake ground motions and the results will be compared. However, for the earthquake analyses, the open joint does not need to be included by adding nodes since joints are modeled in the elements by the smeared crack method. Thus, the damaged model for earthquake analyses only requires softening of the elements at the left abutment.

Chapter 8

Analysis with January 13, 2001 Earthquake Records

The ground motion records from the January 13, 2001 earthquake were used as input to the SCADA model that was calibrated to match the MODE-ID determined properties. Comparing the output motion from the model to the records obtained from the body of the dam during the earthquake can help to assess the validity of the finite element model. Various ground motions generated to reproduce the January 2001 records were also used as input to the model. The output from the generated records can be compared to the output from the actual records. In this way, the ability of the generated records to produce useful results from the model can be assessed. However, it should be noted that due to the low level of excitation associated with the 2001 earthquake, the complete nonlinear capabilities of the model are not tested.

8.1 Actual Records

The analysis of the effect of temperature fluctuations (see Section 7.5) indicated that the contraction joints in the dam are not open at any time during the year and they probably did not open at all during the 2001 earthquake. Therefore, the linear SCADA model may be more appropriate than the nonlinear model for simulating the response to the 2001 earthquake. However, both linear and nonlinear analyses were done to determine whether the difference is important. The SCADA model calibrated to have linear fundamental modes at 4.82 Hz (symmetric) and 5.02 Hz

(antisymmetric) with the water level 38 meters below the crest was used for the analyses. The model was described in Chapter 7. Output time histories and response pictures of maximum compressive stresses and joint opening are shown in Appendix B.

The time histories at the locations corresponding to the accelerometer array are computed first from a linear SCADA analysis excited by the January 13, 2001 earthquake ground motions. A comparison of the computed acceleration time histories at channels 1–8 and the actual records is shown in Figure 8.1. The acceleration

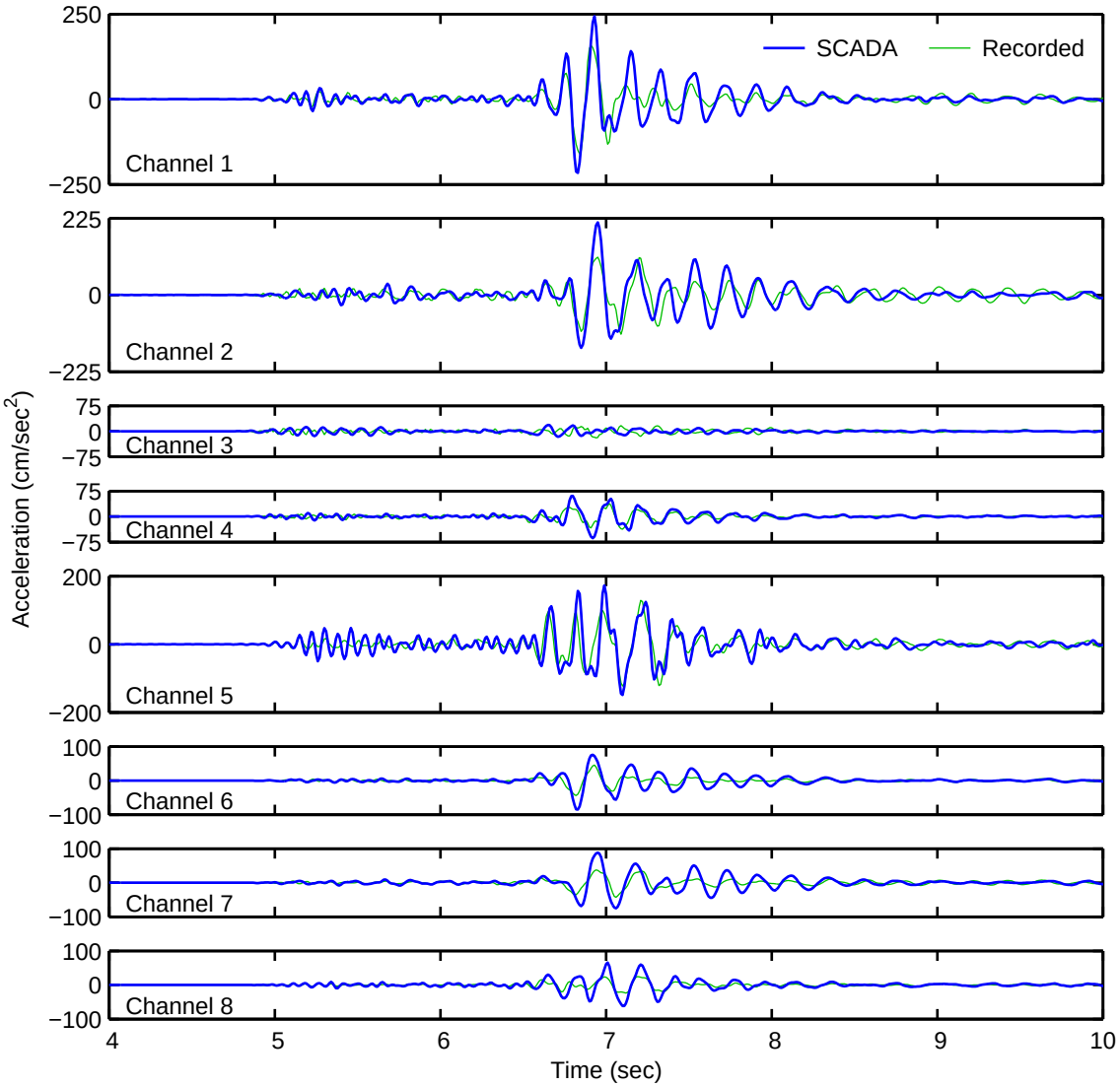

Figure 8.1: Acceleration time histories at locations corresponding to channels 1–8 computed from a linear analysis of the January 13, 2001 earthquake compared to the actual records

computed by SCADA overestimates the acceleration that was actually recorded by as much as 100% at some of the measured locations. This may be partially due to some amplification of the records supplied as input to the model along the abutments due to foundation-structure interaction, meaning that the "input" to the dam at the dam-foundation interface nodes in the model is larger than it actually was during the earthquake. However, as seen in Figure 8.2, the foundation-structure interaction does not alter the interface motions significantly so there must be another reason.

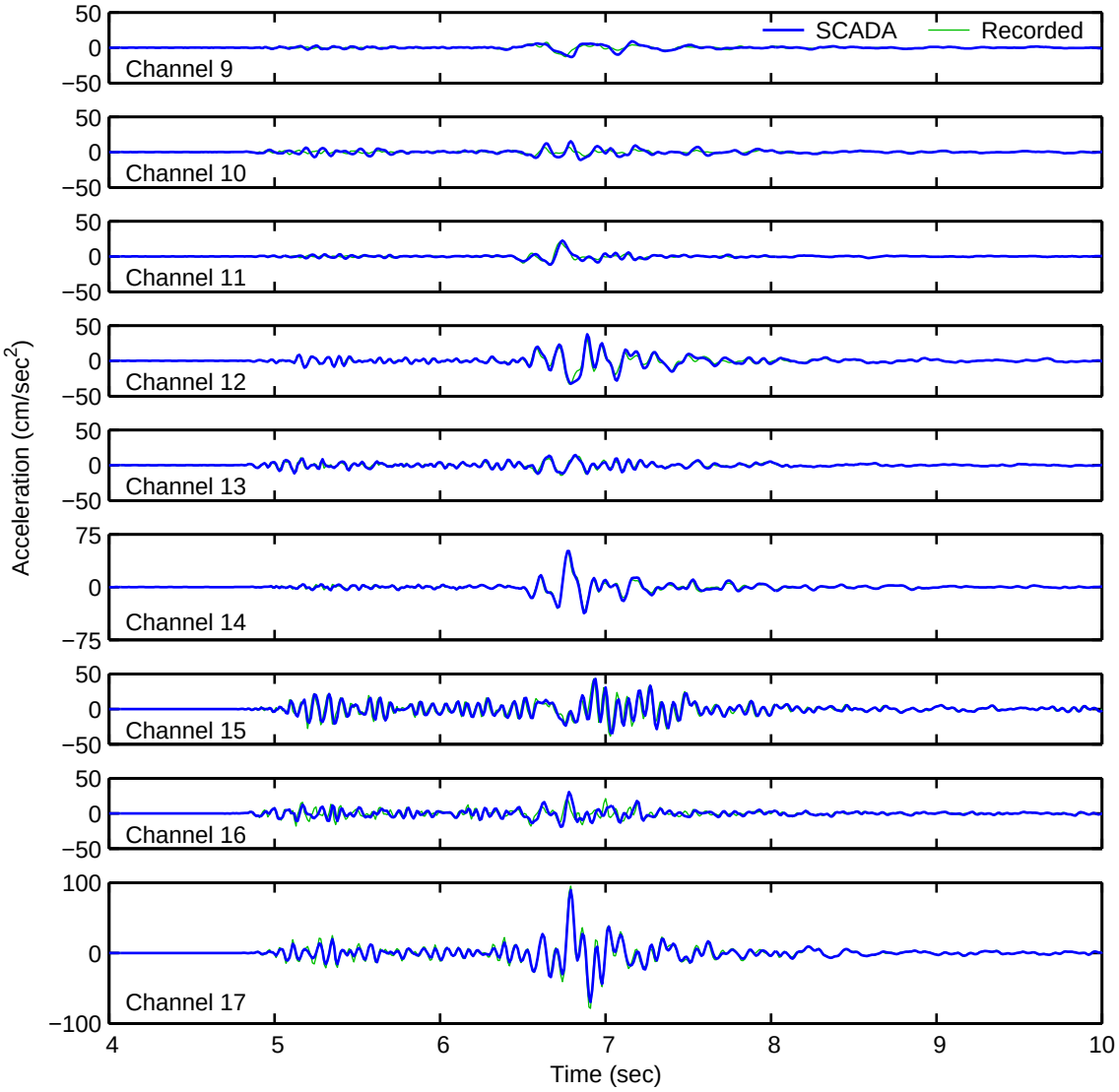

Figure 8.2: Acceleration time histories at locations corresponding to channels 9–17 computed from a linear analysis of the January 13, 2001 earthquake compared to the actual records

One possibility is that the modal damping should actually be higher to reduce the computed response, but there is no basis for an increase in the damping since it was based on system identification using the January 2001 records. The displacements computed at channels 1–8 do agree better with the recordings than the accelerations, which is seen from Figure 8.3. Aside from the overestimation by the computed response, for both accelerations and displacements, the oscillatory behavior agrees well with the records, but the reason for the computed overestimation is not known.

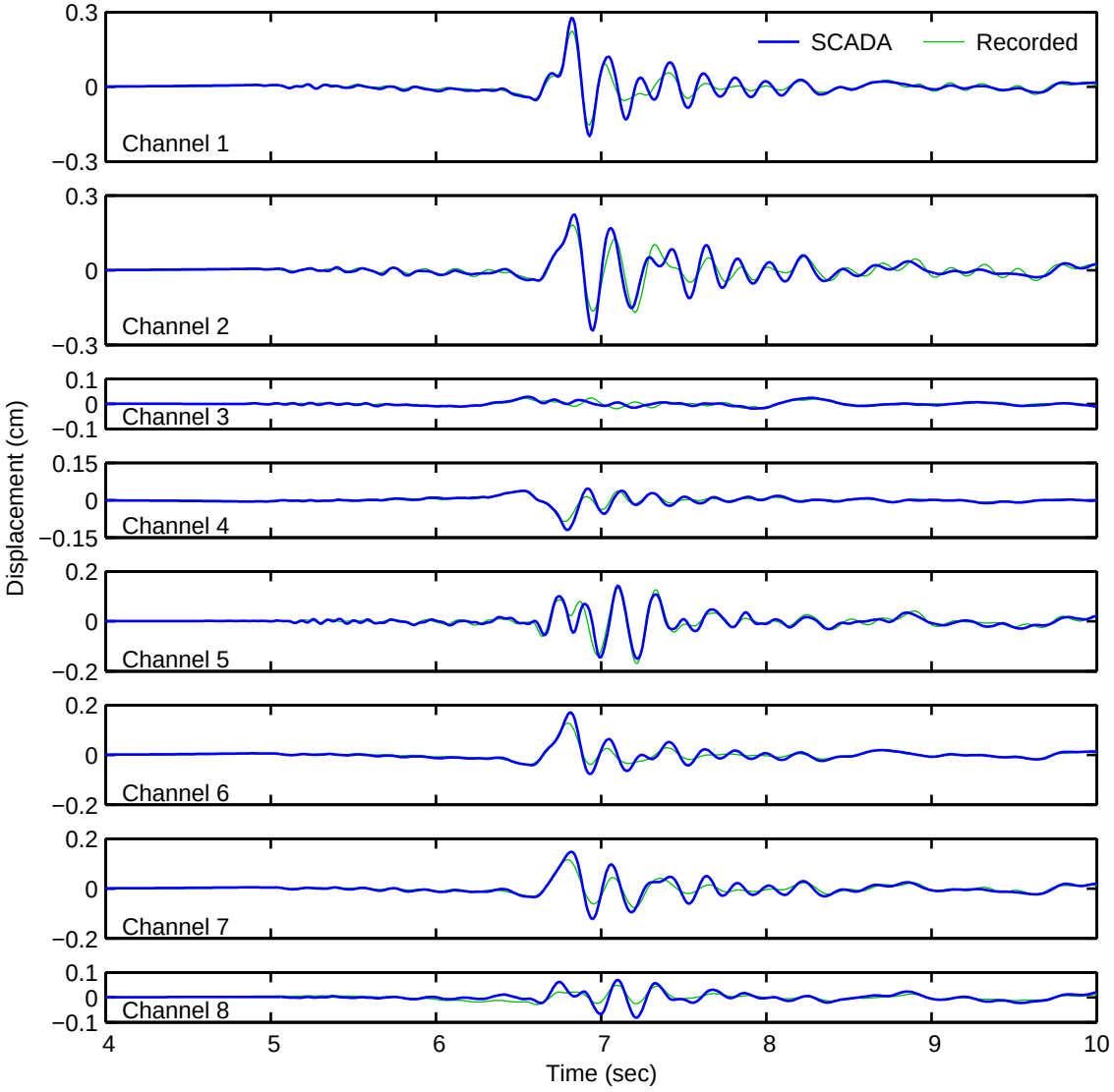

Figure 8.3: Displacement time histories at locations corresponding to channels 1–8 computed from a linear analysis of the January 13, 2001 earthquake compared to the actual records

From comparison of the modeled displacements with the actual records, it can be seen that the computed motion oscillates at a slightly lower frequency at channels 1, 4 and 6 than the records, and the computed motion at channels 2 and 7 oscillates at a slightly higher frequency than the records. Channels 1, 4 and 6 are radial at the right third point and tangential at the center so these channels should predominantly record response from the antisymmetric mode; and channels 2 and 7 are radial at the center so the symmetric mode response should be significant in these channels. This may indicate that the SCADA model has an antisymmetric mode frequency that is too low and a symmetric mode frequency that is too high to match the Pacoima Dam system.

The maximum compressive stresses in the dam in the arch and cantilever directions computed during the linear analysis are shown in Figures 8.4 and 8.5. The stresses on both faces of the dam are shown, and the faces are presented as if an observer was viewing the dam from downstream so the thrust block is to the right side in the figures. The stresses from the analysis with the January 2001 earthquake input are actually so small that they are dominated by the static stresses. The arch and cantilever stresses from the static part of the linear analysis are shown in Figures 8.6 and 8.7. Tensile stresses are positive and compressive stresses are negative. The compressive stresses in the dam are less than 1.4 MPa (200 psi) throughout the static and dynamic analyses and the dynamic component is only a small fraction of this amount. The dam does undergo tension in the arch direction, but it is no larger than 0.35 MPa (50 psi); and tension in the cantilever direction is even smaller.

A nonlinear analysis with the same model and January 2001 earthquake ground motion input gives very similar results to those obtained from the linear analysis. There is no cracking and the largest joint opening is only 0.03 cm with vertical sliding between the joints no larger than 0.04 cm. The presence of vertical joints does affect the stresses slightly, but the overall distribution is not affected much. The maximum compressive stresses in the arch direction during the nonlinear analysis shown in Figure 8.8 can be compared to the stresses in Figure 8.4 to illustrate this.

The motion time histories from the nonlinear analysis are also very similar to

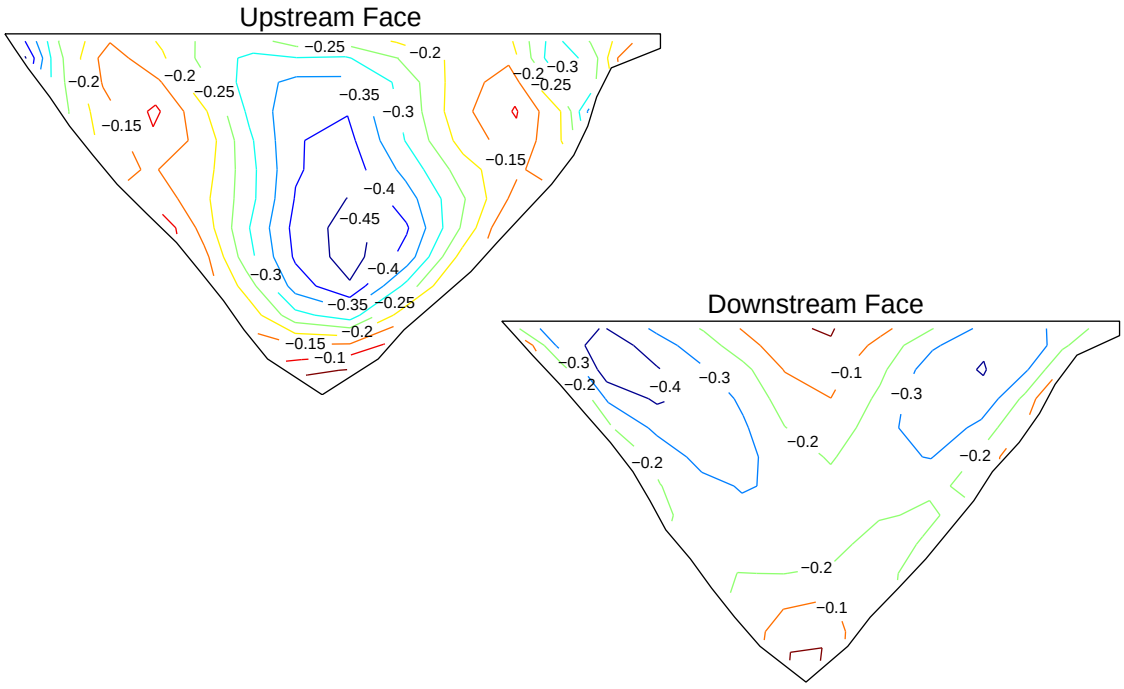

Figure 8.4: Maximum compressive arch stresses (MPa) computed during a linear analysis with the January 13, 2001 earthquake input

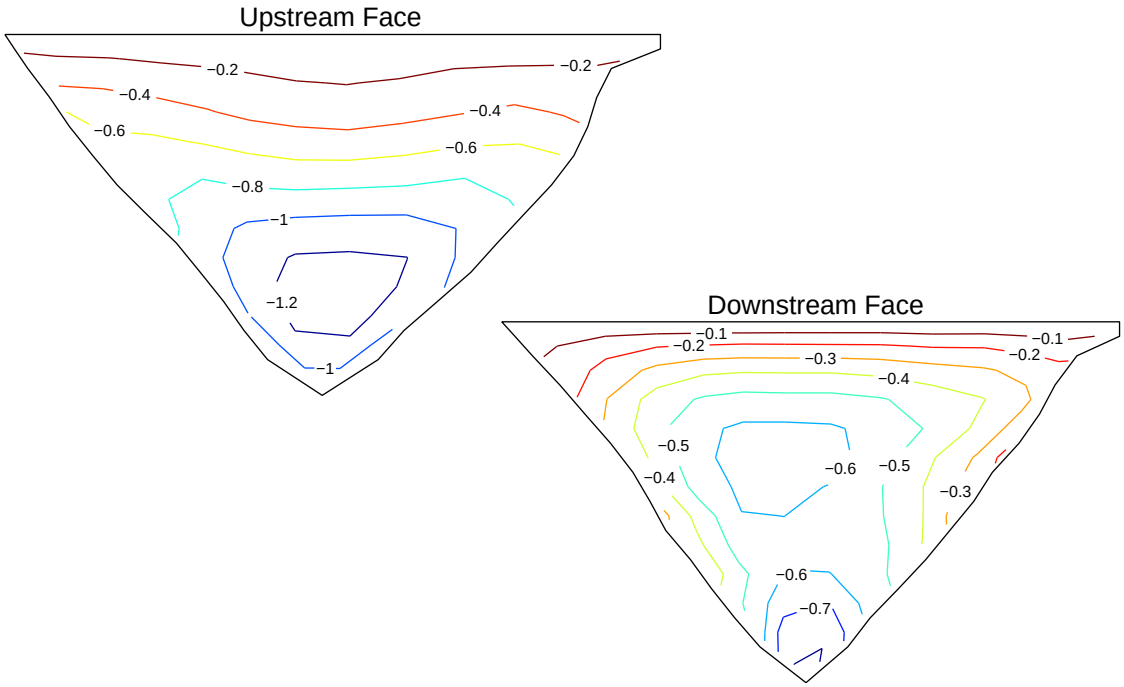

Figure 8.5: Maximum compressive cantilever stresses (MPa) computed during a linear analysis with the January 13, 2001 earthquake input

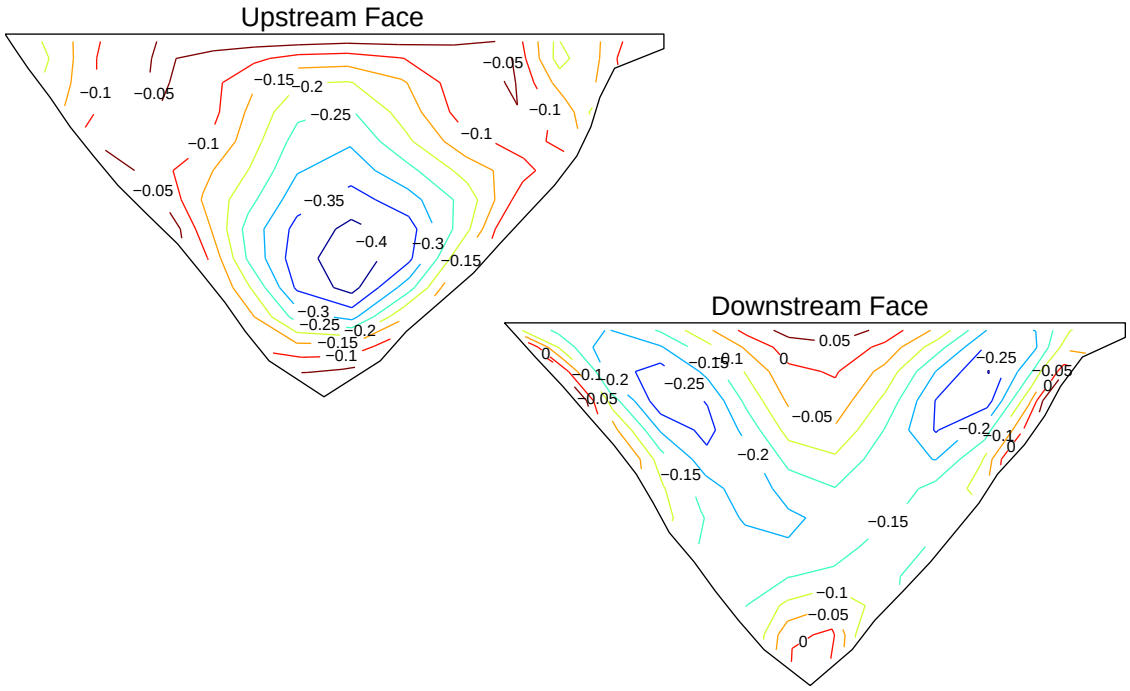

Figure 8.6: Arch stresses (MPa) computed from a linear static analysis

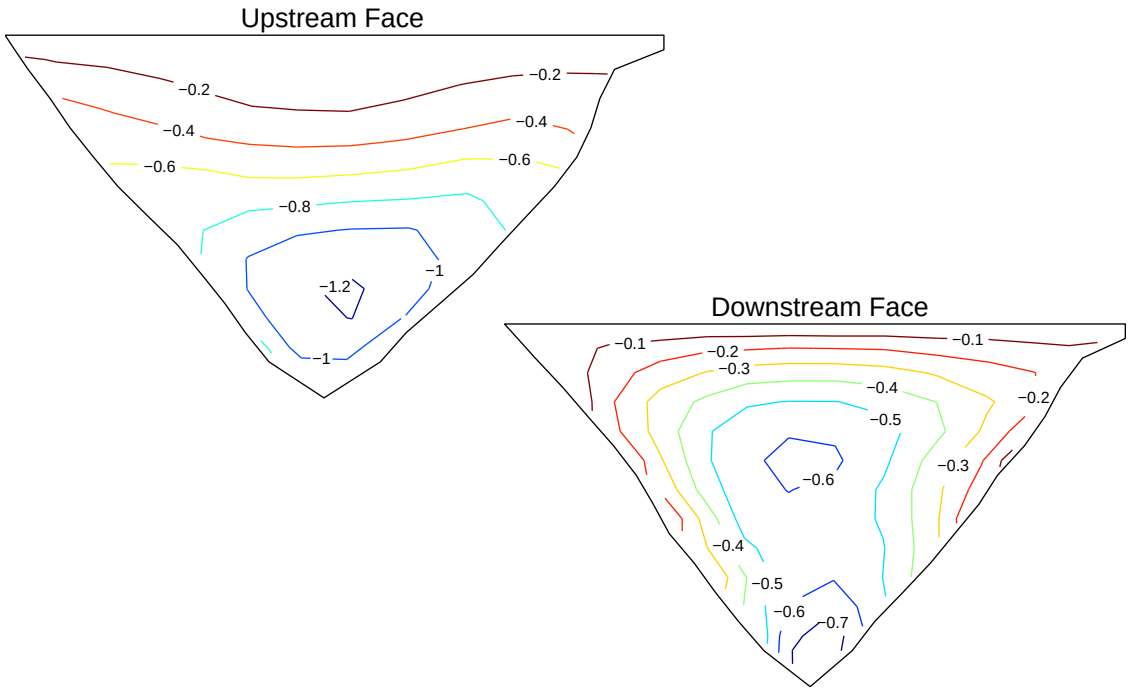

Figure 8.7: Cantilever stresses (MPa) computed from a linear static analysis

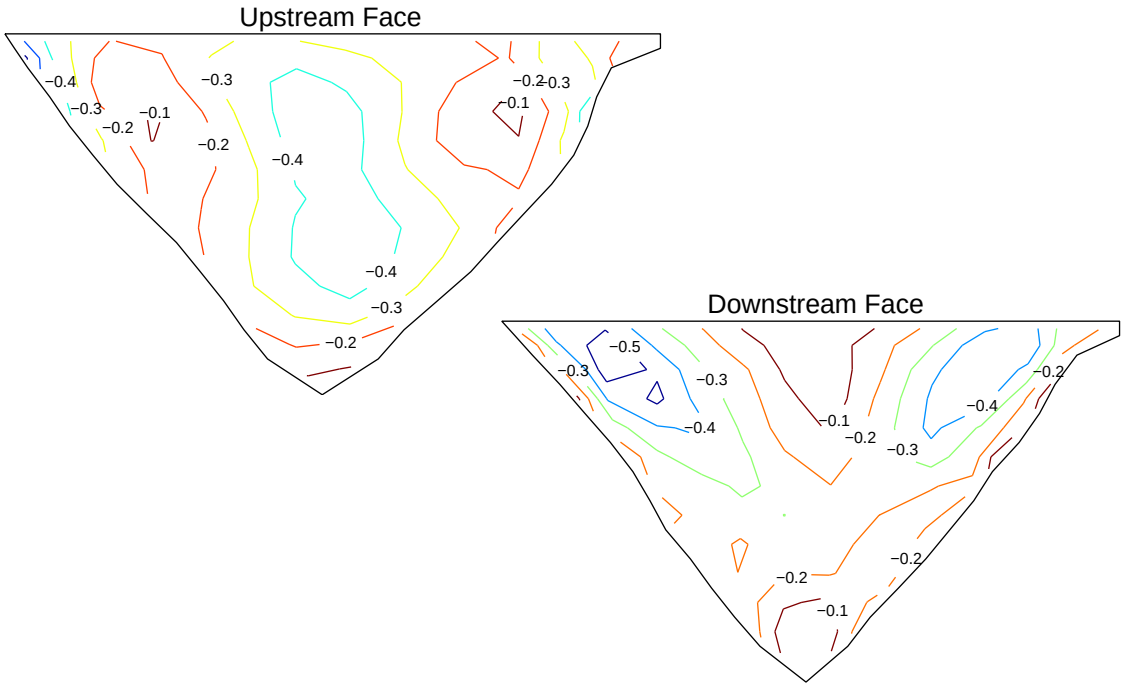

Figure 8.8: Maximum compressive arch stresses (MPa) computed during a nonlinear analysis with the January 13, 2001 earthquake input

those from the linear analysis. The accelerations at channels 2 and 4 are compared from the nonlinear and linear analyses in Figure 8.9. There are some high frequency pulses in the channel 4 acceleration for the nonlinear analysis that do not occur during

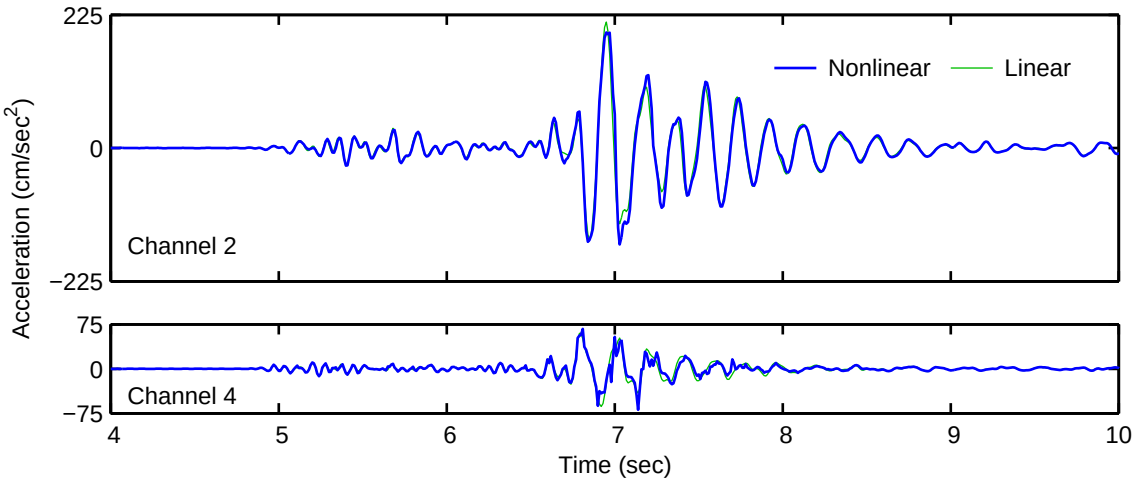

Figure 8.9: Acceleration time histories at locations corresponding to channels 2 and 4 computed from nonlinear and linear analyses of the January 13, 2001 earthquake

the linear analysis. Channel 4 is tangential so the acceleration pulses are from joint impacts. There is a small decrease in oscillation frequency on the order of about 2% when nonlinearity is allowed that can be visually deduced from the time histories upon close inspection. That would correspond to a stiffness decrease of about 4%.

When a nonlinear analysis is done, the response is almost completely linear. However, while the nonlinear analysis does indicate some minimal joint opening, the contraction joints probably did not open during the January 2001 earthquake. Therefore, the linear analysis is more appropriate for analysis of Pacoima Dam when it is subjected to a small earthquake like the one on January 13, 2001, but the difference is not important for an event of that size. This does not mean that a linear analysis is appropriate to model the response of Pacoima Dam to an event the size of the Northridge earthquake.

The agreement of the modeled response with the observed behavior from the January 2001 earthquake is reasonable. The recorded dam acceleration is overestimated by the model, but the modeled displacements agree better with the recorded motion. This indicates that the stresses modeled in the dam are probably conservative. This same behavior can be expected if the model is subjected to stronger earthquake motion.

8.2 Generated Records

Abutment ground motions at channels 12–17 generated by methods 1, 2 and 9 (Table 3.1) for the January 2001 earthquake were input to SCADA with the actual recorded base motions at channels 9–11. Method 1 generates the motion with piecewise linear amplification and frequency-dependent time delays; method 2 uses piecewise linear amplification and constant, component-dependent time delays; and method 9 uses 0% damped spectral displacement ratios and frequency-dependent time delays. The nonlinear SCADA model was used for the comparison of the response to these sets of input ground motion.

The acceleration and displacement time histories and the response pictures of

maximum compressive stresses and joint opening are given in Appendix B for these analyses. The maximum compressive stresses and joint opening computed by the model with the various sets of generated input are very similar to those computed with the actual records, except that records generated by method 2, which uses a constant time delay, yield arch compressive stresses that are a little larger at the upper abutments. The output time histories computed with the generated input exhibit more variance. All three sets of generated input yield motion near the center of the crest that overestimates the actual recorded motion even more than the analysis with the actual records. This is most severe with input generated by method 2. However, output motion closer to the left abutment (channel 5) is actually smaller with the generated input than the actual records. This occurs because the approximate amplification functions most significantly underestimate the input at the left abutment (channels 15–17). It is more apparent with the piecewise linear amplification than the 0% damped spectral displacement ratios.

Despite the differences in the output motion, the stresses and joint opening in the dam do not differ very much. This means that the variation in generated input ground motion does not affect the stresses that the dam is subjected to in the simulations to the same degree. Therefore, the more simple and approximate methods for generating ground motion should yield acceptable results when used in a dynamic finite element analysis. However, it needs to be remembered that only small earthquake input is considered for these results, so significant nonlinear effects are not included.

Chapter 9

Flexible vs. Rigid Foundation

In Chapter 4, MODE-ID was used to identify the modal parameters of Pacoima Dam. However, it is not completely clear what system was identified. The input to the MODE-ID model is given at three locations along the dam-foundation interface, so these locations are theoretically fixed. The effect that this limited input definition has on the amount of foundation-structure interaction that is included in the identified system is not known. With acceleration time histories computed by the linear SCADA finite element model, this issue can be investigated. This model has natural frequencies for the first two modes at 4.82 Hz (symmetric) and 5.02 Hz (antisymmetric). If the foundation is made rigid, the frequencies increase to 5.58 Hz and 5.74 Hz. The 5.58 Hz mode appears to be antisymmetric and the 5.74 Hz mode appears to be symmetric, but the shapes are quite different from those with the flexible foundation.

9.1 Three Input Locations

As in Chapter 4, nine seconds of the accelerations at channels 1–8 and channels 9–17 computed by the linear SCADA model for the January 13, 2001 earthquake (Figures 8.1 and 8.2) are supplied as output and input, respectively, to MODE-ID. The inputs at channels 9–17 that are supplied to MODE-ID are the time histories that are computed from the model with a flexible foundation, not the records that are input to the finite element model. Thus, foundation interaction in the model is included in the accelerations that are input to MODE-ID. The natural frequencies identified

are around 5.36 Hz (antisymmetric) and 5.49 Hz (symmetric). These frequencies are closer to the natural frequencies of the finite element model with a rigid foundation than a flexible foundation, and the mode shapes are more similar to the shapes computed from the model with a rigid foundation. This seems to indicate that the system identified by MODE-ID using the input at three locations is actually closer to having a rigid foundation, but some foundation flexibility is included. If this is the case, then the model calibrated in Chapter 7 to match the MODE-ID identified natural frequencies is actually too stiff.

The finite element model should be calibrated so that the first two natural frequencies coincide with the MODE-ID estimates from the actual records when the model is some hybrid of the models with flexible and rigid foundations. The model with a flexible foundation would be less stiff than this hybrid model. However, if the stiffness of the finite element model is decreased, the agreement of the modeled motions with the recorded motions gets worse. Also, MODE-ID estimates that the symmetric mode is lower than the antisymmetric mode when the recorded accelerations are used, which is not consistent with the estimates using computed accelerations and the frequencies computed for the rigid foundation system.

Taking all of this into consideration, it is concluded that the input along the dam-foundation interface must be more fully characterized at the three measurement locations when the input and output accelerations for MODE-ID are computed by the finite element model than when the actual recorded accelerations are used. For the nodal input to the finite element model, the ground motions along the abutments at intermediate elevations are interpolated based on the motions at the three recording locations (see Section 7.2). This is an approximation to the physical effects of topographic amplification and traveling seismic waves, but the actual process is more complicated so the intermediate elevation ground motions must be more independent from each other and the recording locations. This would mean that the system identified by MODE-ID using the recorded accelerations has more contribution from the foundation than is indicated by the MODE-ID results with modeled accelerations. However, this is only speculation.

9.2 Increasing the Number of Input Locations

As the number of inputs to MODE-ID along the dam-foundation interface is increased, the estimates should theoretically converge to the rigid foundation system. This can be investigated with accelerations computed by the finite element model. The same accelerations computed by the model at channels 1–8 for the January 2001 earthquake are supplied as output to MODE-ID, and three components of acceleration computed at a variable number of nodes along the dam-foundation interface are supplied as input to MODE-ID.

Nine input locations (27 total inputs) spaced along the abutments at vertical intervals of less than 30 meters appear to yield a system that MODE-ID estimates to have mode shapes and frequencies that are consistent with the rigid foundation system. However, the results are not conclusive because as the number of inputs is increased the MODE-ID estimates converge slowly and the solutions are sensitive to initial guesses. Also, more input locations may be required to identify the rigid foundation system if accelerations from an actual earthquake were recorded with that spacing, since accelerations computed from the finite element model seem to give stiffer MODE-ID estimates than actual recordings.

9.3 Cross-Correlation Functions

Further investigation can be done using cross-correlations of the acceleration records as free vibration output for MODE-ID. As is shown in Farrar and James (1997) and Beck et al. (1995), the cross-correlation between two measurements can have the same properties as the free vibration response of the system. This holds for ambient vibration that is assumed to be excited by stationary white noise, so the input and the output need to be statistically independent. Earthquake excitation does not adhere to this condition, but it might be a close enough approximation that the results can be useful. The cross-correlations of the accelerations recorded January 13, 2001, should contain the modal properties of the dam system with complete foundation flexibility

included.

All of the radial and stream direction acceleration records (channels 1, 2, 5–9, 12 and 15) were cross-correlated to the channel 2 record (actually autocorrelated in the case of channel 2). The first 4 seconds of these cross-correlation functions were supplied as output for MODE-ID with no input. The cross-correlation functions for channels 1, 2 and 12 are compared to the free vibration computed by MODE-ID in Figure 9.1. Notice that the functions do not appear as though they are good representations of free vibration, but the estimates from MODE-ID are discussed here anyway. The modes identified have natural frequencies of 3.84 Hz (symmetric) and 5.30 Hz (antisymmetric). The damping for the antisymmetric mode is 4.6%, but it is over 20% for the symmetric mode. The damping is probably not reliable, but the natural frequencies may yield some useful information about the flexible foundation system. The fact that the antisymmetric mode frequency is actually higher than it is for the system that is a hybrid of the systems with rigid and flexible foundations does not make sense, but recall that it was observed in Chapter 8 that the SCADA modeled

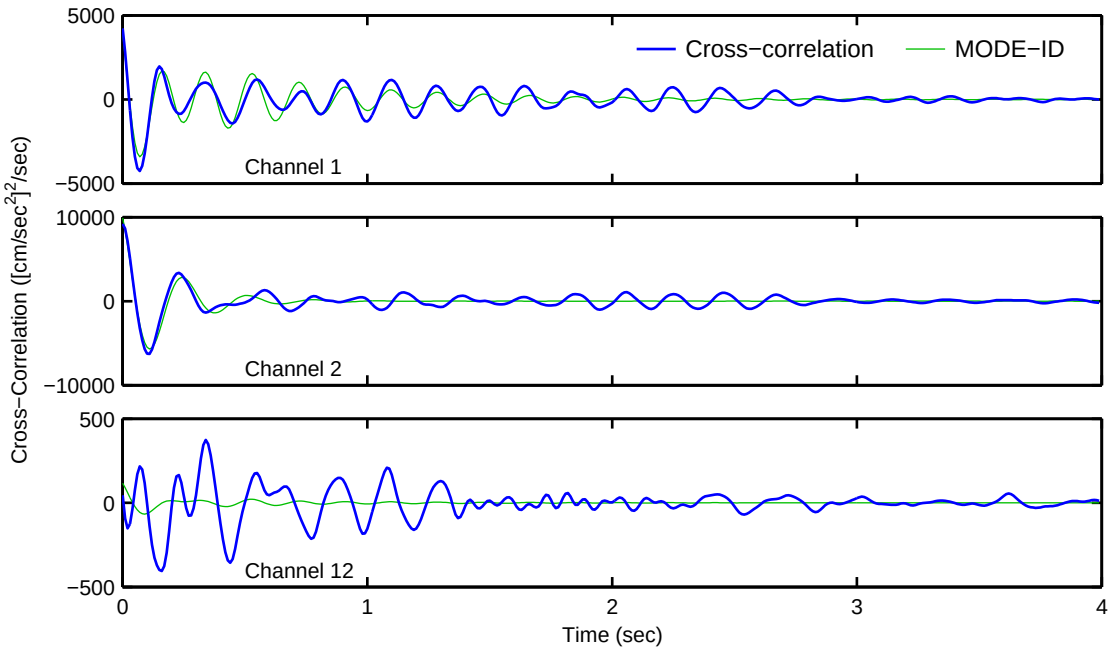

Figure 9.1: Cross-correlation functions for channels 1, 2 and 12 referenced to channel 2 compared to the free vibration computed by MODE-ID to match the cross-correlation functions

time histories would agree better with the records if the symmetric mode frequency was lower and the antisymmetric mode frequency was higher. The symmetric mode frequency does seem to be much too low, but it was also noted in Section 9.1 that MODE-ID finds the symmetric mode frequency lower than the antisymmetric mode frequency when the actual records are used. Making the foundation rigid forces the symmetric mode frequency to be higher than the antisymmetric mode frequency, since rigidity of the foundation has a larger effect on the symmetric mode. This may indicate that the symmetric mode frequency is actually much lower than the antisymmetric mode frequency when foundation flexibility is completely included, which is consistent with the MODE-ID cross-correlation results but not with the forced vibration results. It should be noted that the necessary spread in frequencies does not seem to be attainable for the finite element model with realistic material properties. However, in principle, a stiff dam and a soft foundation are necessary to attain a symmetric mode frequency that is significantly lower than the antisymmetric mode frequency. This would be consistent with the hypothesis given in Chapter 6 that, compared to the system excited by forced vibration, the dam concrete was unaffected and the foundation rock softened during the January 2001 earthquake.

There are unresolved issues dealing with precisely what system is identified by MODE-ID using earthquake records obtained during the January 13, 2001 earthquake. This is a topic that deserves further investigation. However, the calibrated finite element model does yield reasonable results and it can be used for the main purpose of this study, which is to investigate methods for generating spatially nonuniform ground motions to be used for dynamic structural analyses.

Chapter 10

Analysis with Northridge Earthquake Records

The records generated to replace the incomplete set from the 1994 Northridge earthquake (Section 3.3) can be used in nonlinear dynamic analyses. The methods for generating sets of nonuniform ground motion records can be compared to each other through their nonlinear responses; and the response to uniform input can be compared to the response to nonuniform input. A similar investigation was done by Mojtahedi and Fenves (2000), but the data providing information on ground motion nonuniformity had not yet been collected from the 2001 earthquake so it could not be used to guide generation of the nonuniform input.

10.1 Comparing Generation Methods

Unlike the 2001 earthquake, the ground motions generated from the Northridge earthquake base records (channels 9–11) induce a SCADA modeled response that is significantly nonlinear. This provides another opportunity to assess the methods for generating nonuniform ground motion. Results for several analyses run with various sets of ground motion input are included in Appendix C. The records at the locations corresponding to channels 12–17 must be generated from channels 9–11 by the methods described in Chapter 3. Records from eight of the methods summarized in Table 3.1 are discussed here. Also, two other sets of records that are modifications of method 1 are used. One of these is generated by method 1 with each record at

channels 12–17 shifted an extra 0.05 seconds later. The other set is generated with piecewise linear amplification functions like in method 1, but no delay is introduced to the records at channels 12–17. The methods used to generate the input ground motions for the nonlinear dynamic analyses are summarized in Table 10.1.

The input ground motion generated by method 1 is considered to be a representative example of the proposed process for generating nonuniform ground motion to be used in dynamic structural analysis. The computed response from this input ground motion will first be discussed in detail. Then the responses to the ground motion from the other methods of generation will be compared. The same finite element model that was used in Chapter 8 is used for all of these analyses. The model is nonlinear and the water is set to be 38 meters below the crest. The water was about 40 meters below the crest during the Northridge earthquake.

Method	Amplification/Phase
1	Piecewise linear approximation/ Frequency-dependent time delay
2	Piecewise linear approximation/ Constant, component-dependent time delay
3	Piecewise linear approximation/ Constant, component-independent time delay
4	Piecewise linear approximation/ Fourier transfer function phase
5	5% damped spectral displacement ratios/ Frequency-dependent time delay
9	0% damped spectral displacement ratios/ Frequency-dependent time delay
13	Fourier amplitude transfer functions/ Frequency-dependent time delay
16	Fourier amplitude transfer functions/ Fourier transfer function phase
1+0.05 sec	Piecewise linear approximation/ Frequency-dependent time delay with extra 0.05 sec delay
1 no delays	Piecewise linear approximation/ No time delay

Table 10.1: List of the abutment record generation methods used for nonlinear dynamic analysis of the Northridge earthquake

The acceleration and displacement time histories at the locations corresponding to channels 1–8 computed with ground motion generated by method 1 are shown in Figures 10.1 and 10.2. There are large acceleration pulses on the crest that are as high as 6.9g at channel 2. Notice that the large accelerations are only in the upstream direction (downstream is positive), so these accelerations occur when the crest of the dam is moving downstream and then it suddenly changes direction. This happens when the open joints close as the downstream motion compresses the dam in the arch direction. The system gets stiffer when the crest moves downstream and the

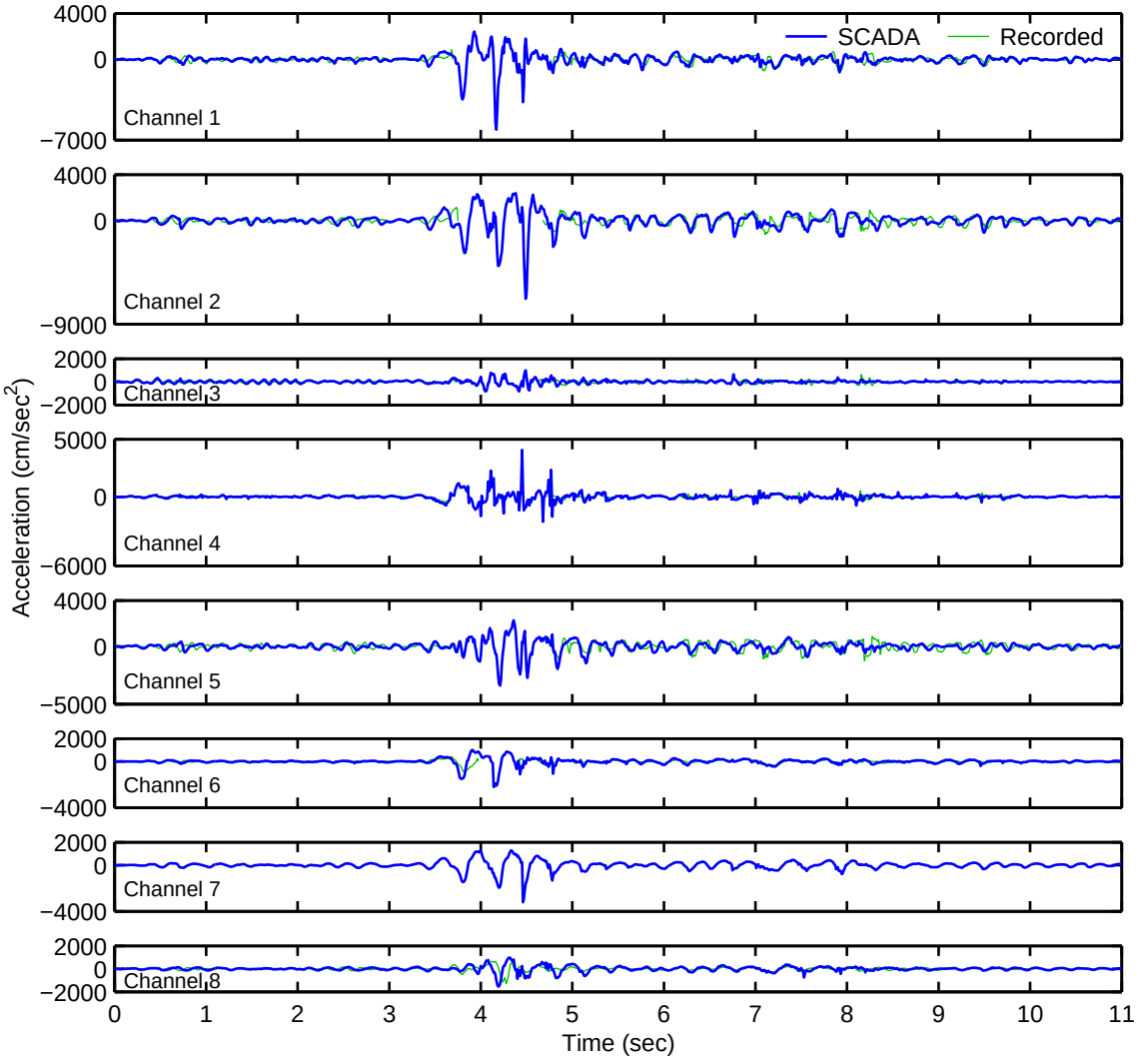

Figure 10.1: Acceleration time histories at locations corresponding to channels 1–8 computed from a nonlinear analysis of the Northridge earthquake compared to the partial records (method 1)

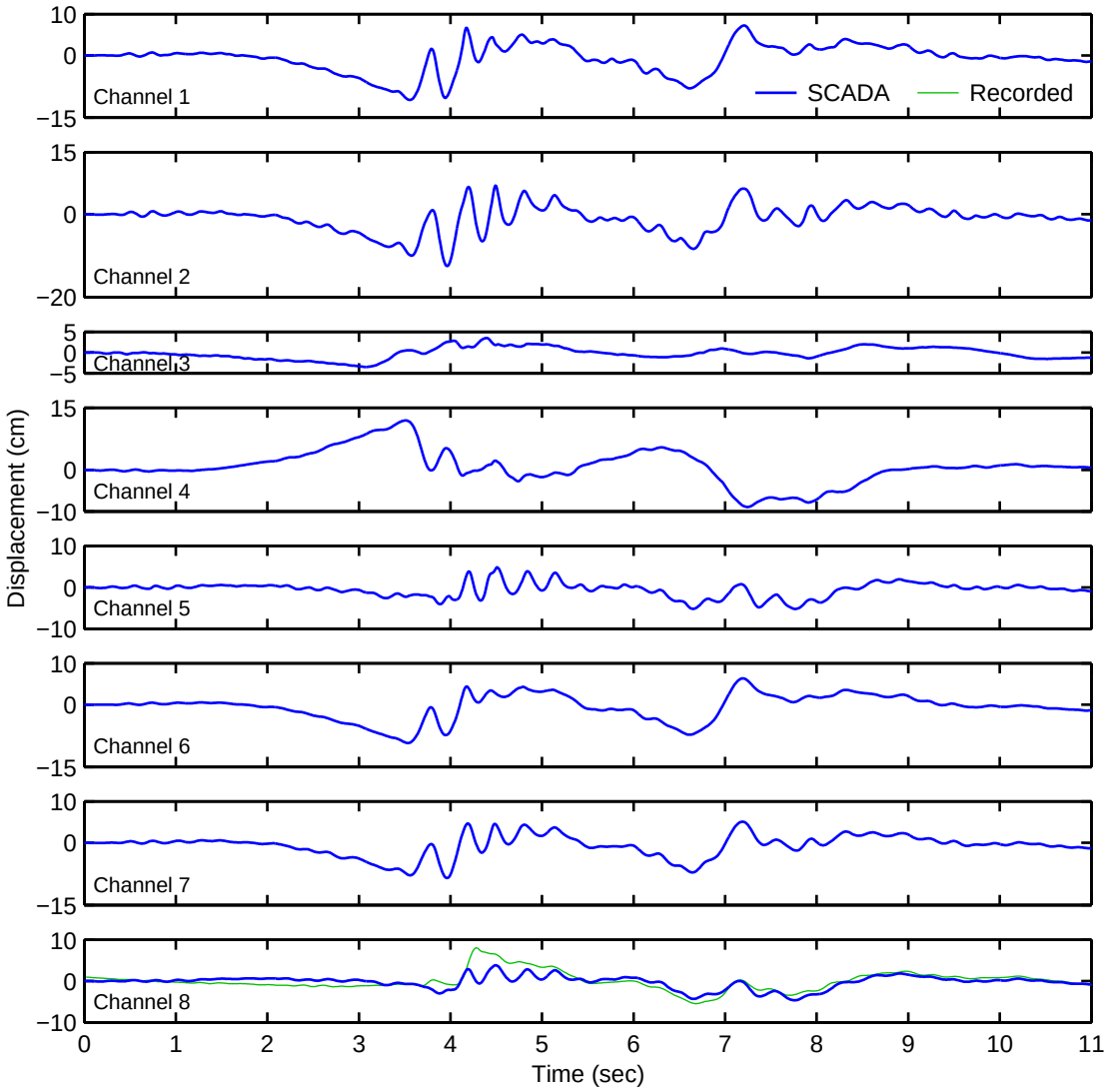

Figure 10.2: Displacement time histories at locations corresponding to channels 1–8 computed from a nonlinear analysis of the Northridge earthquake compared to the partial records (method 1)

joints close, which can be seen from the radial displacements on the crest, particularly channels 1 and 2. Notice that the positive peaks in displacement are sharper than the negative peaks. If a linear analysis is done, the accelerations are almost as high (over 5g) as in the nonlinear analysis and they are approximately equal amplitudes in both directions.

A test can be done to verify that the linear modeled accelerations are consistent with the input ground motion. If the linear model is supplied uniform ground motion

in the stream direction, the output can be theoretically approximated by the product of the modal participation factors, mode shape components and spectral acceleration at the modal frequencies. The participation factors were computed from the mass matrix and the mode shapes for the first two modes of the linear model subjected to uniform ground motion in the stream direction; and the 7% damped spectral accelerations were computed at the modal frequencies from an acceleration that is similar to the motion generated for channel 12. (The model has damping around 7% for the first two modes.) The theoretical values for the maximum acceleration at channel 2 for the first two modes are 3.3g and 4.5g, and the maximum acceleration at channel 2 computed by the linear model is 6.7g when it is subjected to uniform stream direction motion similar to the motion generated for channel 12. Therefore, the theoretical acceleration computed considering the first two modes is consistent with the maximum acceleration that is computed by the model. This indirectly verifies that the large accelerations computed for the nonlinear model shown in Figure 10.1 are theoretically realistic. However, the acceleration that the dam underwent during the Northridge earthquake was probably not that large, since the modal damping should be larger than it was during the 2001 earthquake. Also, recall from Chapter 8 that the acceleration computed from the finite element model did overestimate the acceleration recorded on January 13, 2001.

Of course, a more direct way to verify the nonlinear model is to compare the computed time histories to the recorded motion. The partial acceleration records are included in Figure 10.1 and the processed channel 8 displacement is included in Figure 10.2, since channel 8 was the only record on the dam body that was completely digitized and processed. The agreement of the computed acceleration with the sections recorded before and after the strongest motion is good. Figure 10.3 shows that the computed acceleration for channel 8 agrees fairly well with the recorded acceleration during the strongest motion, except that the computed acceleration is a little larger and leads the record slightly. The computed channel 8 displacement has an oscillation that does not appear in the record. This is a further indication that the modal damping was probably higher during the Northridge earthquake than it was

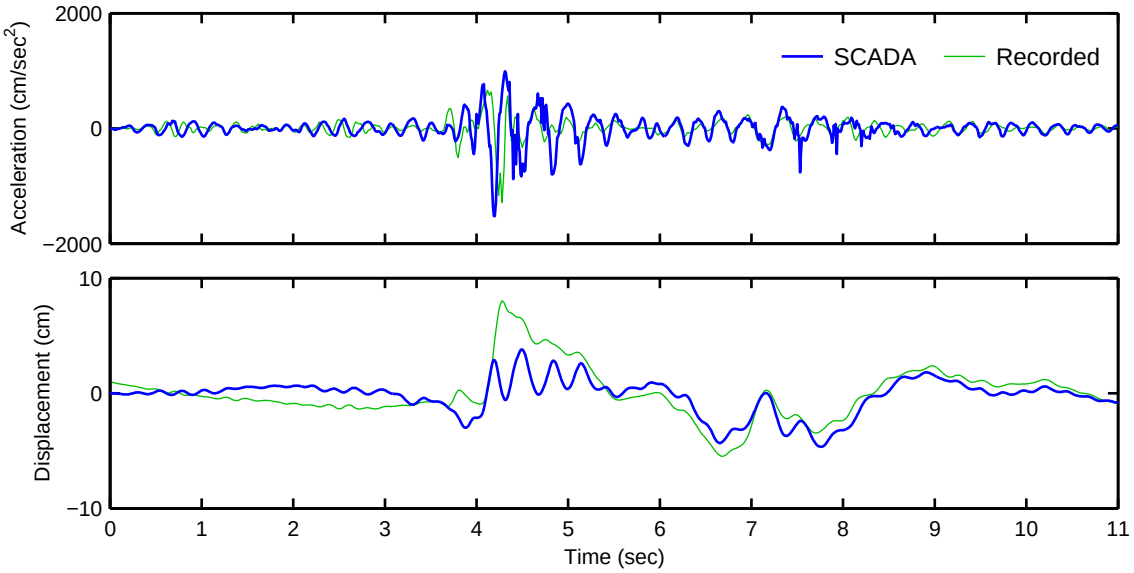

Figure 10.3: Acceleration and displacement time histories at the location corresponding to channel 8 computed from a nonlinear analysis of the Northridge earthquake compared to the actual records (method 1)

during the 2001 earthquake. However, the processing done by CSMIP to obtain the recorded displacement may have introduced errors that account for some of the discrepancy. The oscillation in the computed displacement between 4 and 5 seconds is at a frequency that is about 33% lower than the computed natural frequencies of the linear model (4.82 Hz and 5.02 Hz). Thus, the nonlinearity induced in the model has a significant effect on the stiffness of the system. This is an even more significant effect than the MODE-ID results in Section 4.3 indicate, but those results could not include the period of strongest motion.

Contours of maximum computed compressive stresses in the arch and cantilever directions are shown for both faces of the dam in Figures 10.4 and 10.5. The maximum joint opening and crack opening for each element computed during the analysis are shown in Figures 10.6 and 10.7. The tensile stresses are not shown, because the joints cannot carry tension and the cracks are an indication that the tensile stress in the cantilever direction reached the tensile strength of 3.79 MPa. The largest compressive stresses occur on the upstream face in the arch direction near the thrust block. The highest compressive stress is less than 16.5 MPa (2400 psi), so no crushing

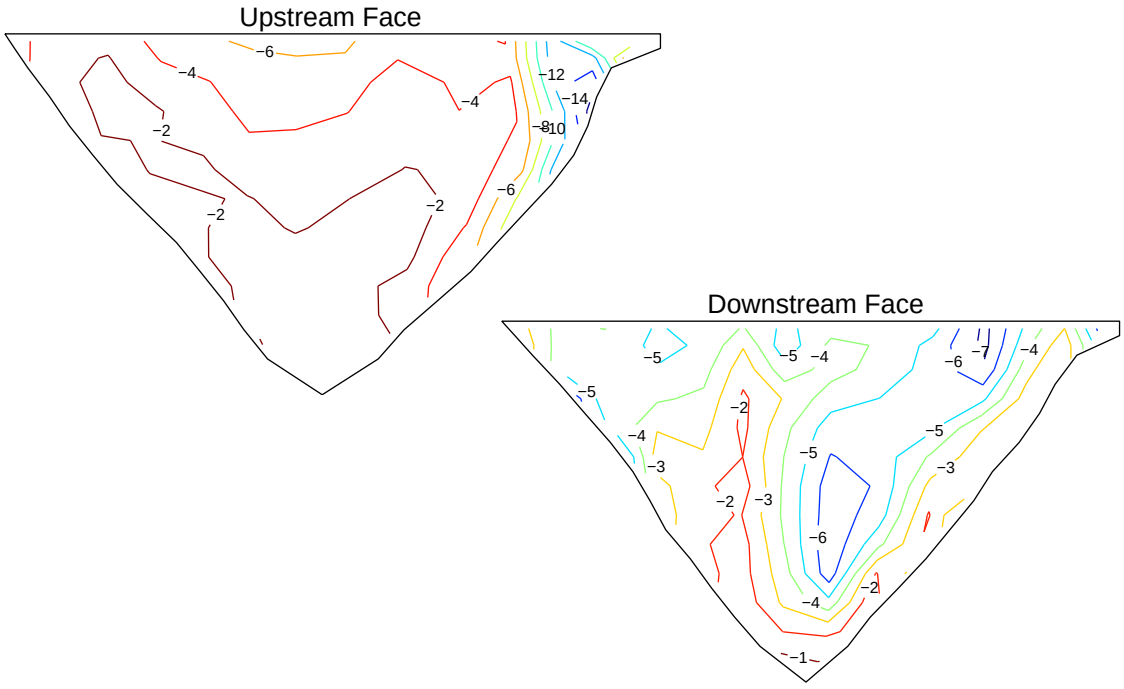

Figure 10.4: Maximum compressive arch stresses (MPa) computed during a nonlinear analysis with the Northridge earthquake input (method 1)

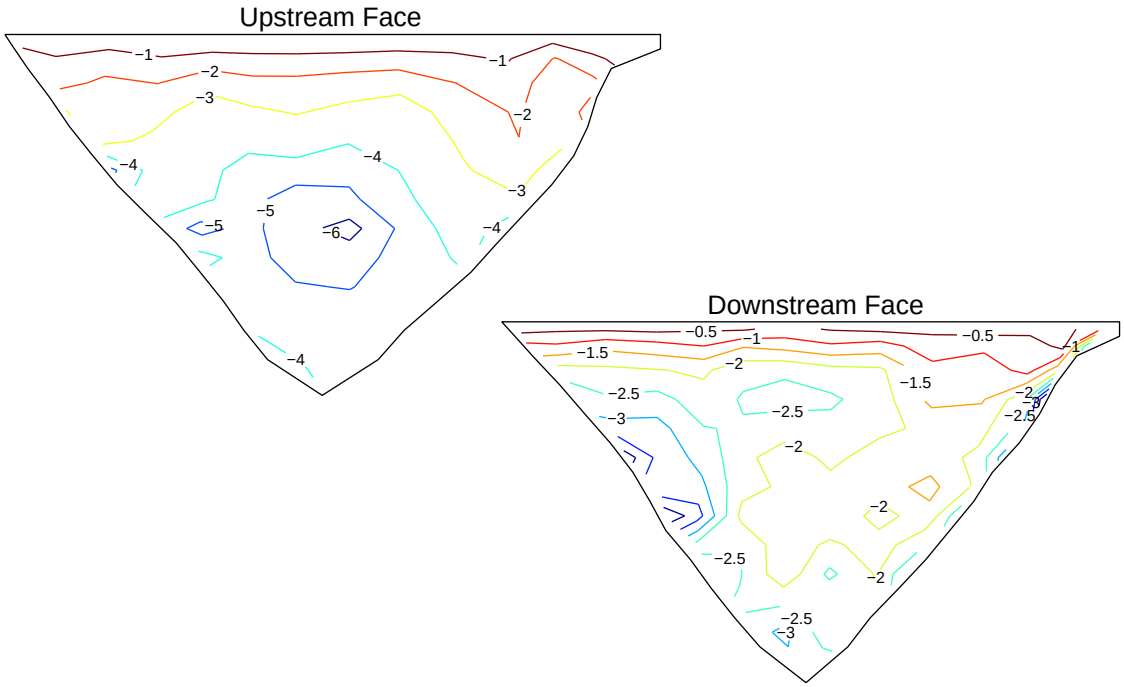

Figure 10.5: Maximum compressive cantilever stresses (MPa) computed during a nonlinear analysis with the Northridge earthquake input (method 1)

0.00	0.93	1.15	1.52	0.68	1.19	2.30	2.54	1.09	2.07	0.58	3.19	0.00	0.00
0.00	0.82	1.06	1.64	0.75	1.08	2.24	2.40	0.89	2.05	0.87	2.90	0.00	0.00
	0.57	1.10	1.80	0.98	0.95	2.12	2.17	0.76	1.94	1.45	2.53	0.00	
	0.24	0.98	1.76	1.18	0.81	1.82	1.96	0.65	1.80	1.86	1.75	0.00	
		0.90	1.55	1.28	0.63	1.32	1.66	0.64	1.65	1.72	1.06		
		0.47	1.42	1.25	0.82	0.79	1.20	0.83	1.57	1.10	0.43		
			1.39	1.03	0.51	0.42	1.18	0.93	1.35	0.95			
			0.60	0.68	0.30	0.44	1.15	1.03	0.92	0.34			
				0.62	0.53	0.41	1.07	1.03	0.70				
				0.26	0.39	0.33	1.06	0.68	0.21				
					0.32	0.21	0.85	0.48					
					0.11	0.09	0.51	0.15					
						0.04	0.15						

Figure 10.6: Maximum joint opening (cm) computed during a nonlinear analysis with the Northridge earthquake input (method 1)

0.00	0.00	0.00	0.00	0.00	0.00	0.00	0.00	0.00	0.00	0.00	0.00	0.00	0.00
0.12	0.00	0.00	0.00	0.00	0.00	0.00	0.00	0.00	0.00	0.00	0.00	0.00	0.00
	0.00	0.00	0.00	0.00	0.00	0.00	0.00	0.00	0.00	0.00	0.00	0.00	
	0.00	0.00	0.00	0.00	0.00	0.00	0.00	0.00	0.00	0.00	0.00	0.27	
		0.00	0.00	0.00	0.00	0.00	0.00	0.00	0.00	0.00	0.00		
		0.32	0.00	0.00	0.00	0.00	0.00	0.00	0.00	0.00	0.26		
			0.00	0.00	0.34	0.51	0.00	0.00	0.00	0.00			
			0.54	0.41	0.00	0.00	0.49	0.31	0.00	0.26			
				0.00	0.00	0.00	0.00	0.00	0.00				
				0.29	0.00	0.00	0.00	0.00	0.22				
					0.00	0.00	0.00	0.00					
					0.00	0.00	0.00	0.00					
						0.00	0.00						

Figure 10.7: Maximum crack opening (cm) computed during a nonlinear analysis with the Northridge earthquake input (method 1)

in compression would be expected. On the downstream face, there is a region of high arch compression that extends from the crest near the thrust block downward to the center of the dam. The compressive stresses in the cantilever direction are generally higher near the base of the dam.

The maximum joint opening is greater than 3 cm at the thrust block and greater than 2 cm near the center of the crest. These are significant, but the joint opening at the thrust block is not as large as the permanent opening of about 5 cm that was observed after the Northridge earthquake. In the actual earthquake, a large section of the foundation slid away from the dam. This permanent displacement is not included in the input ground motion, so the large permanent joint opening is not modeled. The elements with no joint opening are the elements that do not have joints, but the arch tension in some of the thrust block elements is close to the tensile strength of concrete. This tension could cause vertical cracks, and a diagonal crack extending down from the open joint was observed in the thrust block after the Northridge earthquake. There is horizontal cracking in the dam model, but the opening is smaller than 1 cm and most of the cracked elements are along the abutments. Most of the cracks open at both faces of the dam with the larger openings at the downstream face. There is also some lateral sliding in the cracks that is less than 0.5 cm. (The sliding is not shown.) The minimal amount of cracking in the dam is consistent with the observations of Pacoima Dam after the Northridge earthquake. Some cracking was seen near the thrust block along the left abutment and there was a permanent lateral displacement in one of the cracks, but no significant cracking was observed in the rest of the dam. The observations of damage after the Northridge earthquake are described in a report to the Los Angeles County Department of Public Works (Morrison Knudsen, 1994).

The response to the ground motion generated using piecewise linear amplification functions and approximate frequency-dependent time delays (method 1) appears to be a reasonable approximation to the Northridge earthquake response. The responses to the ground motions generated from other methods, which are described in Table 10.1, are shown in Appendix C and the maximums of these responses are summarized in Table 10.2. Generally, the response to ground motion generated by method 1 is

Method	Arch Compression (MPa)	Cantilever Compression (MPa)	Joint Opening (cm)	Number of Elements Cracked	Crack Opening (cm)
1	-16.38	-6.38	3.19	13	0.54
2	-21.04	-6.63	3.56	17	1.49
3	-18.84	-6.16	3.54	17	1.31
4	-19.30	-8.96	6.91	32	1.03
5	-24.47	-6.95	4.55	20	0.92
9	-22.27	-7.11	4.65	19	0.80
13	-11.12	-11.68	4.12	20	2.21
16	-15.58	-10.24	8.33	30	1.70
1+0.05 sec	-18.42	-7.77	3.61	18	1.56
1 no delays	-16.05	-7.14	3.18	10	0.61

Table 10.2: Maximum responses computed from SCADA analyses of the Northridge earthquake with input ground motion generated from various methods

less severe than the other responses. Methods 2 and 3 differ from method 1 only in the phase that is used to delay the abutment ground motions. The computed time histories and stress distributions are similar for all three methods, but there is larger cracking along the abutments and higher arch compression at the thrust block with constant delays (methods 2 and 3). The differences in the response are probably due to the larger delays in the input displacements along the abutments produced by the constant delays. However, the differences are not very significant and the constant delays give the more severe response. Also, notice that the differences between method 2 and method 3 are small, so including smaller delays in the vertical components does not have a significant effect. Therefore, using constant delays, even delays that are component-independent, may be a satisfactory approximation and are more likely to yield conservative results.

Method 4 also uses piecewise linear amplification like methods 1, 2 and 3, but the delays come from the exact Fourier phase difference between the 2001 earthquake records. The response to ground motion generated by method 4 differs more than the other methods. The time histories have noticeable differences and the computed channel 8 acceleration is actually better synchronized with the record when method 4 is used. The stress distribution is similar to the other methods except that there

is much larger arch compression on the upstream face at the center of the crest and larger cantilever compression on the upstream face along the left abutment. The joint opening and cracking are more severe, particularly in the center of the dam away from the abutments. The Fourier phase from the 2001 records yields results that are more severe than the various approximate phase functions. The reason for this is not known, but it is not certain whether this earthquake specific phase is realistic for a general event and analysis of more data is necessary to clarify this. Thus, the approximate relative phases for time delays that are based on physical considerations are preferred for the implementation of the general ground motion generation process.

Methods 5 and 9 generate ground motions using the same phase as method 1, but with amplification from 5% damped and 0% damped spectral displacement ratios, respectively, instead of piecewise linear approximations. The general character of the responses from ground motion produced by methods 5 and 9 is very similar to the response produced by method 1 ground motions. However, both responses have larger stresses and joint opening with more cracking than method 1. Therefore, the piecewise linear amplification may not be sufficient to produce a conservative result. Averaging the spectral ratios over several events, if data were available, should provide smooth functions that are general but induce a larger modeled response than the piecewise linear functions.

Methods 13 and 16 use the amplitude of the Fourier transfer functions between the 2001 earthquake records as amplification. The output acceleration time histories do not agree with the partial records very well, like the input accelerations generated for the Northridge earthquake with the Fourier amplitude transfer functions that are discussed in Section 3.3. The stress distributions in both the arch and cantilever directions are significantly different than those from method 1 ground motion; and the joint opening and cracking are larger, especially in the center of the dam. However, the computed acceleration time histories are substantially unlike the records, so the results are not considered to be realistic.

The ground motions generated by method 1 with an extra 0.05-second delay included in the abutment channels (12–17) can test the impact of slower wave speeds in

the foundation rock for motion that is of larger amplitude than the 2001 earthquake. The response is similar to the response from the method 1 records, but with larger stresses, joint opening and cracking. The computed channel 8 acceleration is better synchronized with the recording. Thus, larger delays may be realistic and the impact they have on the computed response can be important. More study is required to investigate the nonlinear effect of ground motion amplitude on the travel times of the seismic waves along the abutments. On the other hand, if the ground motion is generated with no time delays in the abutment records, the response does not differ very much from the response from ground motion with delays. Without delays the stresses and cracking are only a little less severe along the abutments. Thus, the travel time of the seismic waves is a factor that should be considered, but topographic amplification is the more important effect for modeling the response of the dam.

The process proposed for generating nonuniform ground motion from motion at a single location produces a set of ground motions that can be used in a finite element analysis with reasonable results. Generating nonuniform motion with the level of simplicity captured by methods 1 or 2 is recommended. However, the amplification functions should be averaged over several events from more exact data as from method 9. More study and more data are necessary to refine the process and further define the importance that ground motion amplitude has on the nonuniformity.

10.2 Increased Damping, Softer Foundation, Joint Keys Removed

As mentioned in the previous section, the modal damping in the SCADA model may need to be increased for simulating the Northridge earthquake. Energy is dissipated by cracking and sliding that was not a factor during the January 13, 2001 earthquake. Also, the nonlinear system oscillates at a lower frequency with Northridge earthquake input than it does with 2001 earthquake input. The Rayleigh damping is lower at this frequency than it is at the natural frequencies of the linear model. Therefore, an

analysis was done with increased damping. Another analysis was done with the model described in Section 7.6 that has a region of softened foundation at the upper left abutment. This is an attempt to simulate the effect of the fractures that occurred during the Northridge earthquake. This analysis was run with the original modal damping. Finally, an analysis was done with the keys that prevent lateral sliding in the joints removed, also with the original modal damping. For all three of these analyses, the Northridge earthquake ground motion generated by method 1 was used as input. The computed responses are included in Appendix C.

The damping was increased to be 10% of critical at 4 Hz, compared to 7% at 5 Hz. The stresses, joint opening and cracking are reduced in the center of the dam, but they are not affected significantly along the abutments. The peak acceleration at channel 2 is reduced to 5.0g from 6.9g; and the amplitude of the computed channel 8 acceleration agrees better with the recording, but the oscillation in the computed channel 8 displacement is not damped out nearly enough to agree with the recorded displacement (see Figure 10.8). Perhaps, there was even more energy dissipation in Pacoima Dam during the Northridge earthquake, possibly in the form of radia-

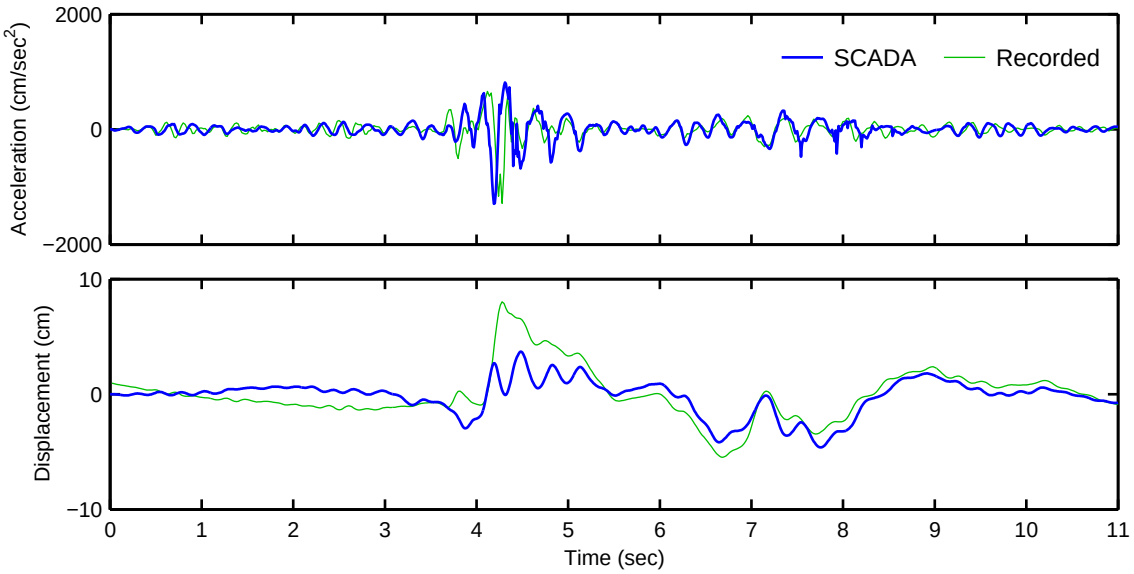

Figure 10.8: Acceleration and displacement time histories at the location corresponding to channel 8 computed from a nonlinear analysis of the Northridge earthquake with increased damping compared to the actual records (method 1)

tion damping, which is not explicitly included in the model. Mojtahedi and Fenves (2000) believed that the lack of radiation damping was an important factor in causing overestimation by the computed motions. However, the difference in the computed and recorded displacements may be due to another unknown cause. Perhaps, the processing done to obtain the recorded displacement removed some oscillation.

The response of the model with a softened region of foundation at the left abutment is very similar to the response with a homogeneous foundation. The compressive stresses in the dam along the upper left abutment are slightly reduced, but the computed motion is mostly unaltered. The simulation of foundation damage does not have a significant impact on the response of the dam.

An analysis was done with the joint sliding keys removed even though there are keys present in Pacoima Dam. The keys are beveled so when a joint is open there is some freedom for lateral sliding, and in the worst case, the keys could be sheared off. The maximum joint sliding is shown in Figure 10.9. The joint sliding has a significant effect on the overall response. The arch compressive stress and joint opening are larger

0.00	1.64	-5.68	-9.59	-8.37	-8.09	10.29	16.35	7.67	3.74	-2.91	-2.53	0.00	0.00
0.00	1.24	-5.01	-9.07	-7.28	-6.86	9.15	14.17	6.66	-2.95	-2.43	-2.36	0.00	0.00
	0.78	-4.13	-8.29	-5.62	-5.24	7.58	11.59	5.43	-2.59	-2.07	-2.21	0.00	
	0.27	-2.91	-6.85	-5.23	-3.68	6.08	9.06	4.29	-2.01	-1.78	-1.60	0.00	
		-1.82	-5.23	-5.19	-1.79	4.69	7.11	3.11	-1.36	-1.78	-0.86		
		-0.77	-3.71	-5.35	1.86	3.16	5.13	-2.45	-1.27	-1.56	-0.23		
			-4.09	2.85	1.58	2.04	2.77	-1.66	-1.53	-1.12			
			-1.65	2.98	-1.47	1.97	1.08	-1.06	-1.63	-0.43			
				-2.69	1.03	1.53	0.71	-1.12	-1.26				
				-1.04	0.84	0.70	0.46	-1.21	-0.46				
					0.82	0.32	0.19	-0.97					
					0.28	0.19	-0.14	-0.30					
						0.11	-0.09						

Figure 10.9: Maximum joint sliding (cm) computed during a nonlinear analysis of the Northridge earthquake with joint sliding allowed (method 1)

in the interior of the dam near the crest, and there are large cracks lower in the dam. There are also large compressive cantilever stresses on the upstream face where the cracks open. These stresses are large because the surface area of the concrete in contact is decreased when the cracks are open at the downstream face. The effect on the computed motions is significant and the computed channel 8 displacement actually has less oscillation like the recorded displacement. However, this scenario is not a realistic simulation of the Northridge earthquake because the joint sliding is too large at the center of the crest compared to the joint opening. The keys in the joints would need to be sheared off to accommodate this amount of sliding and that did not occur.

10.3 Uniform Ground Motion Input

Uniform ground motion is a common assumption that has been made in dynamic analyses of arch dams. The nonuniform ground motion generated from the Northridge earthquake base records can be used to assess the limitations of this assumption. Again, the nonuniform records generated by method 1 are used. For this comparison, the same finite element model that is used in Section 10.1 is used here, except that the reservoir level is raised to about 20 meters below the crest. This approximately corresponds to the elevation at the invert of the spillway, so this is a full reservoir condition for Pacoima Dam barring the simultaneous occurrence of earthquake and flood. Three different sets of uniform 3-component ground motion are used: the base recordings from the Northridge earthquake (channels 9–11), the generated right abutment motions at about 80% height of the dam (channels 12–14) and the generated left abutment motions at about 80% height of the dam (channels 15–17). The two sets at 80% height are reasonable examples of ground motion that could be used in a uniform analysis. The contours of compressive stress and the response pictures of joint opening and cracking for nonuniform input and the three sets of uniform input are given in Appendix C.

The response of the model to nonuniform input with the water 20 meters below the

Input	Arch Compression (MPa)	Cantilever Compression (MPa)	Joint Opening (cm)	Number of Elements Cracked	Crack Opening (cm)
Nonuniform	-16.58	-7.74	2.84	12	0.90
Uniform (Base)	-4.87	-3.40	1.13	0	0.00
Uniform (Right Abutment)	-19.64	-11.75	10.84	28	4.99
Uniform (Left Abutment)	-11.89	-9.00	7.17	21	4.65

Table 10.3: Maximum responses computed from SCADA analyses with nonuniform and uniform input ground motion from the records generated for the Northridge earthquake by method 1

crest is very similar to the response with the water 38 meters below the crest, except that the stresses and openings are slightly larger in the interior of the dam. The maximums of the responses to the nonuniform ground motion and the three different uniform input motions are summarized in Table 10.3. The ground motion from the base of the dam (channels 9–11) gives a much smaller response than the nonuniform input. There is actually no cracking in the dam. The responses to the uniform ground motion from the records generated for the right abutment (channels 12–14) and left abutment (channels 15–17) locations are generally larger than the nonuniform input. The joint opening and cracking are much more severe in the interior of the dam for uniform input than they are anywhere in the dam for nonuniform input. The maximum joint opening and crack opening computed with uniform input defined by channels 12–14 are shown in Figures 10.10 and 10.11. The stresses are also larger in the interior of the dam for the uniform input, but nonuniform input does yield comparably large compressive arch stresses at the upper part of the left abutment. Contours of maximum arch compression computed with the uniform input defined by channels 12–14 and the nonuniform input are shown in Figures 10.12 and 10.13.

The responses to uniform input from the right and left abutment records are somewhat similar, but the right abutment records generally yield a larger response.

0.00	0.80	1.86	2.71	1.95	4.83	7.03	10.84	4.75	2.31	1.83	1.53	0.00	0.00
0.00	0.77	1.87	3.01	3.10	4.61	6.20	9.17	4.69	3.27	2.08	1.50	0.00	0.00
	0.69	1.75	3.29	5.10	3.76	4.29	5.23	3.44	3.72	2.45	1.46	0.00	
	0.36	1.33	3.06	4.20	2.42	2.96	1.52	1.62	2.35	2.40	1.22	0.00	
		1.02	2.67	2.98	1.06	2.56	1.40	0.60	2.14	1.98	0.85		
		0.42	1.81	2.38	0.29	1.44	1.18	0.36	2.13	1.32	0.36		
			1.01	1.59	0.94	0.59	0.82	0.29	1.82	0.97			
			0.31	1.23	0.44	0.19	0.43	0.27	1.42	0.34			
				0.79	0.31	0.12	0.30	0.38	0.92				
				0.26	0.37	0.08	0.14	0.29	0.30				
					0.38	0.05	0.14	0.34					
					0.16	0.03	0.11	0.13					
						0.04	0.04						

Figure 10.10: Maximum joint opening (cm) computed during a nonlinear analysis with uniform ground motion input (method 1 right abutment channels 12–14)

0.00	0.00	0.00	0.00	0.00	0.00	0.00	0.00	0.00	0.00	0.00	0.00	0.00	0.00
0.00	0.00	0.00	0.00	0.00	0.00	0.00	0.00	0.00	0.00	0.00	0.00	0.00	0.00
	0.00	0.00	1.03	0.00	0.00	2.48	1.71	0.52	0.00	0.00	0.00	0.00	
	0.00	0.00	0.00	2.09	3.15	4.12	4.99	2.95	0.73	0.00	0.00	0.00	
		0.00	0.00	0.00	0.00	0.00	0.00	0.00	0.26	0.00	0.00		
		0.00	0.00	0.45	0.30	0.00	0.00	0.75	1.04	0.00	0.00		
			0.00	0.98	1.18	0.00	0.00	0.48	0.00	0.00			
			0.00	0.00	2.26	4.28	4.08	2.22	0.27	0.75			
				0.00	0.00	0.61	0.99	1.17	0.90				
				0.00	0.00	0.00	0.00	0.00	0.00				
					0.00	0.00	0.00	0.00					
					0.00	0.00	0.00	0.00					
						0.00	0.00						

Figure 10.11: Maximum crack opening (cm) computed during a nonlinear analysis with uniform ground motion input (method 1 right abutment channels 12–14)

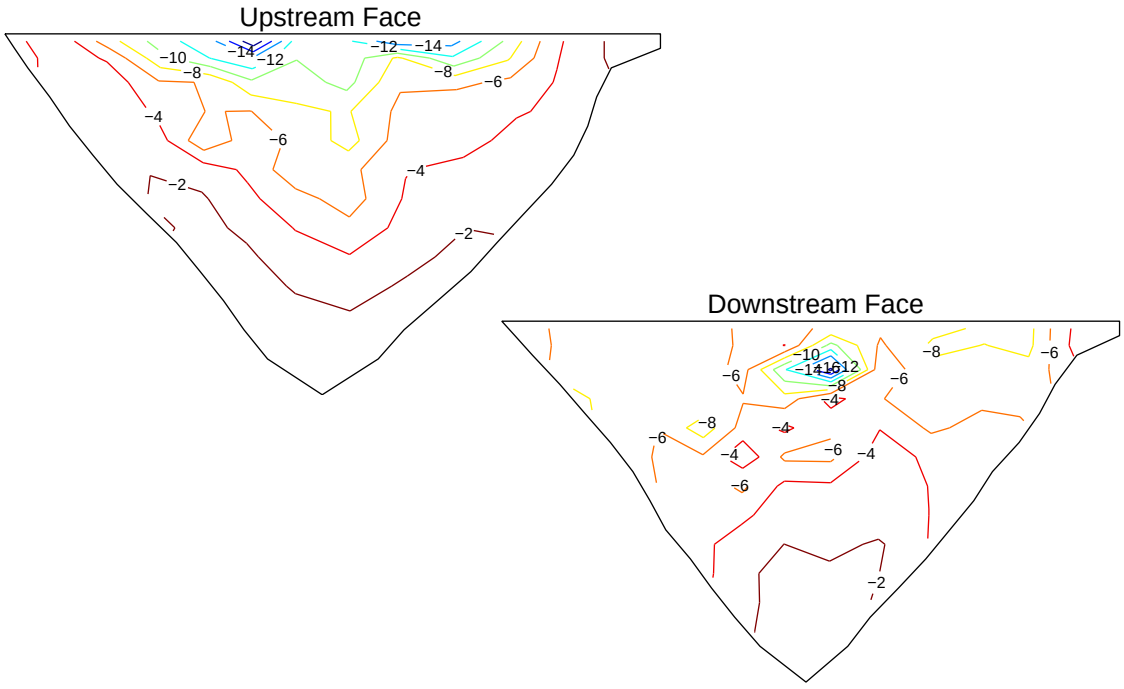

Figure 10.12: Maximum compressive arch stresses (MPa) computed during a nonlinear analysis with uniform ground motion input (method 1 right abutment ch. 12–14)

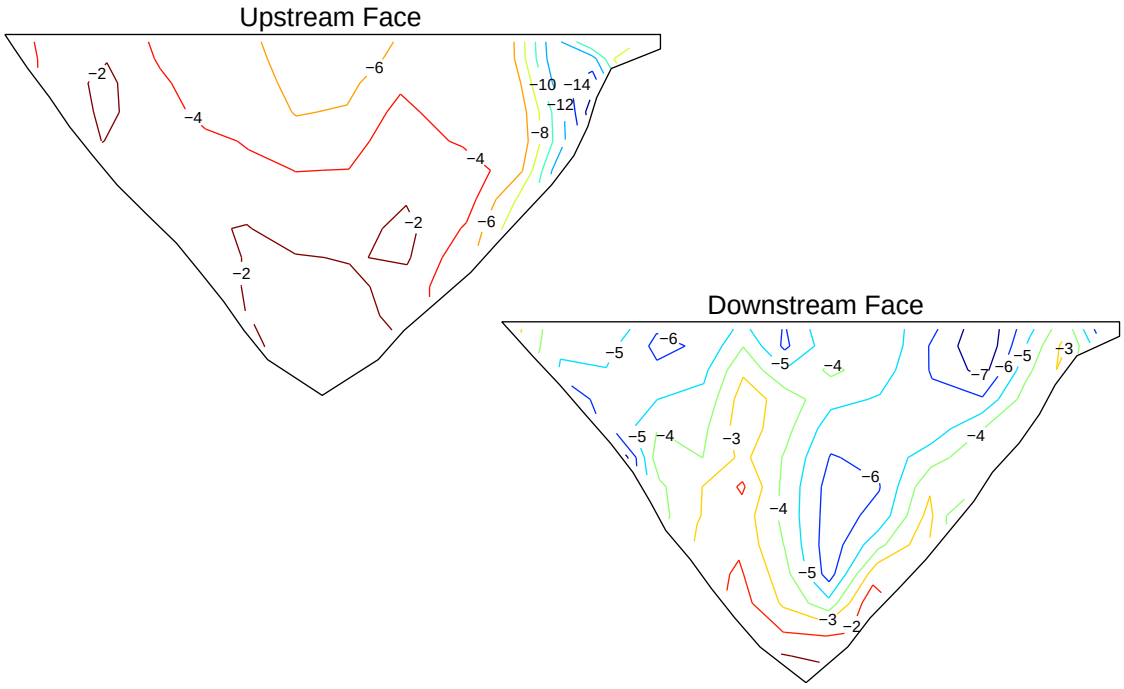

Figure 10.13: Maximum compressive arch stresses (MPa) computed during a nonlinear analysis with nonuniform ground motion input (method 1)

These two sets of uniform input were separately applied one component at a time. In both cases, the strongest response was produced with the stream direction input (channels 12 and 15). This indicates that the stream direction ground motion is the most important component for response to uniform ground motion, so the generated channel 12 record (right abutment) is more severe than the generated channel 15 record (left abutment) when method 1 is used to generate the ground motion. The importance of the stream component for nonuniform input is even further illustrated by the fact that the cross-stream component is obviously larger on the left abutment (channel 17) than the right abutment (channel 14), but the response is larger when 3-component uniform input is supplied from the right abutment records.

One might want to say that the three variations of uniform input ground motion yield responses that are lower and upper bounds for the response to nonuniform input. However, the severity of the responses is not the only difference between uniform and nonuniform input. The response of the dam to uniform ground motion has a significantly different character than nonuniform motion. Generally, for uniform input, the stresses and joint opening are largest in the center of the dam away from the abutments. Cracks open mostly in the center of the dam with very little cracking along the abutments. The major difference between the responses to uniform and nonuniform input is the pseudostatic component of the response. The pseudostatic response is that which would occur if the ground motions are applied very slowly so that inertial and damping effects are negligible. For uniform input, the pseudostatic component is a rigid body motion, but the differential displacements in the nonuniform input cause pseudostatic deformations of the dam, which are most significant near the abutments.

10.4 Pseudostatic Analysis

The pseudostatic response of the model was computed for the nonuniform input generated from the Northridge earthquake base records by method 1. The reservoir is omitted, but a hydrostatic pressure is applied for the static part of the analysis up

to 20 meters below the crest. Results of the analysis are shown in Appendix C. The displacement time histories computed at locations corresponding to channels 2–4 are compared from the pseudostatic analysis and the full dynamic analysis in Figure 10.14. The dynamic analysis does include the pseudostatic component of the response. The dynamic analysis that is compared here uses the model with the water 20 meters below the crest. There is significant dynamic oscillation at channel 2, but the motion at channels 3 and 4 is dominated by the pseudostatic component. Channel 2 is radial at the center of the crest, channel 3 is vertical and channel 4 is tangential at the center of the crest. The time histories indicate that most of the dynamic oscillation of the dam is in the stream direction.

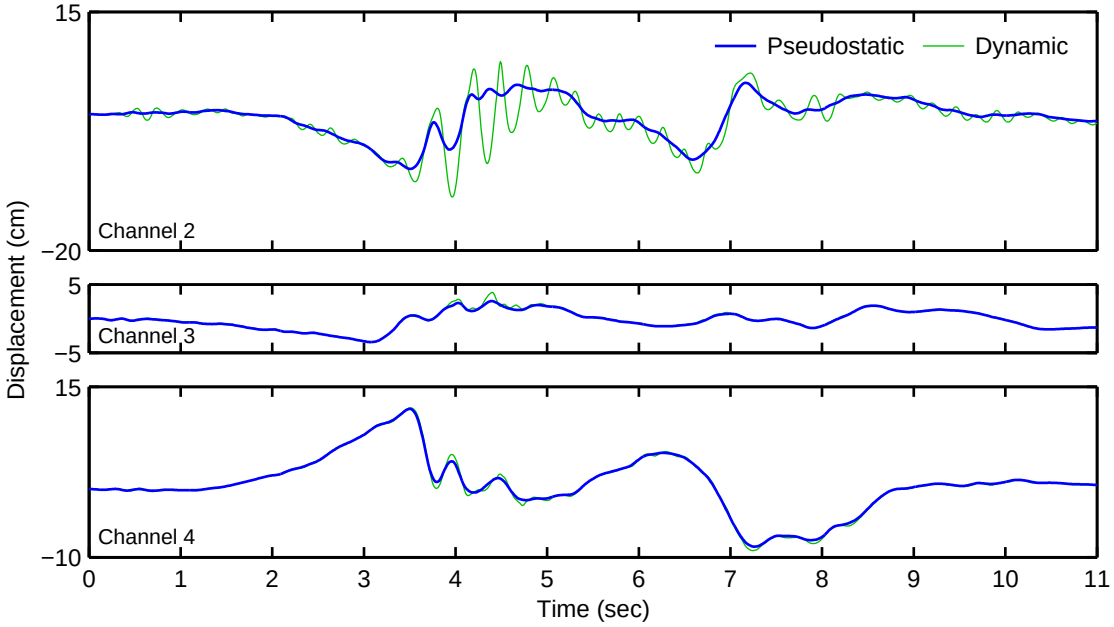

Figure 10.14: Displacement time histories at locations corresponding to channels 2–4 computed from a nonlinear pseudostatic analysis compared to the time histories from a nonlinear dynamic analysis (method 1)

The maximum compressive stresses in the arch direction are shown in Figure 10.15. On the upstream face, the pseudostatic stresses are large along the upper abutments, particularly the left abutment. On the downstream face, the pseudostatic stresses are largest near the upper left abutment, but there are also significant compressive stresses in the entire half of the dam that is closer to the left abutment. The stresses

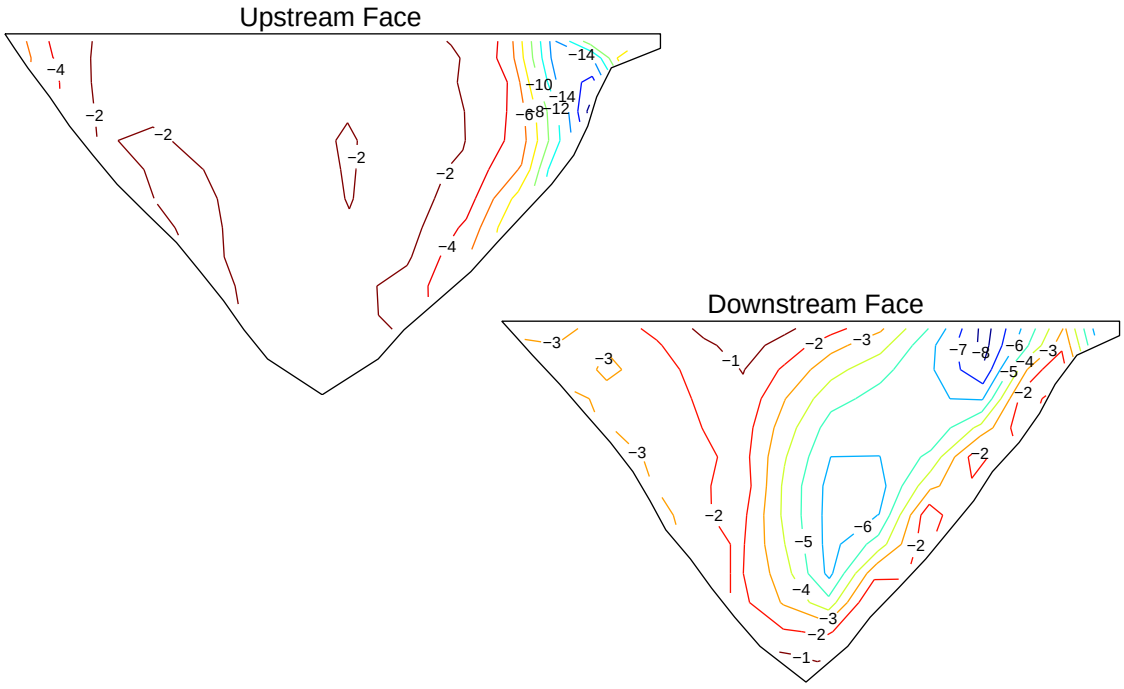

Figure 10.15: Maximum compressive arch stresses (MPa) computed during a nonlinear pseudostatic analysis with nonuniform ground motion input (method 1)

for the dynamic analysis along the abutments and in the center of the downstream face are dominated by these pseudostatic stresses, and the dynamic effects are important near the center of the crest. The maximum joint opening throughout the dam has a similar distribution to the arch compression on the upstream face. Like the stresses, the joint opening along the abutments is pseudostatic and the joint opening in the interior of the dam is caused by oscillation of the dam. Cracking is minimal for the pseudostatic analysis. Only three elements along the abutments crack and the opening is small.

The high stresses at the upper left abutment are not the result of a stress concentration that may be present, because the singularity would also cause similar high stresses for uniform ground motion input. However, that is not the case so any stress concentration is too weak to show an effect. The large pseudostatic stresses at the upper left abutment appear to be related to the large cross-stream displacement in the generated input along the left abutment. The largest amplification of displacement in the generated ground motions is the cross-stream component along the left abut-

ment. Channel 17 illustrates this large displacement. The high stresses do not arise from an overall compression of the arch of the dam, but from the local differential in displacement input as the elevation increases along the abutment. This is shown by prescribing the ground motions generated for the left abutment to both abutments at the same time, so that the arch is not compressed along the crest. The pseudostatic analysis with this input shows large arch compression at both abutments (see Figure 10.16). Thus, the large input cross-stream displacement causes large stresses at each abutment at the times when the input motion locally compresses each side of the dam. This effect is the reason that nonuniform ground motions generated by methods 5 and 9 induce larger maximum arch compression at the upper left abutment than ground motion from method 1. The generated channel 17 displacement is larger in the direction causing compression of the dam for methods 5 and 9 than it is for method 1.

While the pseudostatic component of the response does not cause significant crack-

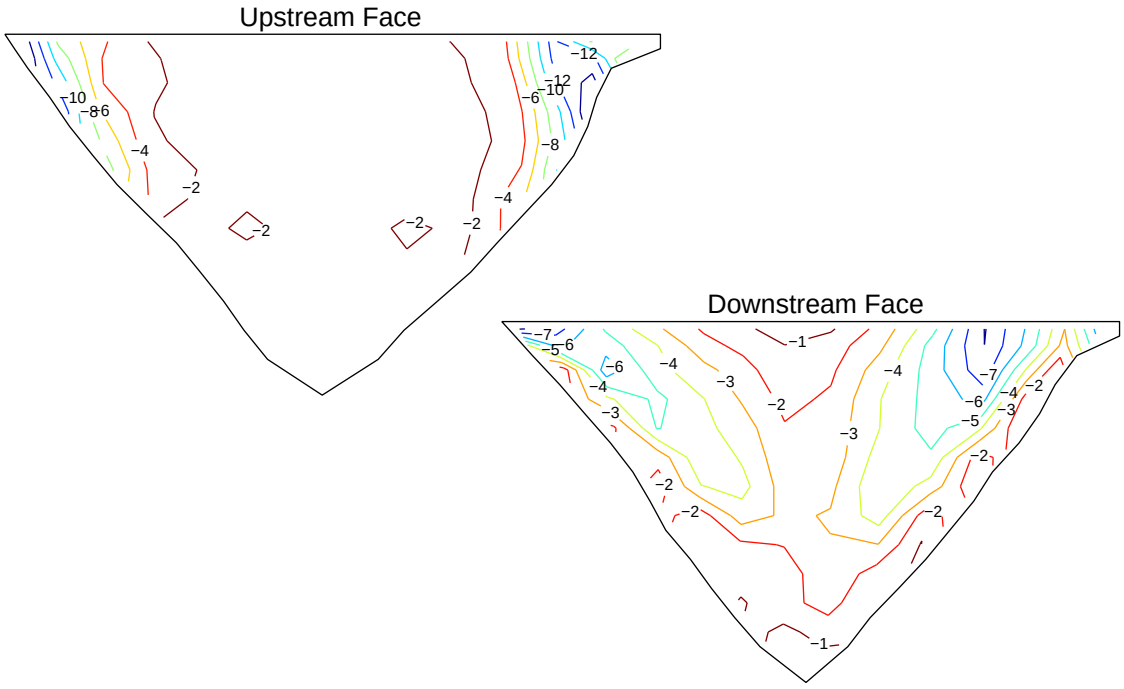

Figure 10.16: Maximum compressive arch stresses (MPa) computed during a nonlinear pseudostatic analysis with nonuniform ground motion input (method 1) with the left abutment input also prescribed on the right abutment

ing, the pseudostatic stresses and joint opening are an important part of the response for nonuniform ground motion. The pseudostatic component of the response to nonuniform ground motion has been observed to be important by other researchers (Lin et al., 1996; Mojtahedi and Fenves, 2000), but in another study with nonuniform ground motion it was not as important (Nowak and Hall, 1990). Therefore, the degree of importance of the pseudostatic response can depend significantly on the nonuniform seismic input that is used, and care should be taken in choosing the input. The displacements, in particular, need to be carefully integrated from the accelerations. Recall that the method 1 generated ground motions for the 2001 earthquake agree best in terms of displacements when being compared to the actual records. This is good since accurately capturing the pseudostatic response is important. The approach used here to generate ground motions shows promise based on the available data, but more data and more analysis is necessary for validation.

Chapter 11

Summary and Conclusions

The occurrence of a relatively small earthquake (magnitude 4.3) on January 13, 2001, at Pacoima Dam presented an opportunity to study the spatial nonuniformity of the ground motion along the abutments of an arch dam. The ground motion is amplified by the topography of the canyon in which the dam is situated, and assuming that the seismic waves propagate upward, the ground motion arrives at the top of the dam later than at the base. The spatial nonuniformity was captured by an array of accelerometers located at Pacoima Dam that includes 3-component measurements at three locations along the canyon.

In studying the ground motion, a system identification study was done with MODE-ID using the acceleration records from the January 2001 earthquake. The estimates from MODE-ID indicate that the response was dominated by the first two modes. The modes are generally symmetric (4.73 Hz–4.83 Hz) and antisymmetric (5.06 Hz), but Pacoima Dam is not a perfectly symmetric structure so the modes are not perfectly symmetric and antisymmetric. The estimated modal damping is around 6% to 7% of critical for both modes. It was initially believed that Pacoima Dam responded elastically to the 2001 earthquake. However, the natural frequencies identified by MODE-ID are significantly lower than the frequencies for the symmetric and antisymmetric modes determined from forced vibration tests performed in 1980 (5.45 Hz and 5.60 Hz). The mode shapes are somewhat similar, but the decrease in frequencies is substantial for both modes. The significant stiffness reduction shows that either the system has been damaged since 1980 and left unrepaired, which is not

the case, or the 2001 earthquake induced a nonlinear response from Pacoima Dam. When short windows of the 2001 records are provided to MODE-ID, the natural frequencies are shown to vary during the course of the earthquake. The frequencies tend to increase as the motion from the earthquake dies out, but the frequencies do not reach the values determined from the 1980 forced vibration tests.

Partial records were also recorded by the accelerometer array at Pacoima Dam during the 1994 Northridge earthquake, and these records were also provided in short windows to MODE-ID. The results identify a system that has significant nonlinearity. At the beginning of the earthquake, the system is similar to the system identified from the 2001 earthquake, but as the Northridge earthquake progresses the natural frequencies decrease significantly, indicating a reduction of stiffness. This makes sense because the Northridge earthquake was observed to cause substantial damage to Pacoima Dam and its foundation. However, no damage was reported after the 2001 earthquake and the motion was not believed to be large enough for the dam to leave the elastic range.

In order to investigate the apparent nonlinear response during the 2001 earthquake, a forced vibration experiment was performed in July and August 2002. These tests yielded modal frequencies and mode shapes that were similar to the 1980 findings. The symmetric mode and antisymmetric mode frequencies were determined to be bounded by 5.35 Hz–5.45 Hz and 5.65 Hz–5.75 Hz, respectively, compared to 5.45 Hz and 5.60 Hz in 1980. The modal damping determined from the 2002 experiment ranges from 4% to 7% for the symmetric mode and 4.5% to 5.5% for the antisymmetric mode. The damping computed from the 1980 tests is higher, but it is believed to be overestimated based on the quality of the data. The reservoir was actually 13 meters deeper in 1980 so the natural frequencies identified in 1980 should be lower due to the added mass of the water. The fact that the symmetric mode frequency was lower in 2002 indicates that the Pacoima Dam system may have lost stiffness in the 22 years between experiments. This most likely happened in 1994 when the dam and foundation were damaged by the Northridge earthquake. Repairs after the earthquake may not have returned the dam to its pre-earthquake state, but

the difference does not explain the much larger decrease in stiffness that the system identification with the 2001 records seems to indicate. The differences are far too large to explain by the fact that the modes are closely spaced. The frequencies are believed to be good estimates from both MODE-ID and forced vibration. The slightly lower damping from the forced vibration tests could possibly be a result of closely spaced modes that make accurate damping estimates difficult, but there must have been some form of nonlinearity during the 2001 earthquake to explain the stiffness changes.

The nonlinearity in the 2001 earthquake response is believed to be in the foundation rock, particularly at the upper left abutment. The rock at the upper left abutment was fractured after both the 1971 San Fernando earthquake and the 1994 Northridge earthquake, and in both cases repairs were made. The foundation must remain in a state in which stiffness can be lost during even low level excitation, but the foundation does not permanently lose stiffness if no permanent displacements of the rock are caused. The nonlinear behavior must not be engaged by the forced vibration tests because that excitation is orders of magnitude smaller than the 2001 earthquake. Also, while seismic waves travel to the dam through the foundation, forced vibration excitation originates on the crest of the dam. Thus, the earthquake excitation may more easily affect the foundation. The dam concrete is believed to have behaved elastically during the 2001 earthquake.

This nonlinear effect may be even more significant than initially thought. The MODE-ID identified system is a hybrid of the systems with flexible and rigid foundations, so this system should actually be stiffer than the system with a flexible foundation. The cross-correlation functions of ambient measurements can actually be shown to oscillate at the natural frequencies of the flexible foundation system, and cross-correlations of earthquake records may be a close enough approximation to have the same properties. When cross-correlation functions for the 2001 records are provided as free vibration output for MODE-ID, the symmetric mode frequency is much lower than the estimate using the records directly. However, the antisymmetric mode frequency is actually found to be higher through the cross-correlation functions.

Also, the computed response from a finite element model that is calibrated to match the MODE-ID estimates from the records seems to indicate that the symmetric mode frequency is too high and that the antisymmetric mode frequency is too low to match the actual recorded response. These results are not completely intuitive because the antisymmetric mode frequency is not expected to be higher for what seems to be a more flexible system. While the specific nature of the system that is identified by MODE-ID is not clear, it is apparent that the dam oscillated as a stiffer system during the forced vibration tests than it did during the January 2001 earthquake.

The variation of stiffness has implications for structural health monitoring. The state of a structure can be monitored by tracking the modal properties of the system. In the case of Pacoima Dam, the January 2001 earthquake was believed to be small enough to induce a linear response, which theoretically should be able to be compared to forced vibration tests to determine whether the state of the dam has changed between the two events. However, this was shown not to be the case, because while the 2002 forced vibration tests indicate a different state than the 2001 earthquake, there were no significant changes to the dam system between the events. If the earthquake response was compared to the 1980 forced vibration tests without knowledge of the 2002 tests, the frequency variations could have been interpreted as a permanent stiffness reduction that did not actually happen. The same problem may exist when comparing forced vibration data to ambient data. Perhaps, nonlinear response is significant even for these excitations. It is believed that structural health monitoring should be useful as long as responses from the same type of excitation are compared, but even this may not be true for all structures. The precise level of the excitation may even be important. Comparisons for structural monitoring need to be made before and after an event based on ambient vibration or forced vibration. This is not a significant limitation, especially if ambient data can be collected in real-time. Comparisons from different excitations are not reliable, at least for Pacoima Dam, and more study is necessary to fully understand the nonlinear mechanism in Pacoima Dam.

A main goal of this research is to develop a useful method for generating nonuni-

form ground motion to be used in structural analyses of dams. The SCADA finite element program was modified to accept nonuniform input along the abutments of the dam. A preprocessor was also created to interpolate ground motion to each node of a finite element model from a nonuniform set of ground motion records that include at least three locations along the abutments: one near the base of the dam and one each at higher elevations along the right and left abutments. The interpolation is done in the frequency domain so that amplitude and phase can both be interpolated. The input to the model is assumed to be free-field. This is not the reality when actual recordings from a dam are used, but the approximation is necessary since no free-field data is available.

The finite element model that was constructed has 110 dam elements (6 of which model the thrust block), 1320 water elements and 728 foundation elements. The dam elements can include contact nonlinearities through the smeared crack method. The water and foundation are modeled linearly with water compressibility neglected and mass omitted from the foundation. This model can be reasonably calibrated to match the results from the 2002 forced vibration experiment, and softened to calibrate to the modal estimates from the 2001 earthquake records. The model can be subjected to temperature cycles, and if joints are omitted from the dam the computed response at the crest of the dam agrees well with annual cycles of GPS and temperature data that were analyzed in the late 1990s. This indicates that the contraction joints in Pacoima Dam are closed throughout the year. Also, damage that was sustained during the 1971 San Fernando earthquake can be simulated with the model by softening a section of the foundation and disconnecting three nodes between the dam and the thrust block. The modal properties of the damaged model reasonably match results from forced vibration tests done in 1971 before repairs were made.

The SCADA analysis can be run in a linear mode or a nonlinear mode. The analysis with the January 2001 earthquake ground motion indicates that the dam probably did vibrate linearly, but no conclusion can be made about the foundation. The modeled response compares well to the recorded motion, but the computed accelerations on the dam body overestimate the records during the strongest motion.

The computed displacements agree with the records better than the accelerations. The reason for the overestimation is not known. Perhaps, the modal damping should be higher, but the damping was based on system identification that was done with the 2001 earthquake records so there is no basis for increasing the damping. The agreement of the modeled response with the recorded response is good enough to use for assessing the method that is proposed for generating nonuniform ground motion.

The approach for generating ground motion is based on the recordings from the abutments on January 13, 2001. The topographic amplification is characterized by transfer functions comparing the records on the abutments to the records at the base of the dam. The amplification is frequency-dependent. Spectral displacement ratios, both 0% and 5% damped, and Fourier amplitude spectra are considered. For the generation method, the amplification would, ideally, be implemented as an average amplification determined from several events. In order to be consistent with this, a piecewise linear approximation to the spectral displacement ratios is also considered. The time for the seismic waves to travel from the base of the dam upward along the abutments is considered through time delays based on cross-correlations and the actual relative phase between records from the Fourier spectra. In order to characterize the ground motion with time delays, the importance of reflections of the traveling waves is assumed to be small, which appears to be reasonable. Frequency-dependent delays are computed by taking the time at which the maximum value occurs from the cross-correlation of the displacement responses of 5% damped single degree of freedom oscillators at each frequency excited by the acceleration records. Frequency-independent delays are computed by taking the time at which the maximum value occurs from the cross-correlation of the acceleration records. The delays are converted to relative phase for generating ground motions. The various amplification functions and relative phase functions are used to generate motions at points along the abutments from a reference 3-component ground motion at the base of the dam. This is done in the frequency domain, and then the ground motions are converted back to the time domain for use in dynamic analyses.

Nonuniform ground motions were generated from the base records of the Jan-

uary 2001 earthquake and the Northridge earthquake. The generated motions were compared to the full records from the 2001 earthquake and the partial records from the Northridge earthquake. From these comparisons, it was concluded that smooth functions are better for the general method, because specific features from the Fourier transfer functions from one event can be unrealistic for another event. The amplification and delays may be ground motion amplitude-dependent. There is evidence that the amplification may be larger for stronger ground motion, but the effect does not appear to be important based on comparison of the generated Northridge motions with the partial records. Comparison of the generated motions with the records does indicate that the time delays may increase for larger motion. This may happen because the stronger motion softens the foundation rock so the wave speeds decrease.

Ground motions were generated from the 2001 earthquake base records using various amplification and relative phase functions. When these ground motions are supplied as input to the SCADA model, the computed stresses are similar for different methods of generation. Also, the stresses computed with generated input do not differ significantly from the stresses computed with the actual records supplied as input. The response to the 2001 earthquake is small and predominantly linear, so a larger earthquake needs to be considered to determine whether the good agreement still occurs for nonlinear response. However, while the stresses show very good agreement, the computed motions on the dam differ more noticeably when comparing the generated inputs and the recorded input. Therefore, at least for linear analysis, the various approximate generated ground motions can yield reasonable modeled results, in terms of stresses, even though the computed motions on the dam are not identical.

While the results from the 2001 earthquake are good, comparing the generation methods for the Northridge earthquake can yield more information since nonlinearity is important for this event. The responses from the generated ground motion can be compared to the partial set of recordings and the observations of damage made after the earthquake. The smoother amplification functions yield motions that agree with the partial records better than motions generated with the amplification from Fourier amplitude transfer functions. The Fourier amplification does produce a severe

response in the dam, but it is considered unrealistic because of the motions that are computed. The piecewise linear amplification functions yield results that are realistic, but the motion is underestimated somewhat so the general size of the response is probably underestimated, as well. The 0% and 5% damped spectral displacement ratios yield results that are generally larger and more severe for the dam. The proposed way to create amplification functions is to average 0% damped spectral displacement ratios from several events. However, it is likely that the required amount of data will not be available, so an attempt to simulate this would be necessary. If sufficient data were actually available, averaging Fourier transfer functions from several events may actually be the best option.

The frequency-dependent time delays are used for generating ground motions in an attempt to physically account for dispersive traveling waves. However, the frequency-independent (constant) delays yield a computed finite element response that is similar. Also, if the smaller delays for the vertical components determined from the 2001 earthquake are neglected and a single frequency-independent delay is used for all three components at a single location, the computed response is still not affected very much. Thus, the constant delays, even component-independent, are a satisfactory approximation for the purposes of modeling the response and obtaining useful results. The relative phase from the Fourier transfer functions yields a somewhat more severe response, but the general applicability of this phase is questioned because it is event specific for the 2001 earthquake, so the approximated phases based on physical considerations are recommended. The computed motions on the dam for the Northridge earthquake appear as though they agree better with the partial records if the delays are increased. This is further evidence that the wave travel times between the recording stations are ground motion amplitude-dependent. However, the differences in the responses from ground motions with various implementations of time delays are not as important as the differences from the various amplification functions. The time delay is a factor that should be considered when generating nonuniform motion, but the topographic amplification is more important for the modeled response, so more effort should be directed toward accurately characterizing the amplification.

The nonuniform ground motion generated for the Northridge earthquake with piecewise linear amplification and frequency-dependent time delays produces a computed response that agrees with the partial records fairly well. The nonlinearity in the model significantly decreases the dominant oscillation frequency of the dam, which was also observed in the frequencies estimated by MODE-ID using the Northridge records. The joint opening and cracking agree reasonably well with the observed damage, except that there is no computed permanent joint opening at the thrust block because the permanent displacement of the foundation at the upper left abutment is not simulated by the input ground motion. Other than the lack of a permanent joint opening at the thrust block, the computed damage is actually a little more severe for the dam than what was observed after the Northridge earthquake. This assessment only pertains to the dam and not the foundation, since the foundation is modeled elastically. An attempt was made to simulate damage to the upper left abutment by softening that portion of the foundation, but there was little effect on the computed response.

One concern about the model is that the computed accelerations are too large. The damping used in the analysis is based on modal damping determined for the 2001 earthquake. The energy dissipation during the Northridge earthquake was probably higher due to friction and other nonlinear effects. Thus, the damping was increased to be around 10% near the first two frequencies for the model and the response was reduced. However, more damping still seems necessary to obtain good agreement with the recorded displacement at channel 8, the one record on the dam that was digitized. Perhaps, there is even more dissipation that is not accounted for, but the damping used is already quite high. Another modification was made to the model by allowing lateral sliding in the joints. While this does have a substantial effect on the response, the results are unrealistic since failure of the joint keys would have to occur and that did not happen.

Another important goal of this research is to compare the computed responses to generated nonuniform ground motion and uniform ground motion. If the motion recorded at the base of the dam is used as uniform input, the response is less severe

than the nonuniform input. Uniform motion that is taken as the motion generated for the Northridge earthquake at 80% of the height of the dam on either abutment is considered to be a realistic ground motion that would be used in an analysis with uniform input. For uniform ground motion, the stream component is the most important direction of input for determining the response. The response is more severe compared to the nonuniform input in terms of joint opening and cracking, but the general character is significantly different from the response to nonuniform input. The major difference between uniform input and nonuniform input is the pseudostatic component of the response. While the pseudostatic component is a rigid body motion for uniform input, the pseudostatic component of the response to nonuniform input causes deformations in the dam that dominate along the abutments. Large pseudostatic stresses can occur along the abutments for nonuniform input. These stresses are directly related to the displacements of the ground motion input. This means that one of the most important characteristics of nonuniform ground motion for input to a dam model is the displacements. Therefore, generating realistic displacements is critical for the nonuniform ground motion used in dynamic analyses. At least for the 2001 earthquake, the generation method does produce ground motions for which the displacements agree well with the actual records.

The proposed method to generate nonuniform ground motions based on actual recorded earthquake data is fairly simple, but it does account for two major physical phenomena that affect the ground motion in a canyon. The results show some promise, but a lot more data is required to refine and validate the process. The issue of nonuniform ground motion applies not only to dams, but bridges as well. More instrumentation of these structures, particularly along the abutments, is necessary to acquire more data. The instrumentation along the abutments of Pacoima Dam is good, but even better coverage on the abutments would provide important information. Another product of studying data of this nature is possible insight into the cause of the variation in the modal properties observed for small events, which may have implications for structural health monitoring and system identification, in general.

Bibliography

ANCO Engineers, Inc. (1982). Dynamic Testing of Concrete Dams. Final report prepared for National Science Foundation.

Beck, J. L. and P. C. Jennings (1980). Structural identification using linear models and earthquake records. *Earthquake Engineering and Structural Dynamics 8*(2), 145–160.

Beck, J. L., B. S. May, D. C. Polidori, and M. W. Vanik (1995). Ambient Vibration Surveys of Three Steel-Frame Buildings Strongly Shaken by the 1994 Northridge Earthquake. Earthquake Engineering Research Laboratory, California Institute of Technology, Pasadena, CA. Report No. EERL 95–06.

Behr, J. A., K. W. Hudnut, and N. E. King (1998). Monitoring structural deformation at Pacoima Dam, California using continuous GPS. In *Proceedings of the 11th International Technical Meeting of the Satellite Division of the Institute of Navigation*, Nashville, TN, pp. 59–68.

Bell, D. K. and B. J. Davidson (1996). Response identification of Pacoima Dam for the 1994 Northridge earthquake. In *Eleventh World Conference on Earthquake Engineering*, Oxford, England. Disc 2, Paper No. 774.

CSMIP (1994). Processed Data for Pacoima Dam—Channels 8 through 11 from the Northridge Earthquake of 17 January 1994. California Strong Motion Instrumentation Program. Report OSMS 94–15A.

CSMIP (1995). Phase 1 Data for Pacoima Dam—Channels 1–6, 12, 13 and 15–17

from the Northridge Earthquake of 17 January 1994. California Strong Motion Instrumentation Program. Report OSMS 95–05.

CSMIP (2001a). Processed Data for Pacoima Dam—Channels 1 through 17 from the M 4.3 Earthquake of 13 January 2001. California Strong Motion Instrumentation Program. Report OSMS 01–02.

CSMIP (2001b). Processed Data for Pacoima Dam—Channels 22 through 24 (Upper Left Abutment) from the M 4.3 Earthquake of 13 January 2001. California Strong Motion Instrumentation Program. Report OSMS 01–03.

Darragh, R., T. Cao, C. Cramer, M. Huang, and A. Shakal (1994a). Processed CSMIP Strong-Motion Records from the Northridge, California Earthquake of January 17 1994: Release No. 1. California Strong Motion Instrumentation Program. Report No. OSMS 94–06B.

Darragh, R., T. Cao, M. Huang, and A. Shakal (1994b). Processed Data for Pacoima—Upper Left Abutment from the Northridge Earthquake of 17 January 1994. California Strong Motion Instrumentation Program. Report OSMS 94–12A.

Duron, Z. H. and J. F. Hall (1986). New techniques in forced vibration testing. In G. C. Pardoen (Ed.), *Recent Advances in Structural Dynamics: Proceedings of a session sponsored by the Aerospace Division of the American Society of Civil Engineers in conjunction with the ASCE Convention in Seattle, Washington, April 10, 1986*, pp. 16–33. ASCE.

Earthquake Engineering Research Institute (1995). Northridge Earthquake of January 17, 1994 Reconnaissance Report: Volume 1. *Earthquake Spectra*. Supplement C to Volume 11. J. F. Hall (Ed.). EERI 95–03.

Farrar, C. R. and G. H. James III (1997). System identification from ambient vibration measurements on a bridge. *Journal of Sound and Vibration 205*(1), 1–18.

Hall, J. F. (1988). The dynamic and earthquake behaviour of concrete dams: review of experimental behaviour and observational evidence. *Soil Dynamics and Earthquake Engineering* 7(2), 57–121.

Hall, J. F. (1996). Efficient Nonlinear Seismic Analysis of Arch Dams: User's Manual for SCADA (Smeared Crack Arch Dam Analysis). Earthquake Engineering Research Laboratory, California Institute of Technology, Pasadena, CA. Report No. EERL 96–01 (Modified July 1997).

International Engineering Company, Inc. (1972). Pacoima Arch Dam: Investigation and Evaluation of Effects of San Fernando Earthquake: Volume I. Report prepared for Los Angeles County Flood Control District.

Lin, G., J. Zhou, and J. Wang (1996). Seismic response of arch dams to wave scattering and spatial variation of ground motions. In *Eleventh World Conference on Earthquake Engineering*, Oxford, England. Disc 3, Paper No. 1704.

Mickey, W. V., V. Perez, and W. K. Cloud (1974). Amplification studies of the Pacoima Dam from aftershocks of the San Fernando earthquake. In *Proceedings: Fifth World Conference on Earthquake Engineering*, Volume 1, Rome, pp. 755–762.

Mojtahedi, S. and G. Fenves (2000). Effect of Contraction Joint Opening on Pacoima Dam in the 1994 Northridge Earthquake. California Strong Motion Instrumentation Program. Data Utilization Report CSMIP/00–05 (OSMS 00–07).

Morrison Knudsen Corporation, Transportation and Water Resources Group (1994). Report on Initial Assessment of the Effects of the January 17, 1994 Northridge/San Fernando Earthquake on Pacoima Dam: Phase 1. Report prepared for Department of Public Works, County of Los Angeles.

Nowak, P. S. and J. F. Hall (1990). Arch dam response to nonuniform seismic input. *Journal of Engineering Mechanics 116*(1), 125–139.

Reimer, R. B. (1973). Deconvolution of Seismic Response for Linear Systems. Earthquake Engineering Research Center, University of California, Berkeley, CA. Report No. EERC 73–10.

Werner, S. D., J. L. Beck, and M. B. Levine (1987). Seismic response evaluation of Meloland Road Overpass using 1979 Imperial Valley earthquake records. *Earthquake Engineering and Structural Dynamics 15*(2), 249–274.

Woodward-Lundgren & Associates (1971). Pacoima Dam: Determination of In Situ Dynamic Elastic Foundation Properties: Report of Investigations June–August 1971. Report prepared for International Engineering Company, Inc.

Appendix A

Forced Vibration Experimental Data

Two directions of the shaker were employed: radial and tangential at the shaker location. These directions are approximately N85E and S05E, respectively. Since the shaker was placed near the center of the crest, these two directions are essentially the stream and cross-stream directions, respectively. Frequency sweeps were conducted from 2.5 Hz to 11 Hz.

The testing was carried out using six Ranger seismometers at a time. Since the Rangers were placed at ten locations (see Figure 5.2), it was necessary to do two frequency sweeps for each forcing direction. Channels 1fv and 2fv were left in place for both sweeps for reference. Channels 3fv, 4fv, 7fv and 8fv were in place for what is designated the "right shake," and then these Rangers were moved to channels 5fv, 6fv, 9fv and 10fv for the "left shake." Initially, the right shake frequency sweep was only conducted from 2.5 Hz up to 10 Hz. However, it was determined during the left shake that the sweeps would be conducted up to 11 Hz. The Rangers were moved back to channels 3fv, 4fv, 7fv and 8fv so frequencies between 9 Hz and 11 Hz could be recorded. The plots for the right shake given in this appendix include the additional recordings above 10 Hz. Since the response curves were very similar between 9 Hz and 10 Hz for both sweeps of the right shake, the additional frequencies between 10 Hz and 11 Hz were simply appended to the response curves with a minimal adjustment based on the response values at 10 Hz. The data presented in this appendix have been

calibrated across all of the Rangers based on a calibration run that was performed while on the dam. The adjustments required for calibration were minimal. The amplitude and phase for each channel from 2.5 Hz to 11 Hz are shown here. The amplitude of the Ranger response has been divided by frequency cubed so that the output is proportional to the displacement of the dam per unit shaker force. The phases are relative to the force of the shaker and a negative phase indicates that the Ranger response lags behind the force.

The N85E shaking excited the dam to a higher degree than the S05E shaking. In order for the plots to be easily viewed, the amplitude scale for the S05E shaking is 5 times smaller than for the N85E shaking. Also, the abutment channels recorded much smaller motion, so the amplitude scale for channels 7fv, 8fv, 9fv and 10fv is a factor of 10 smaller than for the crest channels for both directions of shaking.

Notice that, as expected, the channel 1fv response curves from the right and left shakes are similar, and the same is true for the channel 2fv response curves. This is the case for both directions of shaking. Also, notice that the higher (antisymmetric) mode is dominant in many of the curves. However, as the channel 1fv response to N85E shaking shows, the lower (symmetric) mode is present. In the other curves, the symmetric mode is smaller so it is not as apparent.

The response of channel 7fv around 9.25 Hz demonstrates an anomalous behavior. A discontinuity in the frequency response curve appears for both directions of shaking. This is probably related to vibration of the steel platform where channel 7fv was located. However, notice that the response of channel 8fv does not show the same behavior, so only motion of the platform in the east-west direction, which is close to the stream direction, is affected. The effect appears to be localized near 9.25 Hz.

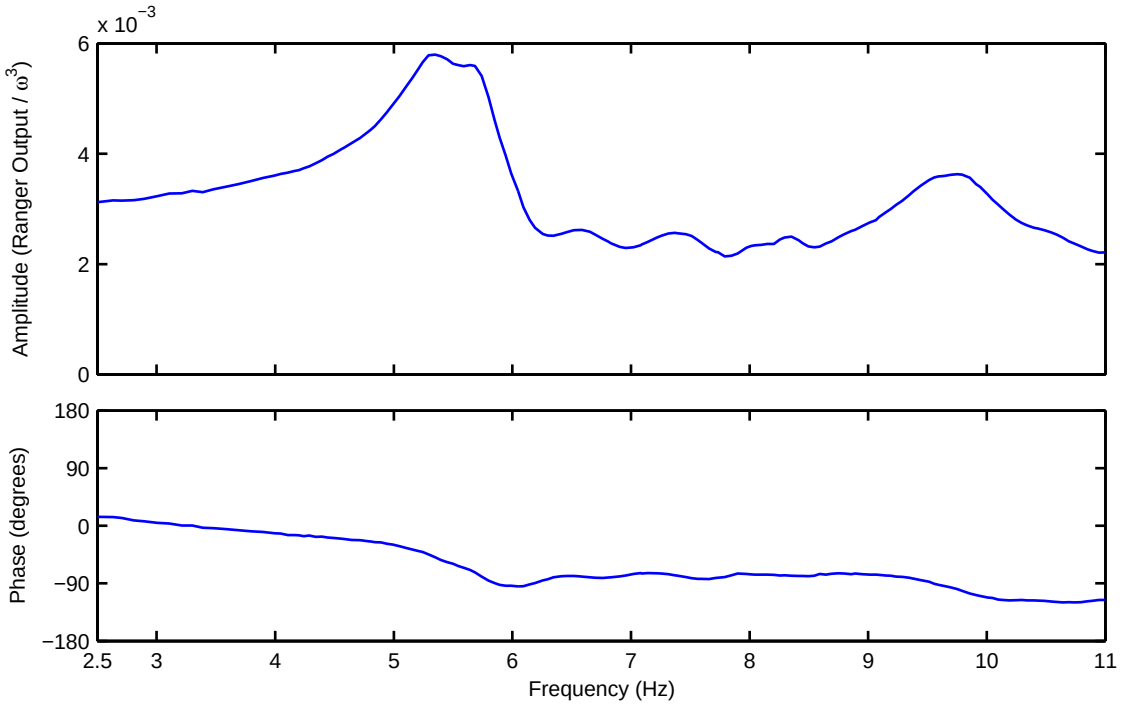

Figure A.1: Channel 1fv amplitude and phase curves for N85E shaking (right shake)

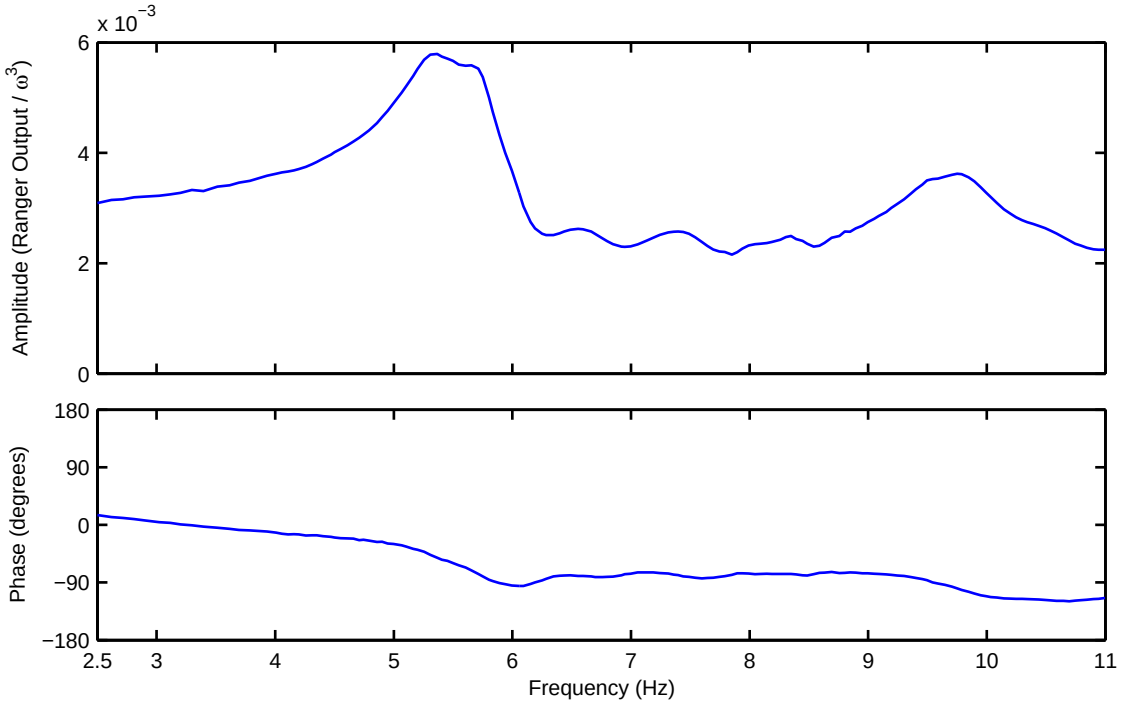

Figure A.2: Channel 1fv amplitude and phase curves for N85E shaking (left shake)

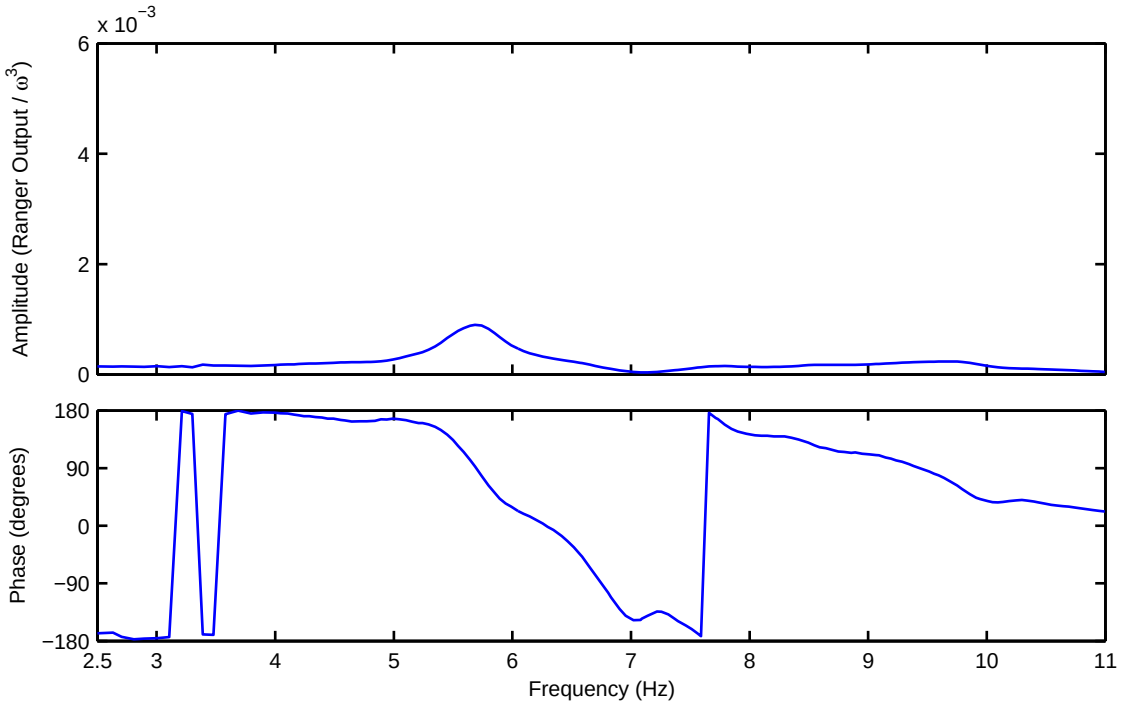

Figure A.3: Channel 2fv amplitude and phase curves for N85E shaking (right shake)

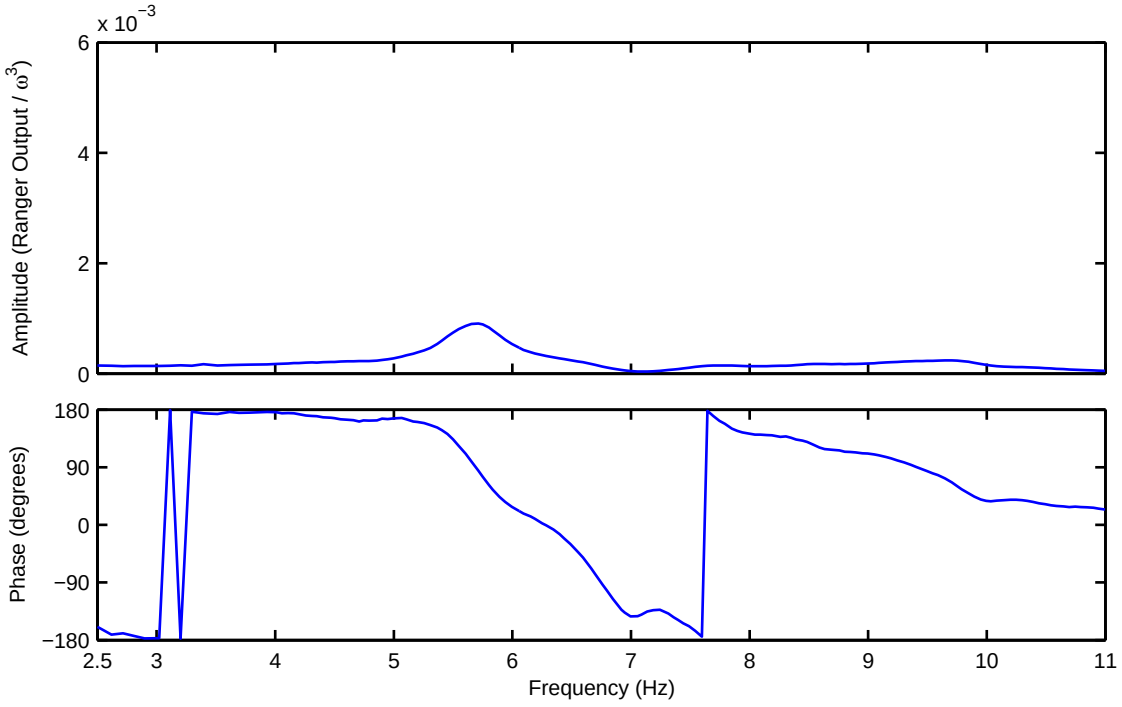

Figure A.4: Channel 2fv amplitude and phase curves for N85E shaking (left shake)

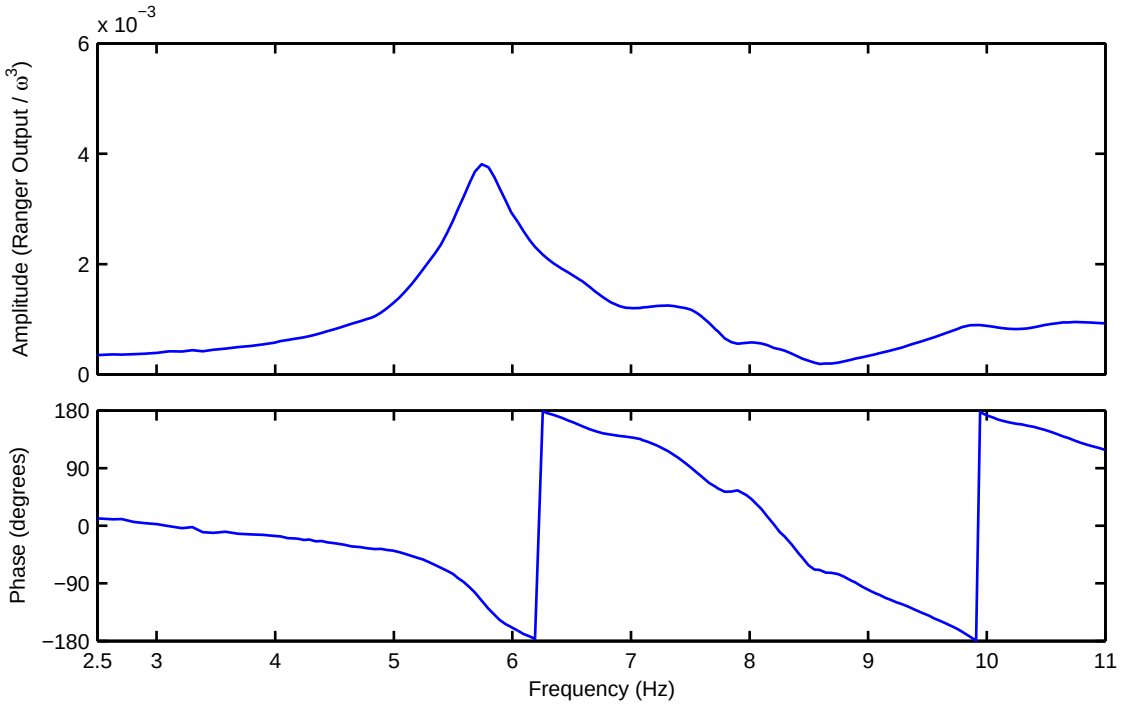

Figure A.5: Channel 3fv amplitude and phase curves for N85E shaking (right shake)

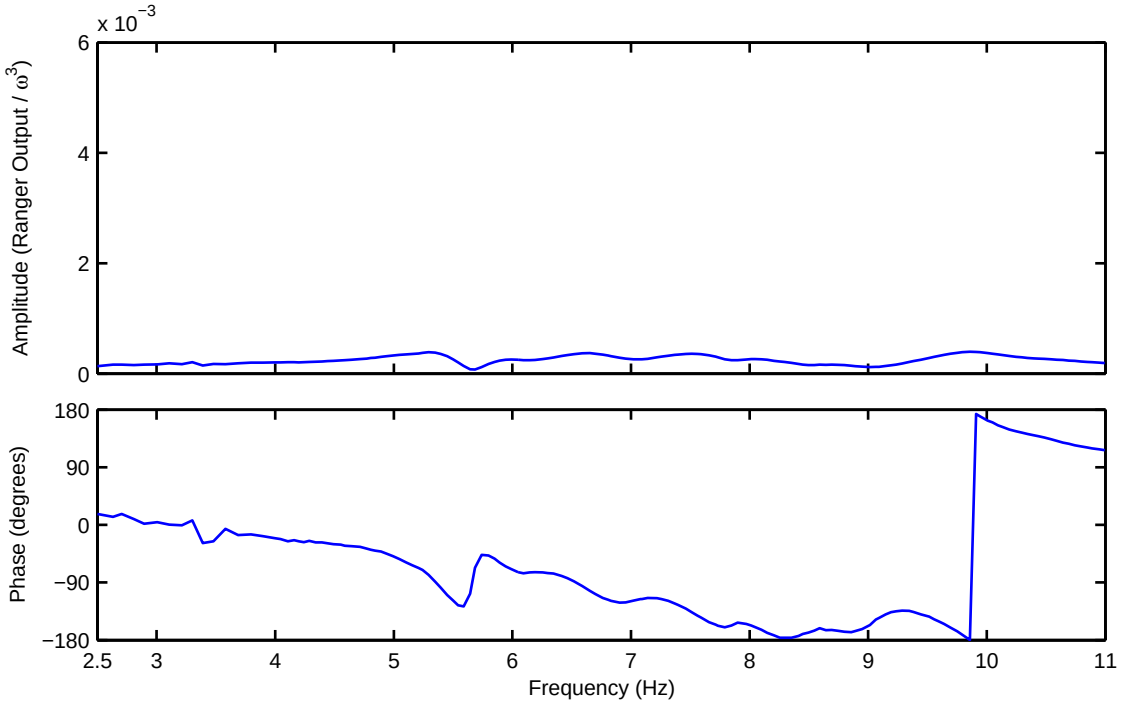

Figure A.6: Channel 4fv amplitude and phase curves for N85E shaking (right shake)

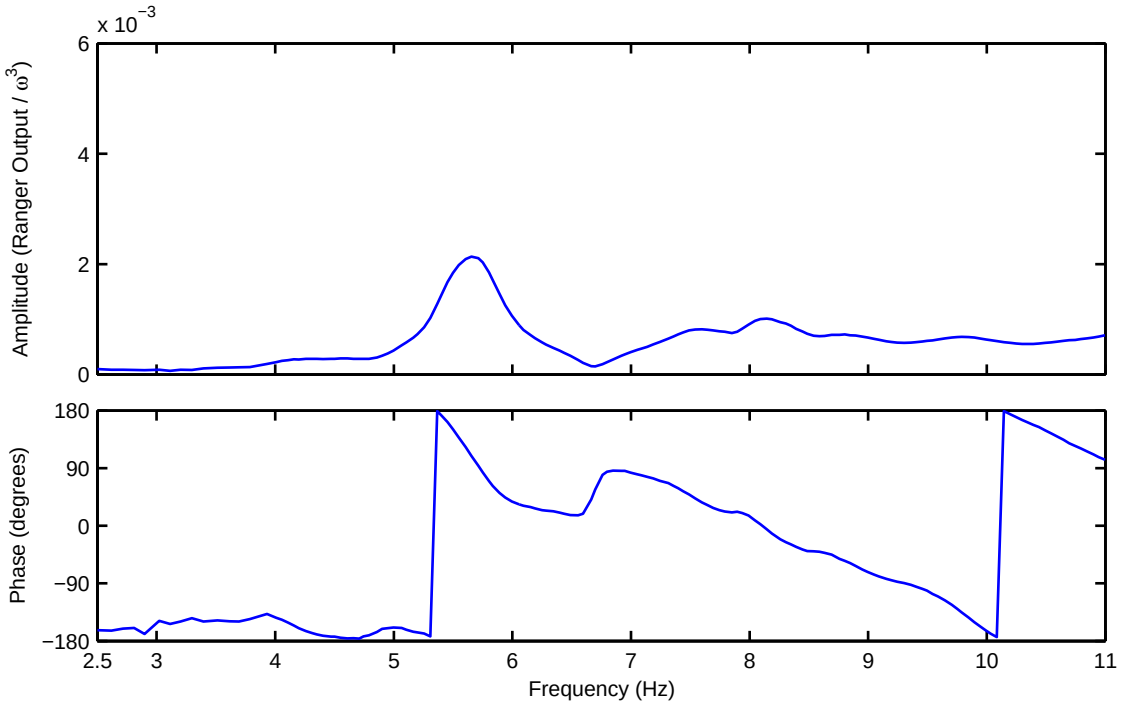

Figure A.7: Channel 5fv amplitude and phase curves for N85E shaking (left shake)

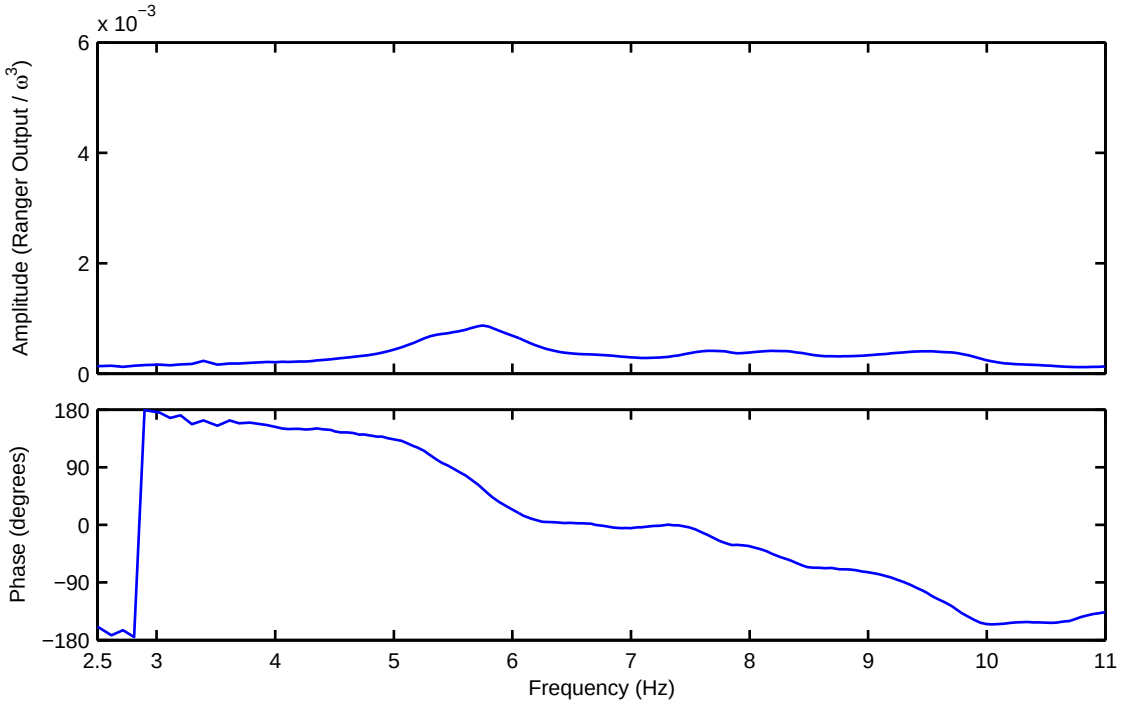

Figure A.8: Channel 6fv amplitude and phase curves for N85E shaking (left shake)

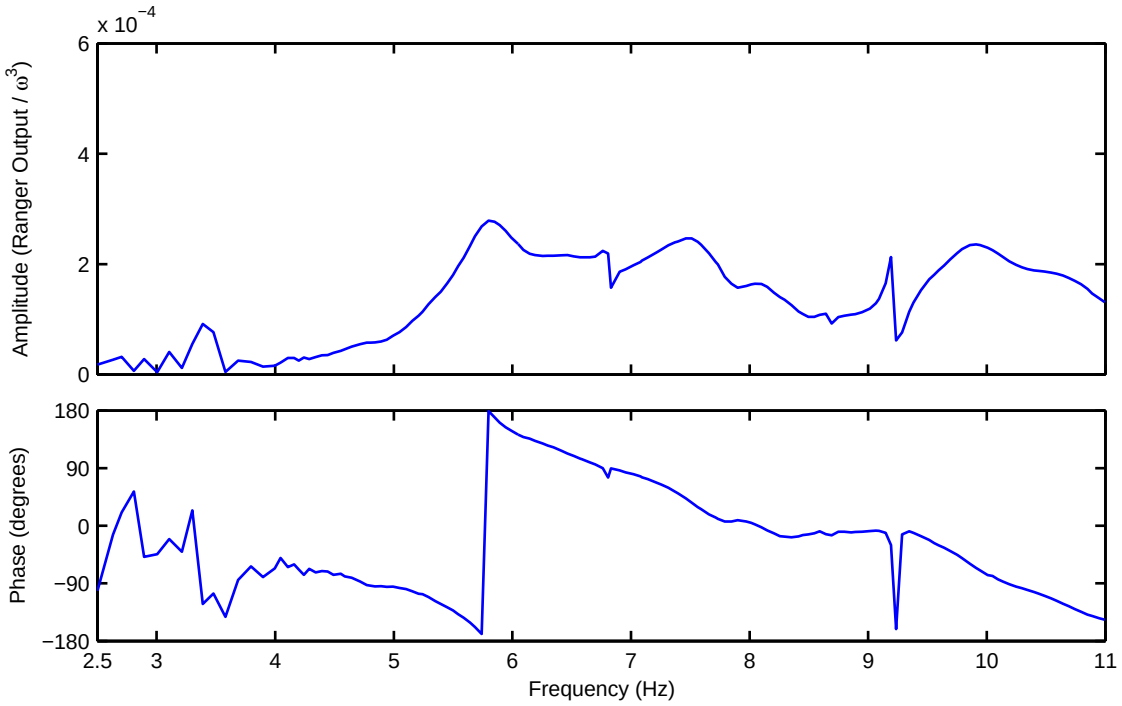

Figure A.9: Channel 7fv amplitude and phase curves for N85E shaking (right shake)

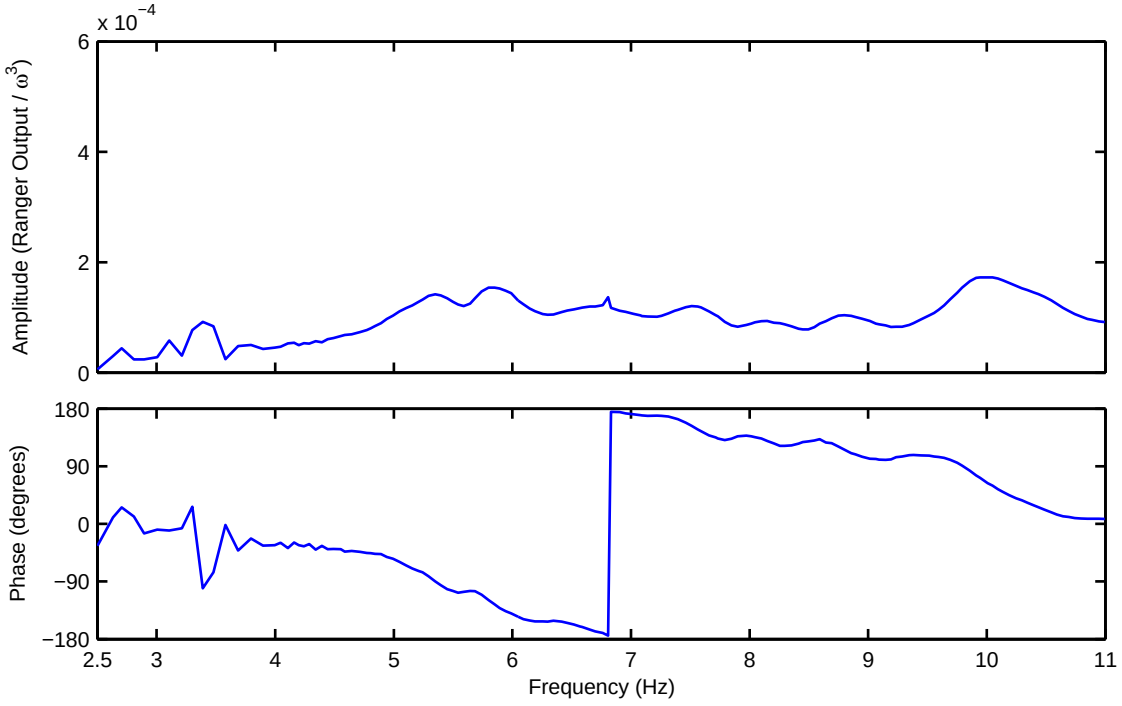

Figure A.10: Channel 8fv amplitude and phase curves for N85E shaking (right shake)

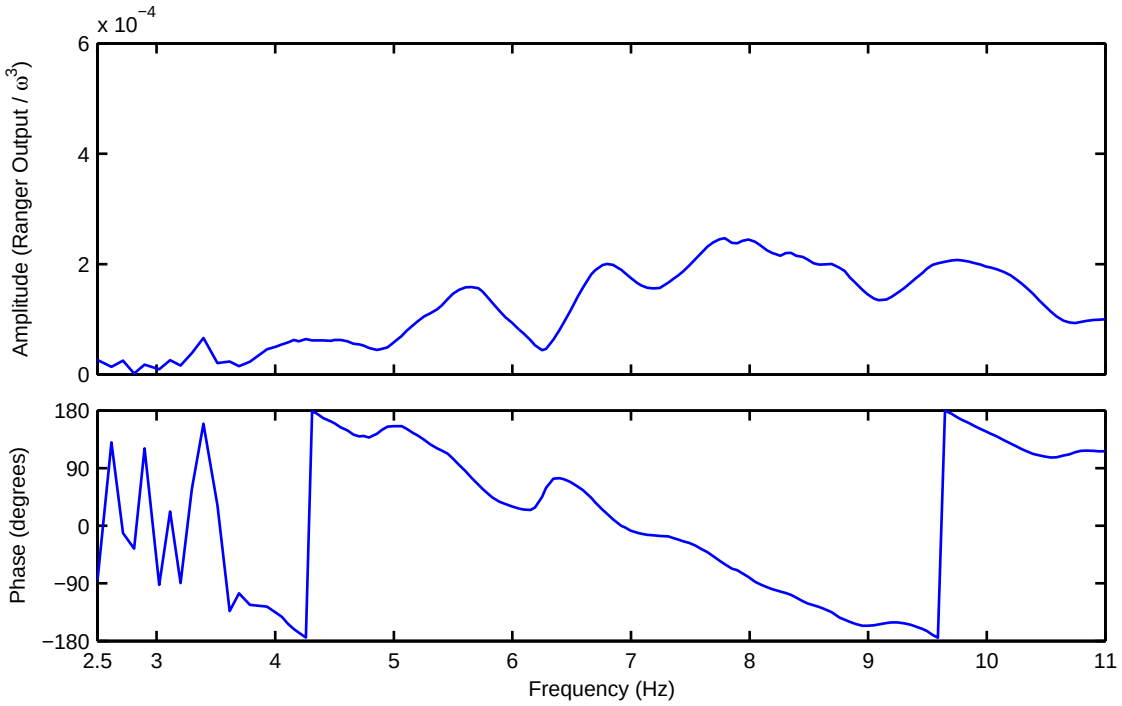

Figure A.11: Channel 9fv amplitude and phase curves for N85E shaking (left shake)

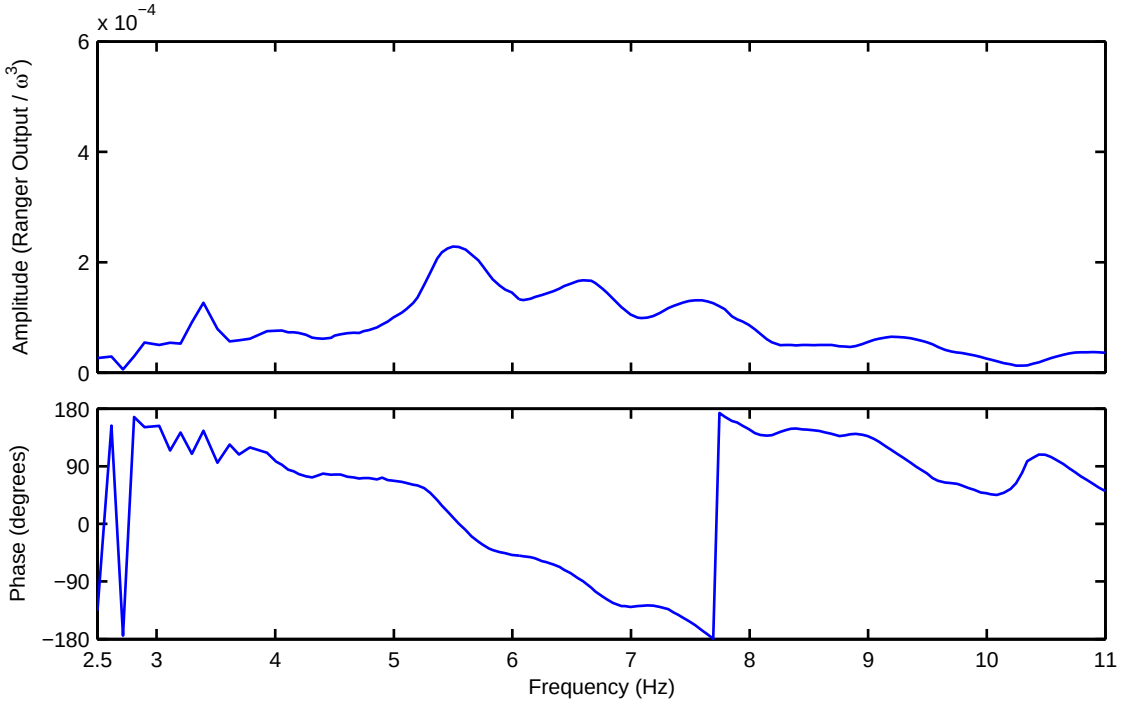

Figure A.12: Channel 10fv amplitude and phase curves for N85E shaking (left shake)

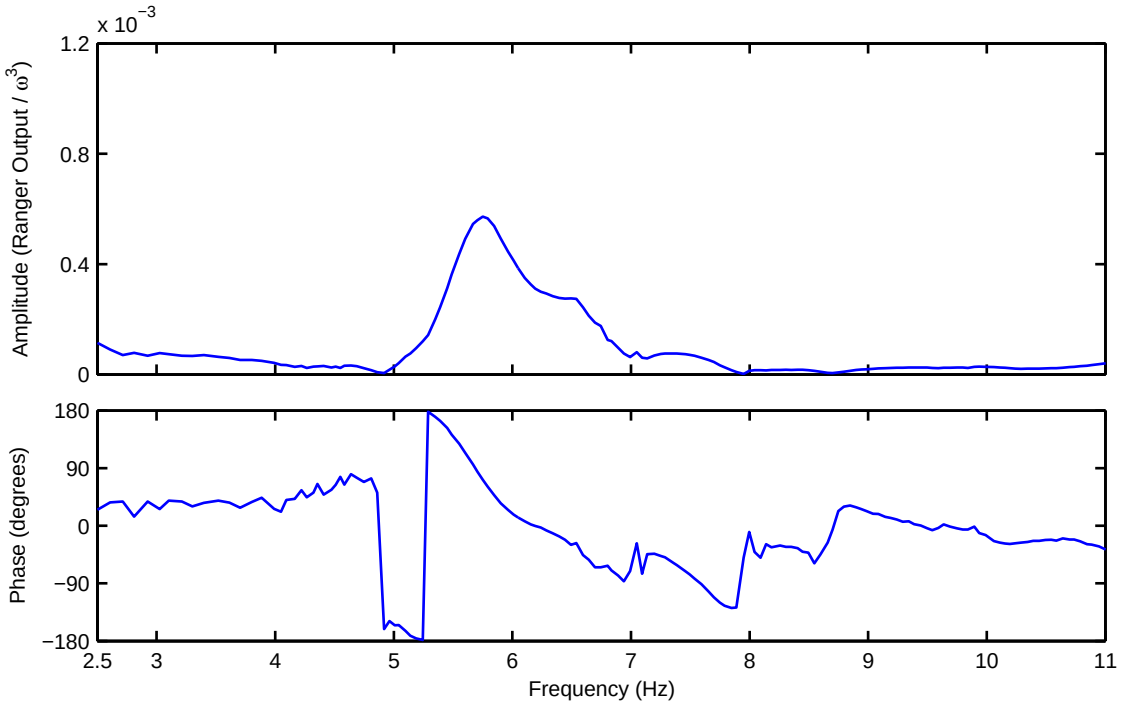

Figure A.13: Channel 1fv amplitude and phase curves for S05E shaking (right shake)

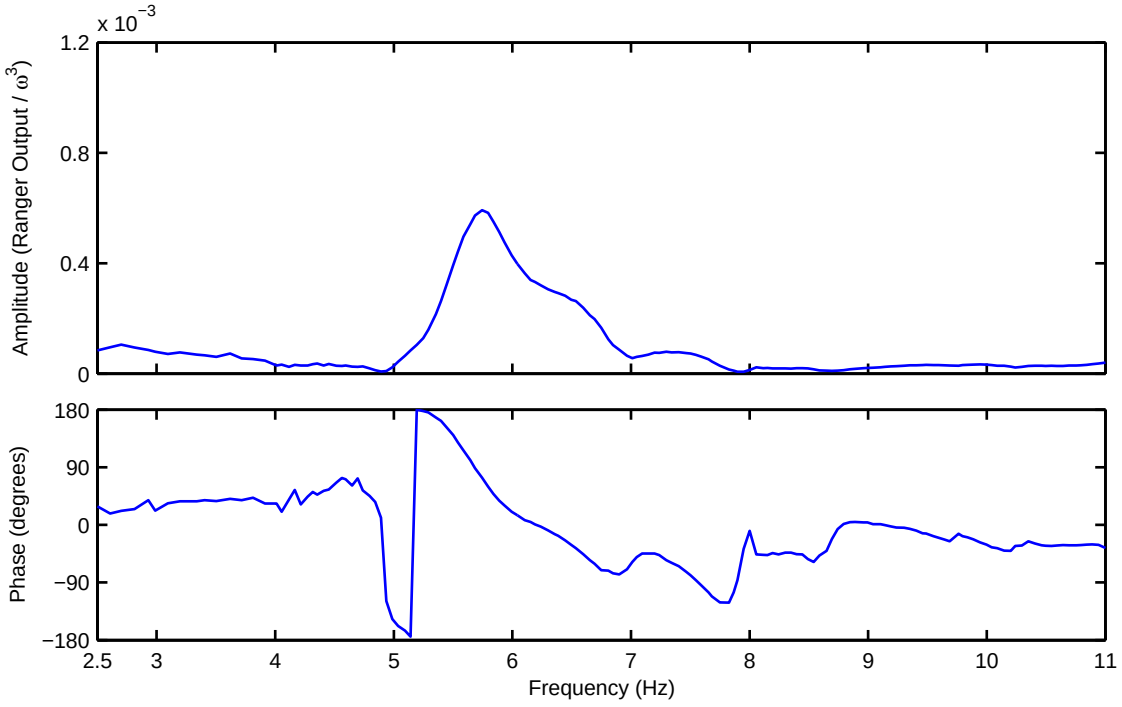

Figure A.14: Channel 1fv amplitude and phase curves for S05E shaking (left shake)

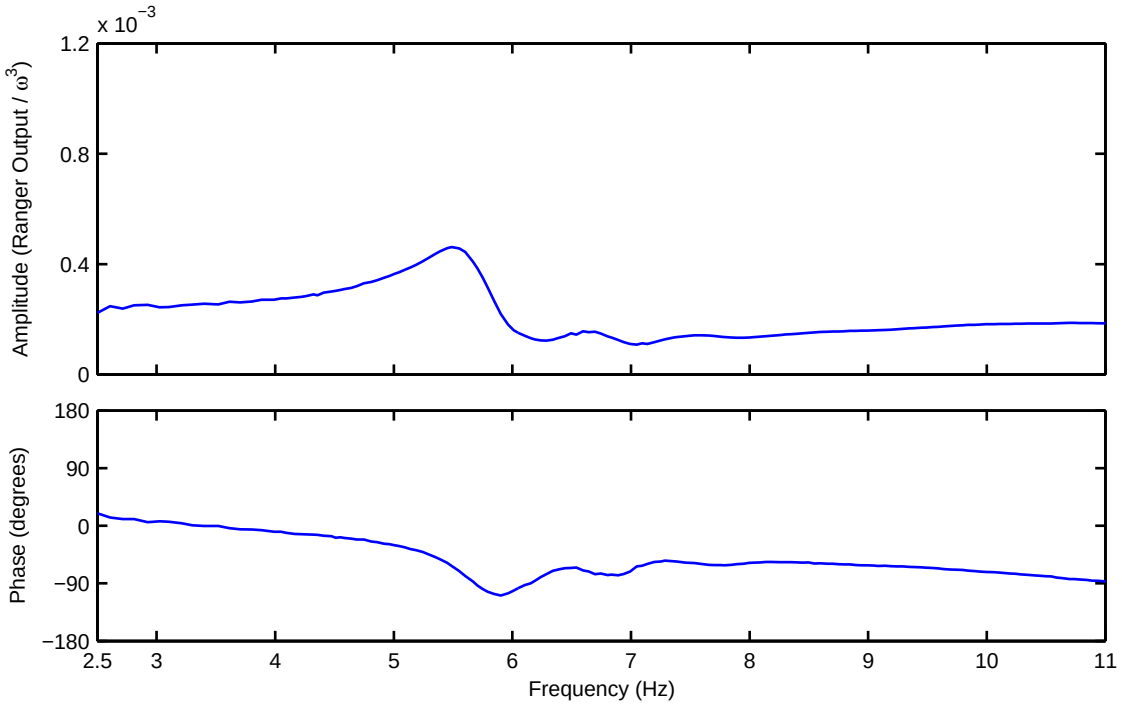

Figure A.15: Channel 2fv amplitude and phase curves for S05E shaking (right shake)

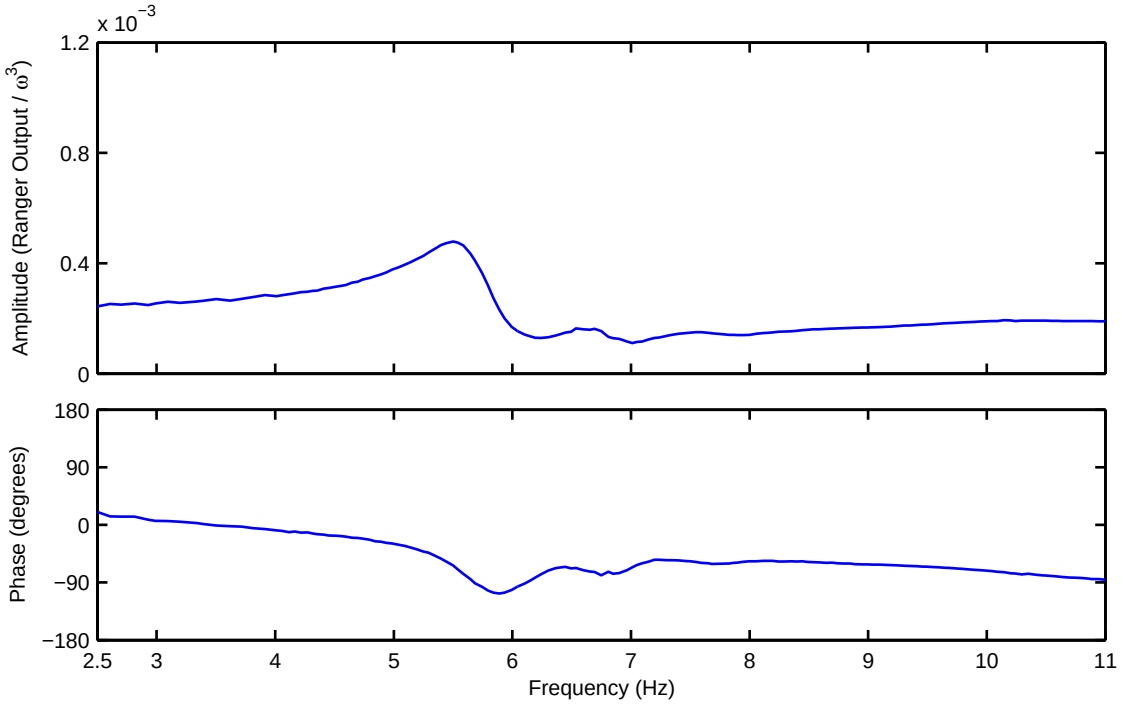

Figure A.16: Channel 2fv amplitude and phase curves for S05E shaking (left shake)

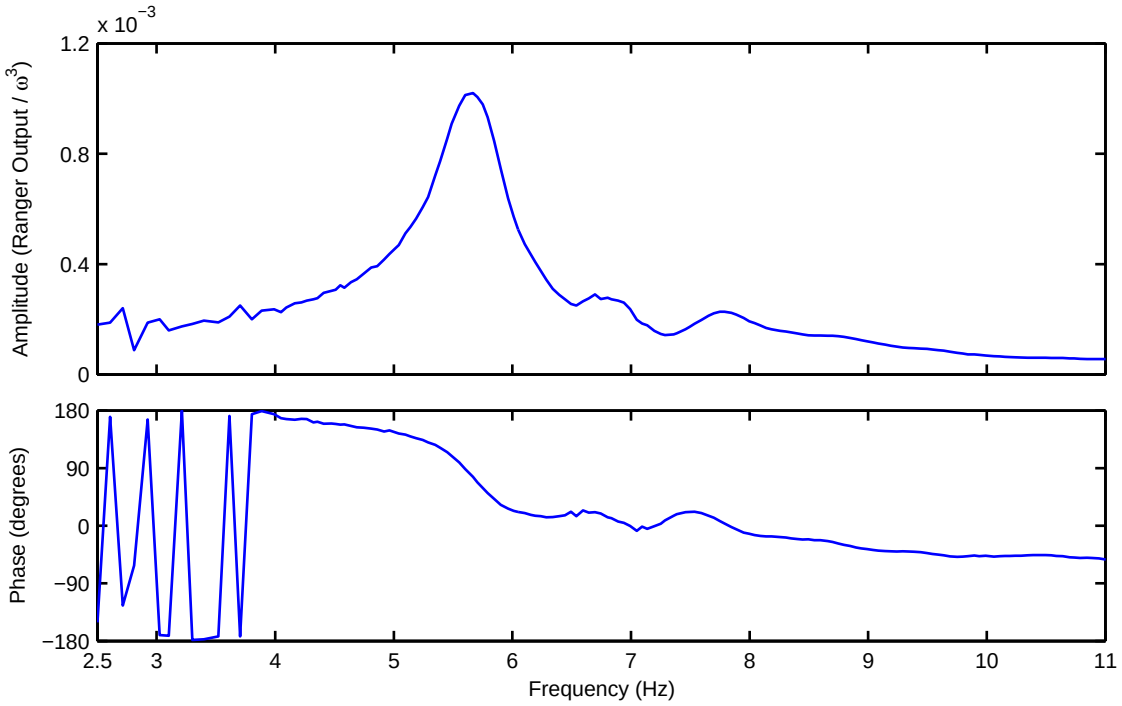

Figure A.17: Channel 3fv amplitude and phase curves for S05E shaking (right shake)

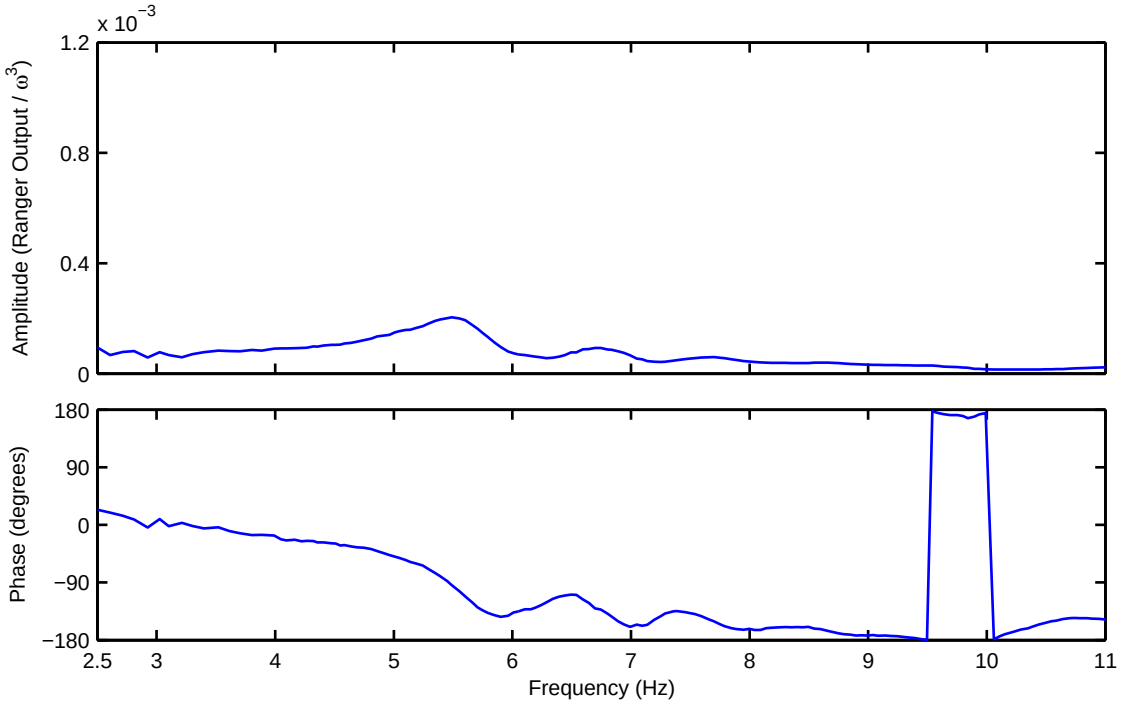

Figure A.18: Channel 4fv amplitude and phase curves for S05E shaking (right shake)

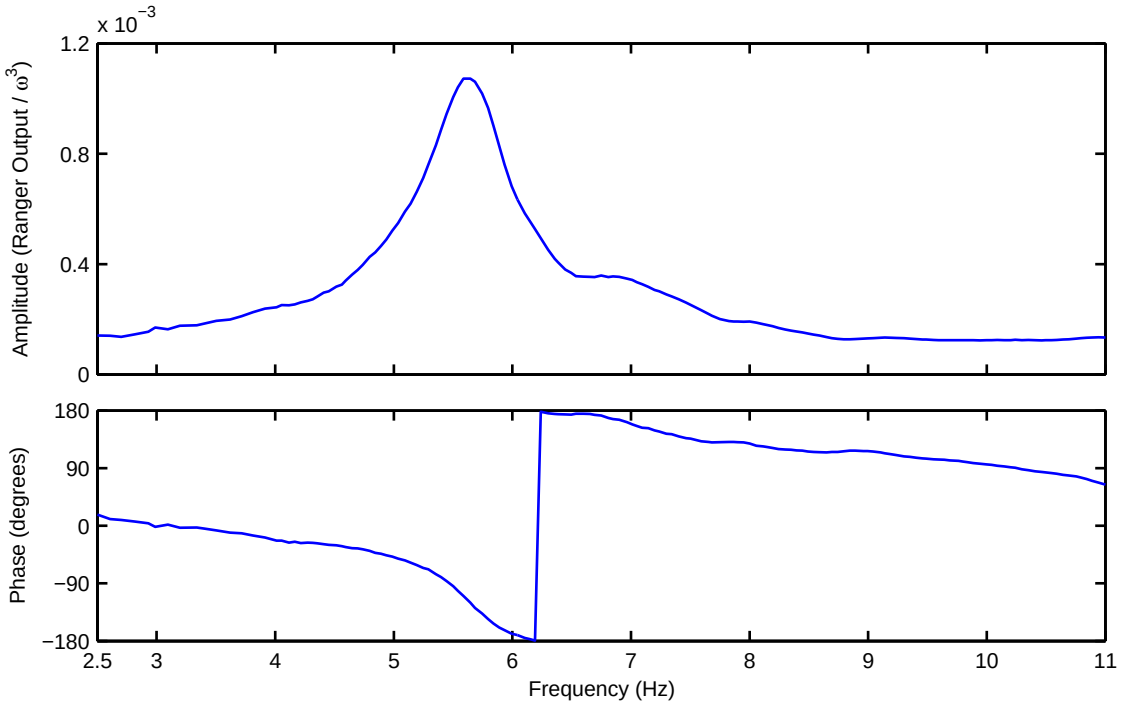

Figure A.19: Channel 5fv amplitude and phase curves for S05E shaking (left shake)

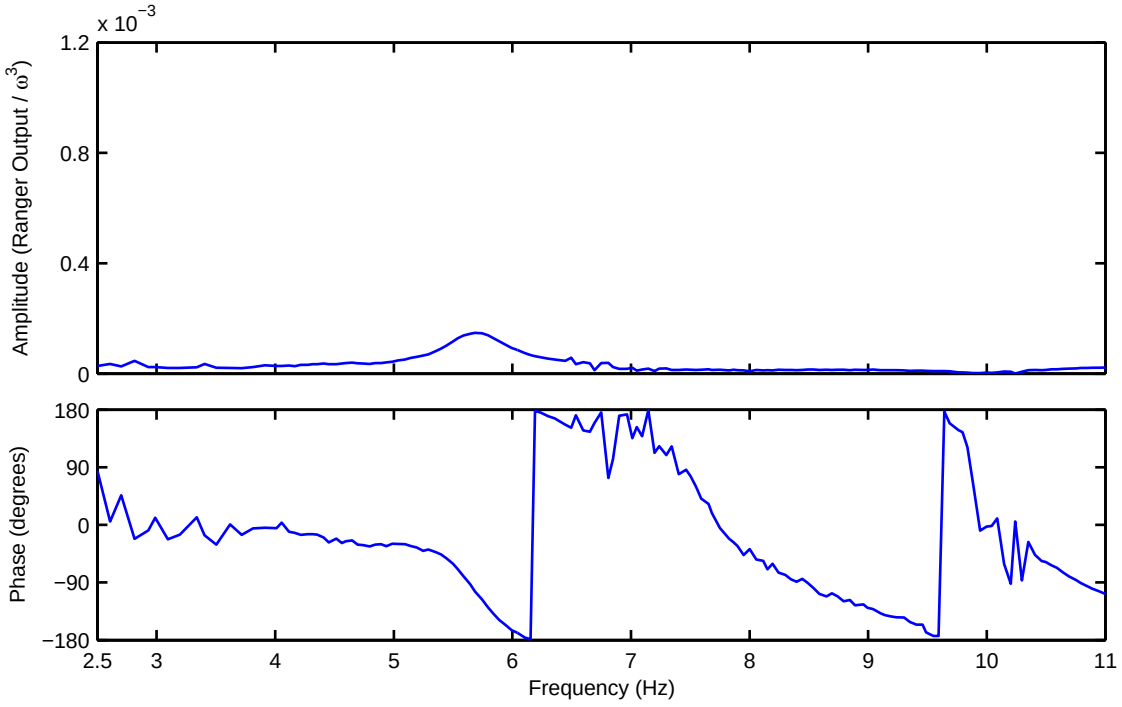

Figure A.20: Channel 6fv amplitude and phase curves for S05E shaking (left shake)

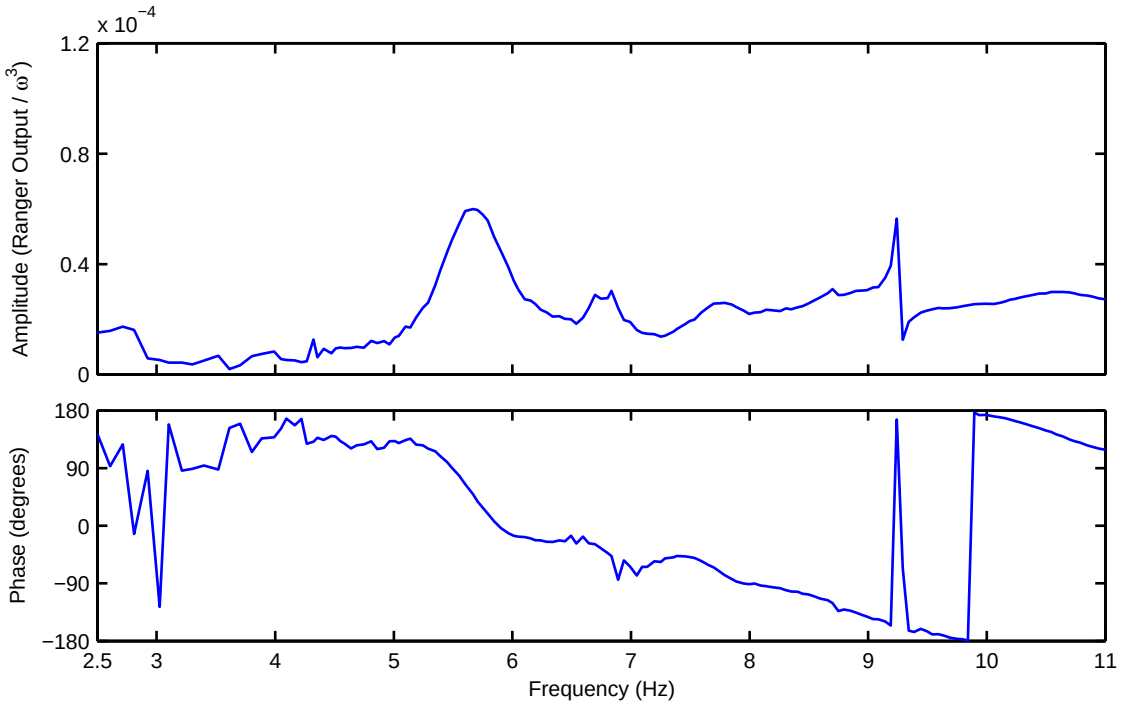

Figure A.21: Channel 7fv amplitude and phase curves for S05E shaking (right shake)

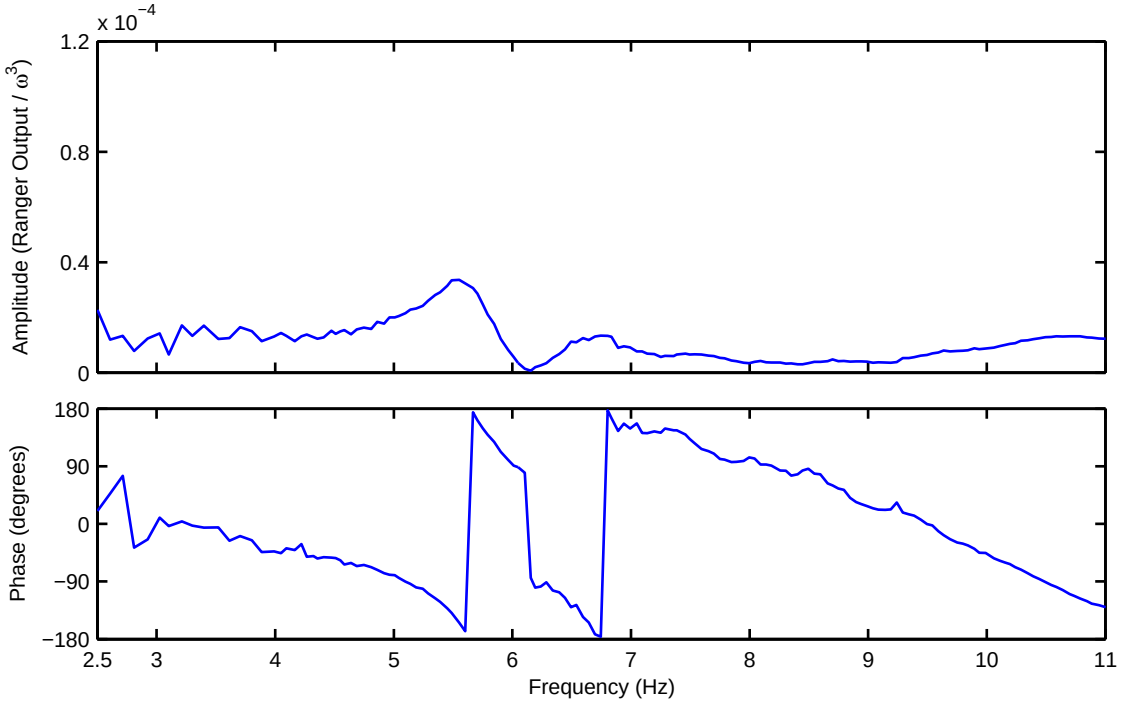

Figure A.22: Channel 8fv amplitude and phase curves for S05E shaking (right shake)

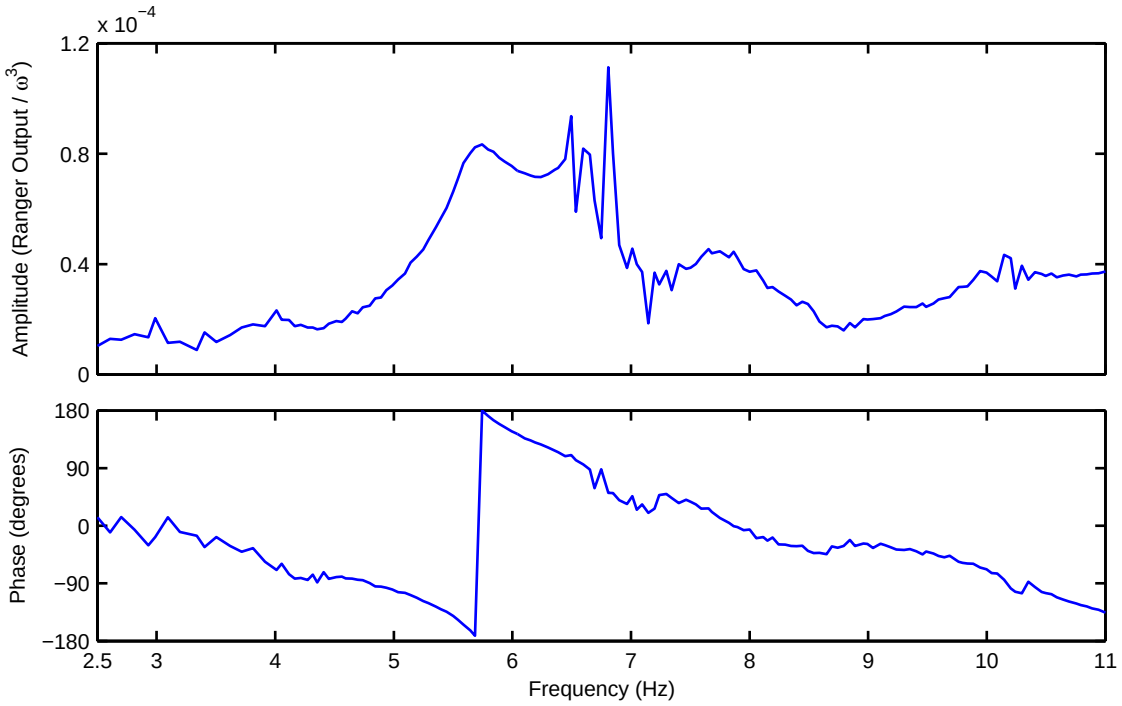

Figure A.23: Channel 9fv amplitude and phase curves for S05E shaking (left shake)

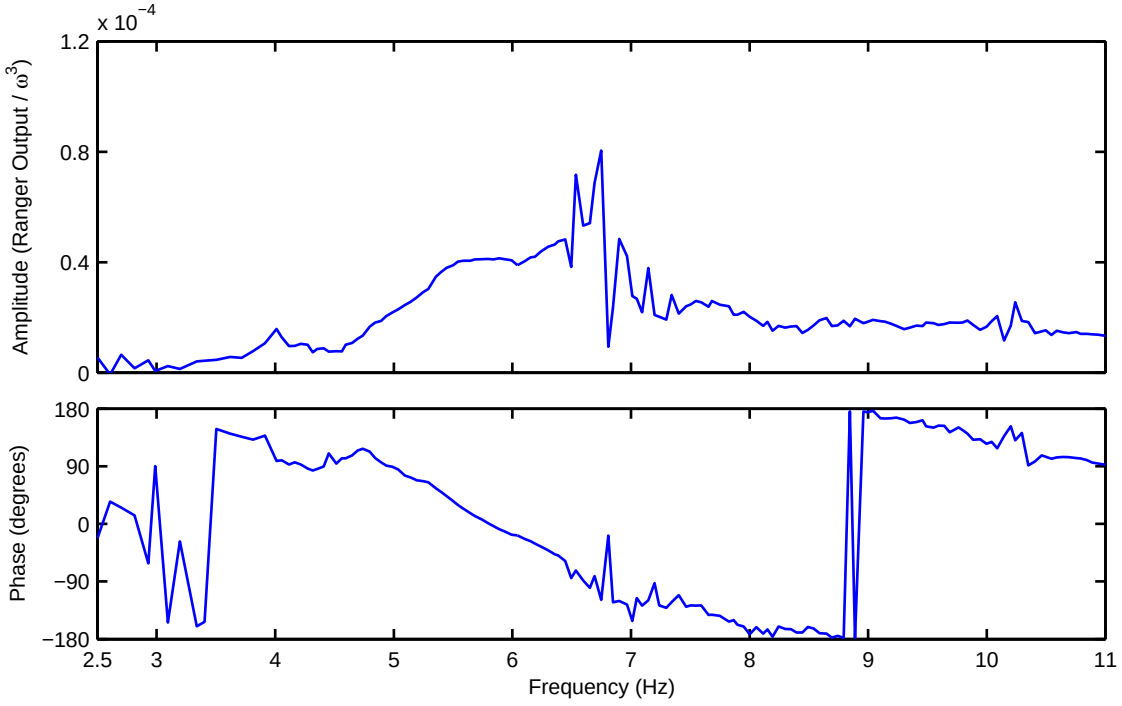

Figure A.24: Channel 10fv amplitude and phase curves for S05E shaking (left shake)

Appendix B

Results from January 13, 2001 Earthquake Analyses

Output responses from SCADA analyses with ground motion input from the January 13, 2001 earthquake are included in this appendix. The actual records from channels 9–17 and the records generated by methods 1, 2 and 9 (Table 3.1) for abutment channels 12–17 along with the actual base records (channels 9–11) are employed as input. Linear and nonlinear analyses were done for the actual records while only nonlinear analyses were done for the generated records. Acceleration and displacement time histories computed at the locations corresponding to the accelerometer array at Pacoima Dam are plotted in comparison to the actual measurements recorded on January 13, 2001. Contour plots of maximum compressive stress in the arch and cantilever directions on both faces of the dam are also included. Plots are not shown for tensile stresses since they are very small. For nonlinear analyses, a response picture that gives the maximum joint opening in each element of the dam is included. The maximum joint opening is determined as the maximum value from either the upstream or downstream face of the element. The stress contour plots and the response pictures are presented as if an observer was viewing the dam from downstream, so north is to the left of the figures and the thrust block is to the right. Some of these response quantities are also presented in Chapter 8, but they are duplicated here for completeness.

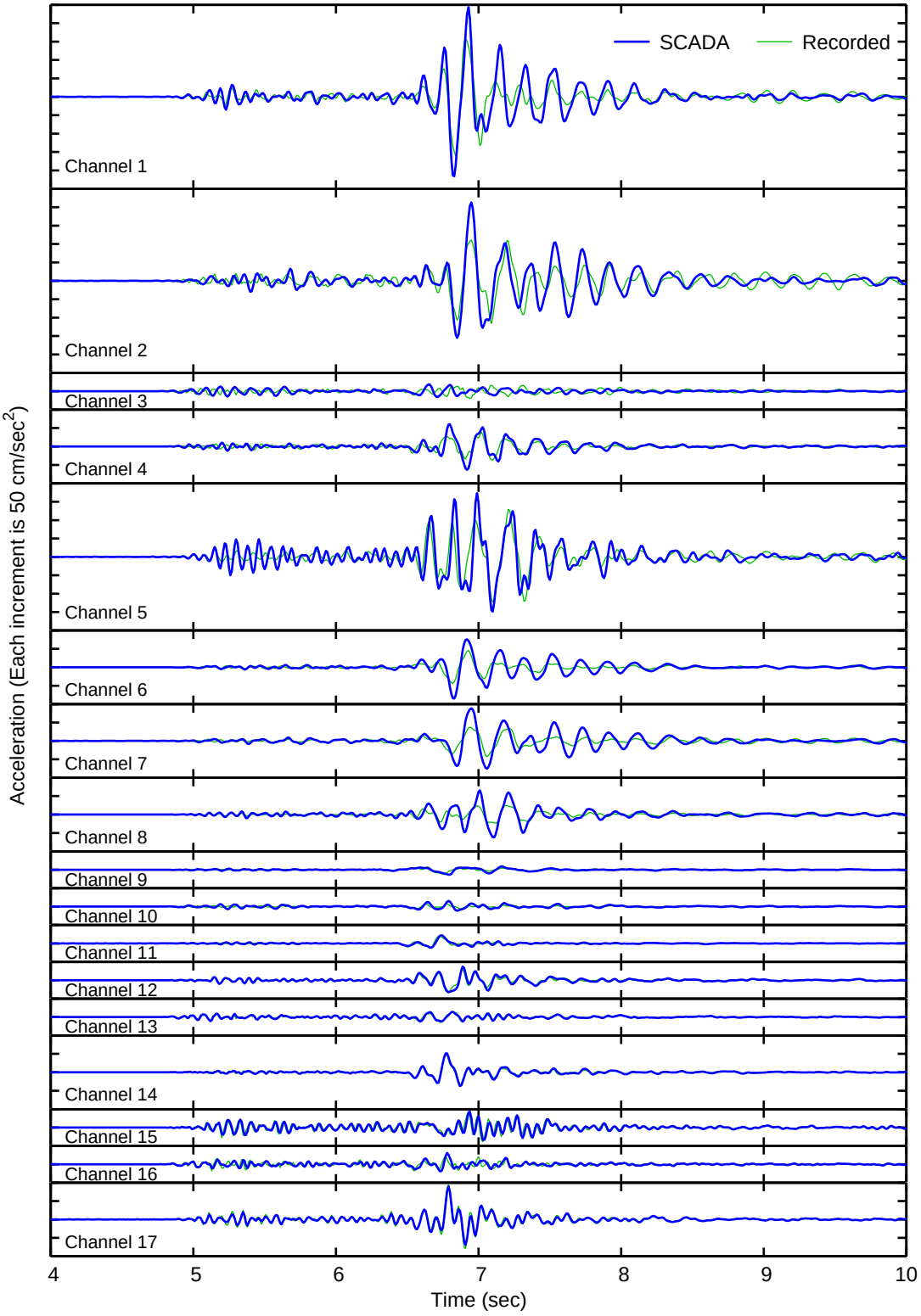

Figure B.1: Acceleration time histories at locations corresponding to channels 1–17 computed from a linear analysis of the January 13, 2001 earthquake compared to the actual records

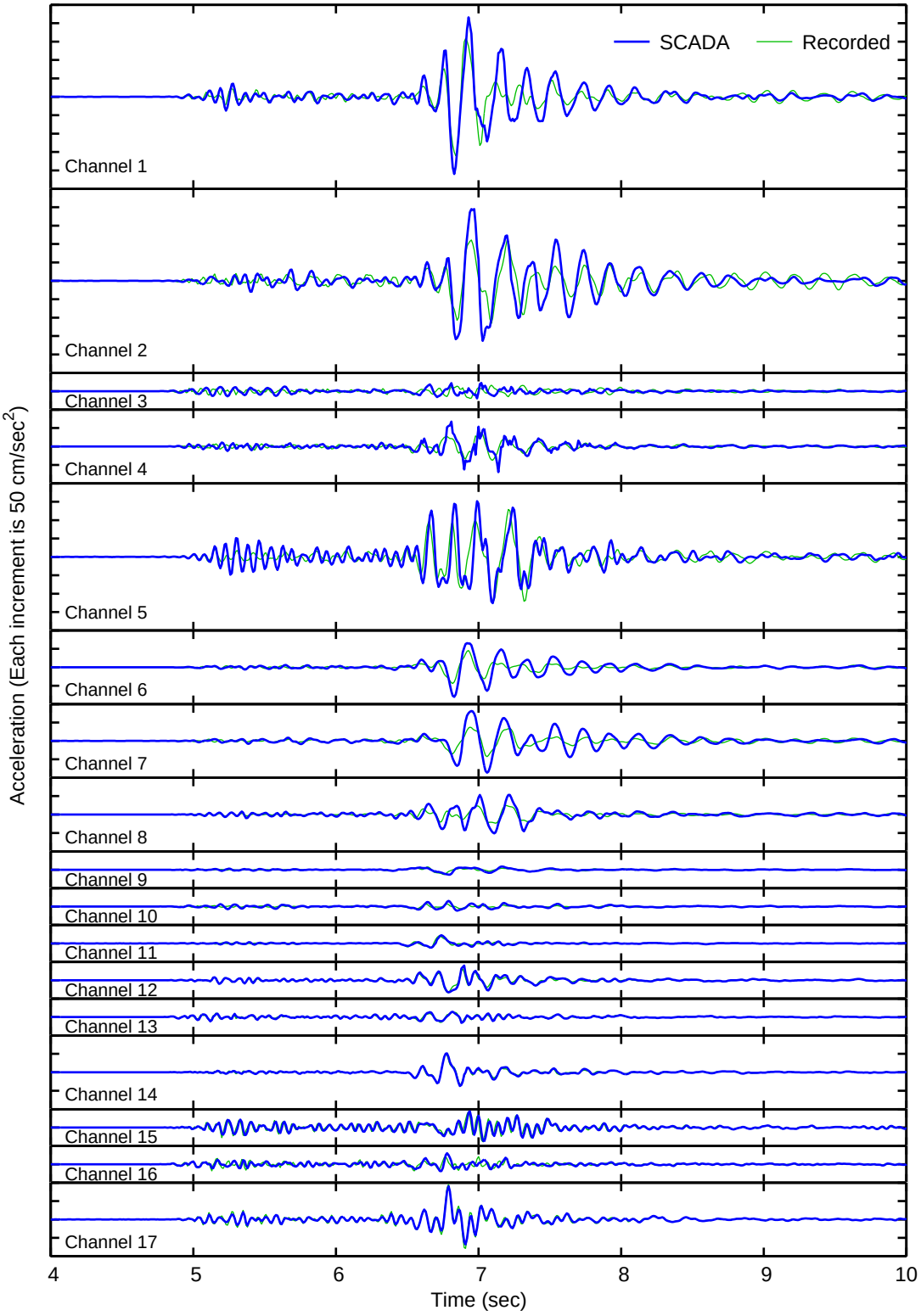

Figure B.2: Acceleration time histories at locations corresponding to channels 1–17 computed from a nonlinear analysis of the January 13, 2001 earthquake compared to the actual records

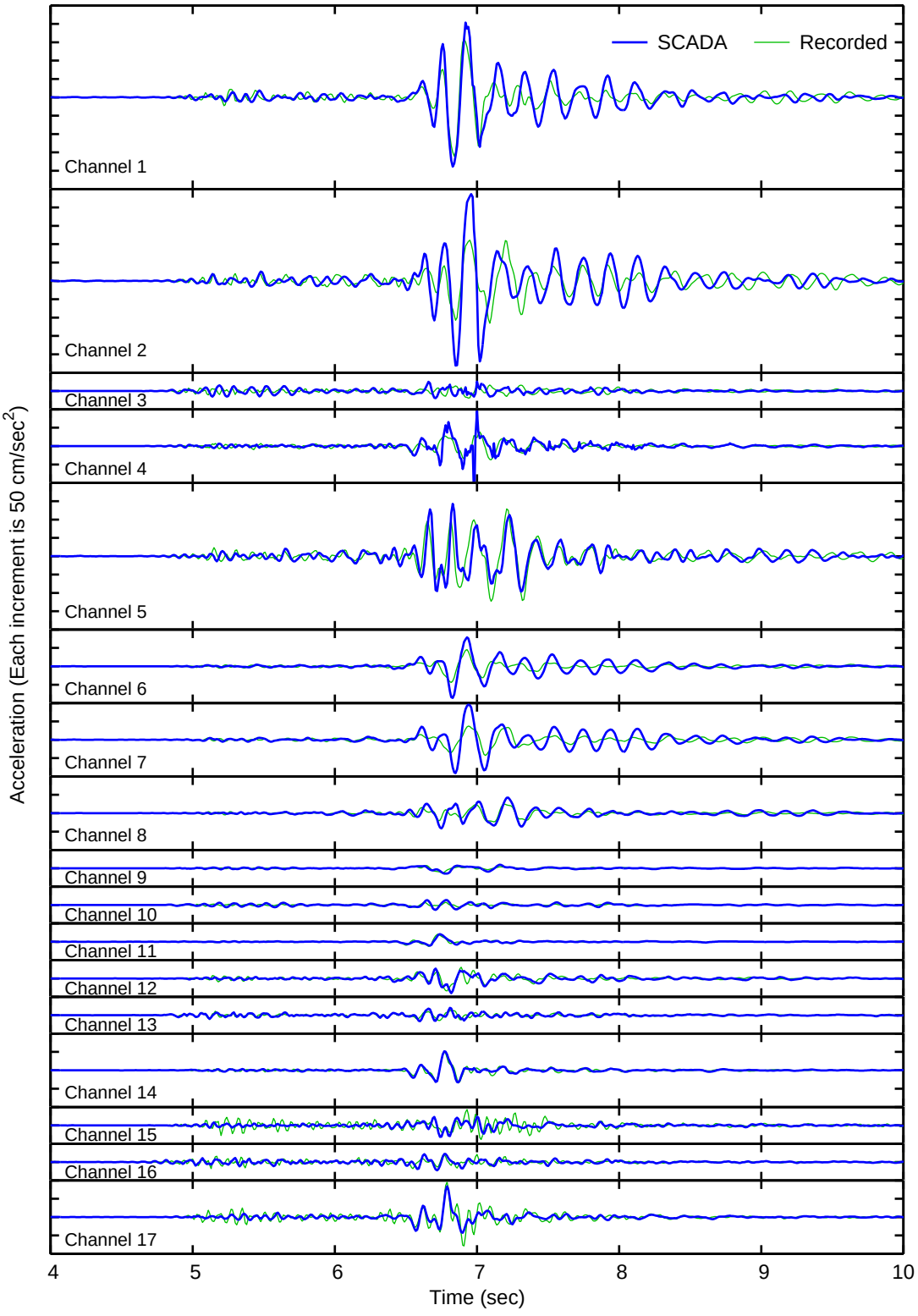

Figure B.3: Acceleration time histories at locations corresponding to channels 1–17 computed from a nonlinear analysis of the January 13, 2001 earthquake generated by method 1 compared to the actual records

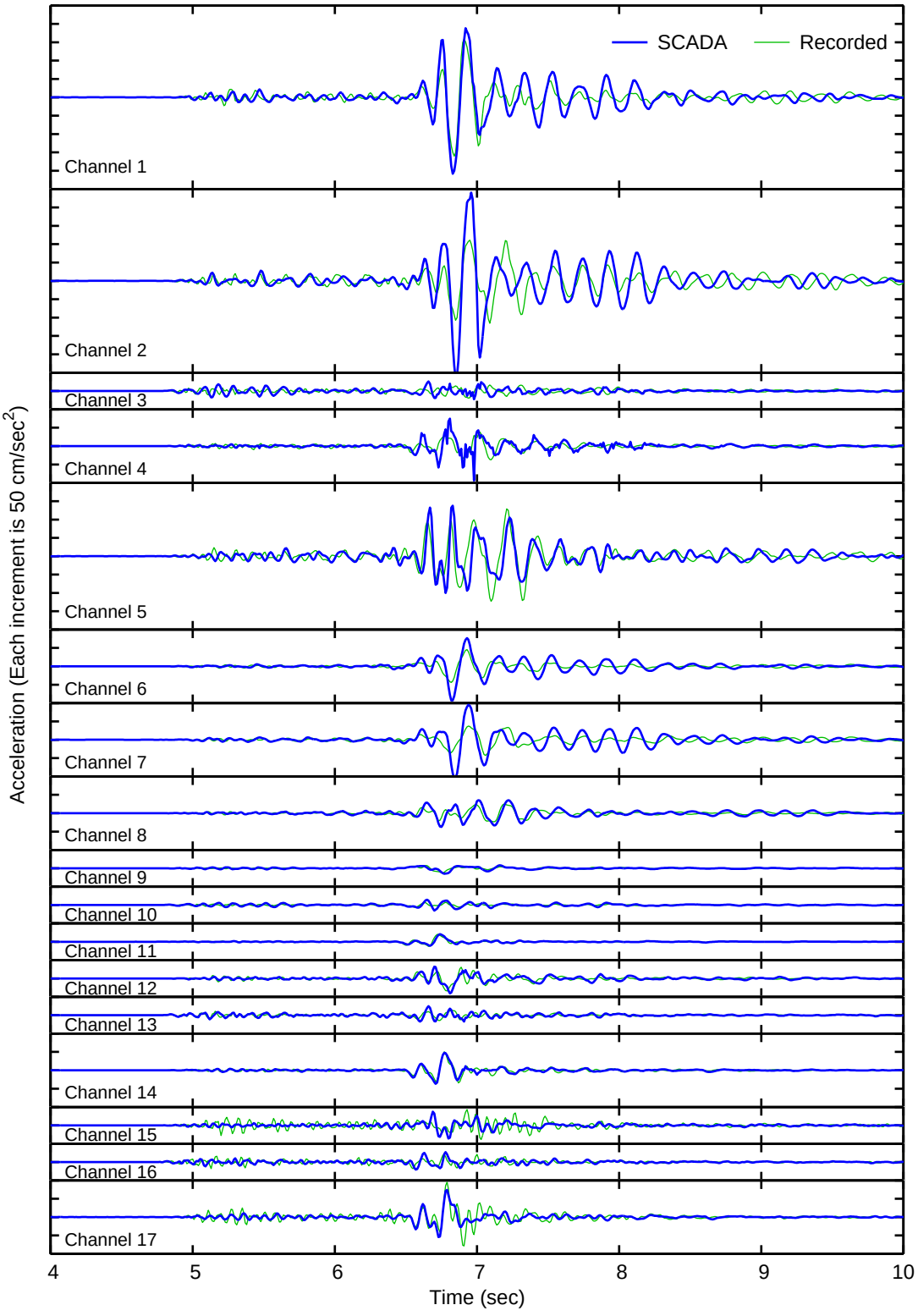

Figure B.4: Acceleration time histories at locations corresponding to channels 1–17 computed from a nonlinear analysis of the January 13, 2001 earthquake generated by method 2 compared to the actual records

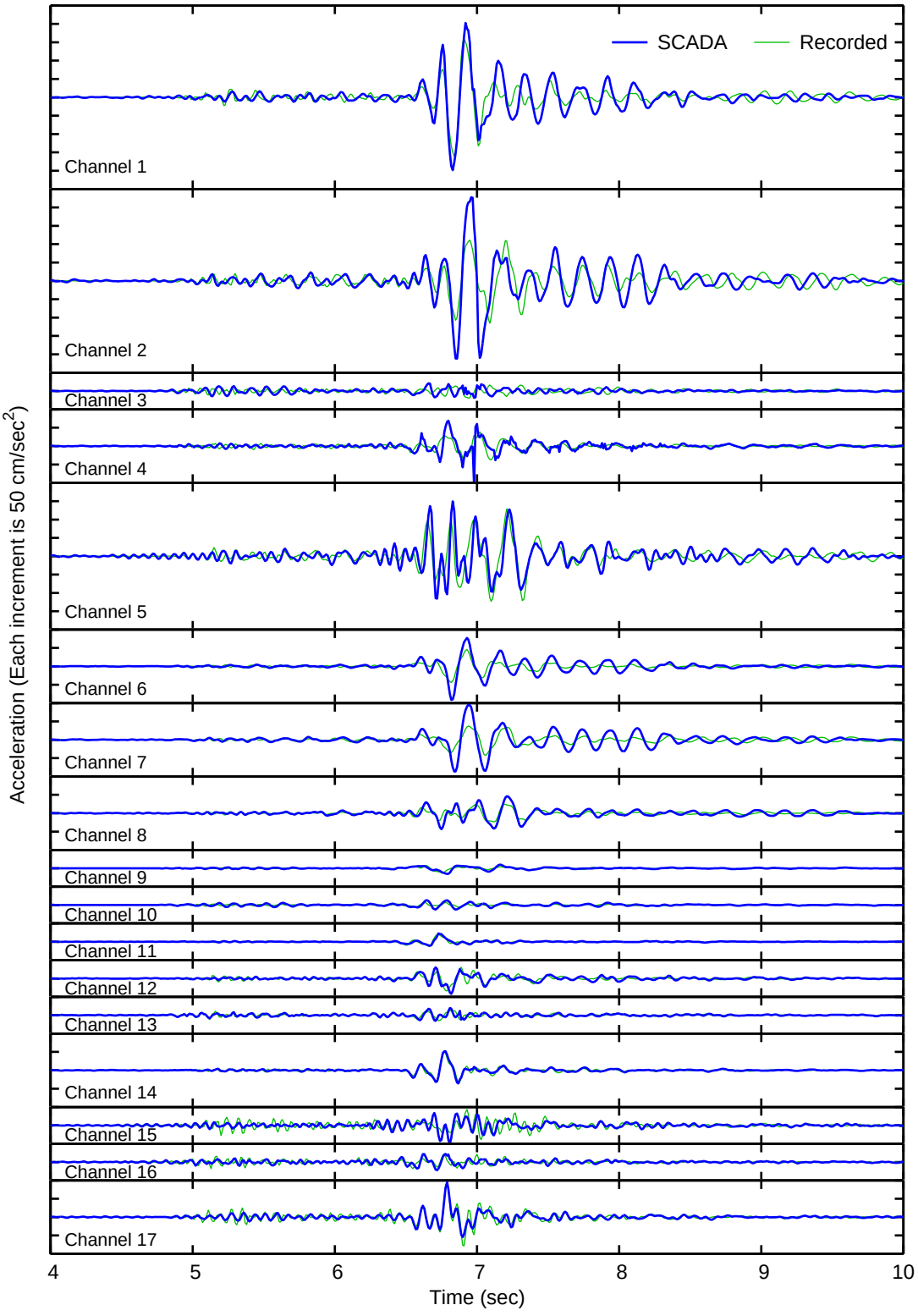

Figure B.5: Acceleration time histories at locations corresponding to channels 1–17 computed from a nonlinear analysis of the January 13, 2001 earthquake generated by method 9 compared to the actual records

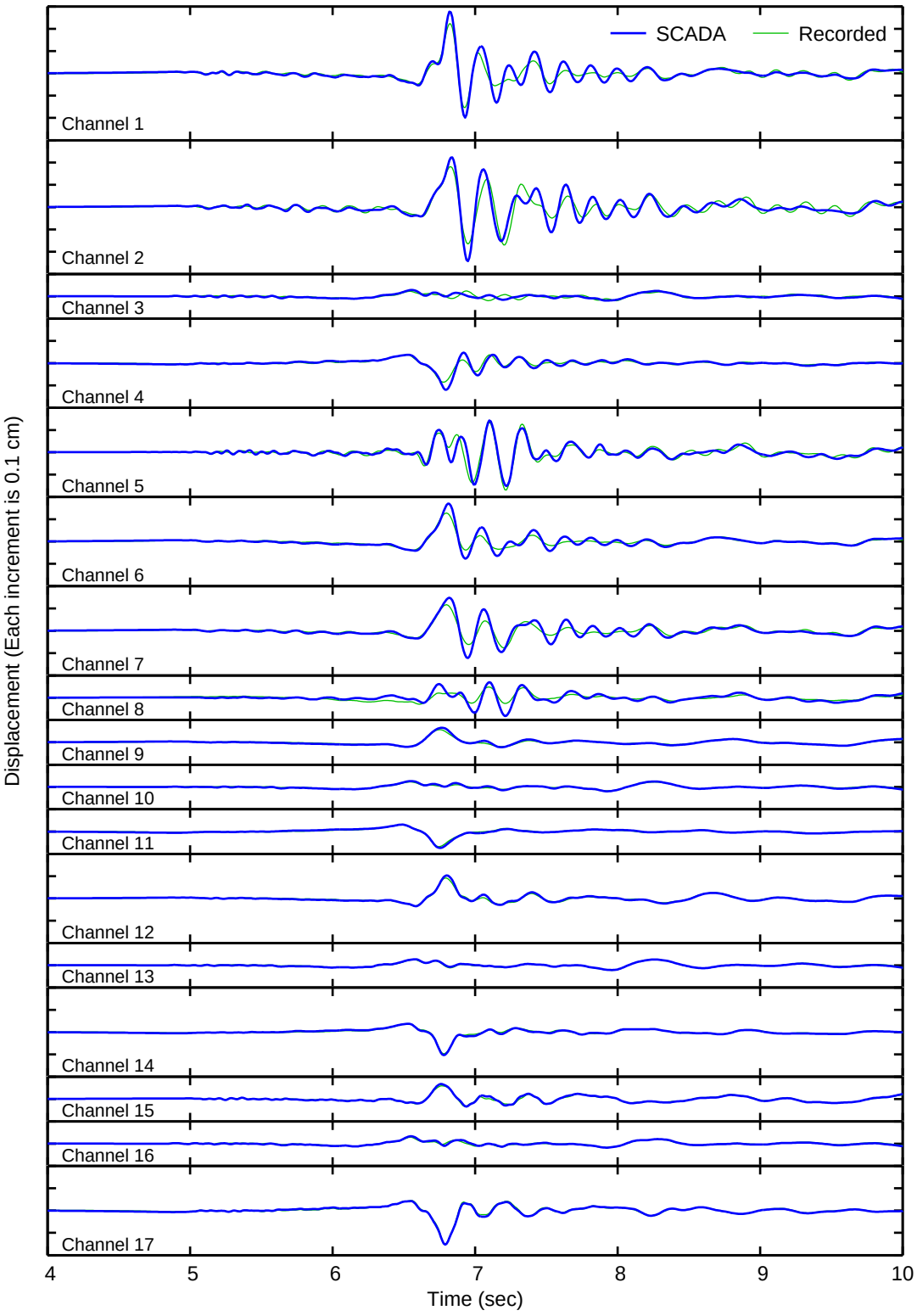

Figure B.6: Displacement time histories at locations corresponding to channels 1–17 computed from a linear analysis of the January 13, 2001 earthquake compared to the actual records

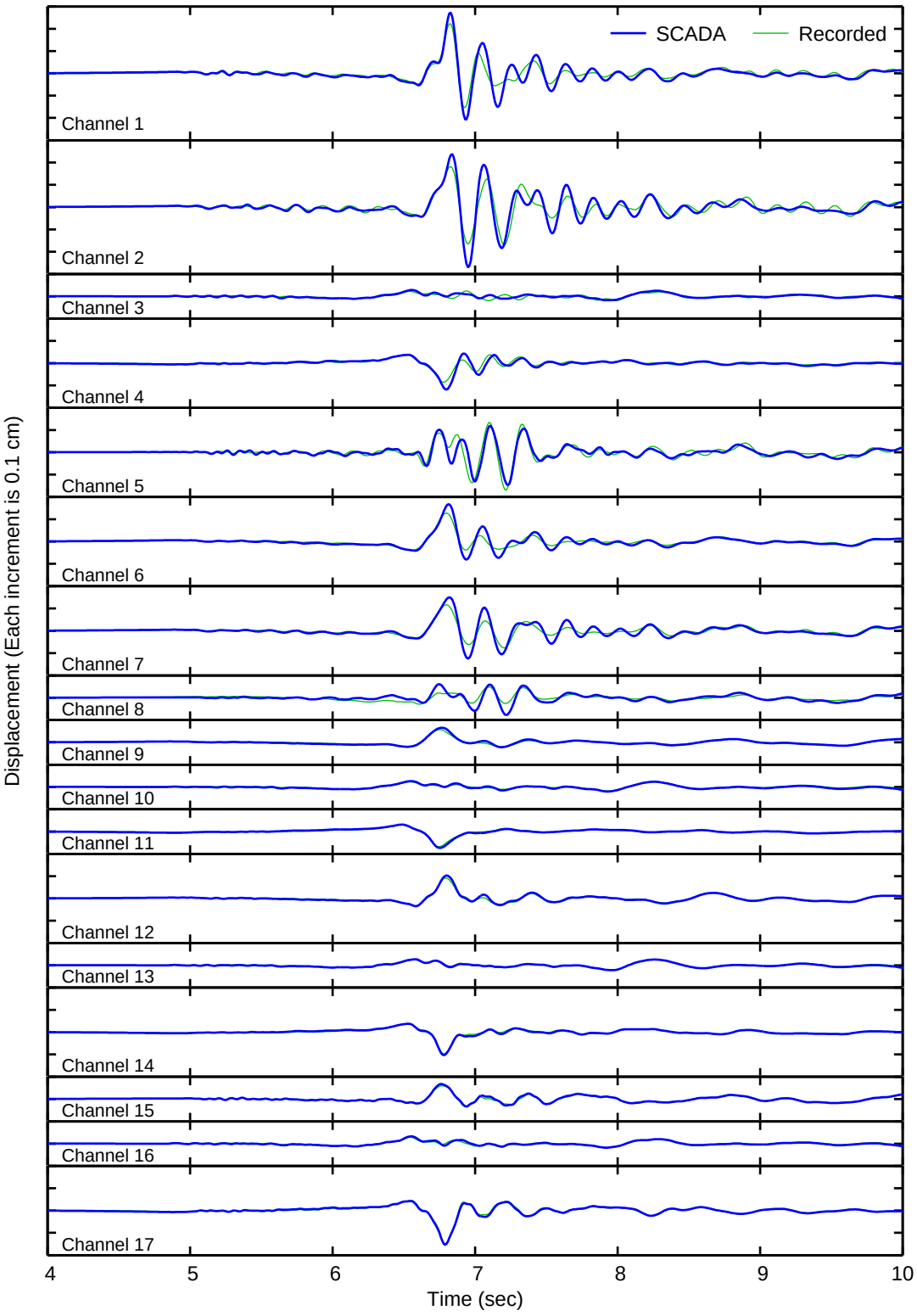

Figure B.7: Displacement time histories at locations corresponding to channels 1–17 computed from a nonlinear analysis of the January 13, 2001 earthquake compared to the actual records

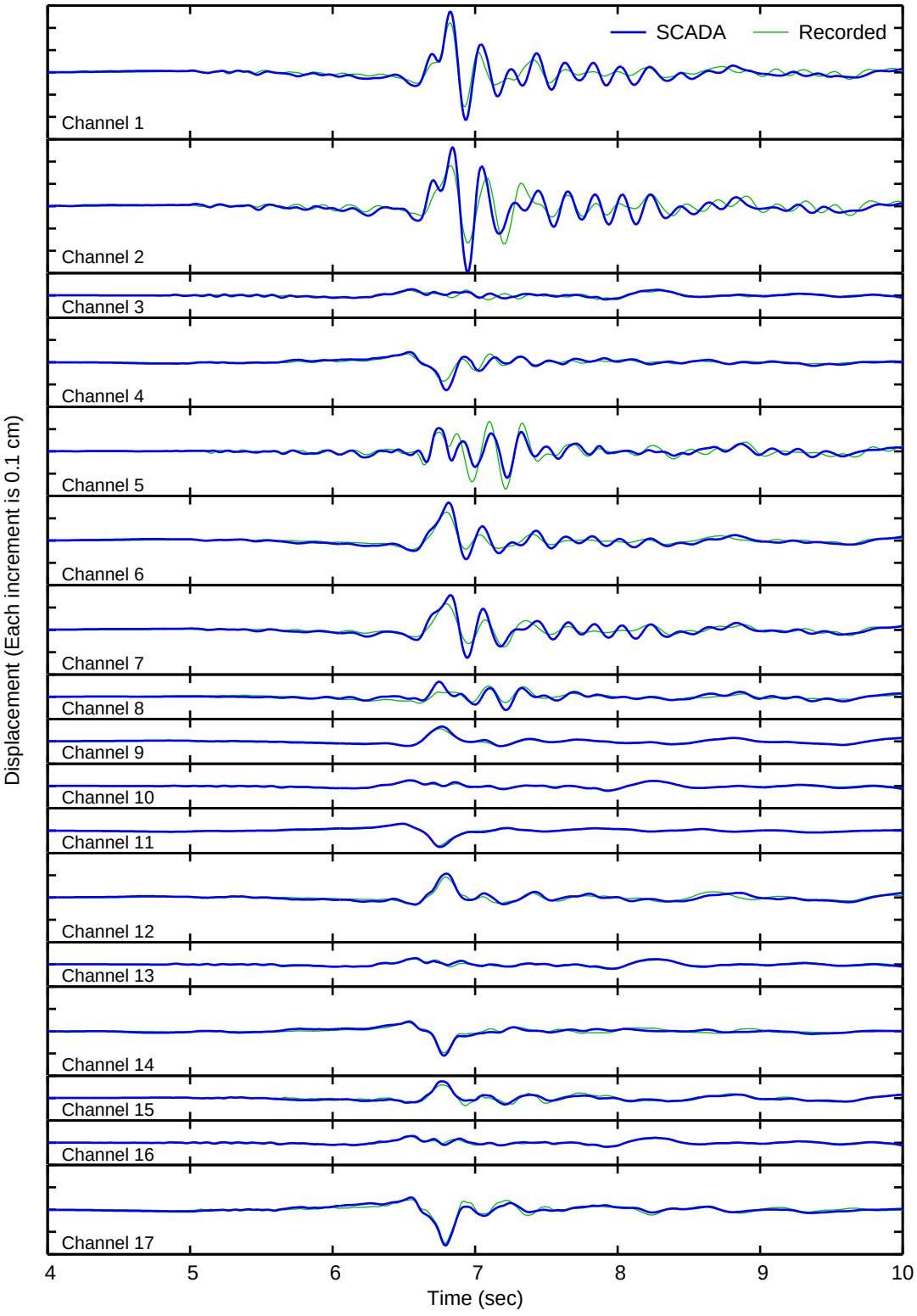

Figure B.8: Displacement time histories at locations corresponding to channels 1–17 computed from a nonlinear analysis of the January 13, 2001 earthquake generated by method 1 compared to the actual records

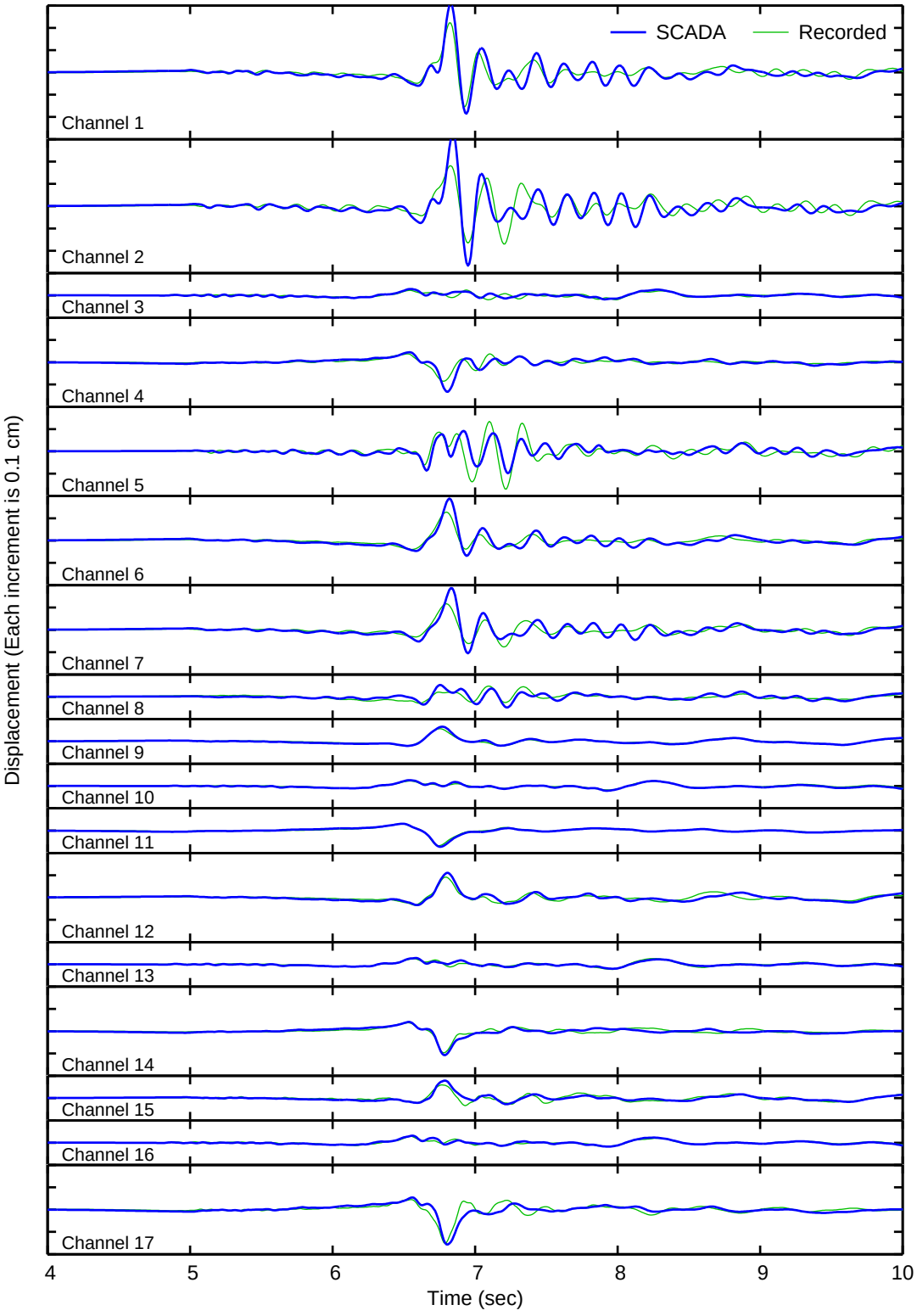

Figure B.9: Displacement time histories at locations corresponding to channels 1–17 computed from a nonlinear analysis of the January 13, 2001 earthquake generated by method 2 compared to the actual records

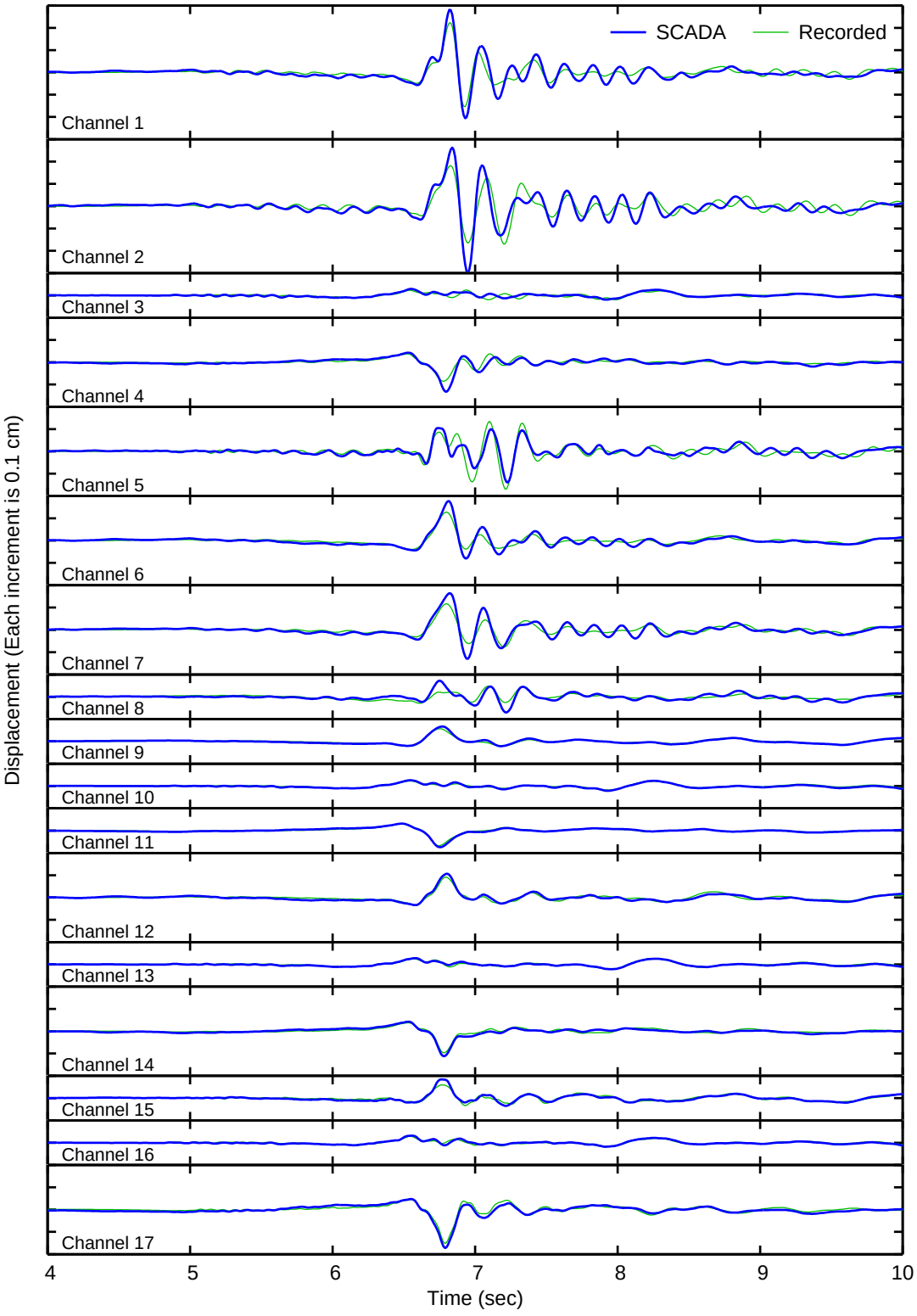

Figure B.10: Displacement time histories at locations corresponding to channels 1–17 computed from a nonlinear analysis of the January 13, 2001 earthquake generated by method 9 compared to the actual records

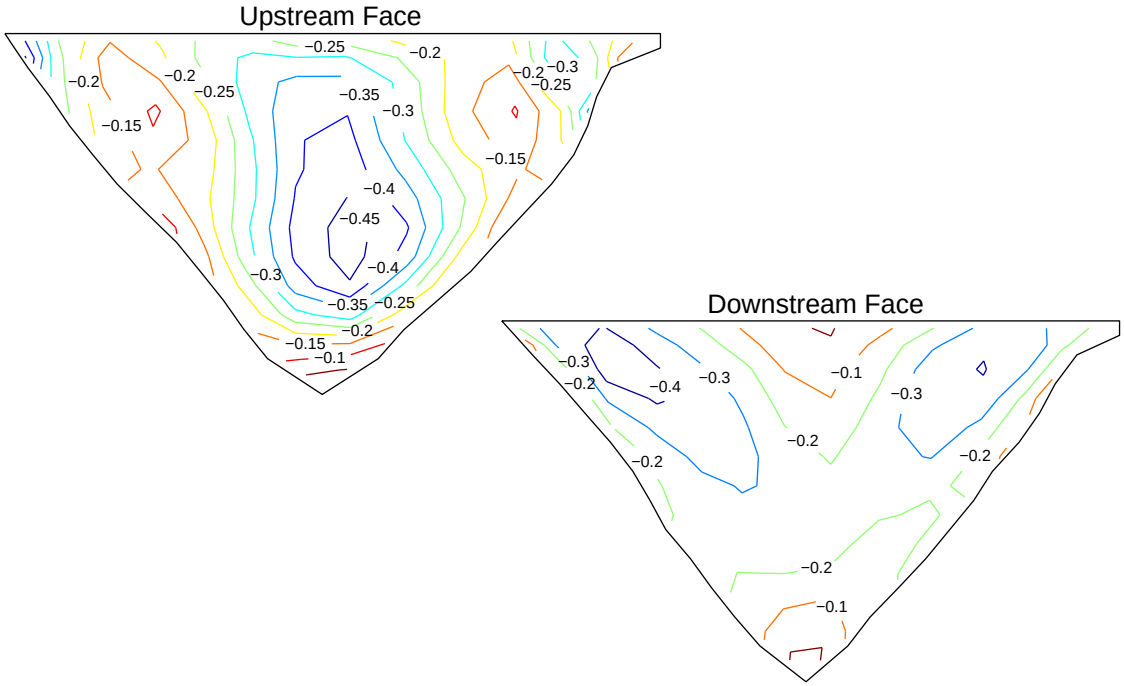

Figure B.11: Maximum compressive arch stresses (MPa) computed during a linear analysis with the January 13, 2001 earthquake input

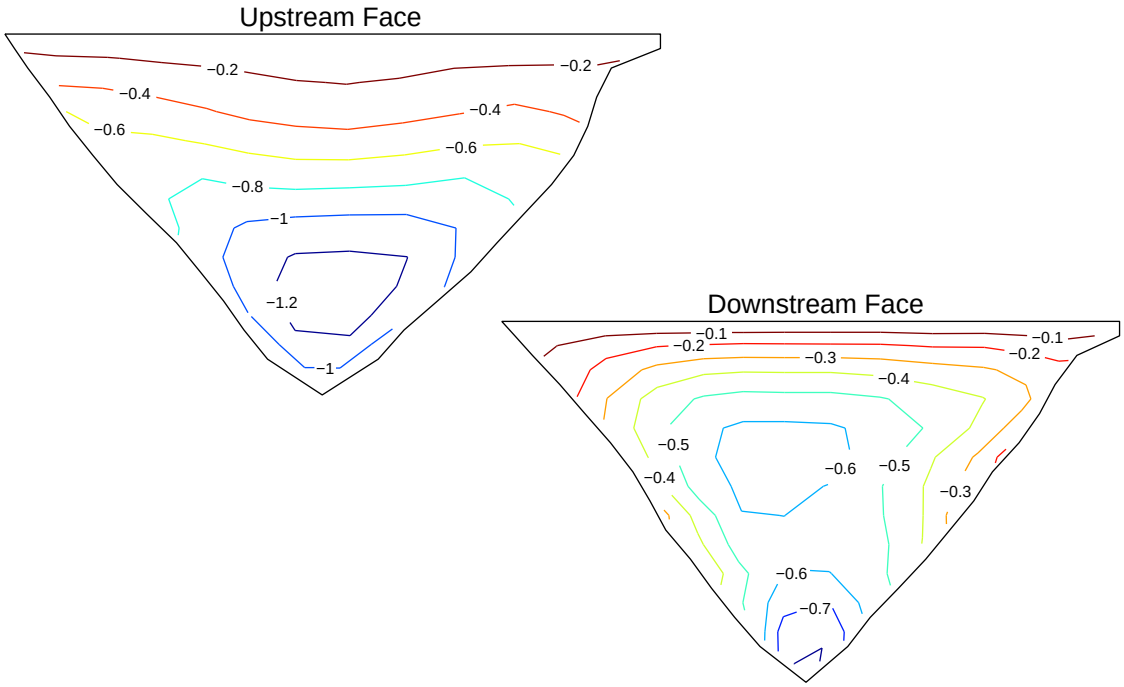

Figure B.12: Maximum compressive cantilever stresses (MPa) computed during a linear analysis with the January 13, 2001 earthquake input

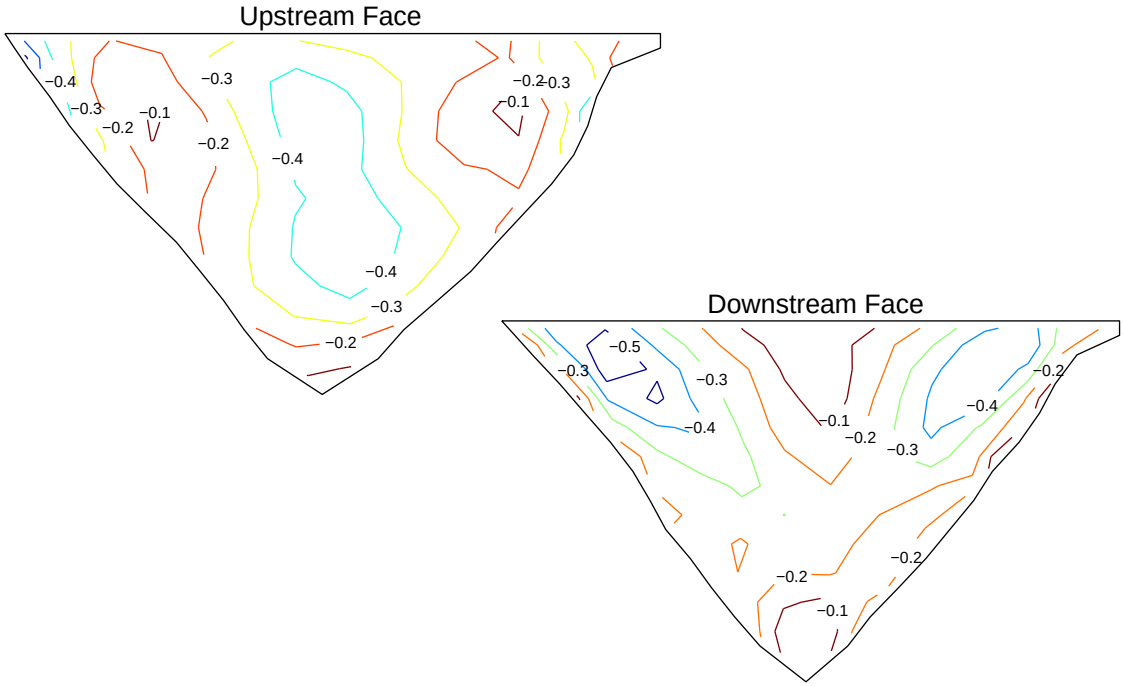

Figure B.13: Maximum compressive arch stresses (MPa) computed during a nonlinear analysis with the January 13, 2001 earthquake input

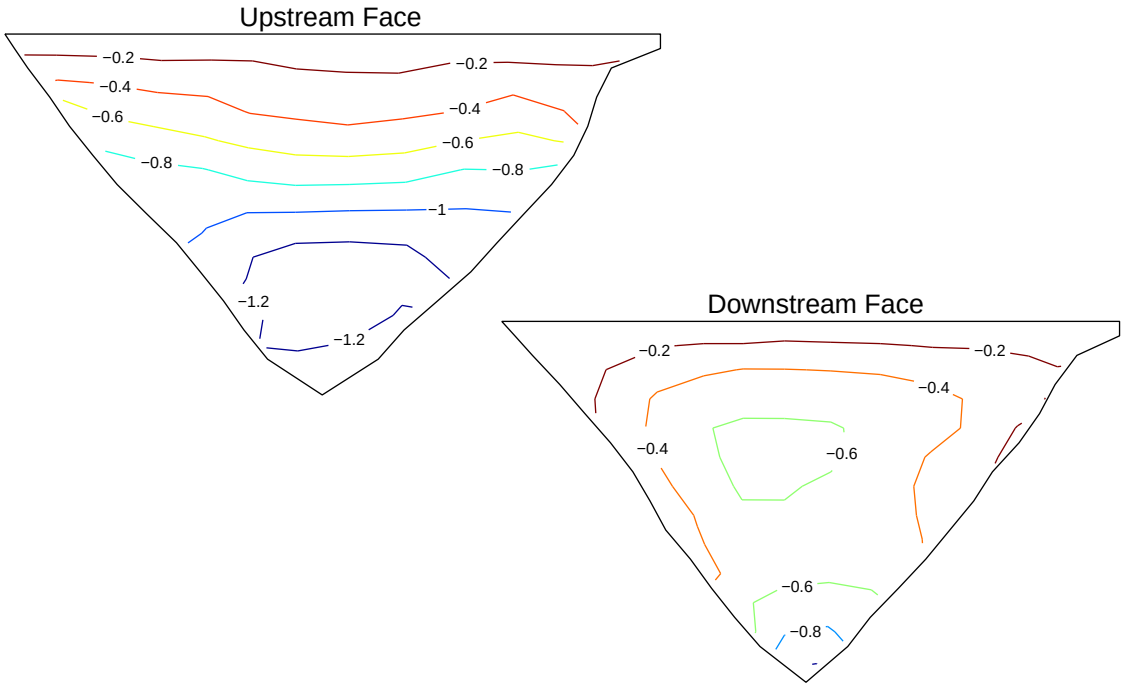

Figure B.14: Maximum compressive cantilever stresses (MPa) computed during a nonlinear analysis with the January 13, 2001 earthquake input

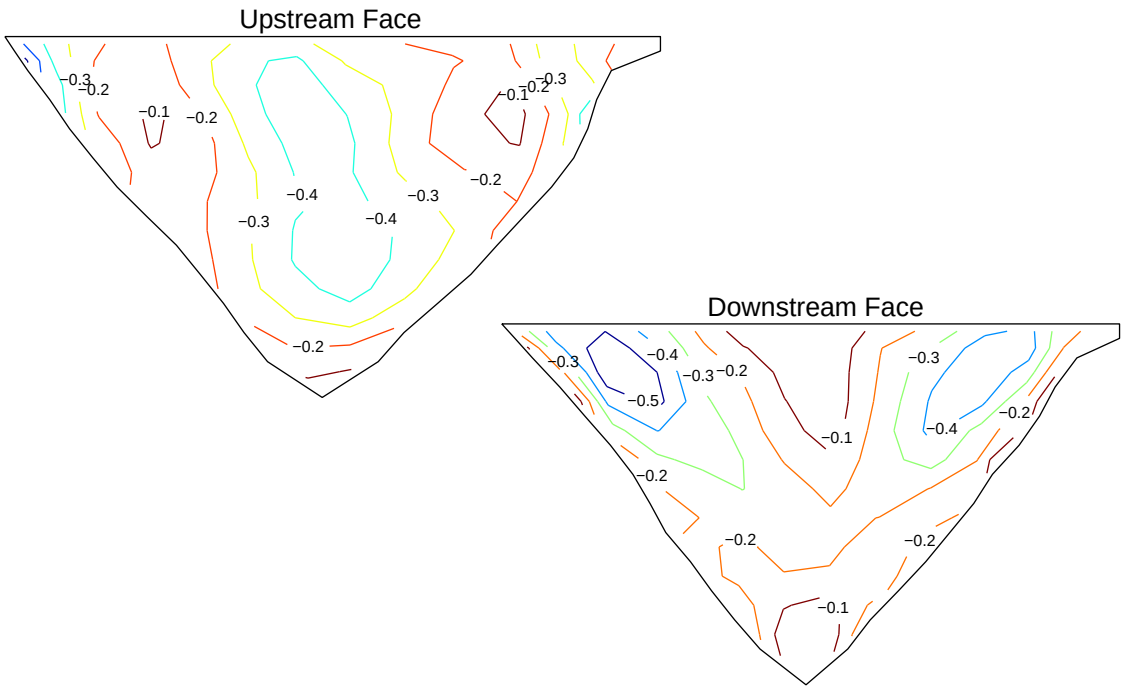

Figure B.15: Maximum compressive arch stresses (MPa) computed during a nonlinear analysis with the January 13, 2001 earthquake input generated by method 1

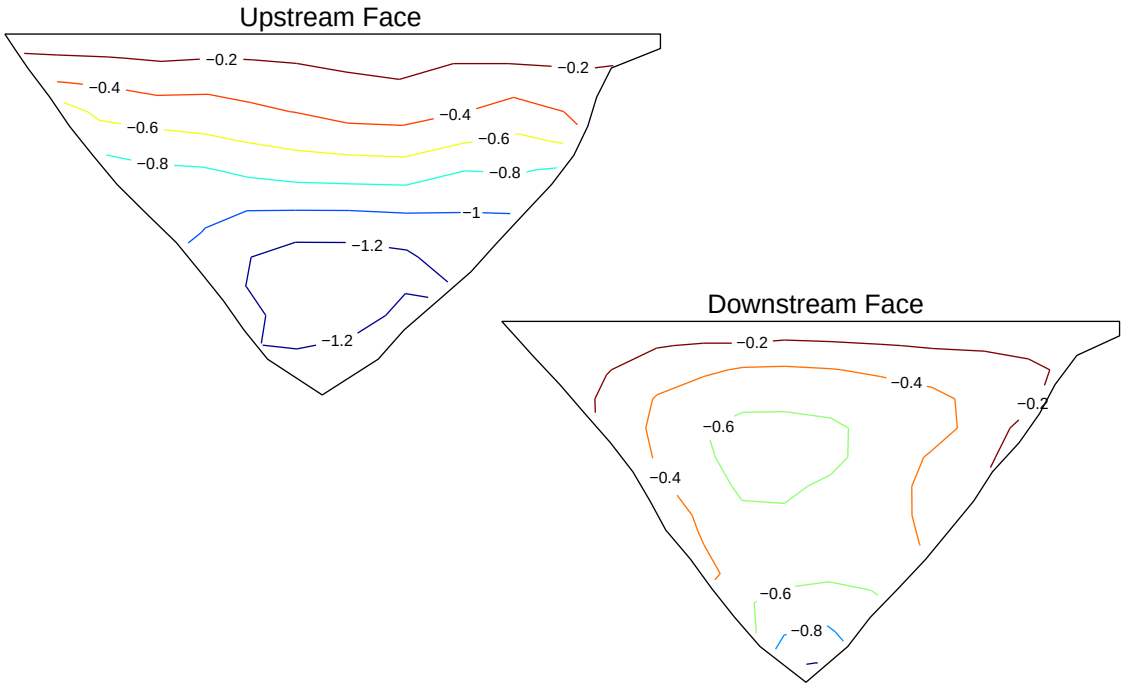

Figure B.16: Maximum compressive cantilever stresses (MPa) computed during a nonlinear analysis with the January 13, 2001 earthquake input generated by method 1

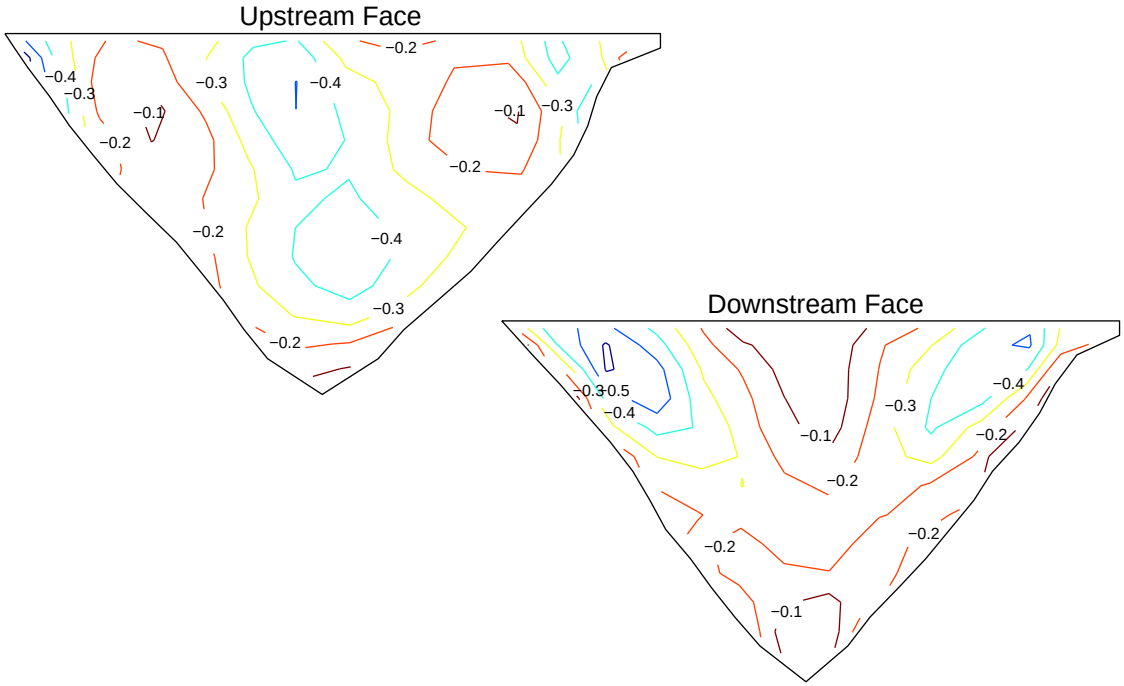

Figure B.17: Maximum compressive arch stresses (MPa) computed during a nonlinear analysis with the January 13, 2001 earthquake input generated by method 2

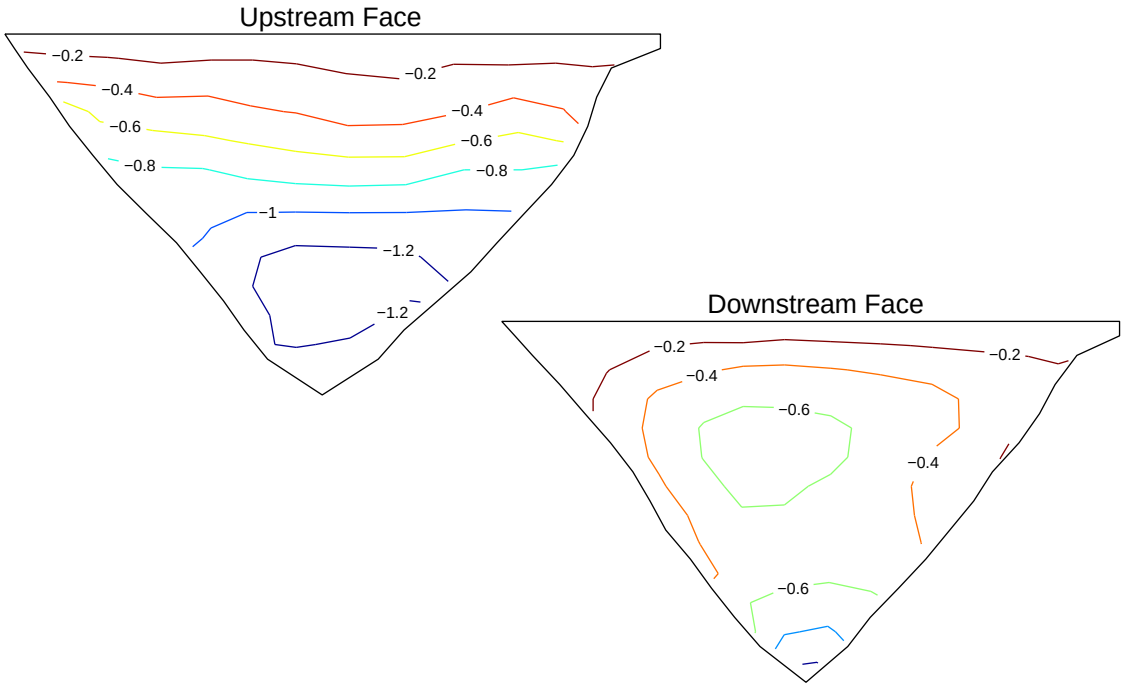

Figure B.18: Maximum compressive cantilever stresses (MPa) computed during a nonlinear analysis with the January 13, 2001 earthquake input generated by method 2

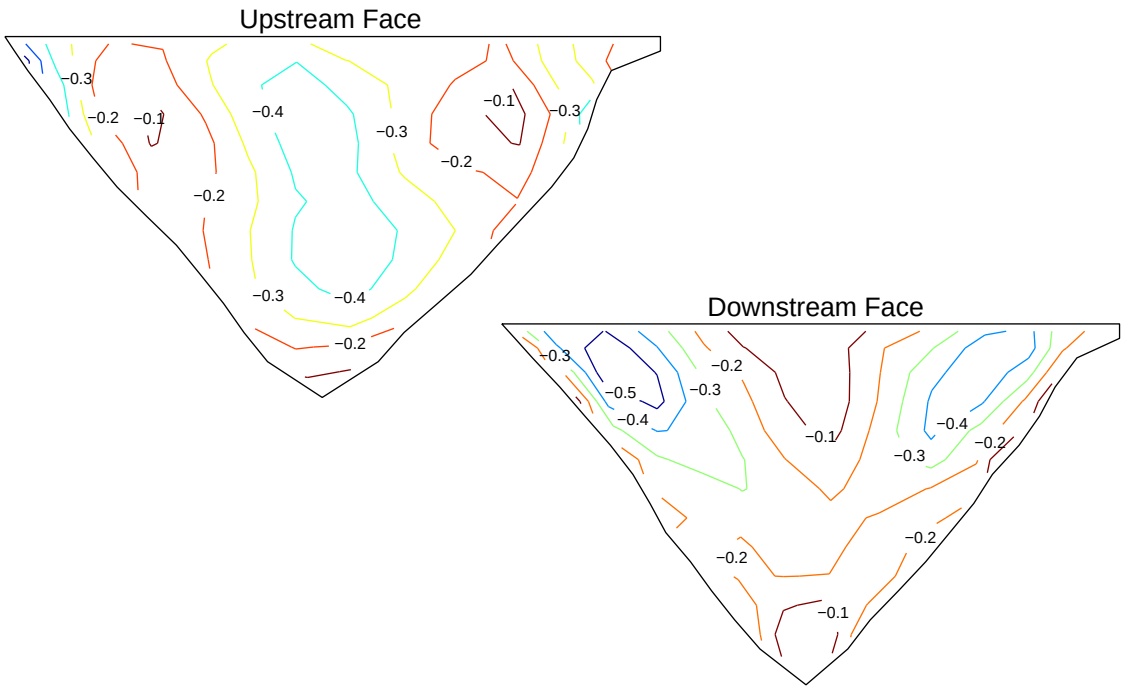

Figure B.19: Maximum compressive arch stresses (MPa) computed during a nonlinear analysis with the January 13, 2001 earthquake input generated by method 9

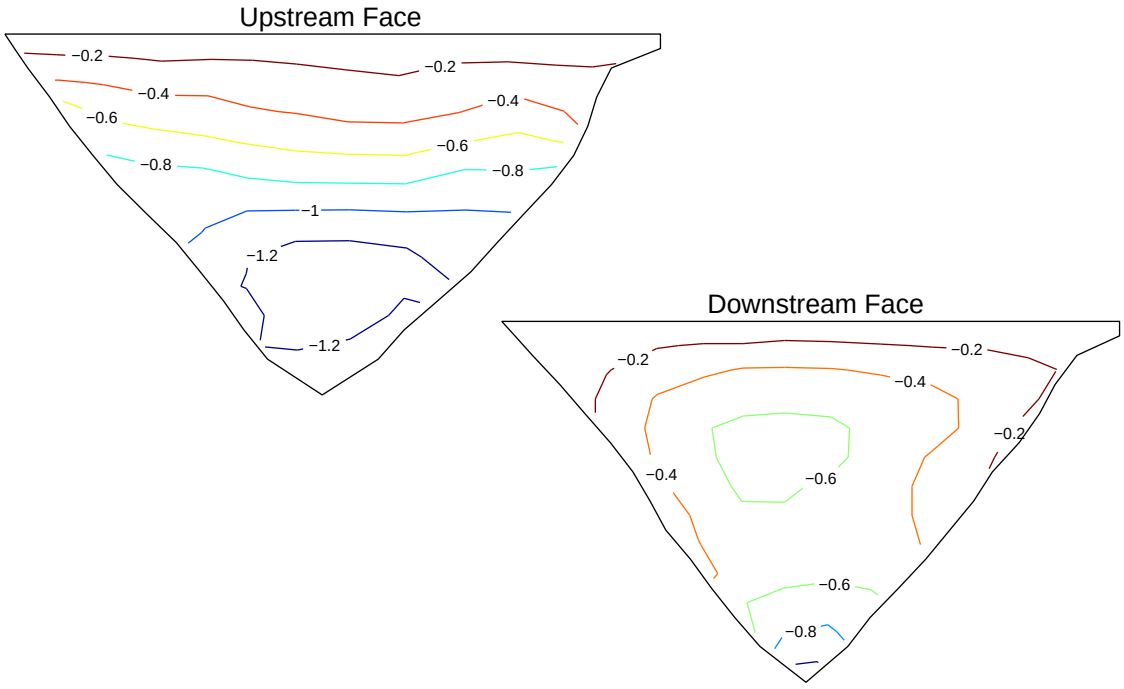

Figure B.20: Maximum compressive cantilever stresses (MPa) computed during a nonlinear analysis with the January 13, 2001 earthquake input generated by method 9

0.00	0.00	0.00	0.00	0.02	0.02	0.03	0.02	0.02	0.01	0.01	0.00	0.00	0.00
0.00	0.00	0.00	0.00	0.01	0.02	0.02	0.01	0.02	0.00	0.01	0.00	0.00	0.00
	0.01	0.00	0.00	0.00	0.01	0.01	0.01	0.01	0.00	0.01	0.00	0.00	
	0.01	0.00	0.00	0.00	0.00	0.01	0.01	0.00	0.00	0.00	0.00	0.00	
		0.01	0.00	0.00	0.00	0.00	0.00	0.00	0.00	0.00	0.01		
		0.01	0.00	0.00	0.00	0.00	0.00	0.00	0.00	0.00	0.01		
			0.00	0.00	0.00	0.00	0.00	0.00	0.00	0.00			
			0.00	0.00	0.00	0.00	0.00	0.00	0.00	0.00			
				0.00	0.00	0.00	0.00	0.00	0.00				
				0.00	0.00	0.00	0.00	0.00	0.00				
					0.00	0.00	0.00	0.00					
					0.00	0.00	0.00	0.00					
						0.00	0.00						

Figure B.21: Maximum joint opening (cm) computed during a nonlinear analysis with the January 13, 2001 earthquake input

0.00	0.00	0.00	0.00	0.02	0.03	0.04	0.02	0.03	0.01	0.01	0.00	0.00	0.00
0.00	0.00	0.00	0.00	0.01	0.02	0.03	0.01	0.02	0.00	0.00	0.00	0.00	0.00
	0.01	0.00	0.00	0.00	0.01	0.01	0.01	0.01	0.00	0.01	0.00	0.00	
	0.01	0.00	0.00	0.00	0.00	0.01	0.01	0.01	0.00	0.00	0.00	0.00	
		0.01	0.00	0.00	0.00	0.00	0.00	0.00	0.00	0.00	0.00		
		0.01	0.00	0.00	0.00	0.00	0.00	0.00	0.00	0.00	0.01		
			0.00	0.00	0.00	0.00	0.00	0.00	0.00	0.00			
			0.00	0.00	0.00	0.00	0.00	0.00	0.00	0.00			
				0.00	0.00	0.00	0.00	0.00	0.00				
				0.00	0.00	0.00	0.00	0.00	0.00				
					0.00	0.00	0.00	0.00					
					0.00	0.00	0.00	0.00					
						0.00	0.00						

Figure B.22: Maximum joint opening (cm) computed during a nonlinear analysis with the January 13, 2001 earthquake input generated by method 1

0.00	0.00	0.00	0.00	0.02	0.03	0.04	0.02	0.03	0.01	0.00	0.00	0.00	0.00
0.00	0.00	0.00	0.00	0.01	0.02	0.03	0.01	0.03	0.01	0.00	0.00	0.00	0.00
	0.01	0.00	0.00	0.01	0.01	0.01	0.01	0.02	0.00	0.01	0.00	0.00	
	0.01	0.00	0.00	0.00	0.00	0.01	0.01	0.01	0.00	0.00	0.00	0.00	
		0.01	0.00	0.00	0.00	0.01	0.00	0.00	0.00	0.00	0.00		
		0.01	0.00	0.00	0.00	0.00	0.00	0.00	0.00	0.00	0.01		
			0.00	0.00	0.00	0.00	0.00	0.00	0.00	0.00			
			0.00	0.00	0.00	0.00	0.00	0.00	0.00	0.00			
				0.00	0.00	0.00	0.00	0.00	0.00				
				0.00	0.00	0.00	0.00	0.00	0.00				
					0.00	0.00	0.00	0.00					
					0.00	0.00	0.00	0.00					
						0.00	0.00						

Figure B.23: Maximum joint opening (cm) computed during a nonlinear analysis with the January 13, 2001 earthquake input generated by method 2

0.00	0.00	0.00	0.00	0.02	0.03	0.04	0.02	0.02	0.01	0.01	0.00	0.00	0.00
0.00	0.00	0.00	0.00	0.01	0.02	0.02	0.01	0.02	0.01	0.01	0.00	0.00	0.00
	0.01	0.00	0.00	0.00	0.01	0.01	0.01	0.01	0.00	0.01	0.00	0.00	
	0.01	0.00	0.00	0.00	0.00	0.01	0.01	0.00	0.00	0.00	0.00	0.00	
		0.01	0.00	0.00	0.00	0.00	0.01	0.00	0.00	0.00	0.00		
		0.01	0.00	0.00	0.00	0.00	0.00	0.00	0.00	0.00	0.01		
			0.00	0.00	0.00	0.00	0.00	0.00	0.00	0.00			
			0.00	0.00	0.00	0.00	0.00	0.00	0.00	0.00			
				0.00	0.00	0.00	0.00	0.00	0.00				
				0.00	0.00	0.00	0.00	0.00	0.00				
					0.00	0.00	0.00	0.00					
					0.00	0.00	0.00	0.00					
						0.00	0.00						

Figure B.24: Maximum joint opening (cm) computed during a nonlinear analysis with the January 13, 2001 earthquake input generated by method 9

Appendix C

Results from Northridge Earthquake Analyses

Output responses from SCADA analyses using ground motion that was generated from the Northridge earthquake base records are included in this appendix. The responses include acceleration and displacement time histories computed at the locations of the accelerometer array at Pacoima Dam, contours of maximum compressive stress in the arch and cantilever directions on both faces of the dam and response pictures showing the maximum joint opening and crack opening in each element of the dam mesh. The stress contour plots and the response pictures are presented as if an observer was viewing the dam from downstream, so north is to the left of the figures and the thrust block is to the right. Some of these response quantities are also presented in Chapter 10, but they are duplicated here for completeness.

C.1 Comparing Generation Methods

The computed responses for nonlinear dynamic analyses with each of the sets of ground motion generated as described in Table 10.1 are given in this section. All of the response quantities are included for each of the ten methods of ground motion generation.

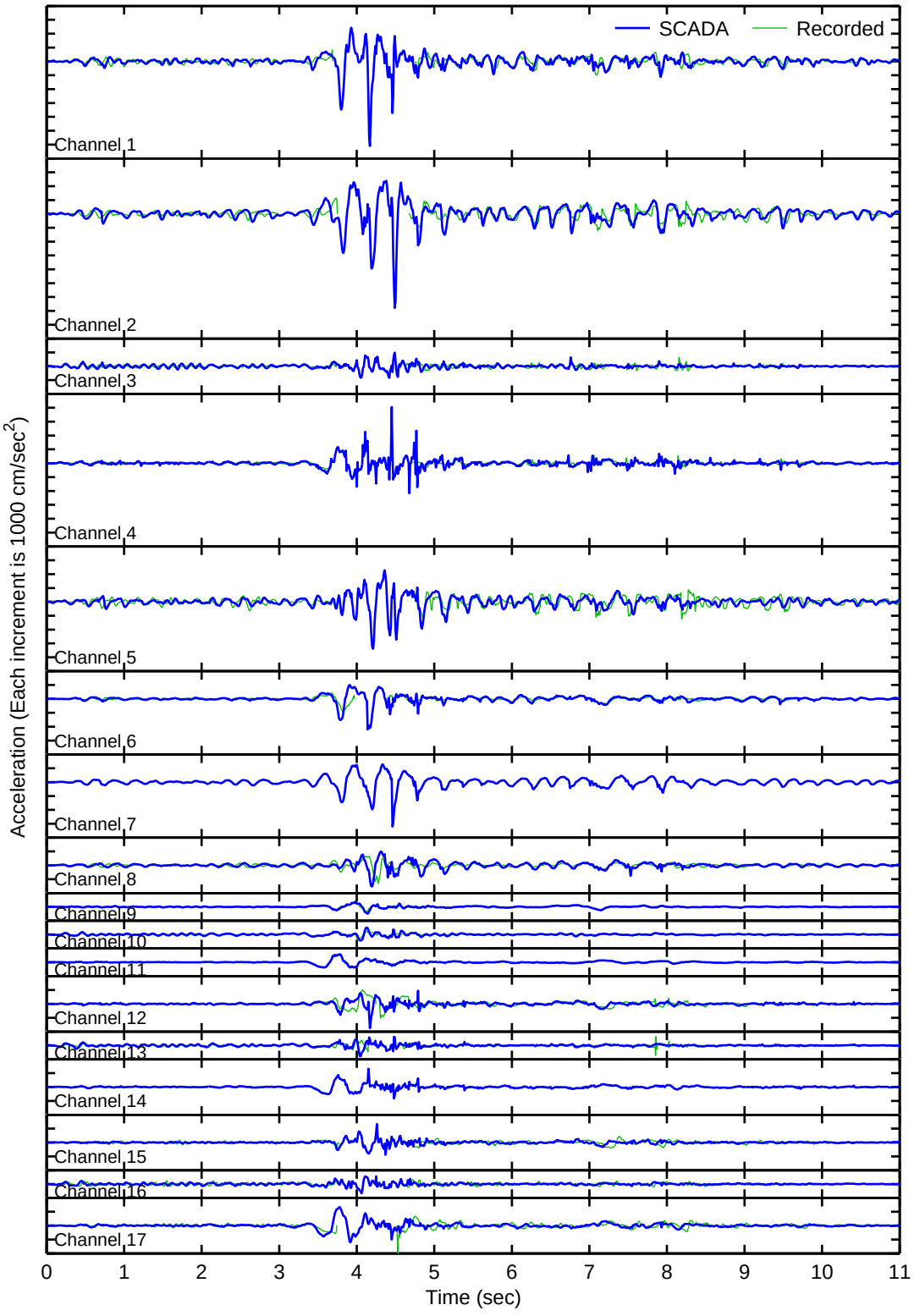

Figure C.1: Acceleration time histories at locations corresponding to channels 1–17 computed from a nonlinear analysis of the Northridge earthquake compared to the partial records (method 1)

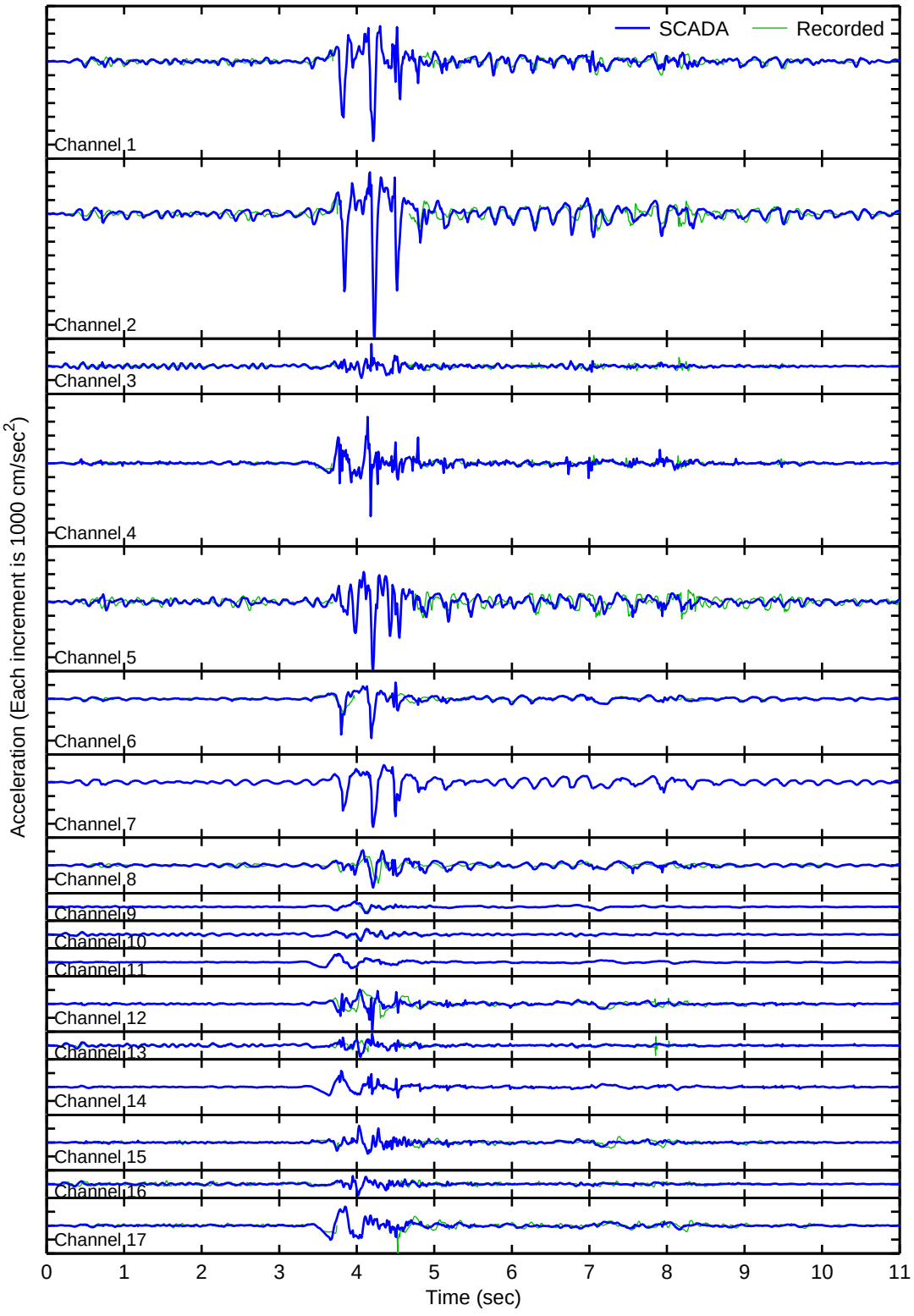

Figure C.2: Acceleration time histories at locations corresponding to channels 1–17 computed from a nonlinear analysis of the Northridge earthquake compared to the partial records (method 2)

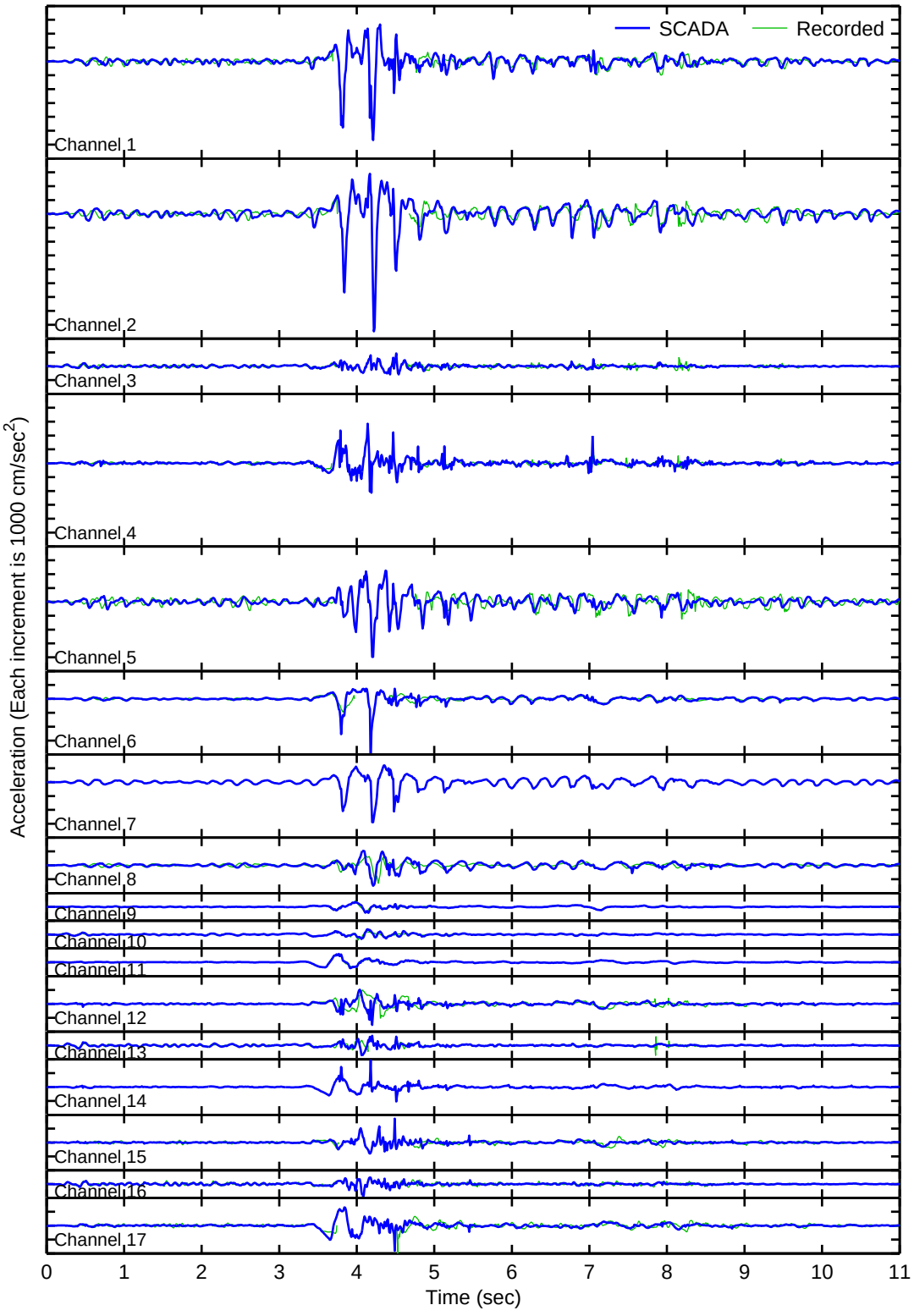

Figure C.3: Acceleration time histories at locations corresponding to channels 1–17 computed from a nonlinear analysis of the Northridge earthquake compared to the partial records (method 3)

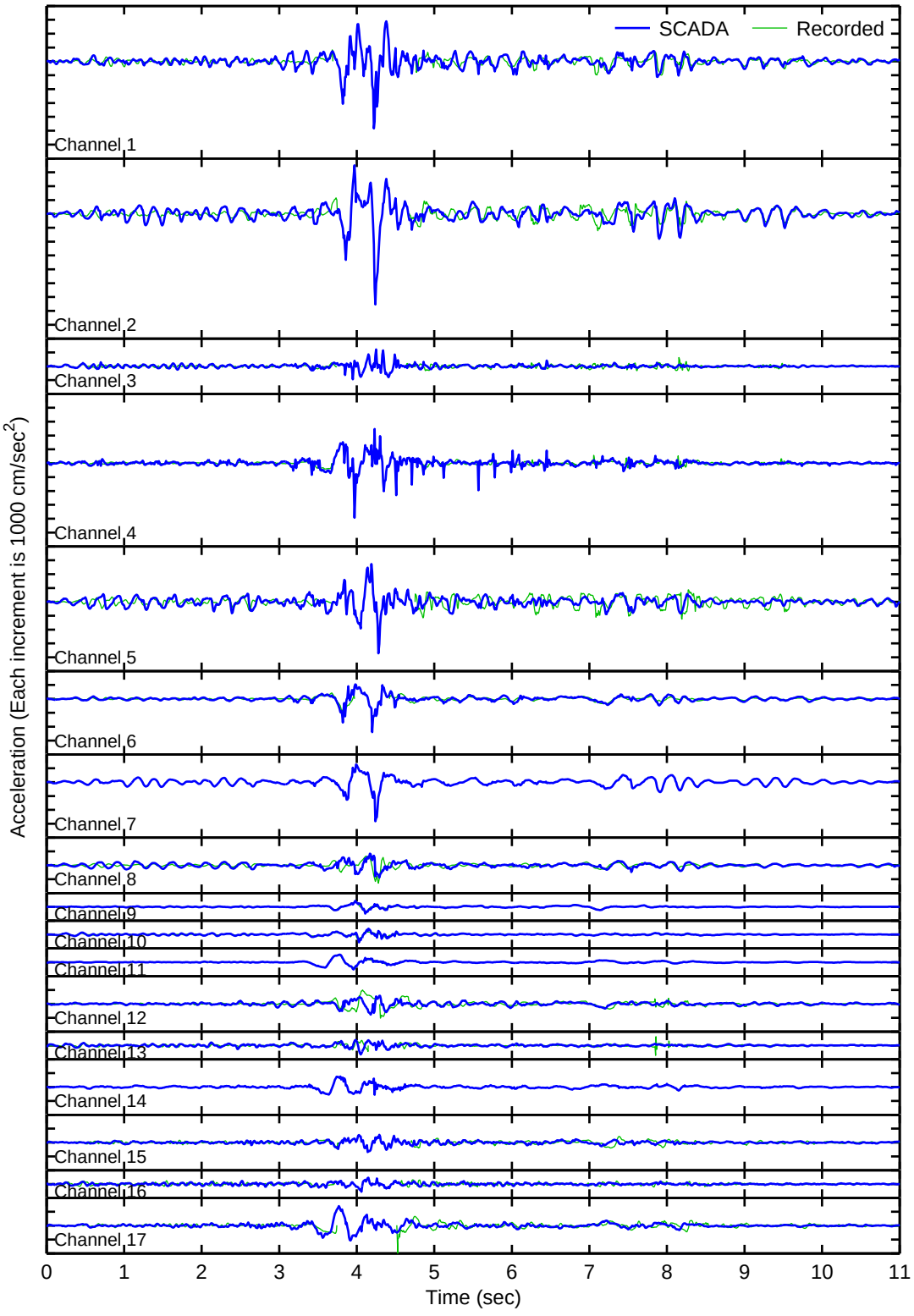

Figure C.4: Acceleration time histories at locations corresponding to channels 1–17 computed from a nonlinear analysis of the Northridge earthquake compared to the partial records (method 4)

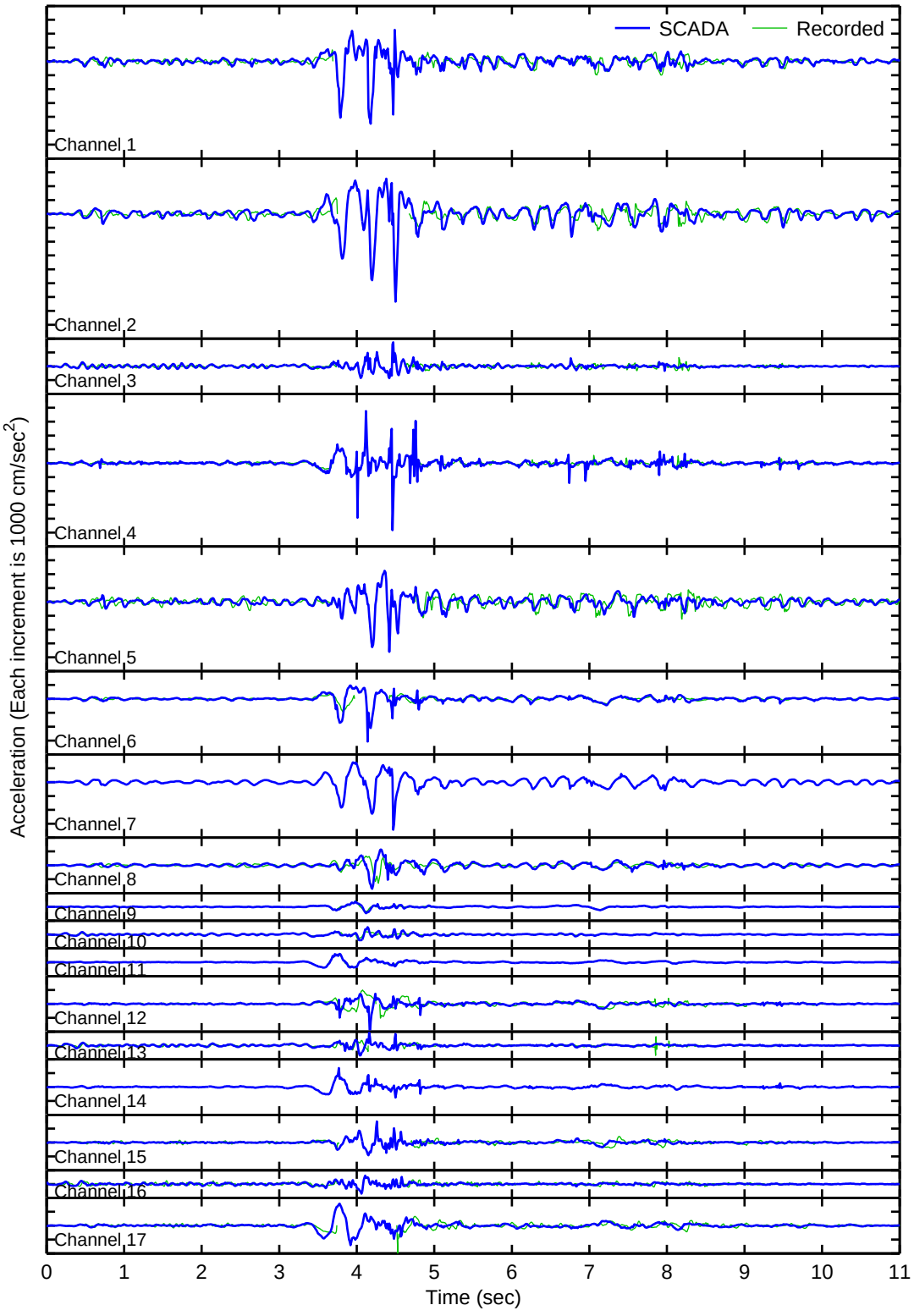

Figure C.5: Acceleration time histories at locations corresponding to channels 1–17 computed from a nonlinear analysis of the Northridge earthquake compared to the partial records (method 5)

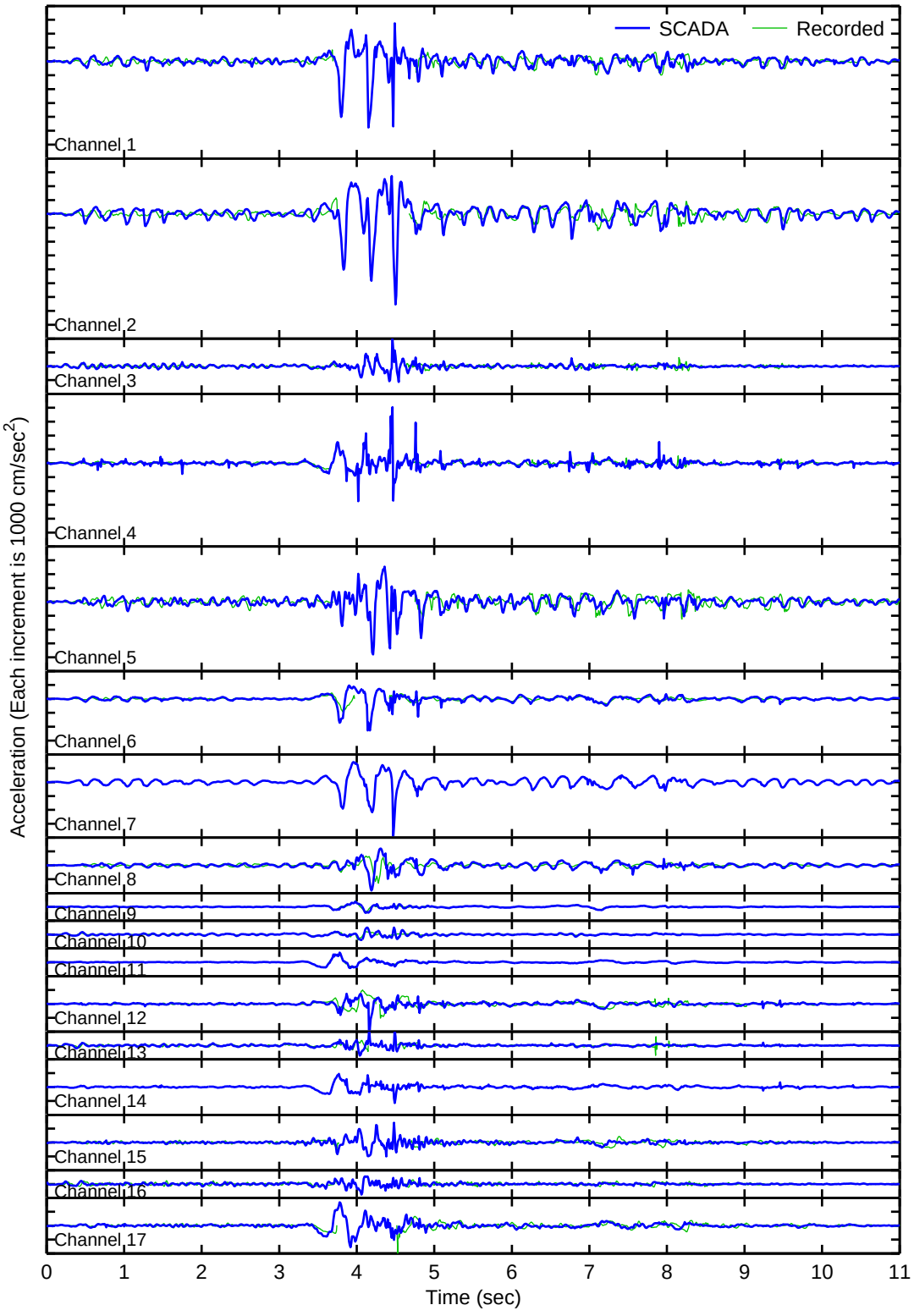

Figure C.6: Acceleration time histories at locations corresponding to channels 1–17 computed from a nonlinear analysis of the Northridge earthquake compared to the partial records (method 9)

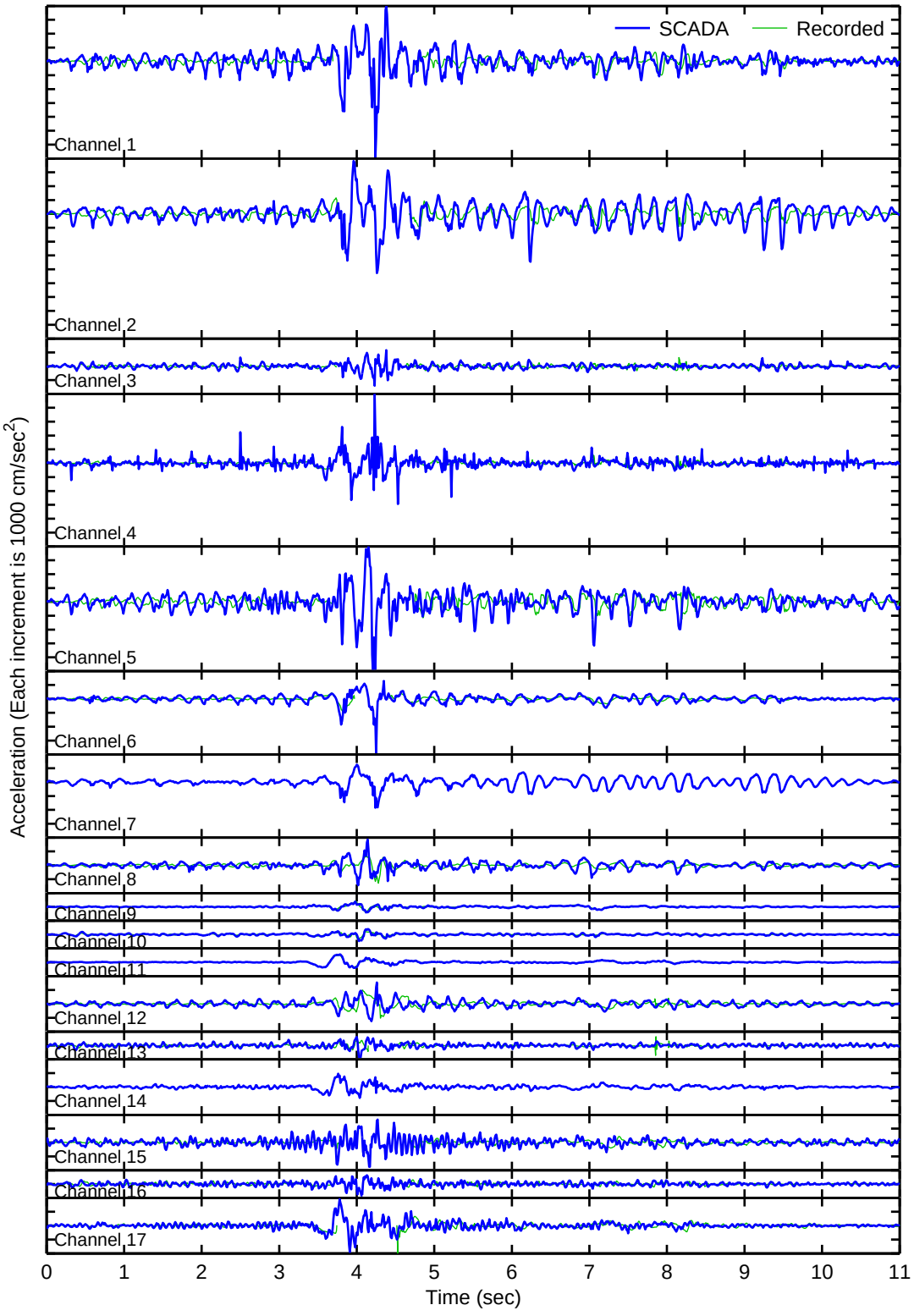

Figure C.7: Acceleration time histories at locations corresponding to channels 1–17 computed from a nonlinear analysis of the Northridge earthquake compared to the partial records (method 13)

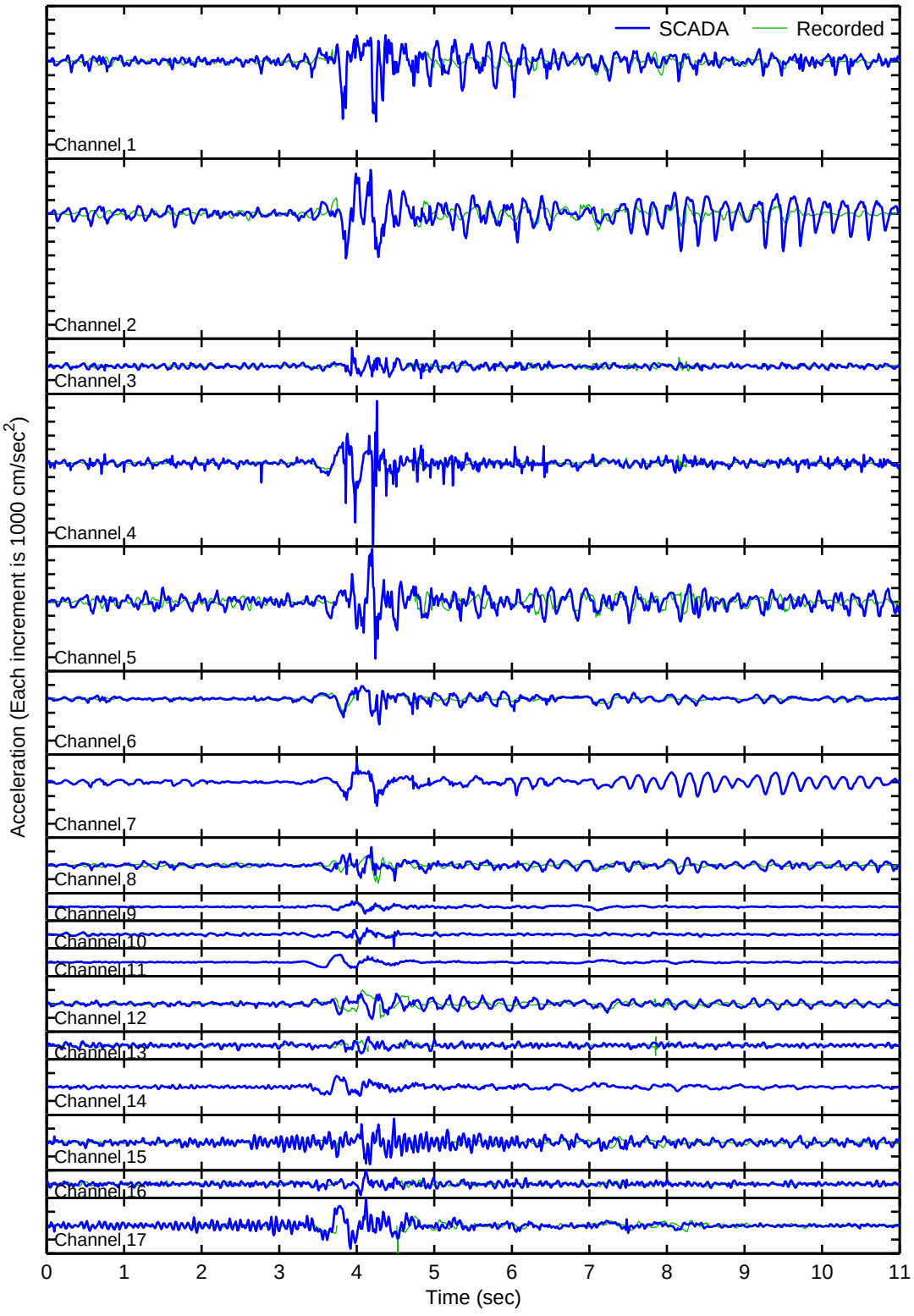

Figure C.8: Acceleration time histories at locations corresponding to channels 1–17 computed from a nonlinear analysis of the Northridge earthquake compared to the partial records (method 16)

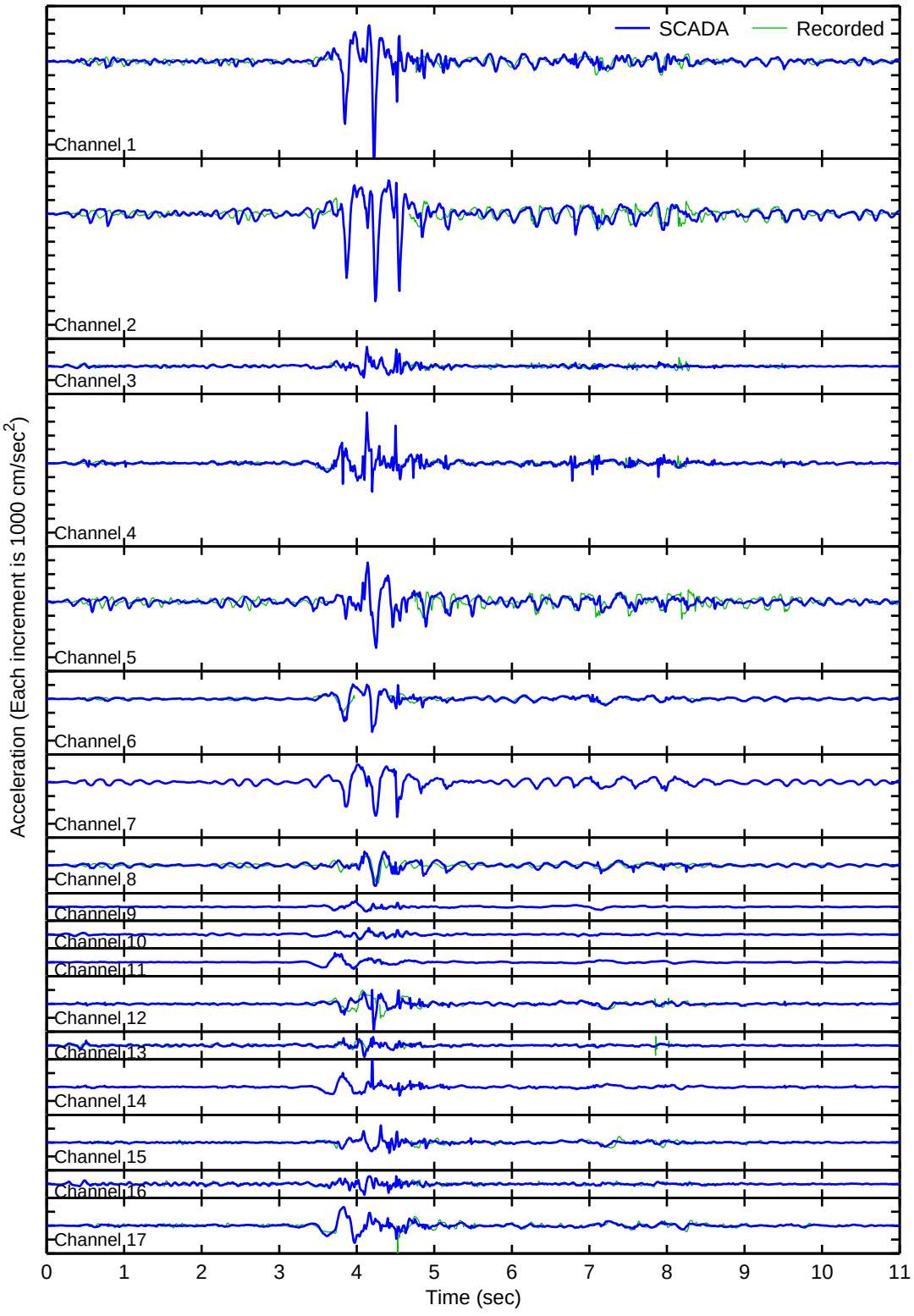

Figure C.9: Acceleration time histories at locations corresponding to channels 1–17 computed from a nonlinear analysis of the Northridge earthquake compared to the partial records (method 1+0.05 sec)

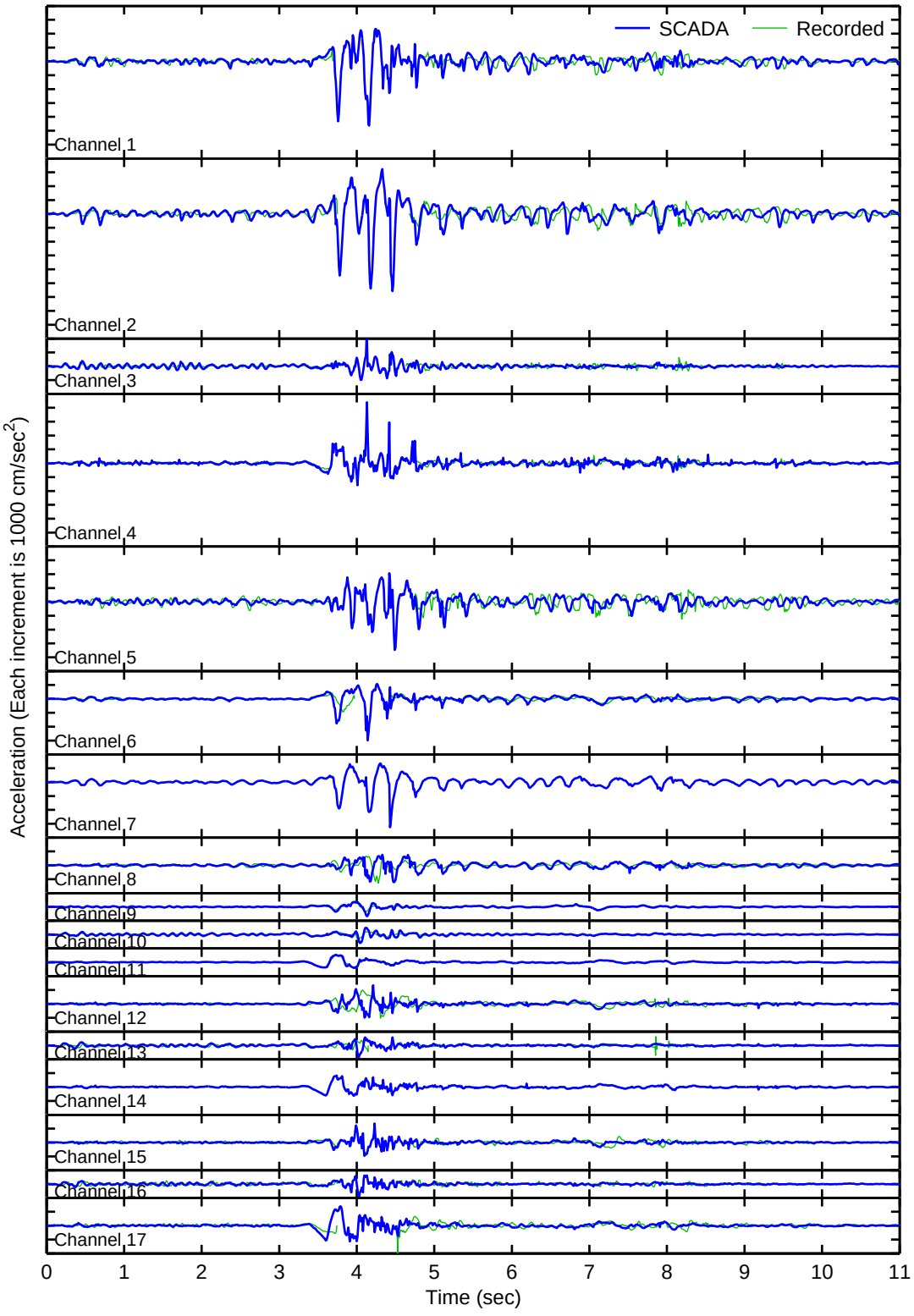

Figure C.10: Acceleration time histories at locations corresponding to channels 1–17 computed from a nonlinear analysis of the Northridge earthquake compared to the partial records (method 1 no delays)

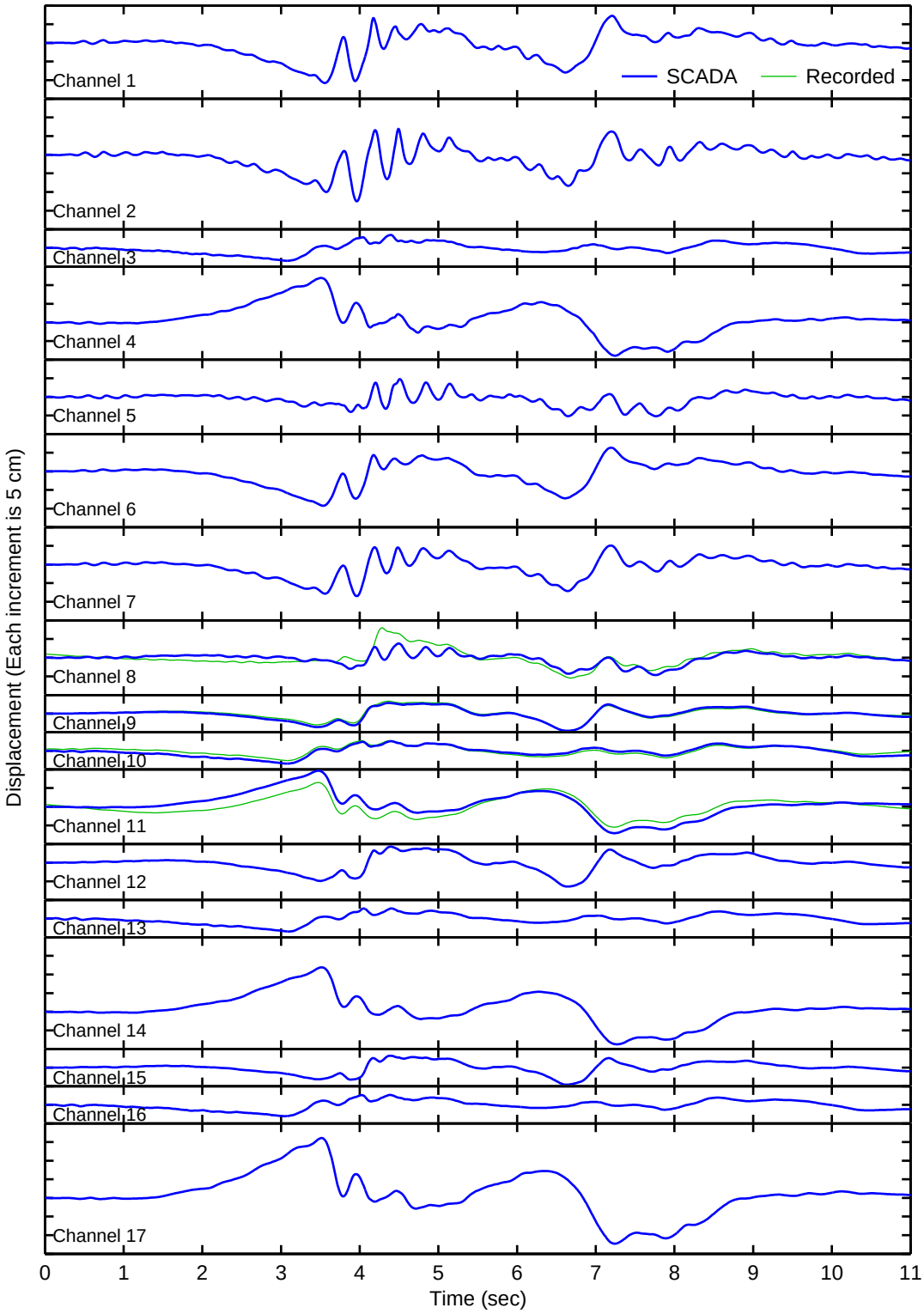

Figure C.11: Displacement time histories at locations corresponding to channels 1–17 computed from a nonlinear analysis of the Northridge earthquake compared to the partial records (method 1)

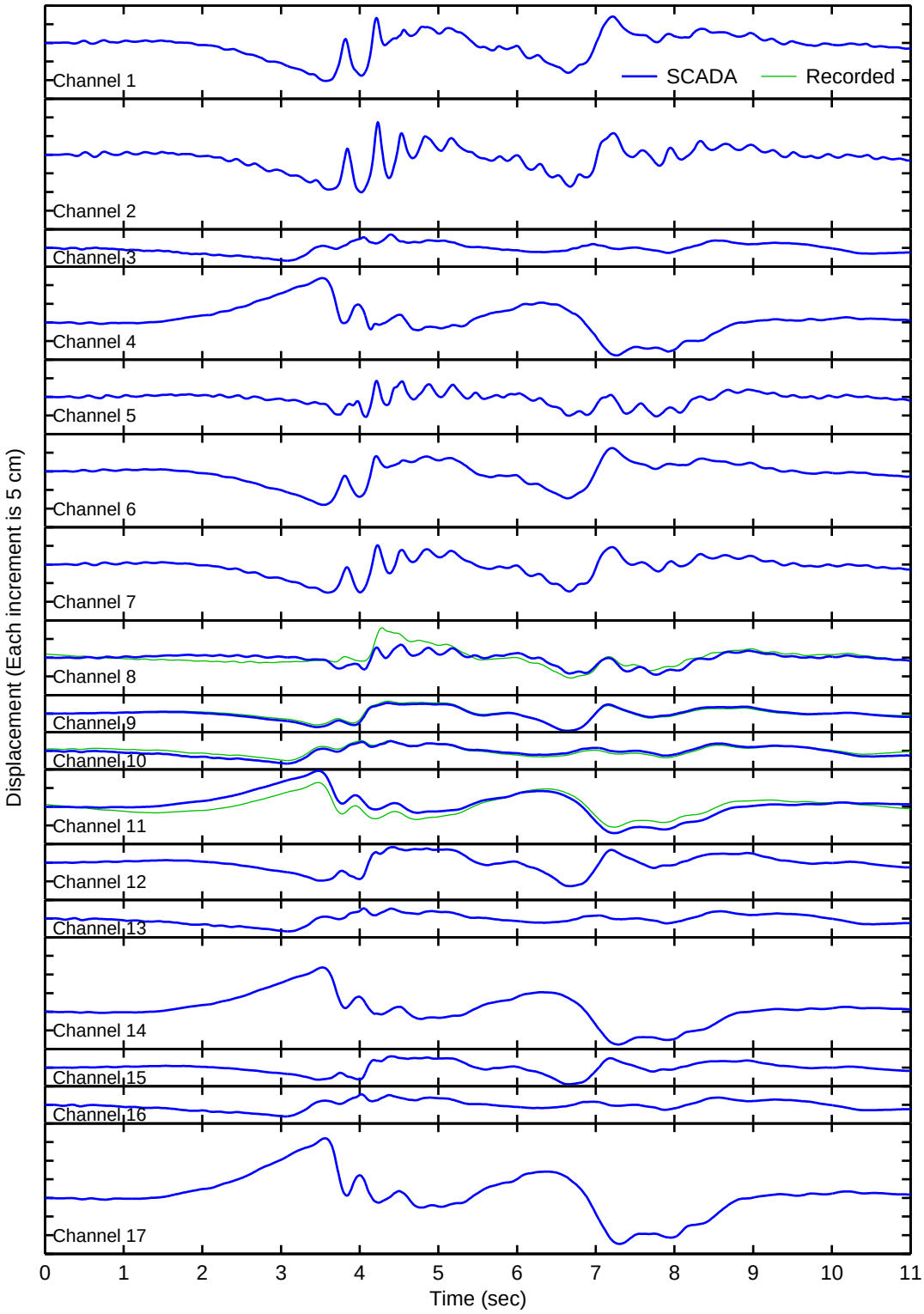

Figure C.12: Displacement time histories at locations corresponding to channels 1–17 computed from a nonlinear analysis of the Northridge earthquake compared to the partial records (method 2)

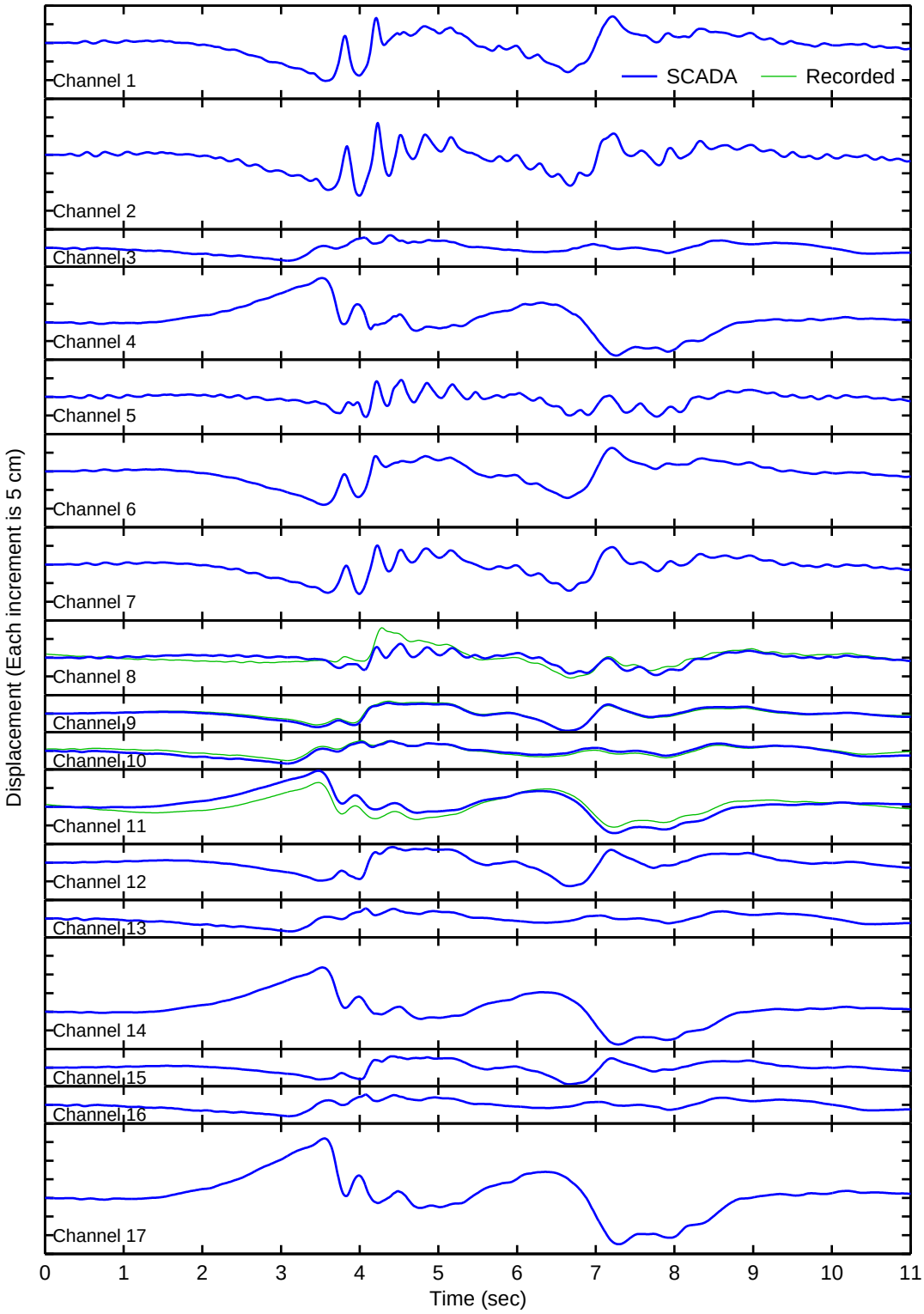

Figure C.13: Displacement time histories at locations corresponding to channels 1–17 computed from a nonlinear analysis of the Northridge earthquake compared to the partial records (method 3)

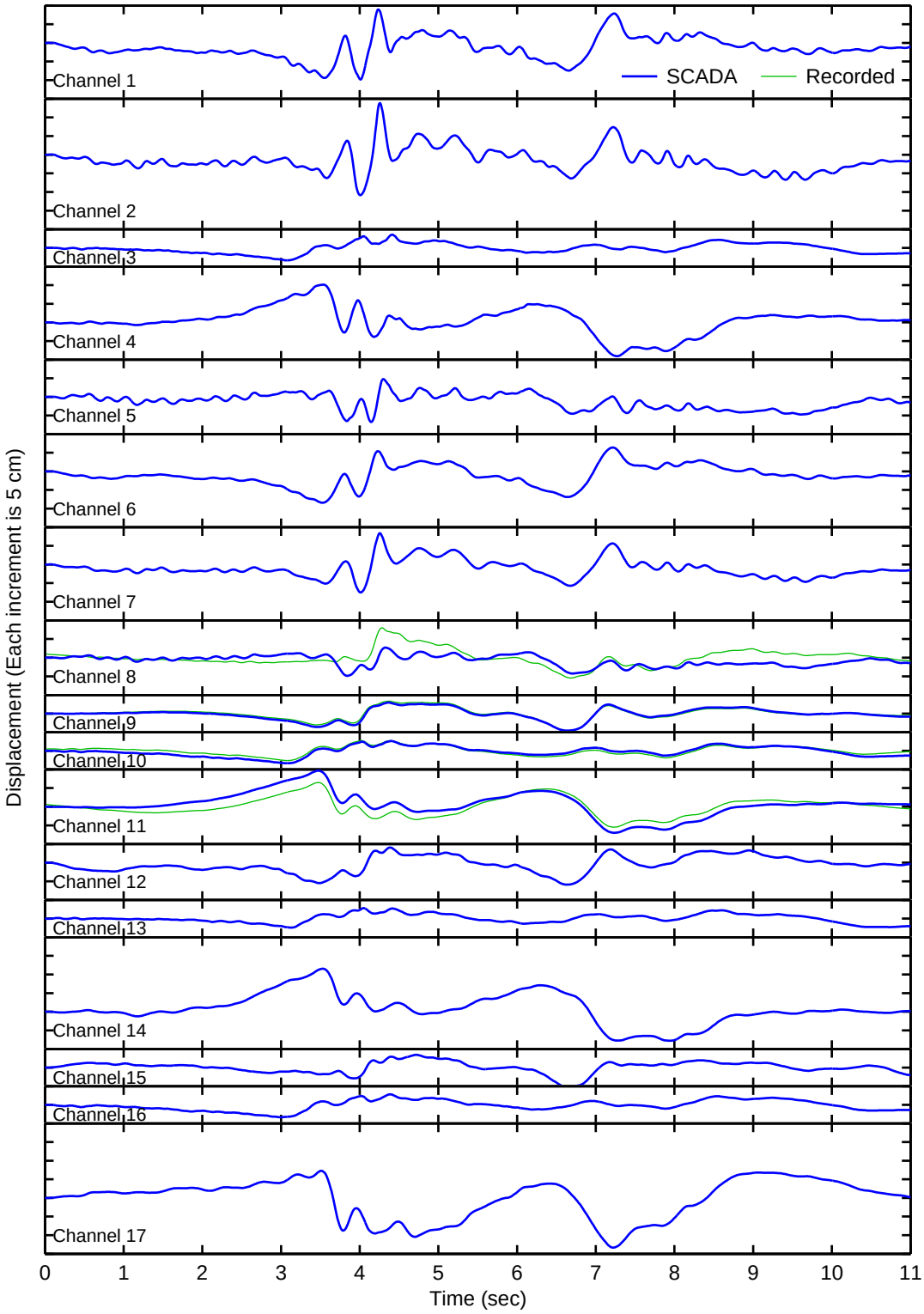

Figure C.14: Displacement time histories at locations corresponding to channels 1–17 computed from a nonlinear analysis of the Northridge earthquake compared to the partial records (method 4)

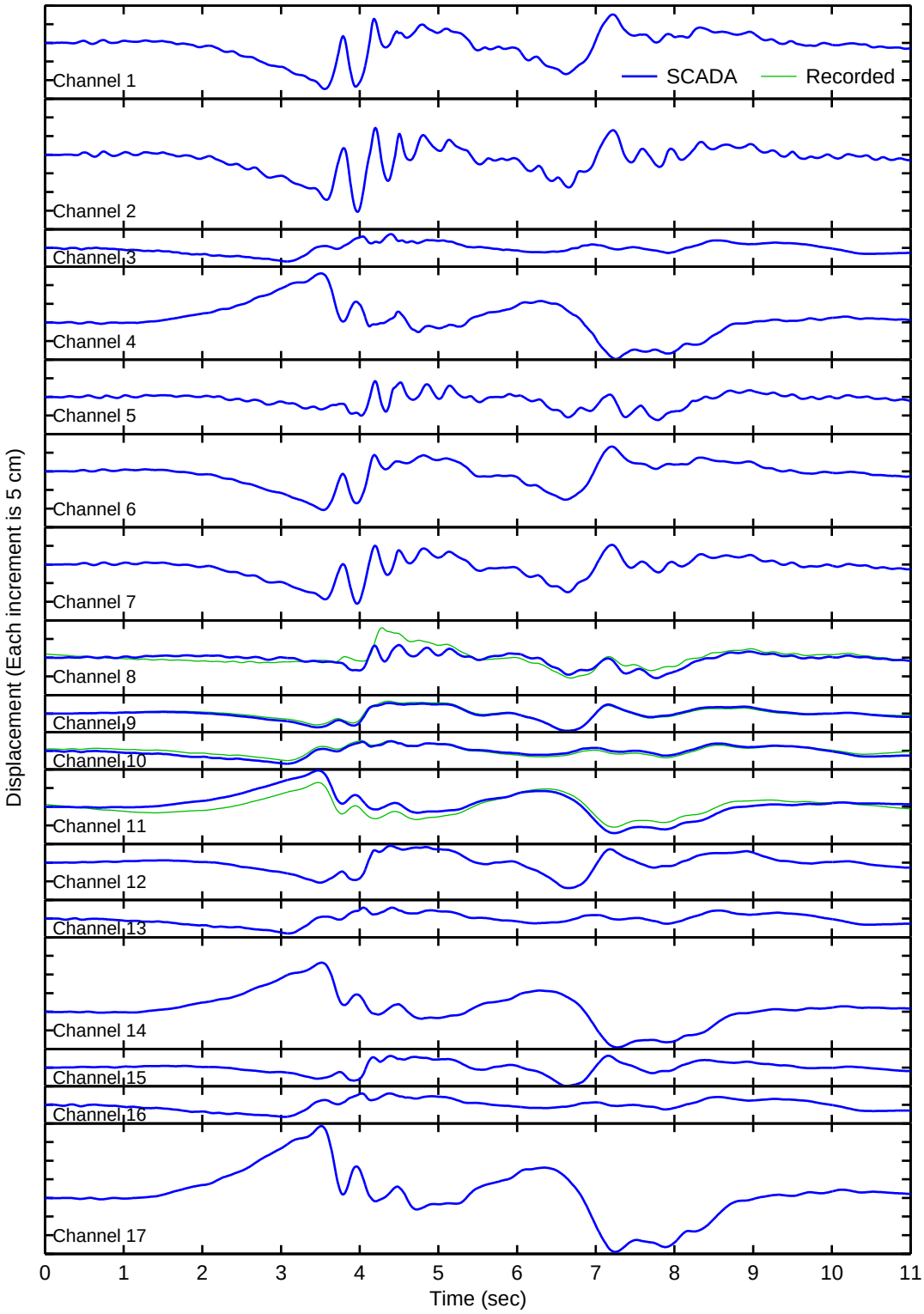

Figure C.15: Displacement time histories at locations corresponding to channels 1–17 computed from a nonlinear analysis of the Northridge earthquake compared to the partial records (method 5)

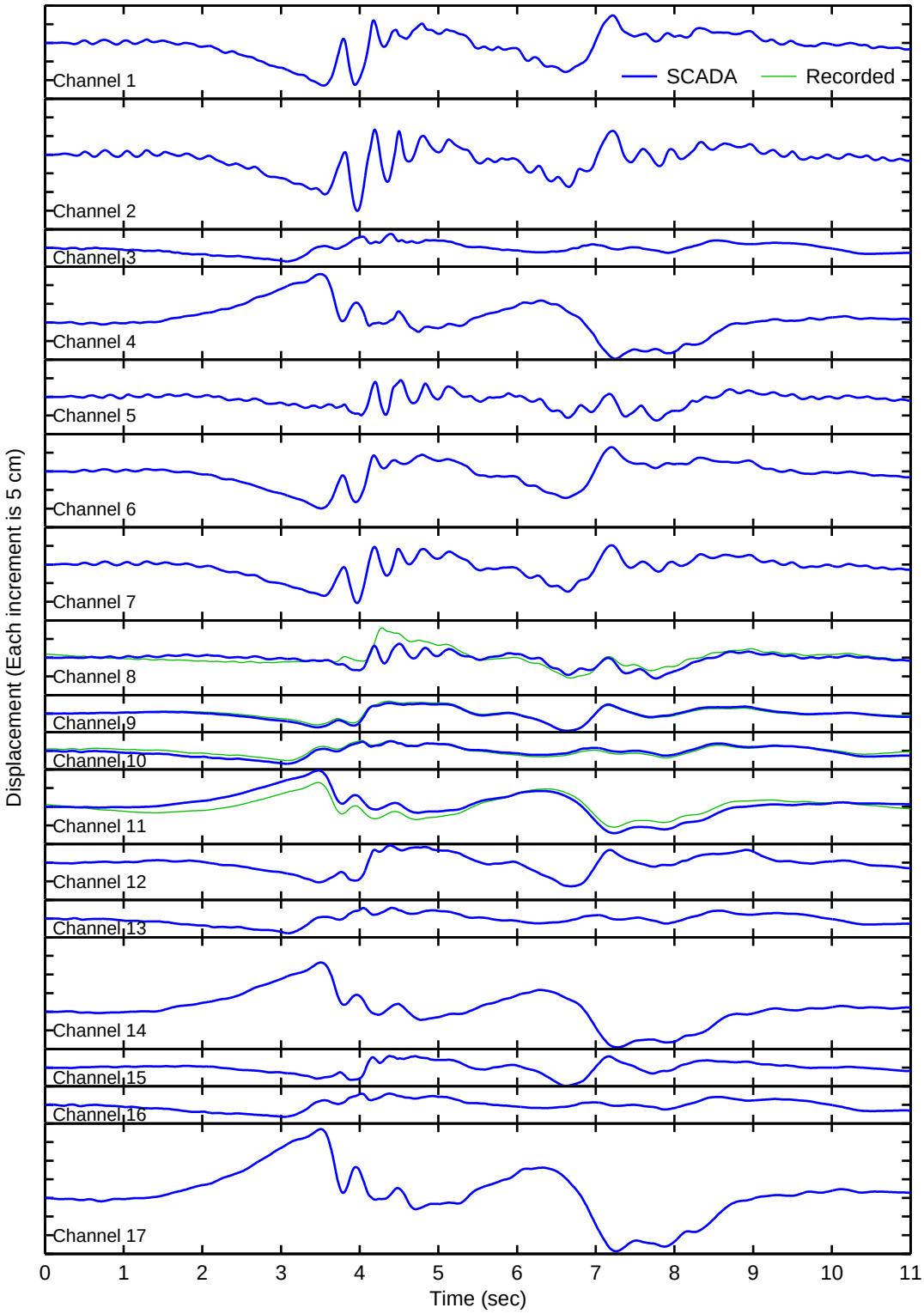

Figure C.16: Displacement time histories at locations corresponding to channels 1–17 computed from a nonlinear analysis of the Northridge earthquake compared to the partial records (method 9)

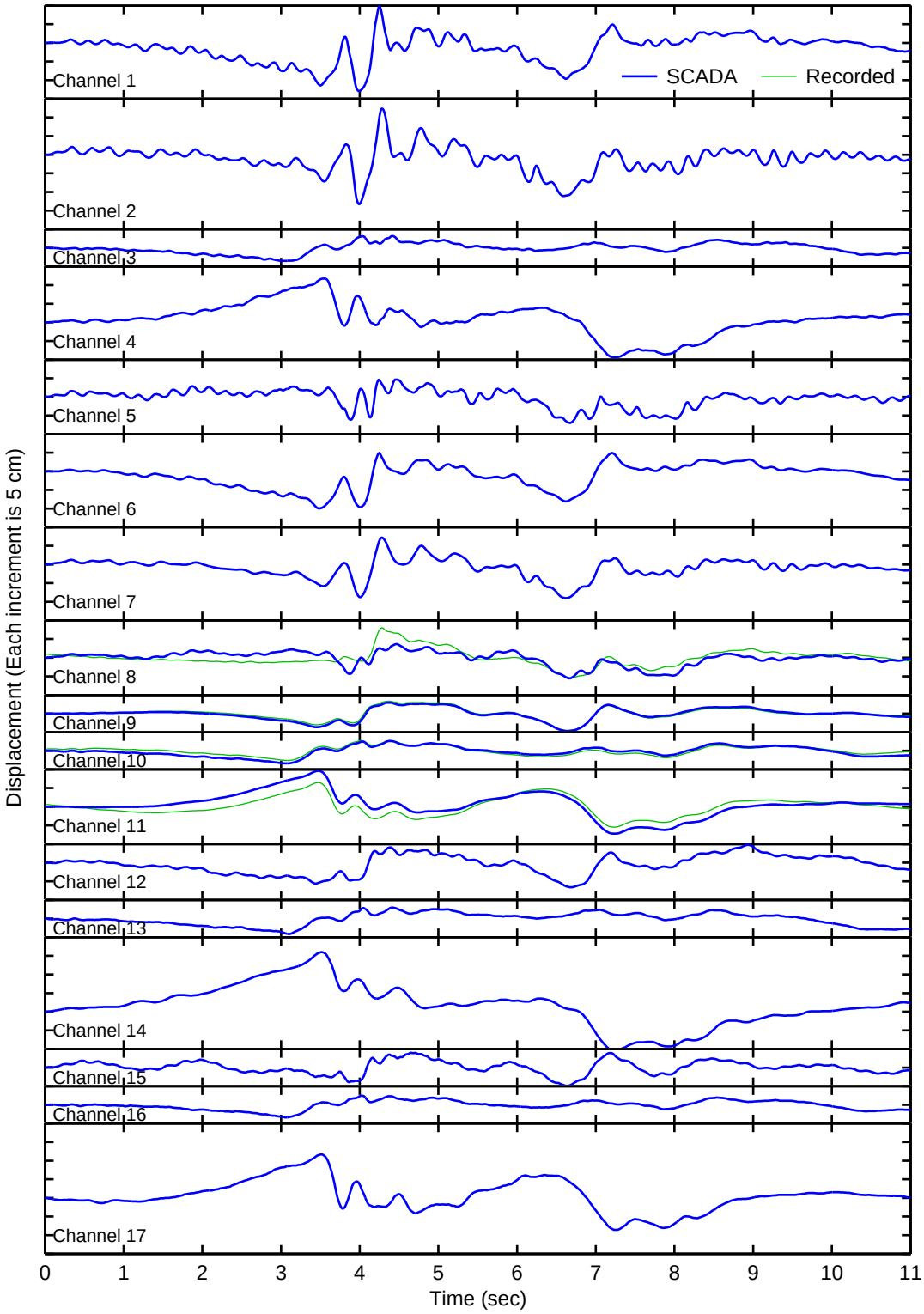

Figure C.17: Displacement time histories at locations corresponding to channels 1–17 computed from a nonlinear analysis of the Northridge earthquake compared to the partial records (method 13)

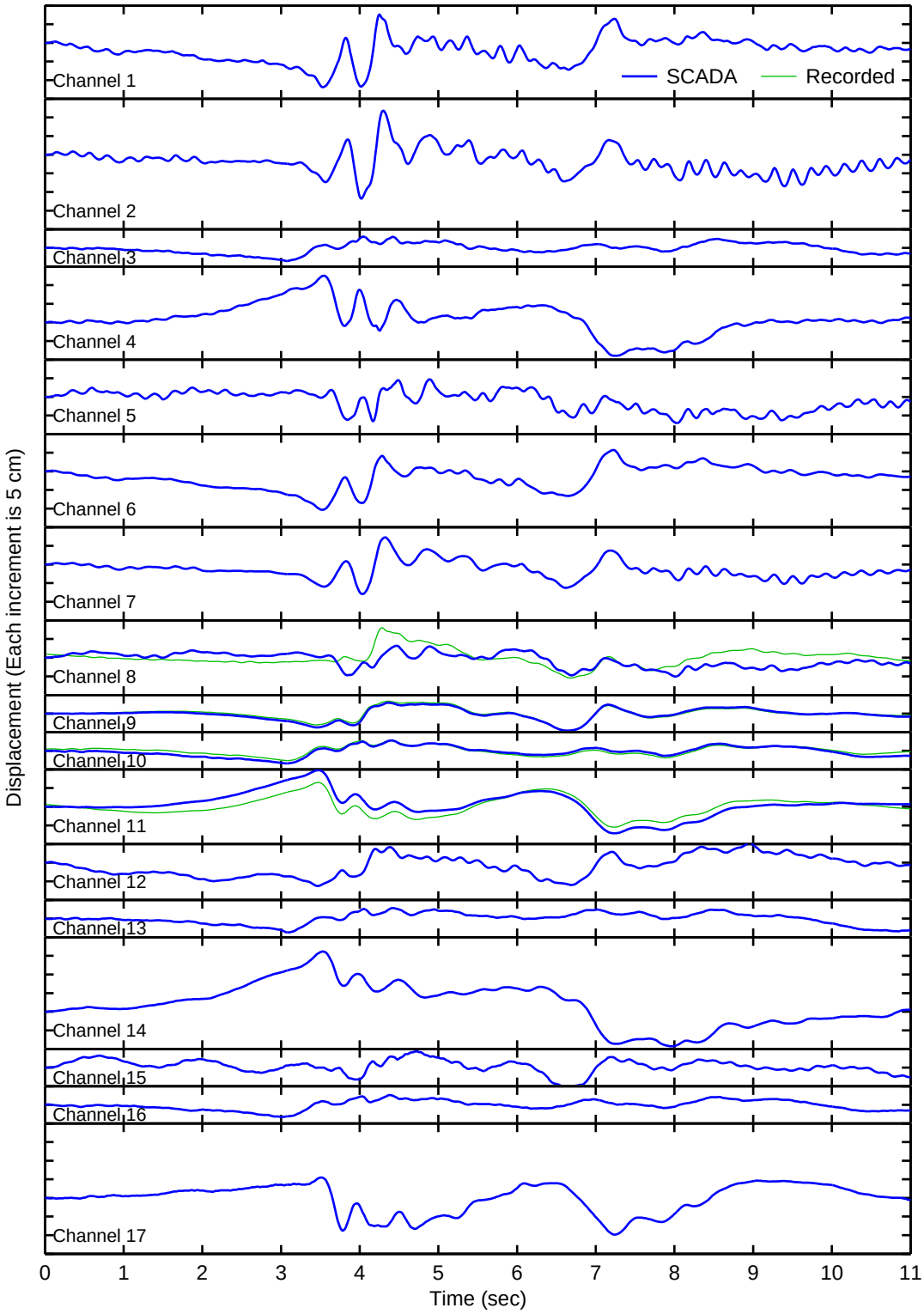

Figure C.18: Displacement time histories at locations corresponding to channels 1–17 computed from a nonlinear analysis of the Northridge earthquake compared to the partial records (method 16)

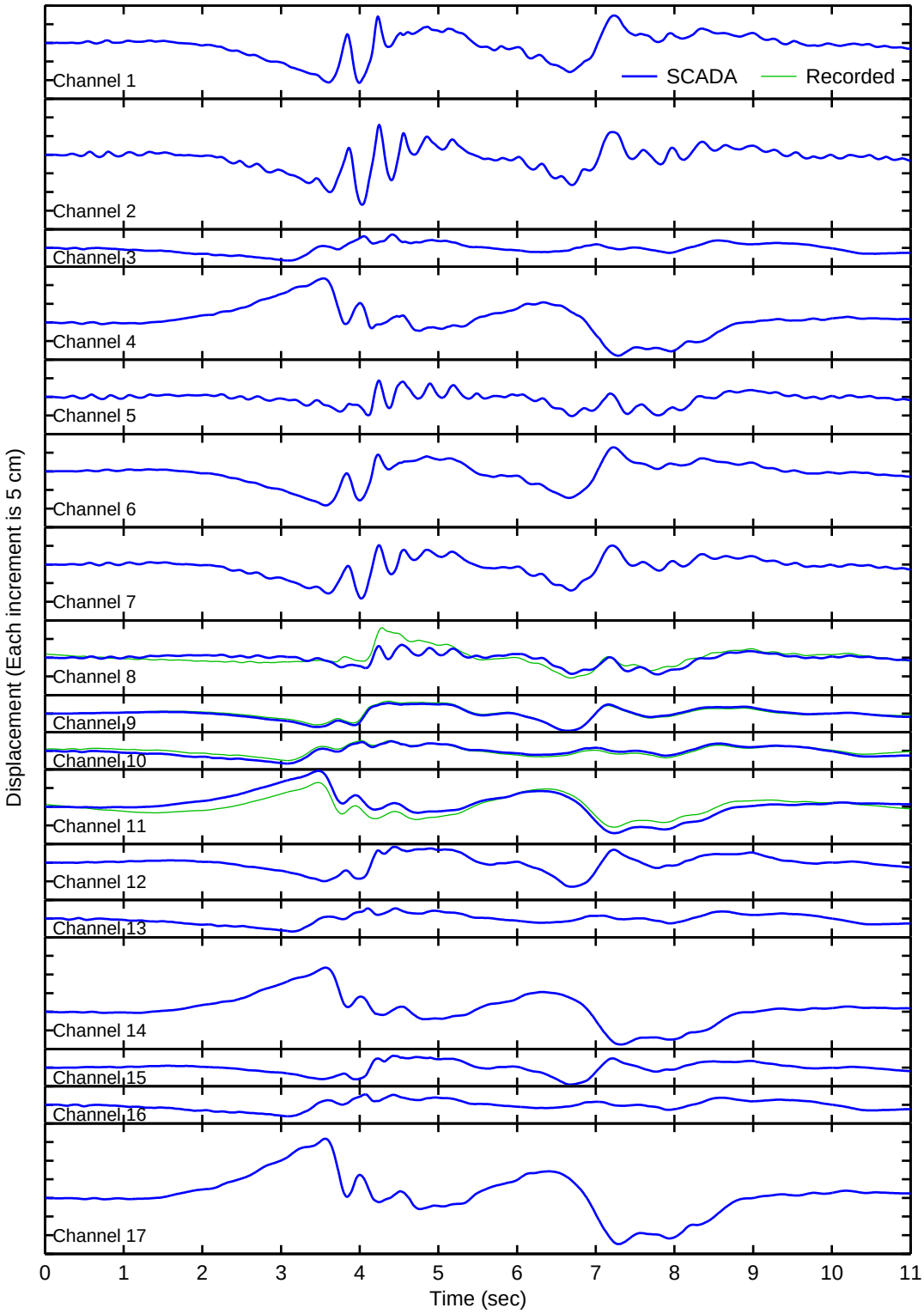

Figure C.19: Displacement time histories at locations corresponding to channels 1–17 computed from a nonlinear analysis of the Northridge earthquake compared to the partial records (method 1+0.05 sec)

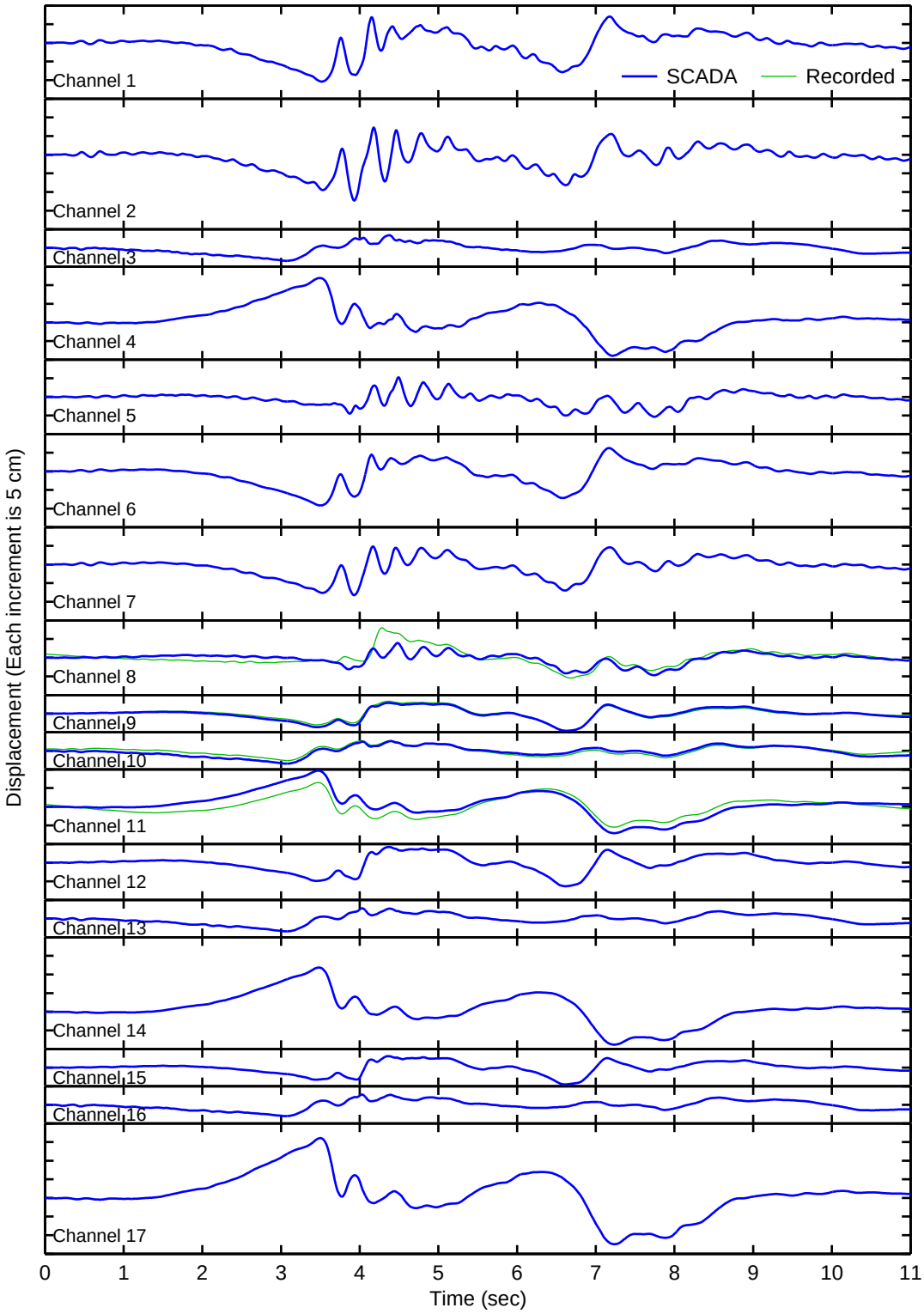

Figure C.20: Displacement time histories at locations corresponding to channels 1–17 computed from a nonlinear analysis of the Northridge earthquake compared to the partial records (method 1 no delays)

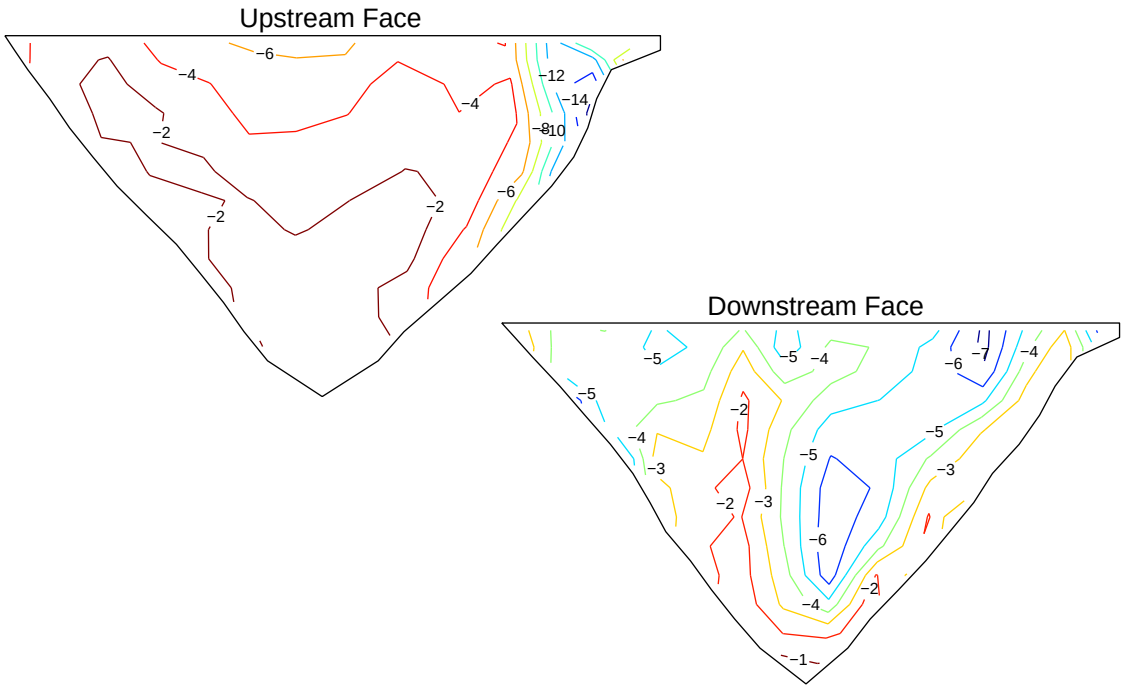

Figure C.21: Maximum compressive arch stresses (MPa) computed during a nonlinear analysis with the Northridge earthquake input (method 1)

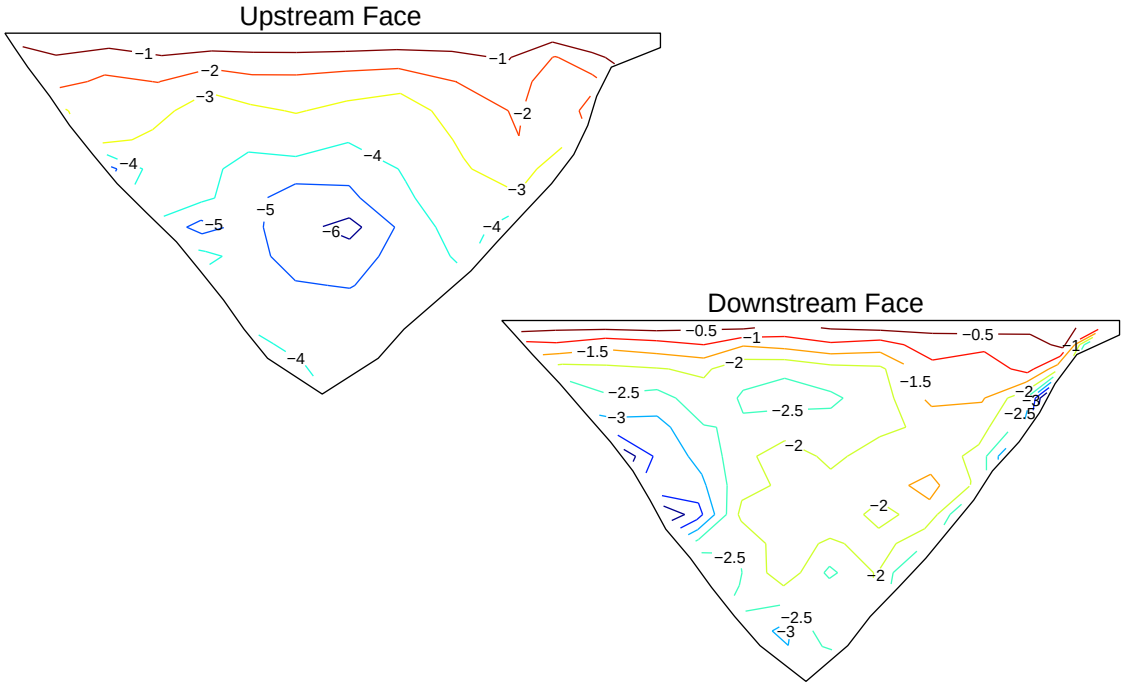

Figure C.22: Maximum compressive cantilever stresses (MPa) computed during a nonlinear analysis with the Northridge earthquake input (method 1)

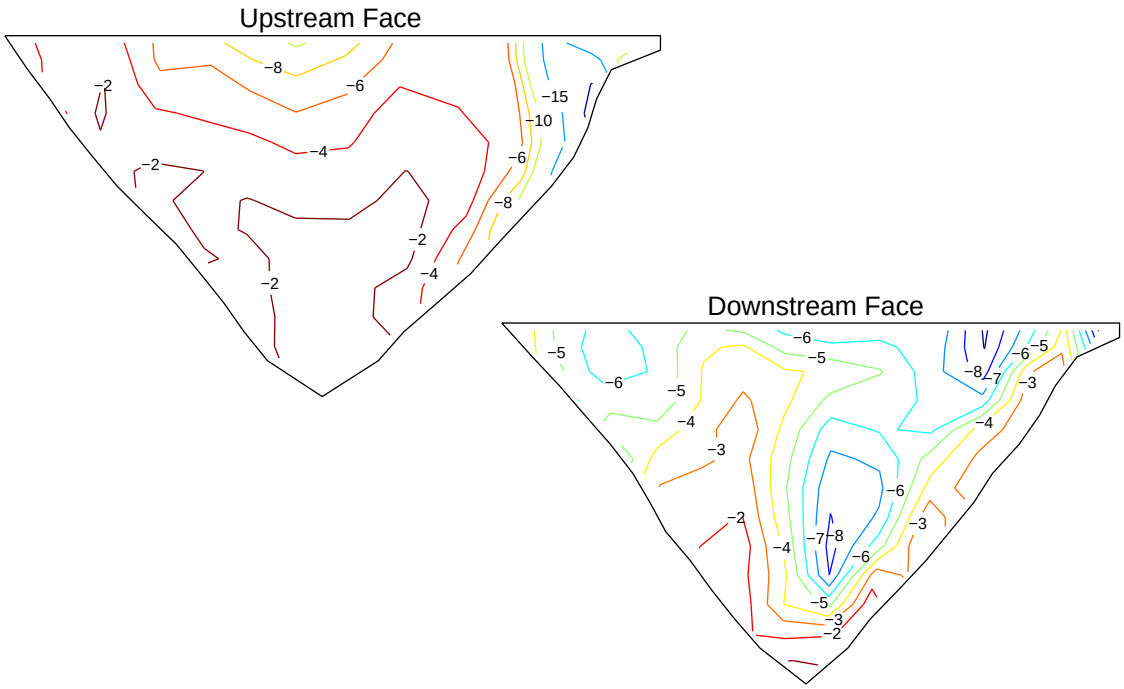

Figure C.23: Maximum compressive arch stresses (MPa) computed during a nonlinear analysis with the Northridge earthquake input (method 2)

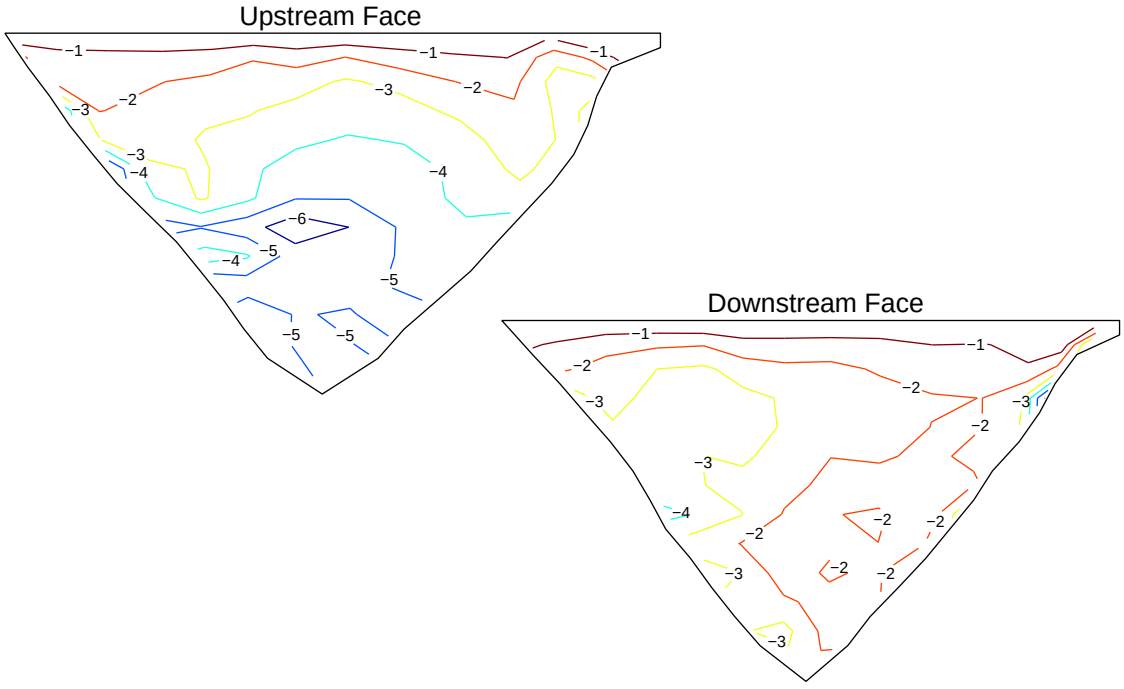

Figure C.24: Maximum compressive cantilever stresses (MPa) computed during a nonlinear analysis with the Northridge earthquake input (method 2)

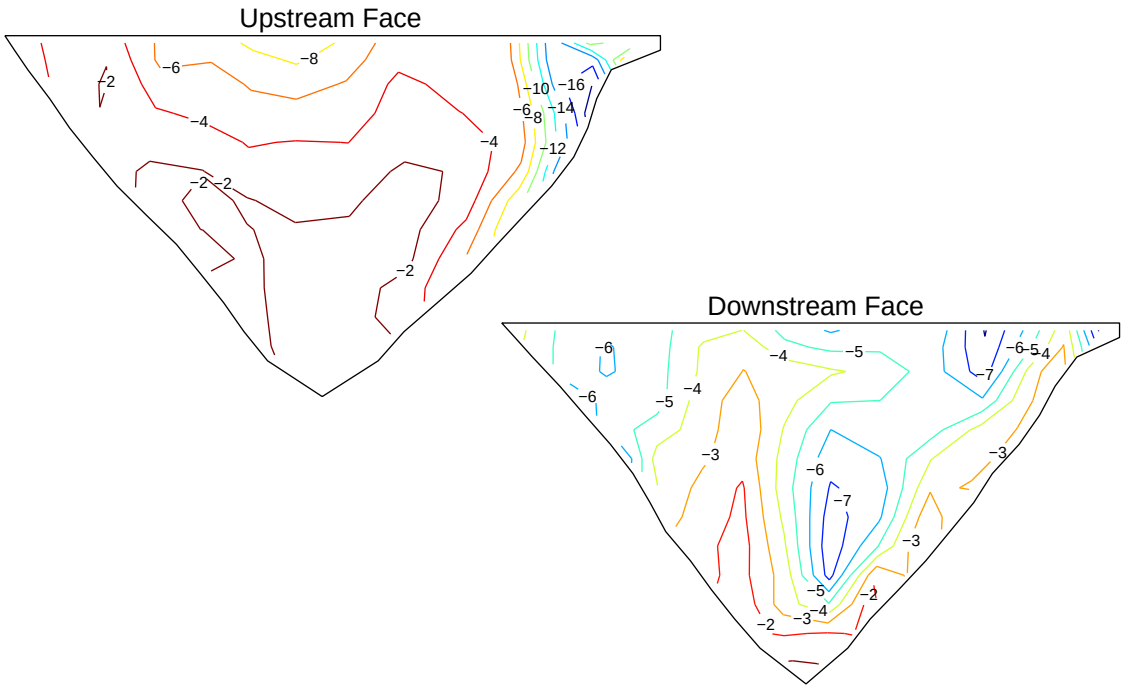

Figure C.25: Maximum compressive arch stresses (MPa) computed during a nonlinear analysis with the Northridge earthquake input (method 3)

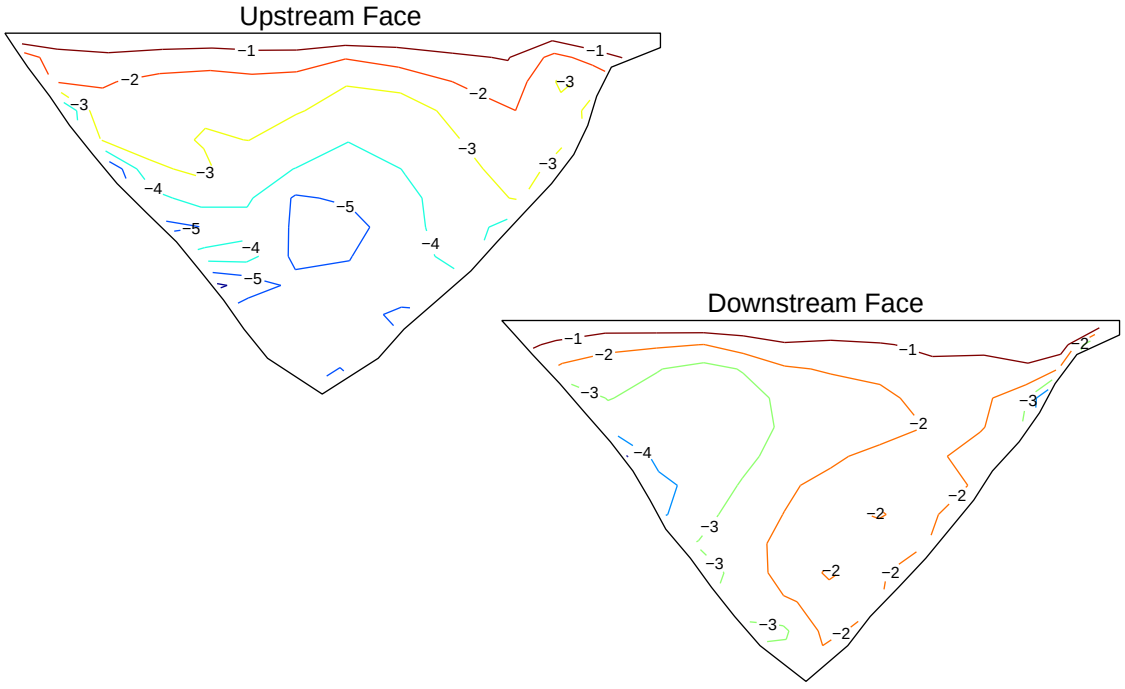

Figure C.26: Maximum compressive cantilever stresses (MPa) computed during a nonlinear analysis with the Northridge earthquake input (method 3)

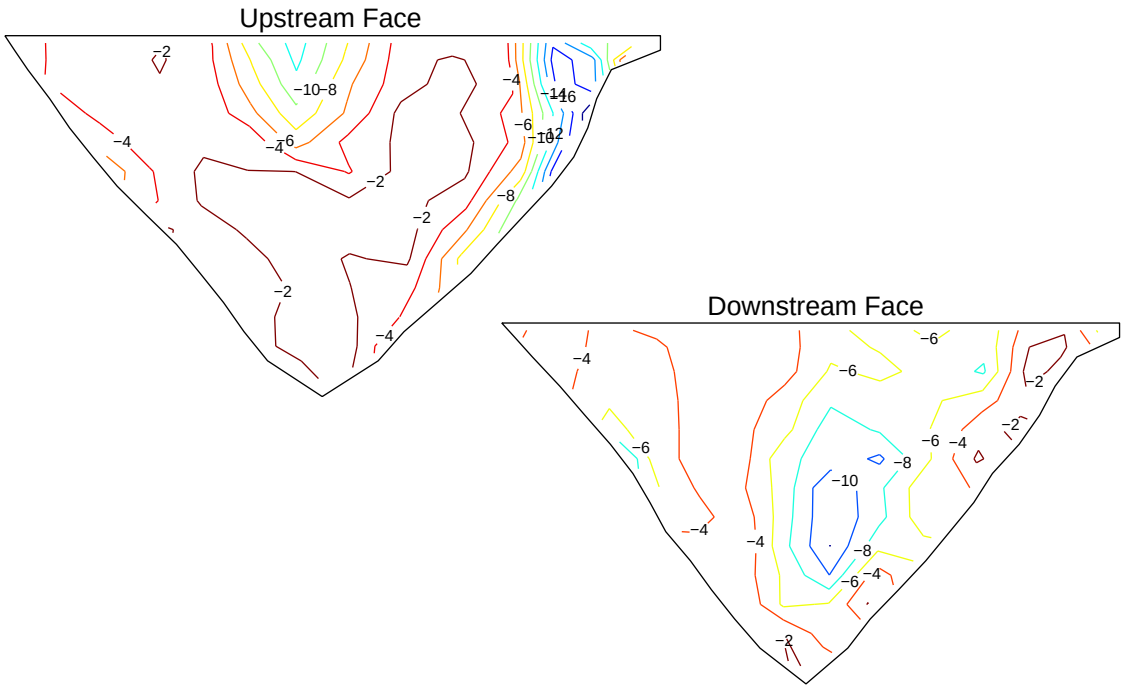

Figure C.27: Maximum compressive arch stresses (MPa) computed during a nonlinear analysis with the Northridge earthquake input (method 4)

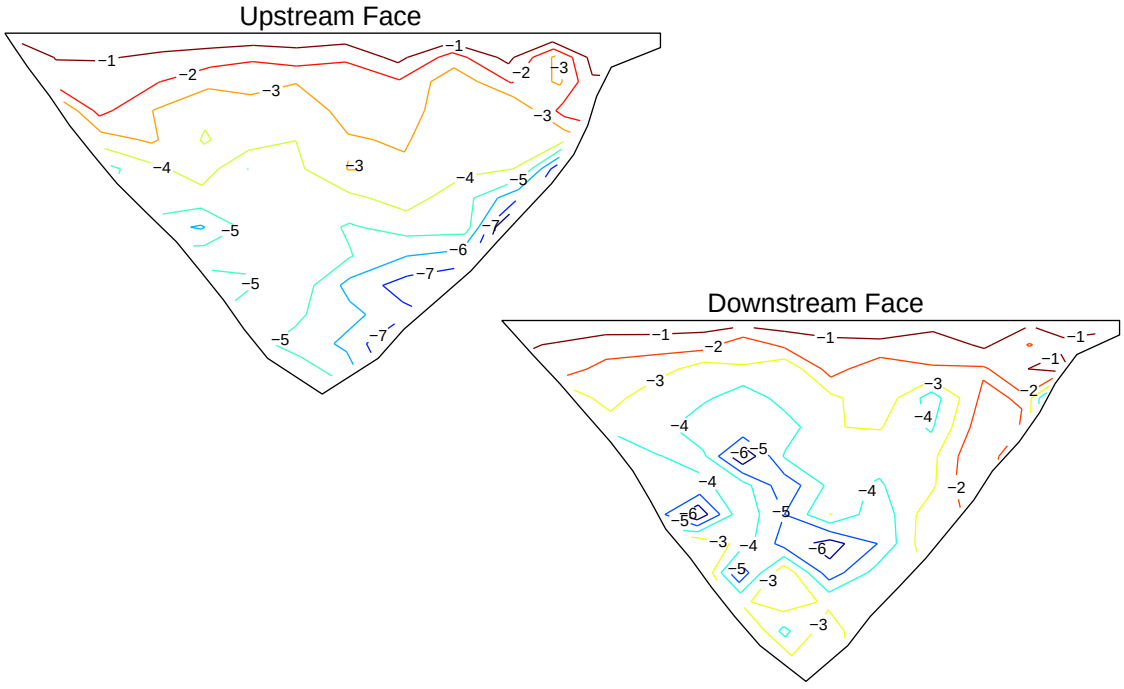

Figure C.28: Maximum compressive cantilever stresses (MPa) computed during a nonlinear analysis with the Northridge earthquake input (method 4)

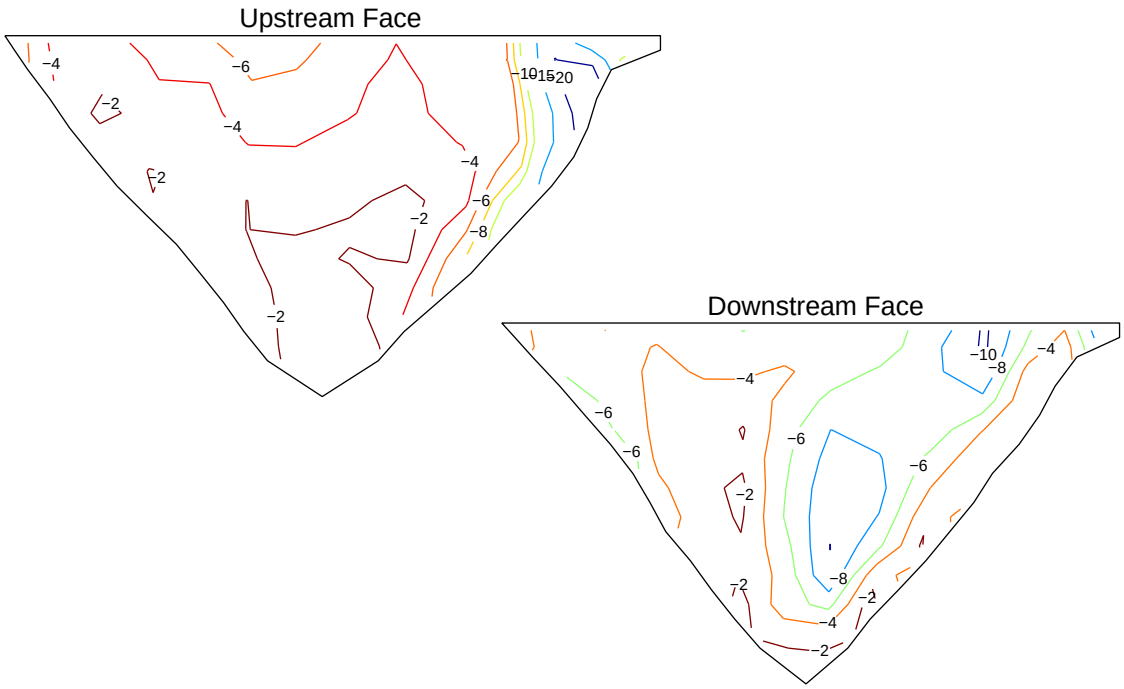

Figure C.29: Maximum compressive arch stresses (MPa) computed during a nonlinear analysis with the Northridge earthquake input (method 5)

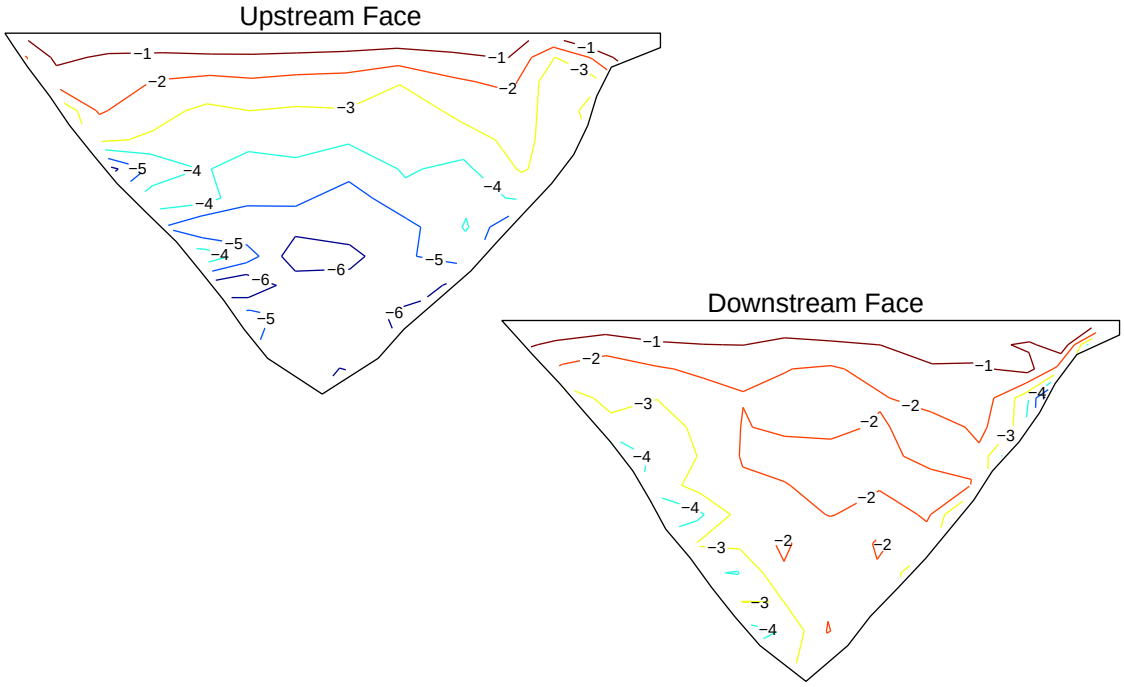

Figure C.30: Maximum compressive cantilever stresses (MPa) computed during a nonlinear analysis with the Northridge earthquake input (method 5)

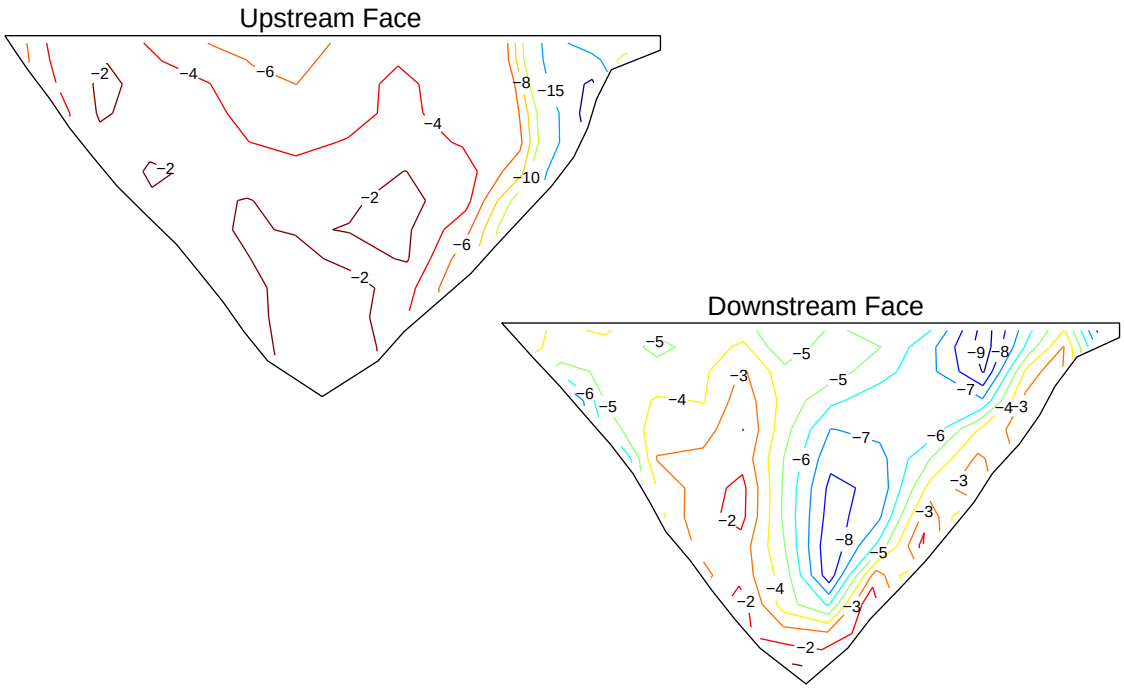

Figure C.31: Maximum compressive arch stresses (MPa) computed during a nonlinear analysis with the Northridge earthquake input (method 9)

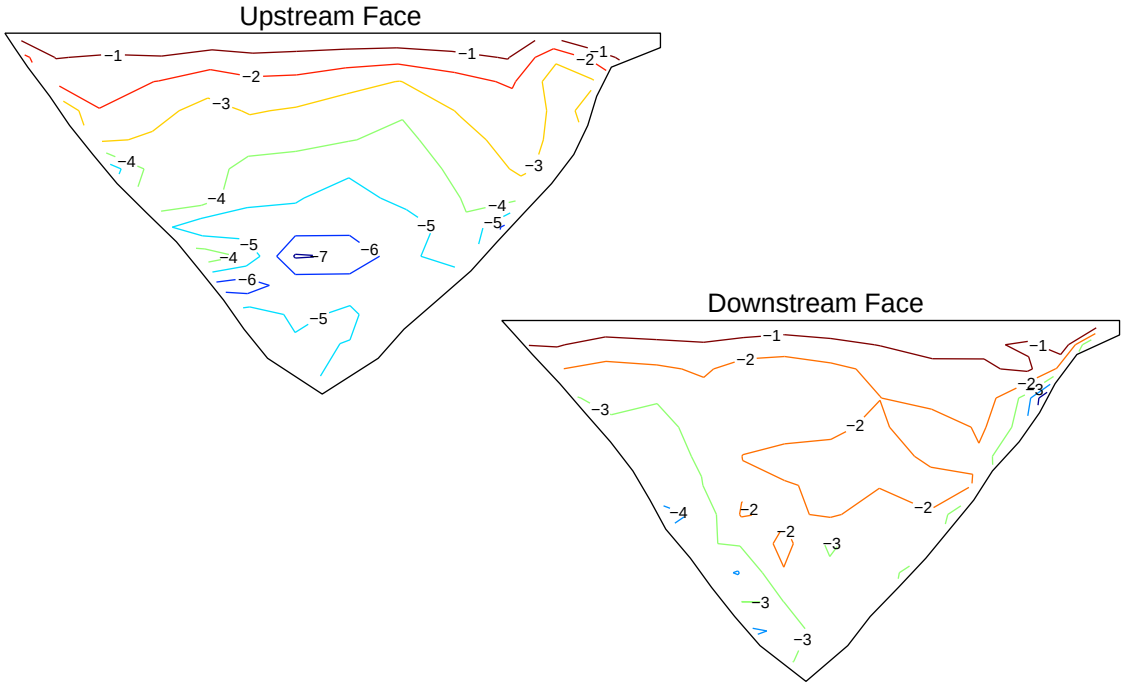

Figure C.32: Maximum compressive cantilever stresses (MPa) computed during a nonlinear analysis with the Northridge earthquake input (method 9)

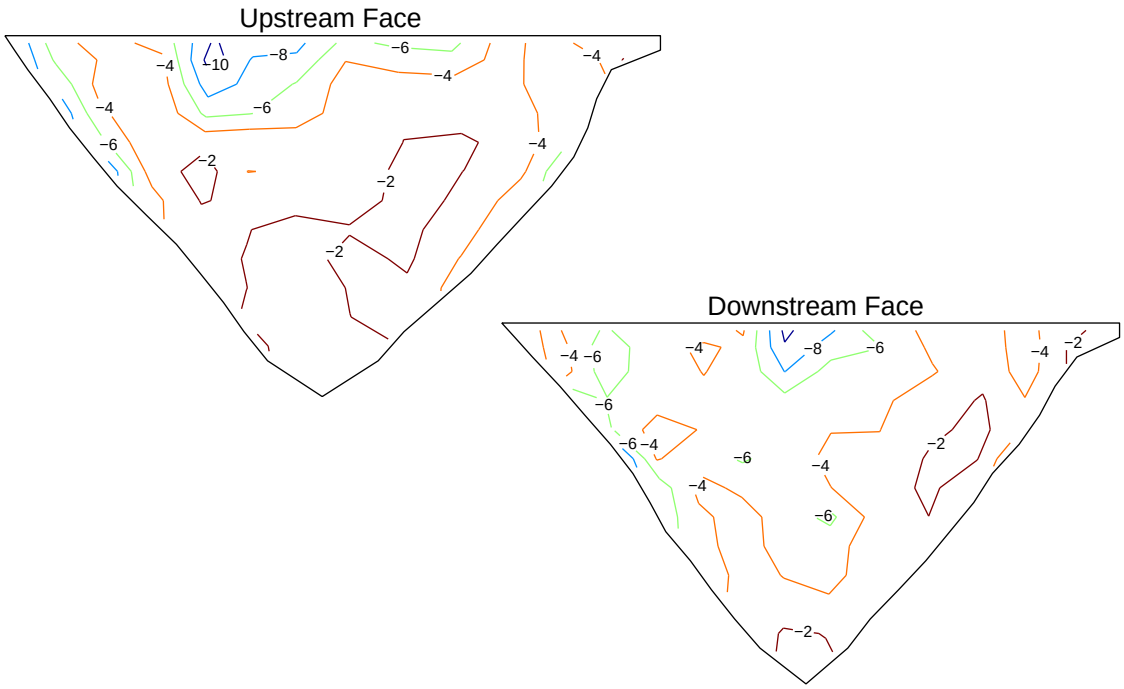

Figure C.33: Maximum compressive arch stresses (MPa) computed during a nonlinear analysis with the Northridge earthquake input (method 13)

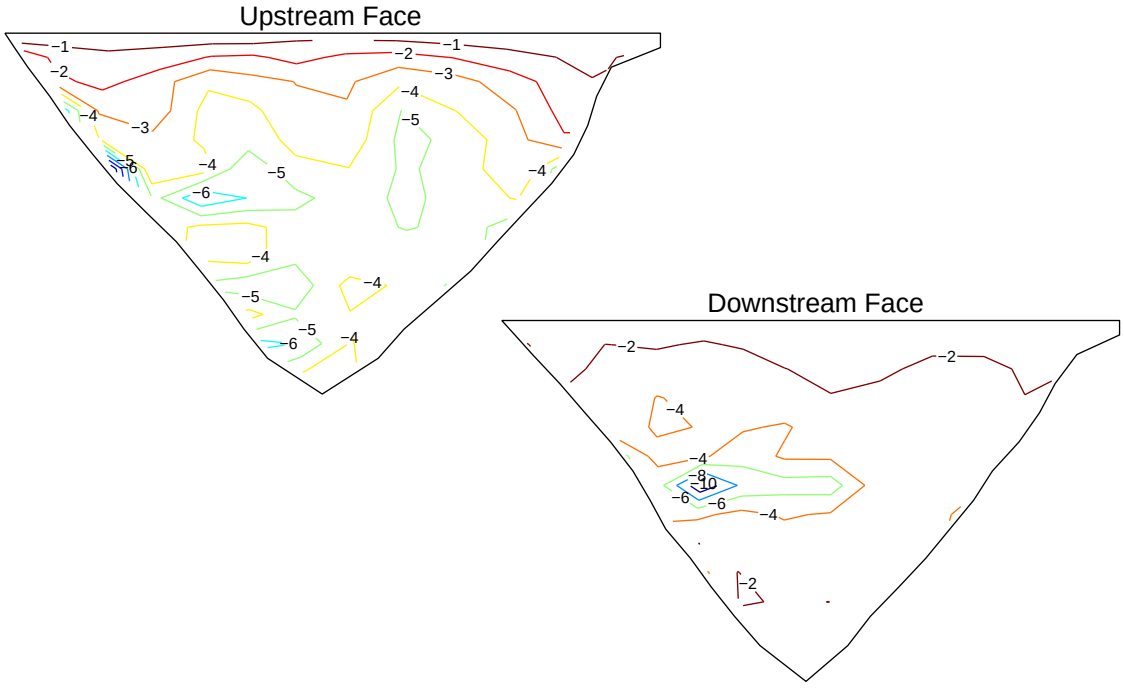

Figure C.34: Maximum compressive cantilever stresses (MPa) computed during a nonlinear analysis with the Northridge earthquake input (method 13)

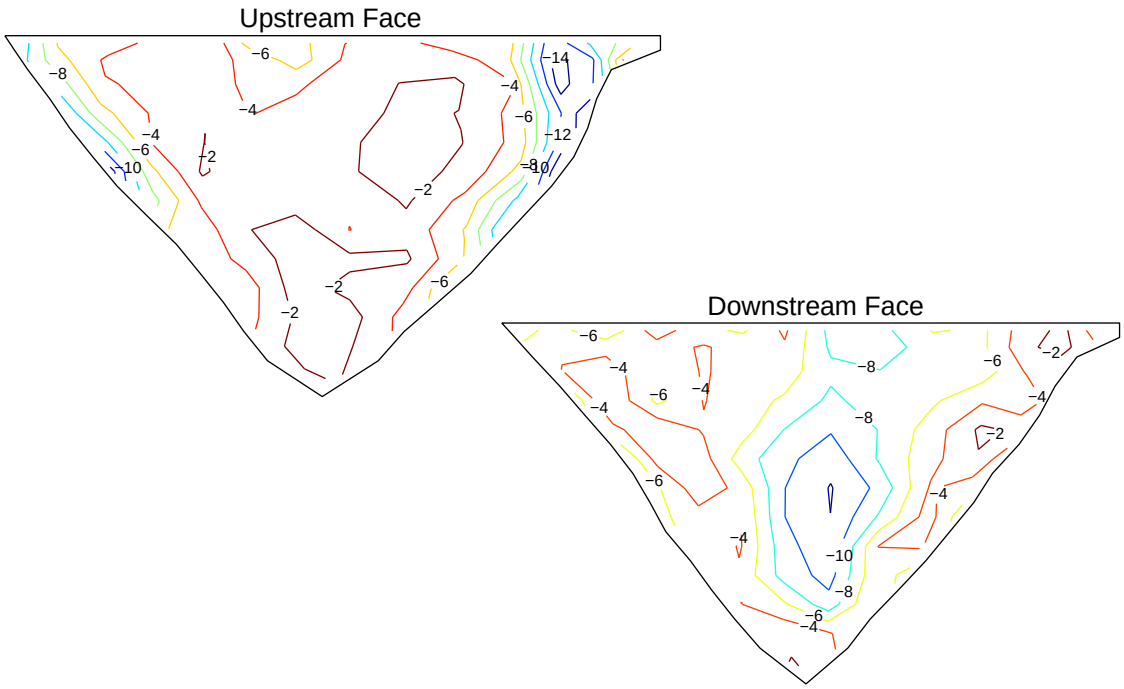

Figure C.35: Maximum compressive arch stresses (MPa) computed during a nonlinear analysis with the Northridge earthquake input (method 16)

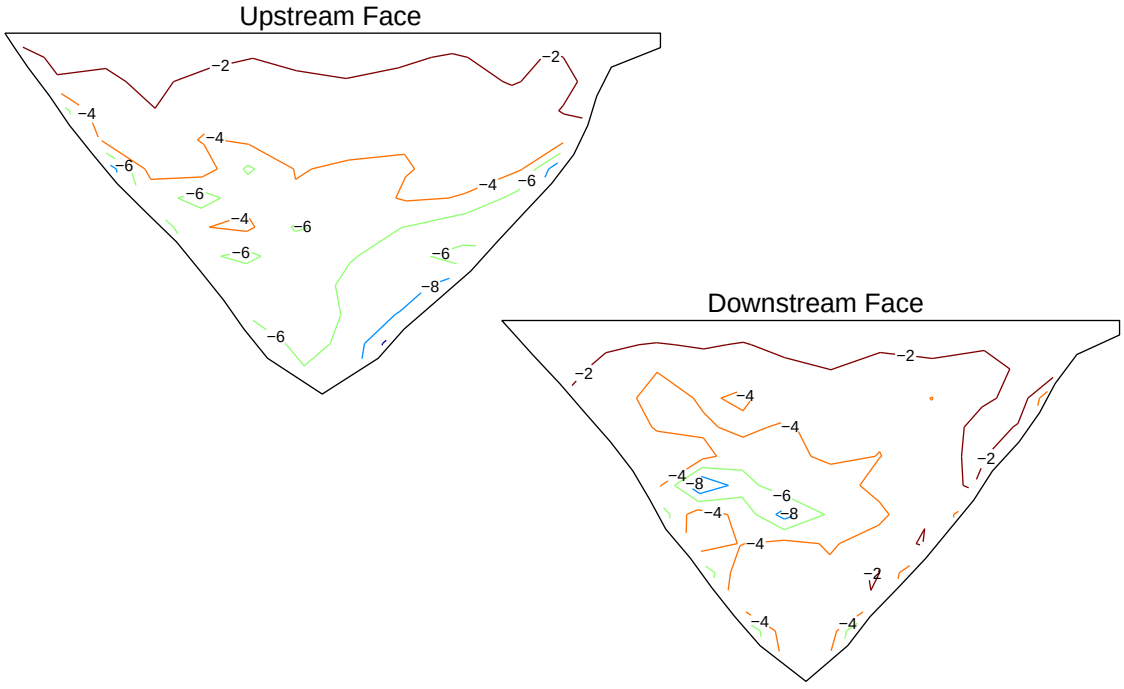

Figure C.36: Maximum compressive cantilever stresses (MPa) computed during a nonlinear analysis with the Northridge earthquake input (method 16)

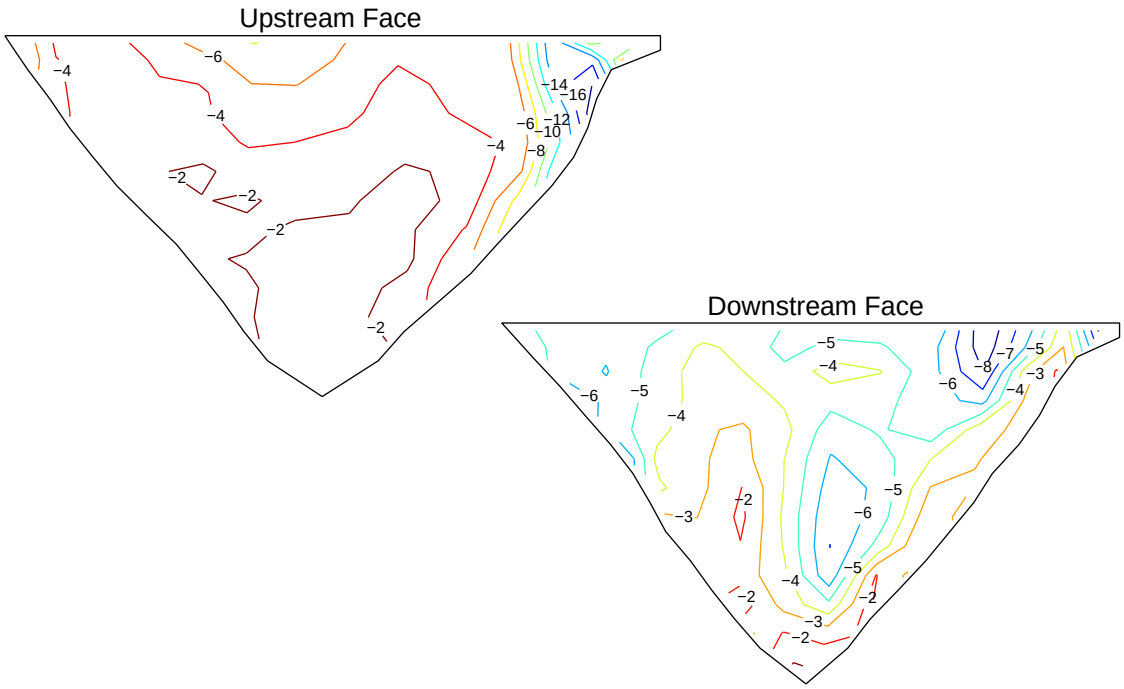

Figure C.37: Maximum compressive arch stresses (MPa) computed during a nonlinear analysis with the Northridge earthquake input (method 1+0.05 sec)

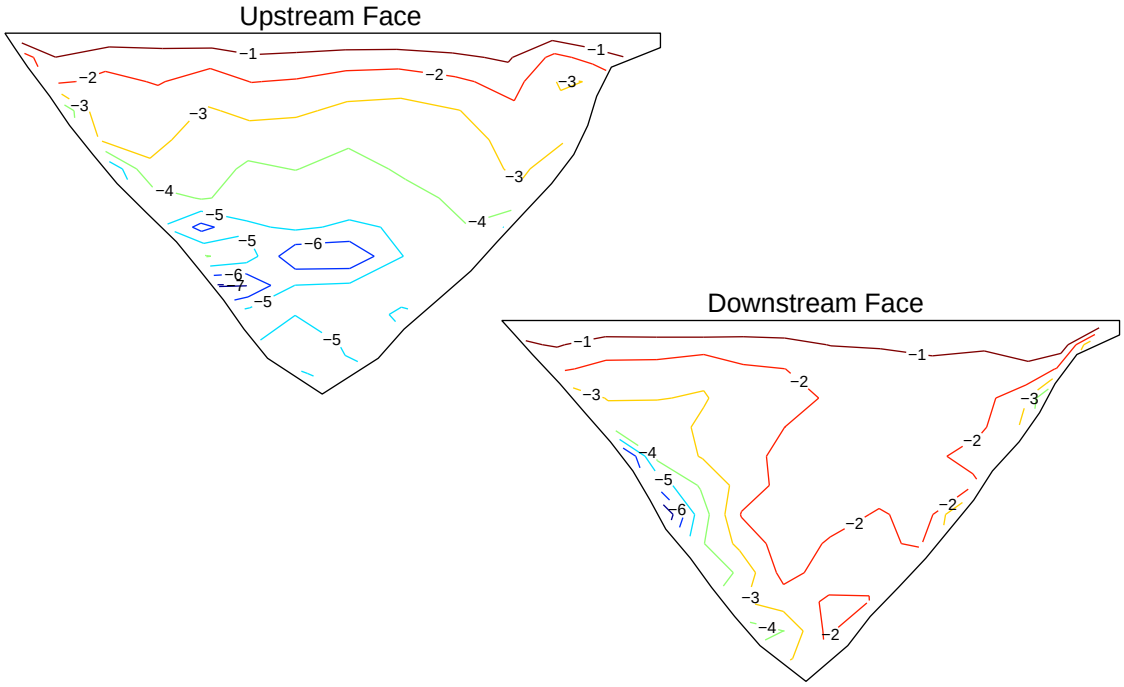

Figure C.38: Maximum compressive cantilever stresses (MPa) computed during a nonlinear analysis with the Northridge earthquake input (method 1+0.05 sec)

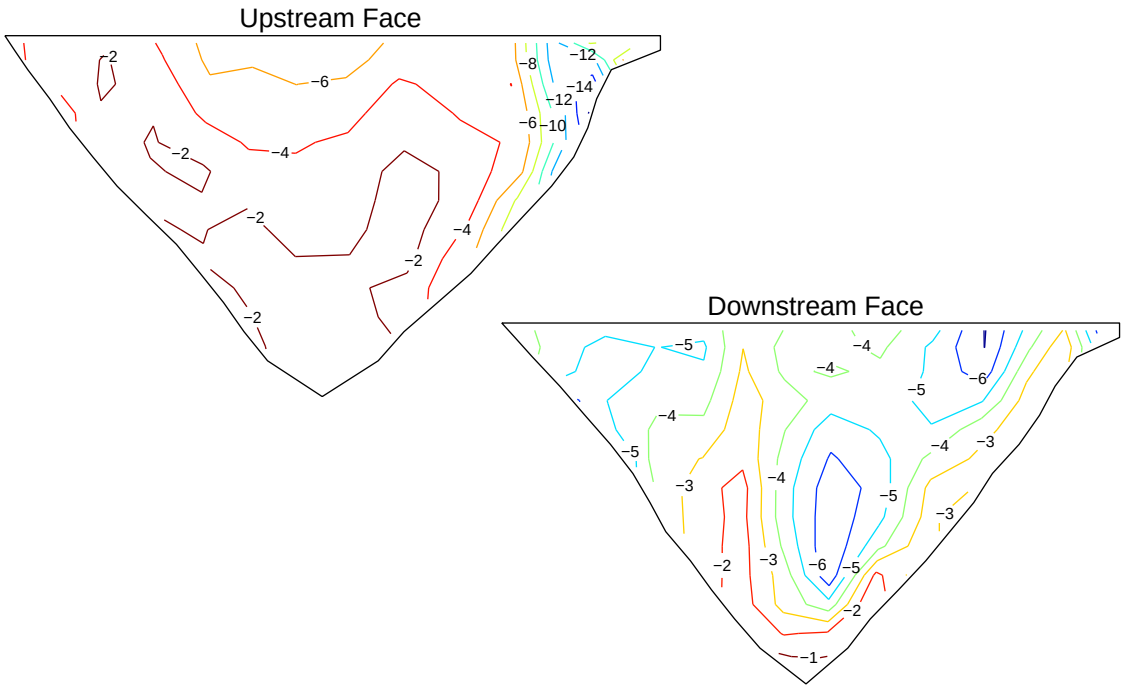

Figure C.39: Maximum compressive arch stresses (MPa) computed during a nonlinear analysis with the Northridge earthquake input (method 1 no delays)

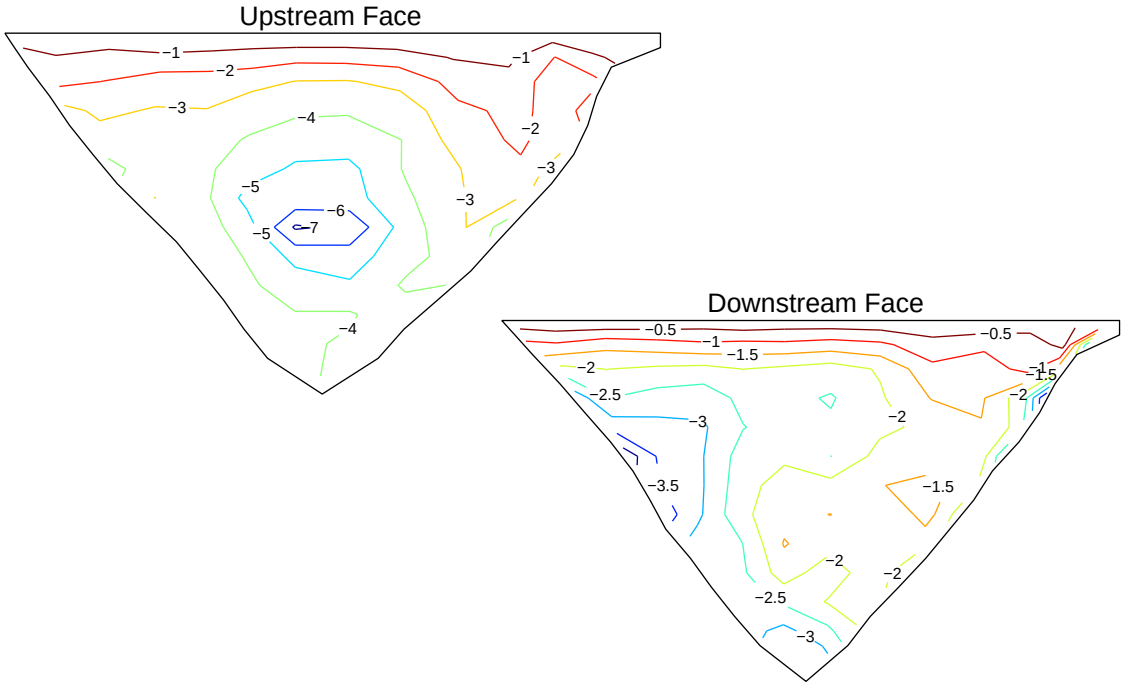

Figure C.40: Maximum compressive cantilever stresses (MPa) computed during a nonlinear analysis with the Northridge earthquake input (method 1 no delays)

0.00	0.93	1.15	1.52	0.68	1.19	2.30	2.54	1.09	2.07	0.58	3.19	0.00	0.00
0.00	0.82	1.06	1.64	0.75	1.08	2.24	2.40	0.89	2.05	0.87	2.90	0.00	0.00
	0.57	1.10	1.80	0.98	0.95	2.12	2.17	0.76	1.94	1.45	2.53	0.00	
	0.24	0.98	1.76	1.18	0.81	1.82	1.96	0.65	1.80	1.86	1.75	0.00	
		0.90	1.55	1.28	0.63	1.32	1.66	0.64	1.65	1.72	1.06		
		0.47	1.42	1.25	0.82	0.79	1.20	0.83	1.57	1.10	0.43		
			1.39	1.03	0.51	0.42	1.18	0.93	1.35	0.95			
			0.60	0.68	0.30	0.44	1.15	1.03	0.92	0.34			
				0.62	0.53	0.41	1.07	1.03	0.70				
				0.26	0.39	0.33	1.06	0.68	0.21				
					0.32	0.21	0.85	0.48					
					0.11	0.09	0.51	0.15					
						0.04	0.15						

Figure C.41: Maximum joint opening (cm) computed during a nonlinear analysis with the Northridge earthquake input (method 1)

0.00	0.00	0.00	0.00	0.00	0.00	0.00	0.00	0.00	0.00	0.00	0.00	0.00	0.00
0.12	0.00	0.00	0.00	0.00	0.00	0.00	0.00	0.00	0.00	0.00	0.00	0.00	0.00
	0.00	0.00	0.00	0.00	0.00	0.00	0.00	0.00	0.00	0.00	0.00	0.00	
	0.00	0.00	0.00	0.00	0.00	0.00	0.00	0.00	0.00	0.00	0.00	0.27	
		0.00	0.00	0.00	0.00	0.00	0.00	0.00	0.00	0.00	0.00		
		0.32	0.00	0.00	0.00	0.00	0.00	0.00	0.00	0.00	0.26		
			0.00	0.00	0.34	0.51	0.00	0.00	0.00	0.00			
			0.54	0.41	0.00	0.00	0.49	0.31	0.00	0.26			
				0.00	0.00	0.00	0.00	0.00	0.00				
				0.29	0.00	0.00	0.00	0.00	0.22				
					0.00	0.00	0.00	0.00					
					0.00	0.00	0.00	0.00					
						0.00	0.00						

Figure C.42: Maximum crack opening (cm) computed during a nonlinear analysis with the Northridge earthquake input (method 1)

0.00	0.94	1.12	2.11	2.53	0.91	2.60	1.93	1.17	2.35	0.98	3.56	0.00	0.00
0.00	0.76	1.34	2.21	2.35	0.80	2.54	1.85	1.10	2.35	0.98	3.30	0.00	0.00
	0.53	1.47	2.28	2.04	0.55	2.37	1.77	0.99	2.11	1.44	2.84	0.00	
	0.24	1.05	2.32	1.47	0.44	2.15	1.58	0.93	1.78	2.00	1.92	0.00	
		0.92	2.03	0.90	0.36	1.81	1.20	0.71	1.68	1.87	1.12		
		0.58	1.77	0.46	0.26	1.25	0.84	0.78	1.63	1.18	0.45		
			1.56	0.69	0.23	0.57	0.89	0.92	1.54	1.01			
			0.47	1.07	0.21	0.22	0.84	1.17	1.15	0.40			
				0.69	0.24	0.18	0.84	1.25	0.80				
				0.35	0.24	0.10	0.92	0.82	0.23				
					0.33	0.08	0.87	0.57					
					0.12	0.04	0.50	0.17					
						0.04	0.15						

Figure C.43: Maximum joint opening (cm) computed during a nonlinear analysis with the Northridge earthquake input (method 2)

0.00	0.00	0.00	0.00	0.00	0.00	0.00	0.00	0.00	0.00	0.00	0.00	0.00	0.00
0.15	0.00	0.00	0.00	0.00	0.00	0.00	0.00	0.00	0.00	0.00	0.00	0.00	0.00
	0.00	0.00	0.00	0.00	0.00	0.00	0.00	0.00	0.00	0.00	0.00	0.00	
	0.33	0.00	0.00	0.00	0.00	0.00	0.00	0.00	0.00	0.00	0.00	0.31	
		0.00	0.00	0.00	0.00	0.00	0.00	0.00	0.00	0.00	0.00		
		0.92	0.00	0.00	0.00	0.00	0.00	0.00	0.00	0.00	0.23		
			0.53	0.00	0.00	0.00	0.00	0.00	0.00	0.00			
			1.49	1.18	0.61	0.78	0.47	0.00	0.00	0.30			
				0.00	0.00	0.00	0.00	0.00	0.00				
				0.71	0.61	0.00	0.00	0.00	0.27				
					0.00	0.00	0.00	0.00					
					0.28	0.22	0.00	0.00					
						0.00	0.00						

Figure C.44: Maximum crack opening (cm) computed during a nonlinear analysis with the Northridge earthquake input (method 2)

0.00	1.02	1.25	1.83	1.86	1.02	2.19	2.71	1.41	2.09	0.79	3.54	0.00	0.00
0.00	0.82	1.40	1.80	1.64	0.98	2.04	2.65	1.31	2.06	0.76	3.29	0.00	0.00
	0.55	1.55	1.98	1.36	0.78	1.82	2.47	1.07	1.86	1.30	2.86	0.00	
	0.26	1.11	2.02	1.02	0.51	1.55	2.19	0.93	1.63	1.89	1.95	0.00	
		0.79	1.77	0.75	0.42	1.16	1.78	0.69	1.51	1.82	1.12		
		0.51	1.48	0.56	0.61	0.84	1.17	0.71	1.55	1.18	0.44		
			1.57	0.57	0.37	0.54	0.82	0.92	1.47	1.00			
			0.55	0.71	0.29	0.30	0.86	1.22	1.10	0.35			
				0.75	0.31	0.22	0.89	1.24	0.78				
				0.35	0.23	0.17	0.93	0.79	0.22				
					0.33	0.13	0.87	0.55					
					0.11	0.08	0.50	0.16					
						0.03	0.15						

Figure C.45: Maximum joint opening (cm) computed during a nonlinear analysis with the Northridge earthquake input (method 3)

0.00	0.00	0.00	0.00	0.00	0.00	0.00	0.00	0.00	0.00	0.00	0.00	0.00	0.00
0.15	0.00	0.00	0.00	0.00	0.00	0.00	0.00	0.00	0.00	0.00	0.00	0.00	0.00
	0.00	0.00	0.00	0.00	0.00	0.00	0.00	0.00	0.00	0.00	0.00	0.00	
	0.35	0.00	0.00	0.00	0.00	0.00	0.00	0.00	0.00	0.00	0.00	0.30	
		0.00	0.00	0.00	0.00	0.00	0.00	0.00	0.00	0.00	0.00		
		0.79	0.00	0.00	0.00	0.00	0.00	0.00	0.00	0.00	0.24		
			0.46	0.00	0.00	0.40	0.30	0.00	0.00	0.00			
			1.31	1.00	0.00	0.00	0.22	0.00	0.00	0.29			
				0.00	0.00	0.00	0.00	0.00	0.00				
				0.66	0.56	0.00	0.00	0.00	0.24				
					0.00	0.00	0.00	0.00					
					0.39	0.28	0.00	0.00					
						0.00	0.00						

Figure C.46: Maximum crack opening (cm) computed during a nonlinear analysis with the Northridge earthquake input (method 3)

0.00	1.30	1.42	2.49	2.97	1.43	2.92	5.27	6.91	3.73	3.43	5.42	0.00	0.00
0.00	1.10	1.47	2.53	2.75	1.46	3.22	5.17	5.94	3.56	3.54	5.06	0.00	0.00
	0.74	1.50	2.41	2.27	1.66	3.53	4.65	5.75	2.84	3.61	4.61	0.00	
	0.29	1.11	2.31	1.87	1.72	3.73	4.56	5.25	2.54	3.50	3.19	0.00	
		1.00	2.05	1.29	1.78	3.81	4.32	4.90	2.25	3.03	2.11		
		0.67	1.77	1.00	1.74	3.73	3.83	5.06	2.02	2.24	1.00		
			1.41	1.11	1.58	3.29	3.94	4.69	2.02	2.13			
			0.54	1.02	1.66	2.84	4.11	4.21	2.22	0.68			
				0.64	1.26	2.10	3.75	3.23	1.66				
				0.33	0.74	1.61	2.78	2.16	0.49				
					0.35	1.33	2.24	1.32					
					0.14	0.52	1.43	0.43					
						0.06	0.47						

Figure C.47: Maximum joint opening (cm) computed during a nonlinear analysis with the Northridge earthquake input (method 4)

0.00	0.00	0.00	0.00	0.00	0.00	0.00	0.00	0.00	0.00	0.00	0.00	0.00	0.00
0.15	0.00	0.00	0.00	0.00	0.00	0.00	0.00	0.00	0.00	0.00	0.00	0.00	0.54
	0.00	0.00	0.00	0.00	0.00	0.00	0.00	0.00	0.00	0.00	0.00	0.50	
	0.00	0.00	0.00	0.31	0.00	0.00	0.00	0.00	0.00	0.00	0.59	0.67	
		0.00	0.00	0.37	0.00	0.00	0.00	0.00	0.00	0.00	0.52		
		0.98	0.00	0.00	0.56	0.00	0.00	0.00	0.00	0.00	0.72		
			0.67	0.00	0.00	0.65	0.00	0.00	0.43	0.68			
			1.02	0.91	1.03	0.36	0.00	0.00	0.00	0.67			
				0.00	0.00	0.51	0.59	0.61	0.61				
				0.75	0.69	0.00	0.00	0.33	0.88				
					0.00	0.00	0.00	0.00					
					0.44	0.40	0.63	0.89					
						0.00	0.00						

Figure C.48: Maximum crack opening (cm) computed during a nonlinear analysis with the Northridge earthquake input (method 4)

0.00	1.16	1.43	2.18	0.86	1.50	2.87	2.15	2.30	1.21	0.69	4.55	0.00	0.00
0.00	1.01	1.42	2.09	0.78	1.53	2.65	2.04	2.04	1.23	1.04	4.19	0.00	0.00
	0.71	1.39	1.85	0.83	1.37	2.42	1.89	1.83	1.07	1.67	3.65	0.00	
	0.29	1.38	1.46	1.09	1.01	2.09	1.74	1.88	1.02	2.27	2.79	0.00	
		1.75	1.53	1.35	0.61	1.60	1.40	1.46	1.40	2.22	1.71		
		1.08	1.17	1.77	0.35	1.13	1.15	1.28	1.83	1.59	0.61		
			1.20	1.92	0.42	0.62	1.19	1.48	1.75	1.31			
			0.54	1.32	0.64	0.44	1.08	1.69	1.15	0.50			
				0.71	0.59	0.45	1.16	1.58	0.92				
				0.35	0.39	0.31	1.40	1.10	0.23				
					0.39	0.16	1.23	0.73					
					0.14	0.12	0.79	0.21					
						0.05	0.23						

Figure C.49: Maximum joint opening (cm) computed during a nonlinear analysis with the Northridge earthquake input (method 5)

0.00	0.00	0.00	0.00	0.00	0.00	0.00	0.00	0.00	0.00	0.00	0.00	0.00	0.00
0.15	0.00	0.00	0.00	0.00	0.00	0.00	0.00	0.00	0.00	0.00	0.00	0.00	0.00
	0.00	0.00	0.00	0.00	0.00	0.00	0.00	0.00	0.00	0.00	0.00	0.00	
	0.29	0.00	0.00	0.00	0.00	0.00	0.00	0.00	0.00	0.00	0.00	0.46	
		0.00	0.00	0.00	0.00	0.00	0.00	0.00	0.00	0.00	0.45		
		0.92	0.61	0.00	0.00	0.00	0.00	0.00	0.00	0.00	0.29		
			0.00	0.00	0.00	0.00	0.33	0.00	0.00	0.00			
			0.80	0.61	0.54	0.00	0.00	0.41	0.00	0.46			
				0.00	0.00	0.68	0.55	0.00	0.00				
				0.61	0.50	0.00	0.00	0.00	0.32				
					0.00	0.00	0.00	0.00					
					0.20	0.00	0.00	0.16					
						0.00	0.00						

Figure C.50: Maximum crack opening (cm) computed during a nonlinear analysis with the Northridge earthquake input (method 5)

0.00	1.16	1.44	1.66	0.86	1.67	2.86	2.31	1.85	2.19	0.93	4.65	0.00	0.00
0.00	1.00	1.35	1.81	0.89	1.53	2.67	2.23	1.74	2.12	1.13	4.27	0.00	0.00
	0.67	1.18	1.96	1.25	1.50	2.45	2.08	1.84	1.80	1.75	3.72	0.00	
	0.29	1.01	1.96	1.69	1.31	2.16	1.91	1.86	1.52	2.26	2.74	0.00	
		1.09	1.81	2.00	0.80	1.76	1.58	1.60	1.63	2.22	1.69		
		0.56	1.54	2.11	0.42	1.46	1.31	1.49	1.83	1.60	0.61		
			1.51	2.19	0.41	1.00	1.38	1.54	1.68	1.40			
			0.60	1.39	0.56	0.47	1.07	1.64	1.20	0.51			
				0.71	0.70	0.37	1.07	1.53	1.01				
				0.36	0.43	0.25	1.38	1.09	0.28				
					0.43	0.12	1.16	0.75					
					0.17	0.09	0.74	0.22					
						0.06	0.23						

Figure C.51: Maximum joint opening (cm) computed during a nonlinear analysis with the Northridge earthquake input (method 9)

0.00	0.00	0.00	0.00	0.00	0.00	0.00	0.00	0.00	0.00	0.00	0.00	0.00	0.00
0.16	0.00	0.00	0.00	0.00	0.00	0.00	0.00	0.00	0.00	0.00	0.00	0.00	0.00
	0.00	0.00	0.00	0.00	0.00	0.00	0.00	0.00	0.00	0.00	0.00	0.00	
	0.23	0.00	0.00	0.00	0.00	0.00	0.00	0.00	0.00	0.00	0.00	0.45	
		0.00	0.00	0.00	0.00	0.00	0.00	0.00	0.00	0.00	0.42		
		0.37	0.00	0.00	0.00	0.00	0.00	0.00	0.00	0.00	0.24		
			0.00	0.00	0.00	0.00	0.33	0.00	0.00	0.00			
			0.73	0.59	0.53	0.00	0.00	0.48	0.00	0.41			
				0.00	0.00	0.80	0.68	0.00	0.00				
				0.58	0.48	0.00	0.00	0.00	0.38				
					0.00	0.00	0.00	0.00					
					0.19	0.00	0.00	0.16					
						0.00	0.00						

Figure C.52: Maximum crack opening (cm) computed during a nonlinear analysis with the Northridge earthquake input (method 9)

0.00	2.28	2.66	3.17	3.28	2.96	4.12	4.00	4.04	2.06	1.74	1.63	0.00	0.00
0.00	1.78	2.66	2.98	2.87	3.24	3.68	3.89	3.68	2.16	1.73	1.50	0.00	0.00
	1.14	2.89	2.62	2.37	3.17	3.46	3.85	3.24	2.16	1.63	1.39	0.00	
	0.44	2.38	3.26	2.45	2.92	3.22	3.86	2.93	2.05	1.49	1.05	0.00	
		2.00	3.16	1.69	2.81	3.19	3.25	2.60	1.60	1.32	0.60		
		1.17	3.35	1.32	2.67	3.09	2.76	2.11	1.01	0.90	0.30		
			2.35	1.59	1.94	3.10	2.60	1.63	0.90	0.75			
			0.25	1.58	1.82	3.25	2.25	1.17	0.77	0.32			
				1.18	1.39	3.19	1.79	0.97	0.63				
				0.57	1.05	2.38	1.52	0.65	0.21				
					0.67	1.35	1.22	0.38					
					0.12	0.74	0.72	0.15					
						0.16	0.30						

Figure C.53: Maximum joint opening (cm) computed during a nonlinear analysis with the Northridge earthquake input (method 13)

0.00	0.00	0.00	0.00	0.00	0.00	0.00	0.00	0.00	0.00	0.00	0.00	0.00	0.00
0.25	0.00	0.00	0.00	0.00	0.00	0.00	0.00	0.00	0.00	0.00	0.00	0.00	0.00
	0.00	0.00	0.00	0.00	0.00	0.00	0.00	0.00	0.00	0.00	0.00	0.00	
	0.49	0.00	0.00	0.00	0.00	0.00	0.00	0.21	0.00	0.00	0.00	0.00	
		0.00	0.00	0.00	0.00	0.33	0.00	0.00	0.29	0.00	0.00		
		1.69	0.00	0.00	0.69	0.00	0.00	0.34	0.00	0.00	0.00		
			1.86	2.21	1.79	1.84	1.08	0.00	0.00	0.00			
			0.35	0.00	0.00	0.00	0.00	0.00	0.00	0.27			
				0.00	0.00	0.00	0.00	0.00	0.00				
				1.14	0.82	0.00	0.00	0.00	0.27				
					0.00	0.00	0.00	0.00					
					0.81	0.54	0.00	0.00					
						0.00	0.00						

Figure C.54: Maximum crack opening (cm) computed during a nonlinear analysis with the Northridge earthquake input (method 13)

0.00	2.62	3.51	4.36	2.52	4.53	5.15	6.66	8.33	2.54	3.12	5.17	0.00	0.00
0.00	2.17	3.02	4.08	2.34	4.09	5.03	6.53	8.03	2.28	2.90	4.93	0.00	0.00
	1.38	2.98	4.07	2.22	3.85	5.09	6.28	7.38	1.77	2.68	4.45	0.00	
	0.59	2.28	5.08	2.53	3.71	4.80	6.16	6.38	1.71	2.70	3.36	0.00	
		2.20	5.56	2.49	3.39	5.04	5.82	5.75	1.63	2.71	2.40		
		1.09	4.65	3.18	3.21	5.31	5.24	5.39	1.87	2.14	1.18		
			2.55	2.99	2.66	5.43	4.96	4.28	1.92	1.94			
			0.53	2.22	2.06	5.12	3.83	3.73	1.98	0.54			
				0.99	1.75	4.30	3.51	2.84	1.43				
				0.29	1.45	3.09	3.35	2.10	0.48				
					0.55	2.24	2.54	1.24					
					0.15	1.21	1.78	0.36					
						0.39	0.61						

Figure C.55: Maximum joint opening (cm) computed during a nonlinear analysis with the Northridge earthquake input (method 16)

0.00	0.00	0.00	0.00	0.00	0.00	0.00	0.00	0.00	0.00	0.00	0.00	0.00	0.00
0.30	0.00	0.00	0.00	0.00	0.00	0.00	0.00	0.00	0.00	0.00	0.00	0.00	0.49
	0.00	0.00	0.00	0.00	0.00	0.00	0.00	0.00	0.00	0.00	0.00	0.46	
	0.35	0.00	0.00	0.00	0.00	0.00	0.00	0.00	0.00	0.00	0.58	0.63	
		0.00	0.00	0.00	0.00	0.00	0.00	0.00	0.00	0.00	0.53		
		1.31	0.00	0.00	0.00	0.00	0.00	0.00	0.00	0.00	1.00		
			0.96	1.43	0.89	0.00	0.00	0.00	0.00	0.59			
			1.70	0.00	0.94	1.12	0.51	0.44	0.66	0.75			
				1.62	1.43	0.00	0.00	0.00	0.00				
				0.52	0.00	0.00	0.00	0.00	0.70				
					0.60	0.00	0.00	0.68					
					0.33	0.00	0.00	0.31					
						1.05	1.07						

Figure C.56: Maximum crack opening (cm) computed during a nonlinear analysis with the Northridge earthquake input (method 16)

0.00	1.70	1.34	2.22	1.58	1.02	2.97	2.88	1.09	2.13	1.01	3.61	0.00	0.00
0.00	1.45	1.56	2.11	1.49	0.93	2.87	2.82	0.97	2.01	1.00	3.30	0.00	0.00
	0.98	1.73	2.05	1.41	0.86	2.68	2.66	0.94	1.74	1.47	2.88	0.00	
	0.38	1.17	2.21	1.13	0.55	2.33	2.33	0.88	1.79	2.03	1.98	0.00	
		1.06	2.10	0.58	0.62	1.75	1.84	0.78	1.89	1.92	1.16		
		0.63	1.70	0.69	0.67	1.19	1.26	0.79	1.75	1.26	0.46		
			1.71	0.81	0.65	0.73	1.14	0.79	1.52	1.10			
			0.52	0.98	0.45	0.36	1.04	0.95	1.10	0.40			
				0.83	0.26	0.38	0.94	1.07	0.83				
				0.42	0.22	0.24	1.02	0.74	0.23				
					0.32	0.08	0.90	0.52					
					0.12	0.10	0.50	0.15					
						0.04	0.15						

Figure C.57: Maximum joint opening (cm) computed during a nonlinear analysis with the Northridge earthquake input (method 1+0.05 sec)

0.00	0.00	0.00	0.00	0.00	0.00	0.00	0.00	0.00	0.00	0.00	0.00	0.00	0.00
0.22	0.00	0.00	0.00	0.00	0.00	0.00	0.00	0.00	0.00	0.00	0.00	0.00	0.00
	0.00	0.00	0.00	0.00	0.00	0.00	0.00	0.00	0.00	0.00	0.00	0.00	
	0.33	0.00	0.00	0.00	0.00	0.00	0.00	0.00	0.00	0.00	0.00	0.30	
		0.00	0.00	0.00	0.00	0.00	0.00	0.00	0.00	0.00	0.00		
		0.89	0.00	0.00	0.00	0.00	0.00	0.00	0.00	0.00	0.28		
			0.56	0.00	0.00	0.00	0.00	0.00	0.00	0.00			
			1.56	1.27	0.47	0.00	0.00	0.42	0.00	0.28			
				0.00	0.00	0.77	0.69	0.00	0.00				
				1.00	0.80	0.00	0.00	0.00	0.27				
					0.00	0.00	0.00	0.00					
					0.59	0.44	0.00	0.00					
						0.00	0.00						

Figure C.58: Maximum crack opening (cm) computed during a nonlinear analysis with the Northridge earthquake input (method 1+0.05 sec)

0.00	0.84	1.54	1.94	0.94	1.46	2.35	2.65	0.98	1.88	0.99	3.18	0.00	0.00
0.00	0.74	1.50	2.13	1.15	1.18	2.22	2.36	0.94	1.88	0.96	2.97	0.00	0.00
	0.63	1.42	2.41	1.46	0.88	2.10	2.03	0.75	1.65	1.31	2.60	0.00	
	0.31	1.19	2.38	1.74	0.76	1.92	1.68	0.70	1.43	1.73	1.78	0.00	
		0.90	2.14	1.81	0.63	1.55	1.30	0.59	1.43	1.53	1.06		
		0.37	1.67	1.79	0.69	1.10	0.88	0.69	1.46	1.07	0.44		
			1.12	1.29	0.80	0.62	0.96	0.90	1.38	0.93			
			0.39	0.87	0.50	0.24	0.92	1.06	0.99	0.31			
				0.72	0.34	0.16	0.96	1.09	0.71				
				0.23	0.31	0.11	0.99	0.76	0.21				
					0.27	0.05	0.84	0.52					
					0.09	0.04	0.50	0.16					
						0.03	0.14						

Figure C.59: Maximum joint opening (cm) computed during a nonlinear analysis with the Northridge earthquake input (method 1 no delays)

0.00	0.00	0.00	0.00	0.00	0.00	0.00	0.00	0.00	0.00	0.00	0.00	0.00	0.00
0.00	0.00	0.00	0.00	0.00	0.00	0.00	0.00	0.00	0.00	0.00	0.00	0.00	0.00
	0.00	0.00	0.00	0.00	0.00	0.00	0.00	0.00	0.00	0.00	0.00	0.00	
	0.00	0.00	0.00	0.00	0.00	0.00	0.00	0.00	0.00	0.00	0.00	0.28	
		0.00	0.00	0.00	0.00	0.00	0.00	0.00	0.00	0.00	0.00		
		0.00	0.00	0.00	0.00	0.00	0.25	0.00	0.00	0.00	0.23		
			0.00	0.00	0.36	0.00	0.00	0.00	0.00	0.00			
			0.27	0.00	0.00	0.61	0.45	0.00	0.00	0.25			
				0.00	0.00	0.00	0.00	0.00	0.00				
				0.24	0.00	0.00	0.00	0.00	0.21				
					0.00	0.00	0.00	0.00					
					0.00	0.00	0.00	0.00					
						0.00	0.00						

Figure C.60: Maximum crack opening (cm) computed during a nonlinear analysis with the Northridge earthquake input (method 1 no delays)

C.2 Increased Damping, Softer Foundation, Joint Keys Removed

Three nonlinear dynamic analyses with the Northridge earthquake ground motion generated by method 1 were done with various modifications to the finite element model: increased Rayleigh damping, a softened region of foundation on the left abutment and joint sliding keys removed. The acceleration and displacement time histories, the contours of maximum arch and cantilever compression on both faces and the response pictures of maximum joint opening and crack opening are given for all three of these analyses.

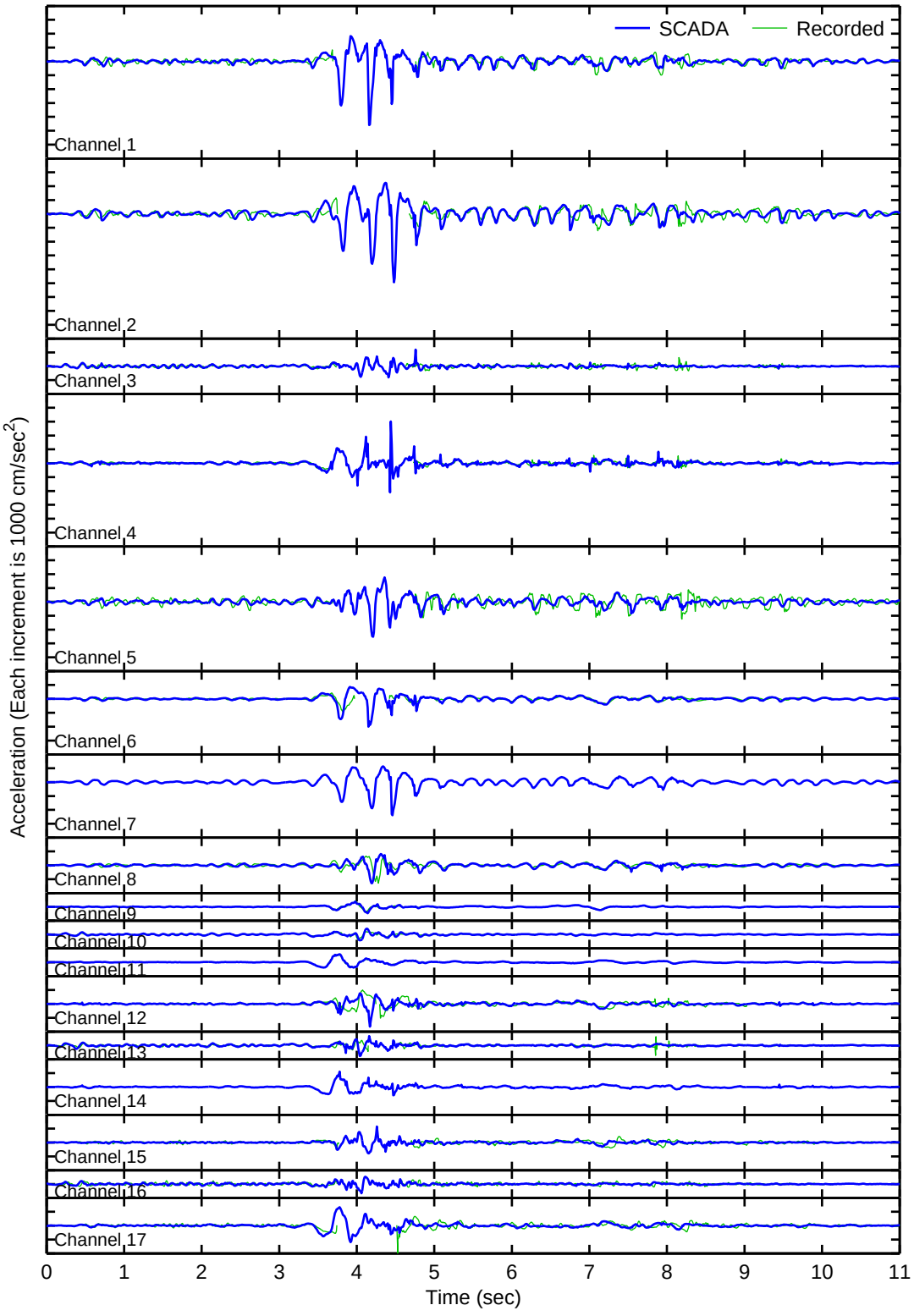

Figure C.61: Acceleration time histories at locations corresponding to channels 1–17 computed from a nonlinear analysis of the Northridge earthquake with increased damping compared to the partial records (method 1)

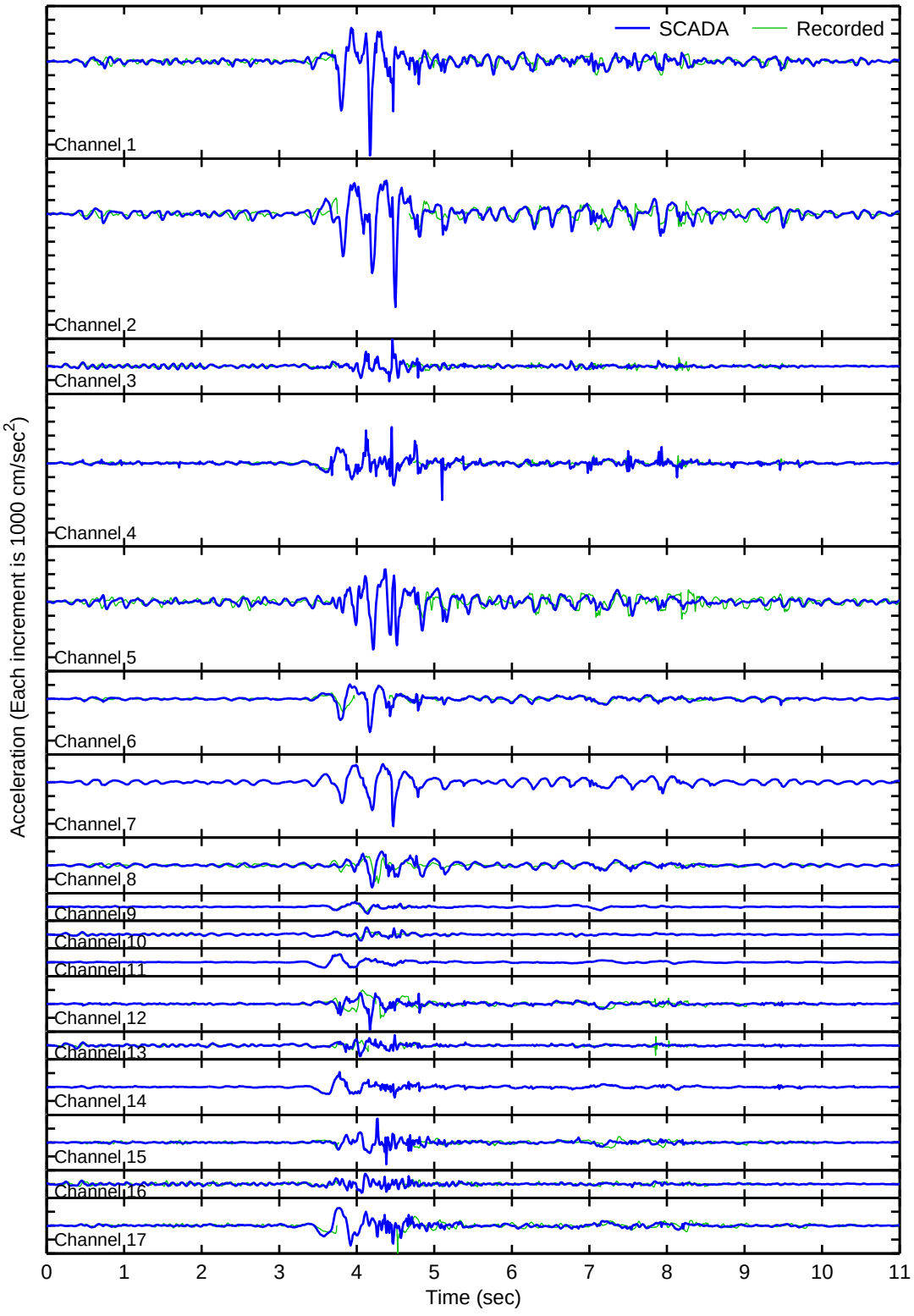

Figure C.62: Acceleration time histories at locations corresponding to channels 1–17 computed from a nonlinear analysis of the Northridge earthquake with a region of softened foundation compared to the partial records (method 1)

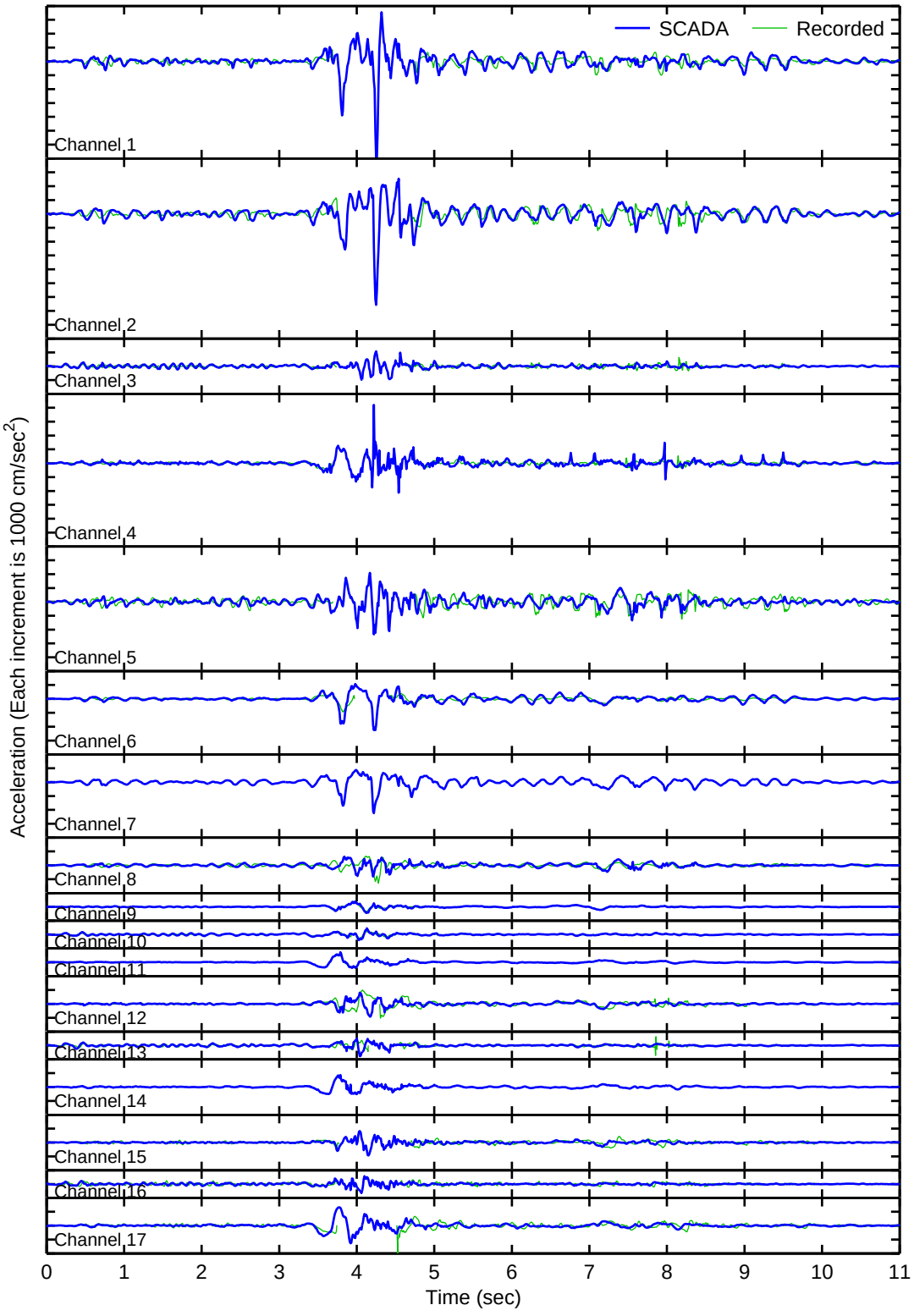

Figure C.63: Acceleration time histories at locations corresponding to channels 1–17 computed from a nonlinear analysis of the Northridge earthquake with joint sliding allowed compared to the partial records (method 1)

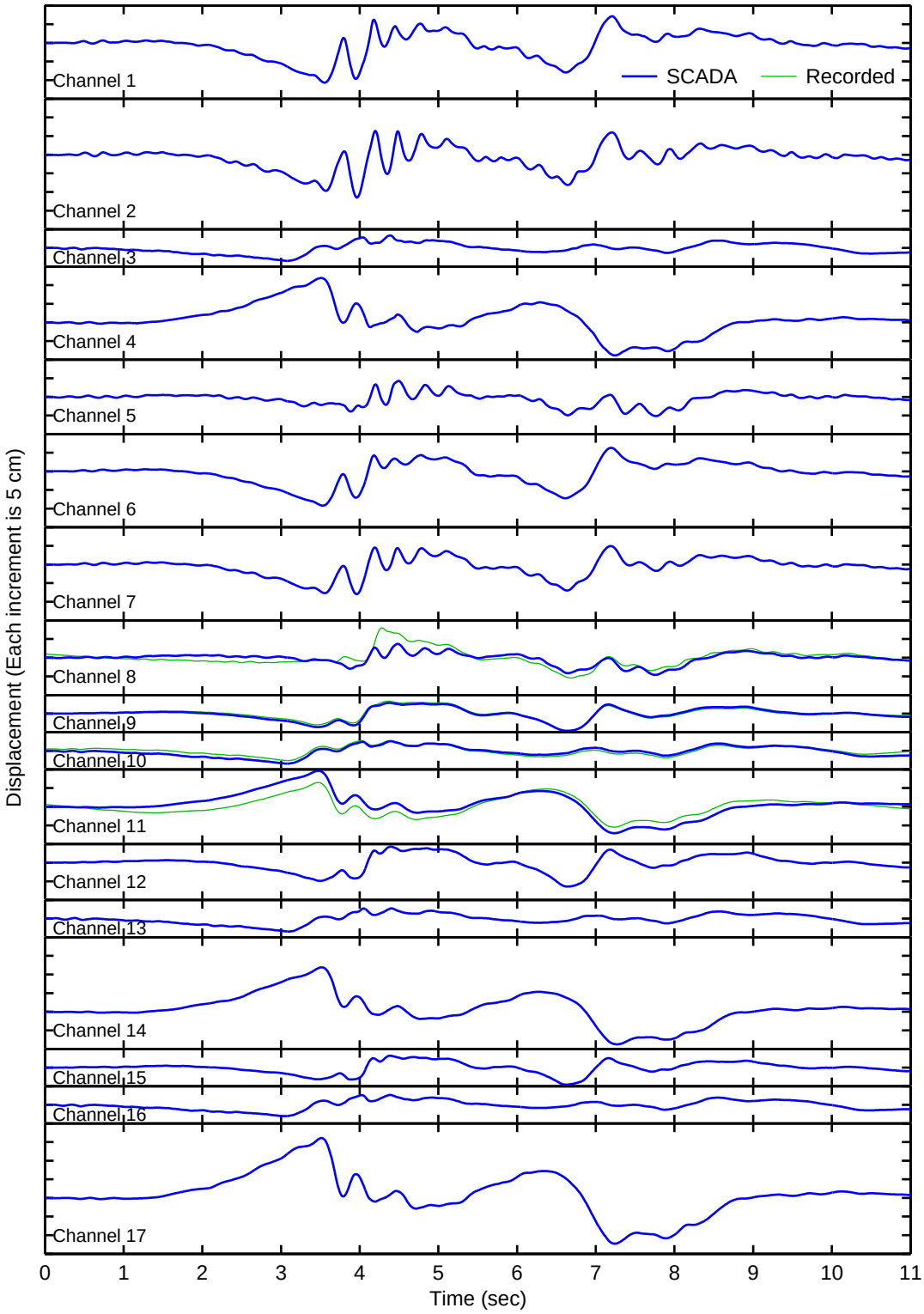

Figure C.64: Displacement time histories at locations corresponding to channels 1–17 computed from a nonlinear analysis of the Northridge earthquake with increased damping compared to the partial records (method 1)

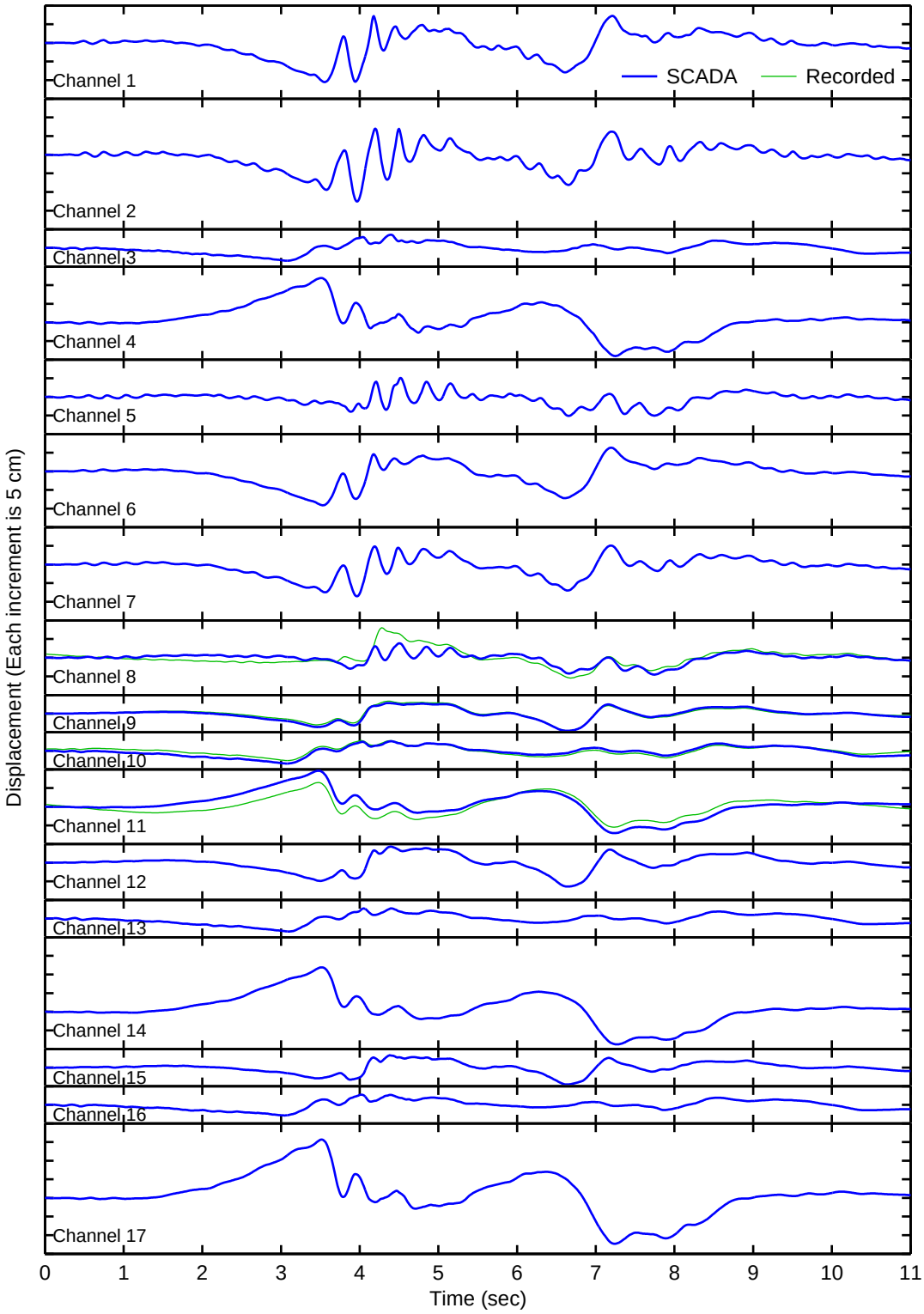

Figure C.65: Displacement time histories at locations corresponding to channels 1–17 computed from a nonlinear analysis of the Northridge earthquake with a region of softened foundation compared to the partial records (method 1)

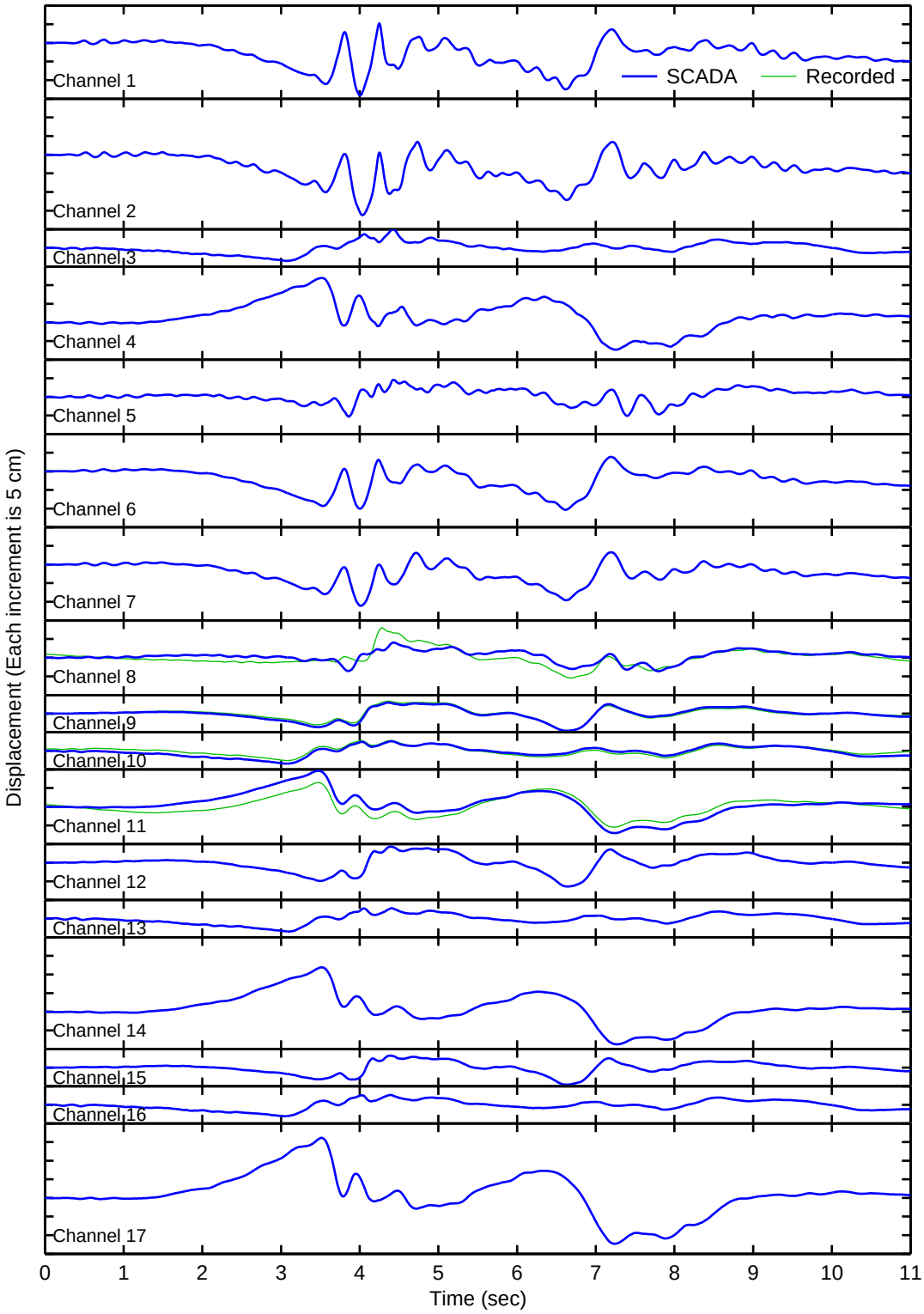

Figure C.66: Displacement time histories at locations corresponding to channels 1–17 computed from a nonlinear analysis of the Northridge earthquake with joint sliding allowed compared to the partial records (method 1)

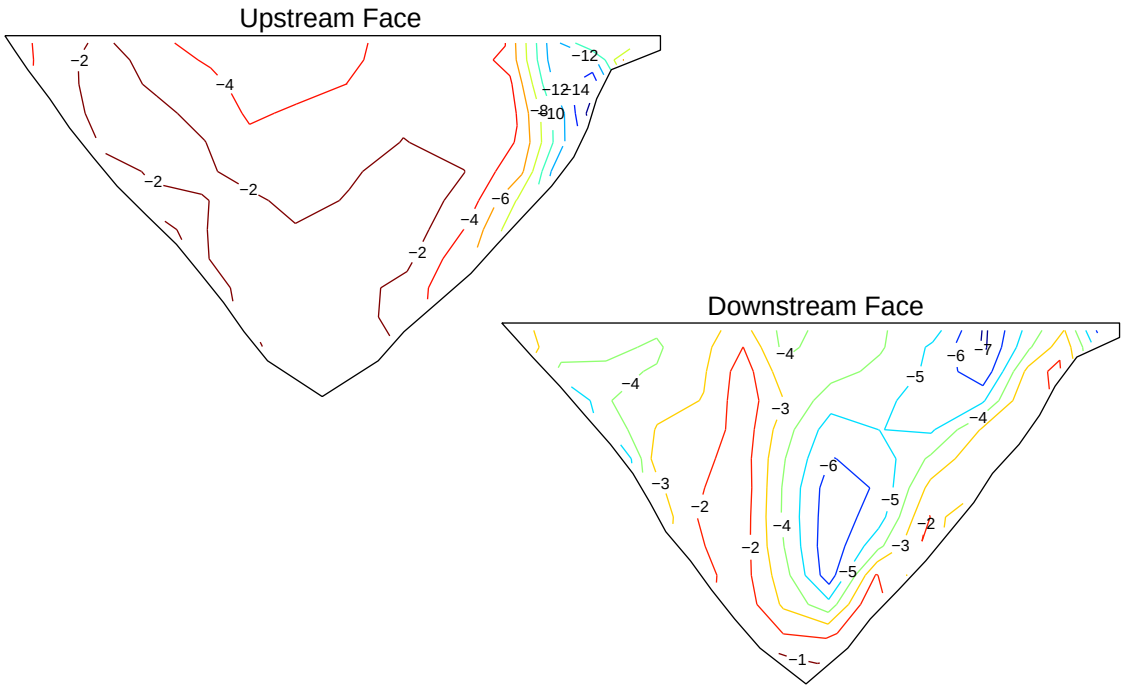

Figure C.67: Maximum compressive arch stresses (MPa) computed during a nonlinear analysis of the Northridge earthquake with increased damping (method 1)

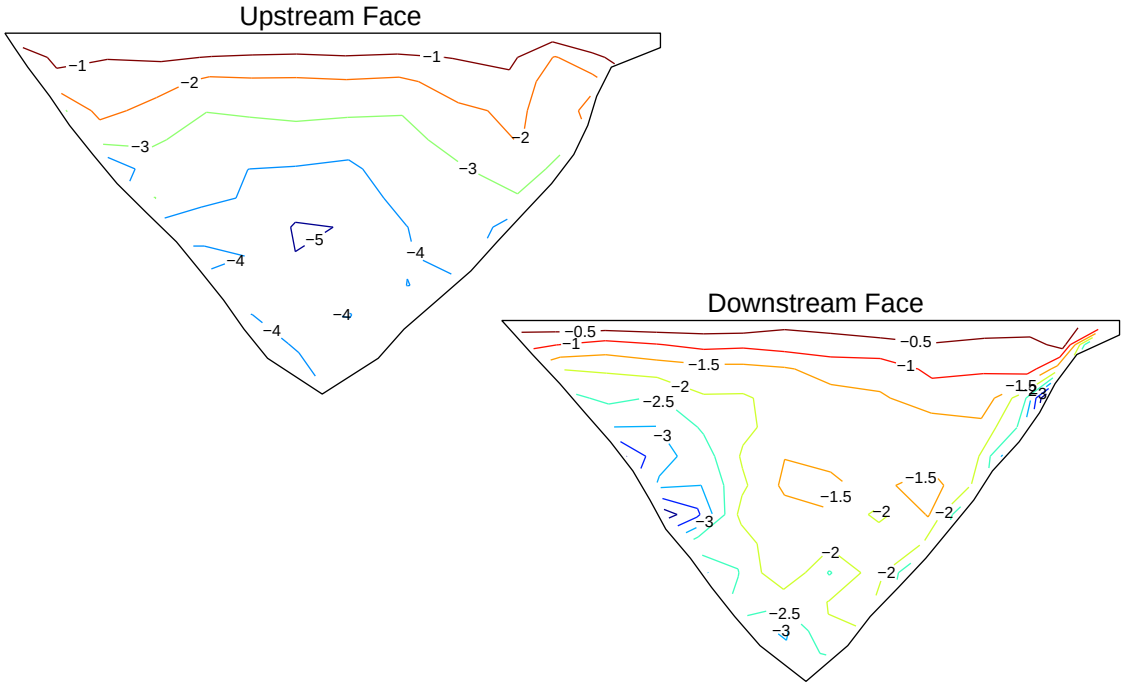

Figure C.68: Maximum compressive cantilever stresses (MPa) computed during a nonlinear analysis of the Northridge earthquake with increased damping (method 1)

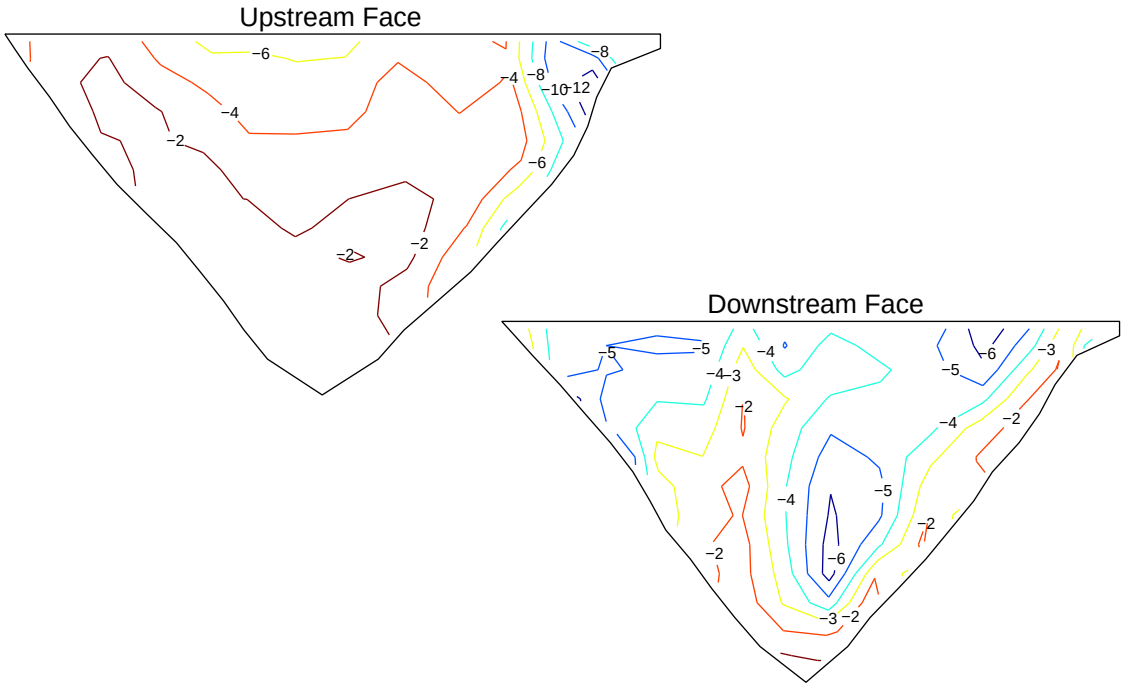

Figure C.69: Maximum compressive arch stresses (MPa) computed during a nonlinear analysis of the Northridge earthquake with a region of softened foundation (method 1)

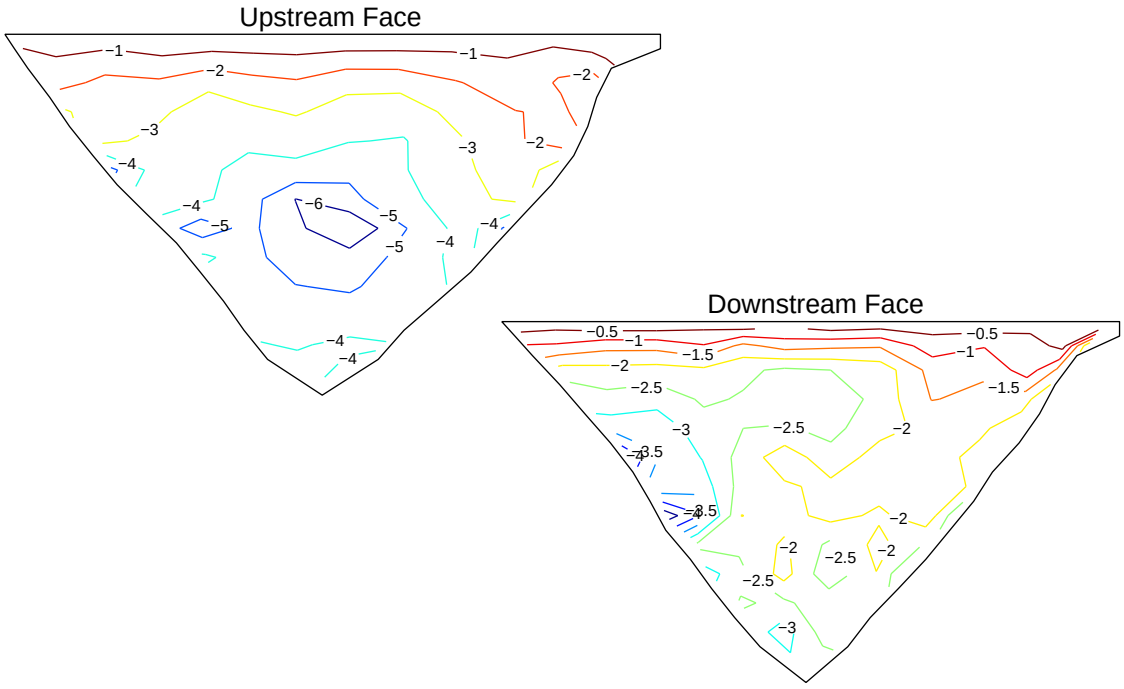

Figure C.70: Maximum compressive cantilever stresses (MPa) computed during a nonlinear analysis of the Northridge earthquake with a region of softened foundation (method 1)

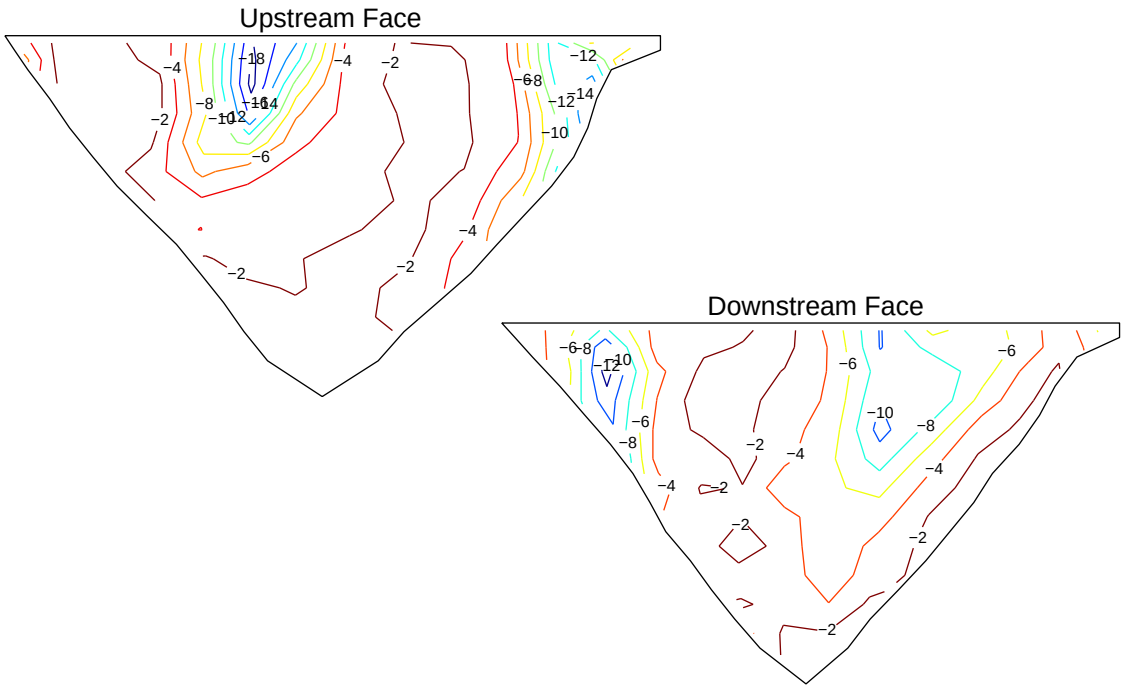

Figure C.71: Maximum compressive arch stresses (MPa) computed during a nonlinear analysis of the Northridge earthquake with joint sliding allowed (method 1)

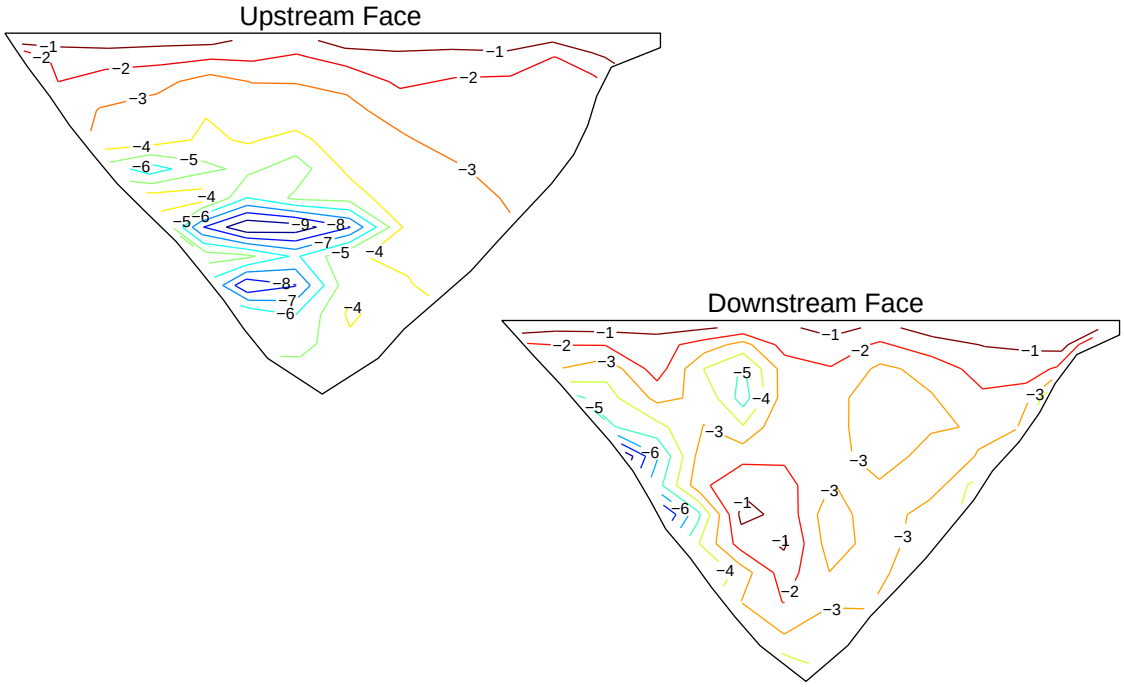

Figure C.72: Maximum compressive cantilever stresses (MPa) computed during a nonlinear analysis of the Northridge earthquake with joint sliding allowed (method 1)

0.00	0.87	1.06	1.25	0.60	0.97	2.04	1.65	0.99	2.19	0.42	3.08	0.00	0.00
0.00	0.76	1.01	1.35	0.61	0.90	1.95	1.59	0.83	2.11	0.69	2.85	0.00	0.00
	0.53	0.94	1.46	0.72	0.81	1.81	1.52	0.69	1.90	1.31	2.49	0.00	
	0.21	0.83	1.38	0.78	0.66	1.52	1.41	0.72	1.70	1.76	1.74	0.00	
		0.79	1.19	0.90	0.60	1.09	1.15	0.77	1.56	1.64	1.07		
		0.41	1.13	0.83	0.74	0.64	0.98	0.88	1.53	1.04	0.42		
			1.16	0.81	0.56	0.35	1.03	0.99	1.34	0.90			
			0.48	0.65	0.48	0.39	1.00	1.09	0.94	0.34			
				0.55	0.52	0.39	1.06	1.03	0.68				
				0.22	0.36	0.32	1.04	0.65	0.20				
					0.27	0.20	0.85	0.46					
					0.09	0.09	0.50	0.14					
						0.04	0.15						

Figure C.73: Maximum joint opening (cm) computed during a nonlinear analysis of the Northridge earthquake with increased damping (method 1)

0.00	0.00	0.00	0.00	0.00	0.00	0.00	0.00	0.00	0.00	0.00	0.00	0.00	0.00
0.12	0.00	0.00	0.00	0.00	0.00	0.00	0.00	0.00	0.00	0.00	0.00	0.00	0.00
	0.00	0.00	0.00	0.00	0.00	0.00	0.00	0.00	0.00	0.00	0.00	0.00	
	0.00	0.00	0.00	0.00	0.00	0.00	0.00	0.00	0.00	0.00	0.00	0.27	
		0.00	0.00	0.00	0.00	0.00	0.00	0.00	0.00	0.00	0.00		
		0.29	0.00	0.00	0.00	0.00	0.00	0.00	0.00	0.00	0.22		
			0.00	0.00	0.00	0.23	0.00	0.00	0.00	0.00			
			0.52	0.39	0.00	0.00	0.00	0.00	0.00	0.25			
				0.00	0.00	0.00	0.00	0.00	0.00				
				0.29	0.00	0.00	0.00	0.00	0.21				
					0.00	0.00	0.00	0.00					
					0.00	0.00	0.00	0.00					
						0.00	0.00						

Figure C.74: Maximum crack opening (cm) computed during a nonlinear analysis of the Northridge earthquake with increased damping (method 1)

0.00	0.94	1.05	1.44	0.75	1.45	2.33	2.54	1.20	1.36	0.85	3.04	0.00	0.00
0.00	0.81	1.12	1.60	0.86	1.27	2.28	2.46	0.95	1.24	0.78	2.85	0.00	0.00
	0.57	1.20	1.81	1.07	1.08	2.18	2.31	0.97	1.01	1.02	2.47	0.00	
	0.27	1.08	1.73	1.18	0.93	1.89	2.11	1.01	1.27	1.48	1.79	0.00	
		1.03	1.42	1.22	0.60	1.39	1.81	0.97	1.39	1.55	1.10		
		0.57	1.30	1.15	0.79	0.84	1.34	0.88	1.31	1.15	0.44		
			1.45	0.91	0.50	0.45	1.18	0.77	1.19	0.98			
			0.62	0.71	0.31	0.43	0.95	0.99	0.87	0.36			
				0.64	0.52	0.42	0.96	1.11	0.67				
				0.26	0.39	0.35	0.98	0.67	0.22				
					0.33	0.22	0.82	0.47					
					0.10	0.10	0.49	0.14					
						0.04	0.15						

Figure C.75: Maximum joint opening (cm) computed during a nonlinear analysis of the Northridge earthquake with a region of softened foundation (method 1)

0.00	0.00	0.00	0.00	0.00	0.00	0.00	0.00	0.00	0.00	0.00	0.00	0.00	0.00
0.13	0.00	0.00	0.00	0.00	0.00	0.00	0.00	0.00	0.00	0.00	0.00	0.00	0.00
	0.00	0.00	0.00	0.00	0.00	0.00	0.00	0.00	0.00	0.00	0.00	0.00	
	0.00	0.00	0.00	0.00	0.00	0.00	0.00	0.00	0.00	0.00	0.00	0.00	
		0.00	0.00	0.00	0.00	0.00	0.00	0.00	0.00	0.00	0.00		
		0.33	0.00	0.00	0.00	0.00	0.00	0.00	0.00	0.00	0.00		
			0.00	0.00	0.40	0.59	0.00	0.00	0.00	0.00			
			0.56	0.43	0.00	0.00	0.61	0.45	0.00	0.27			
				0.00	0.00	0.00	0.00	0.00	0.00				
				0.29	0.00	0.00	0.00	0.00	0.23				
					0.00	0.00	0.00	0.00					
					0.00	0.00	0.00	0.00					
						0.00	0.00						

Figure C.76: Maximum crack opening (cm) computed during a nonlinear analysis of the Northridge earthquake with a region of softened foundation (method 1)

0.00	0.99	1.35	1.29	0.79	3.86	7.77	2.28	2.03	1.55	0.57	3.68	0.00	0.00
0.00	0.80	1.37	1.27	0.79	3.50	7.35	2.10	2.05	1.62	0.70	3.46	0.00	0.00
	0.50	1.42	1.08	0.95	3.08	6.49	1.77	1.89	1.44	1.08	2.72	0.00	
	0.21	1.50	1.13	1.32	3.54	5.48	1.29	1.71	1.38	1.79	1.88	0.00	
		1.63	1.01	1.85	3.29	4.04	0.95	1.46	1.17	2.24	1.14		
		0.94	1.22	2.23	2.32	2.47	1.14	0.78	1.61	1.74	0.39		
			2.40	2.24	0.65	2.01	1.78	0.71	1.88	1.17			
			1.69	1.47	0.26	1.46	0.87	0.85	1.49	0.44			
				1.02	1.14	0.68	0.26	0.66	1.11				
				0.37	0.35	0.35	0.37	0.73	0.41				
					0.24	0.11	0.20	0.71					
					0.09	0.08	0.31	0.23					
						0.07	0.15						

Figure C.77: Maximum joint opening (cm) computed during a nonlinear analysis of the Northridge earthquake with joint sliding allowed (method 1)

0.00	0.00	0.00	0.00	0.00	0.00	0.00	0.00	0.00	0.00	0.00	0.00	0.00	0.00
0.15	0.00	0.00	0.00	0.00	0.00	0.00	0.00	0.00	0.00	0.00	0.00	0.00	0.00
	0.00	0.00	0.00	0.00	0.00	0.00	0.00	0.00	0.00	0.00	0.00	0.00	
	0.00	0.00	0.00	0.00	0.00	0.00	0.00	0.00	0.00	0.00	0.00	0.26	
		0.00	0.00	0.00	0.00	0.00	0.00	0.00	0.00	0.00	0.00		
		1.03	1.43	1.17	0.00	0.00	0.00	0.00	0.00	0.00	0.00		
			0.00	0.00	0.00	0.00	0.00	0.00	0.00	0.00			
			1.95	1.95	3.25	2.70	1.11	0.00	0.00	0.00			
				0.00	0.00	0.00	0.00	0.00	0.00				
				1.16	1.28	0.70	0.00	0.00	0.00				
					0.00	0.00	0.00	0.00					
					0.37	0.29	0.00	0.00					
						0.00	0.00						

Figure C.78: Maximum crack opening (cm) computed during a nonlinear analysis of the Northridge earthquake with joint sliding allowed (method 1)

C.3 Uniform Ground Motion Input

Nonlinear dynamic analyses with the ground motion generated from the Northridge earthquake base records by method 1 are done with the water level in the finite element model at about 20 meters below the crest. The nonuniform ground motion input is compared to three different sets of uniform ground motion input. The 3-component sets at channels 9–11 (base), 12–14 (right abutment) and 15–17 (left abutment) are each applied uniformly. The contours of maximum compressive stress in the arch and cantilever directions on both faces and the response pictures of maximum joint opening and crack opening in each element are given for all four analyses.

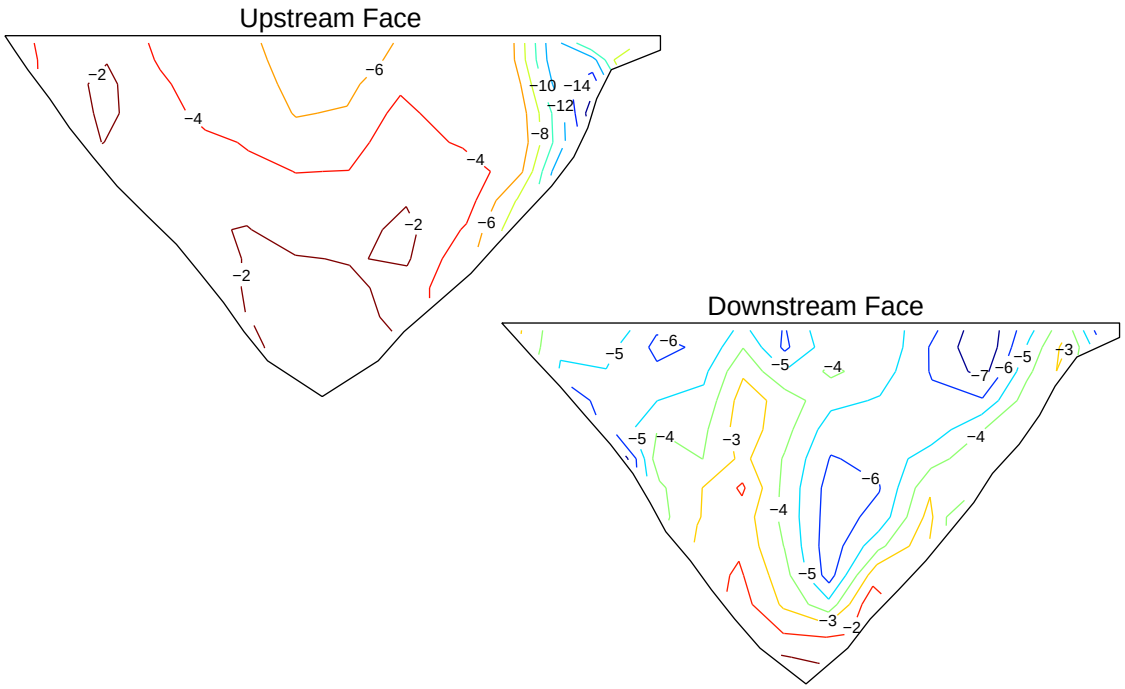

Figure C.79: Maximum compressive arch stresses (MPa) computed during a nonlinear analysis with nonuniform ground motion input (method 1)

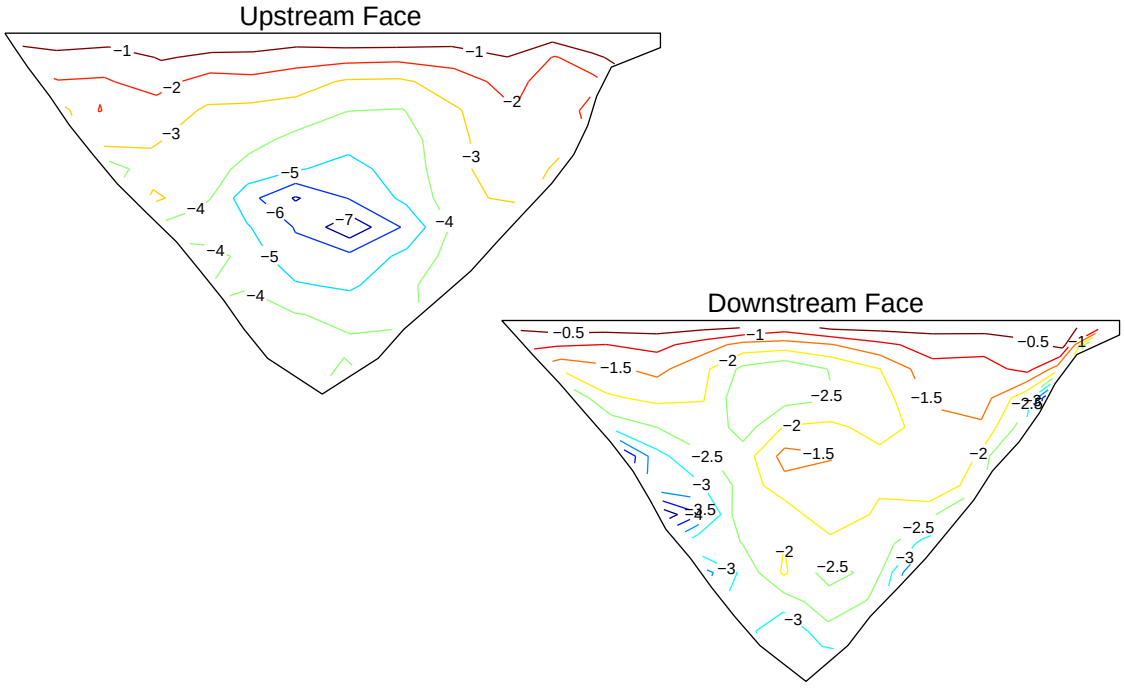

Figure C.80: Maximum compressive cantilever stresses (MPa) computed during a nonlinear analysis with nonuniform ground motion input (method 1)

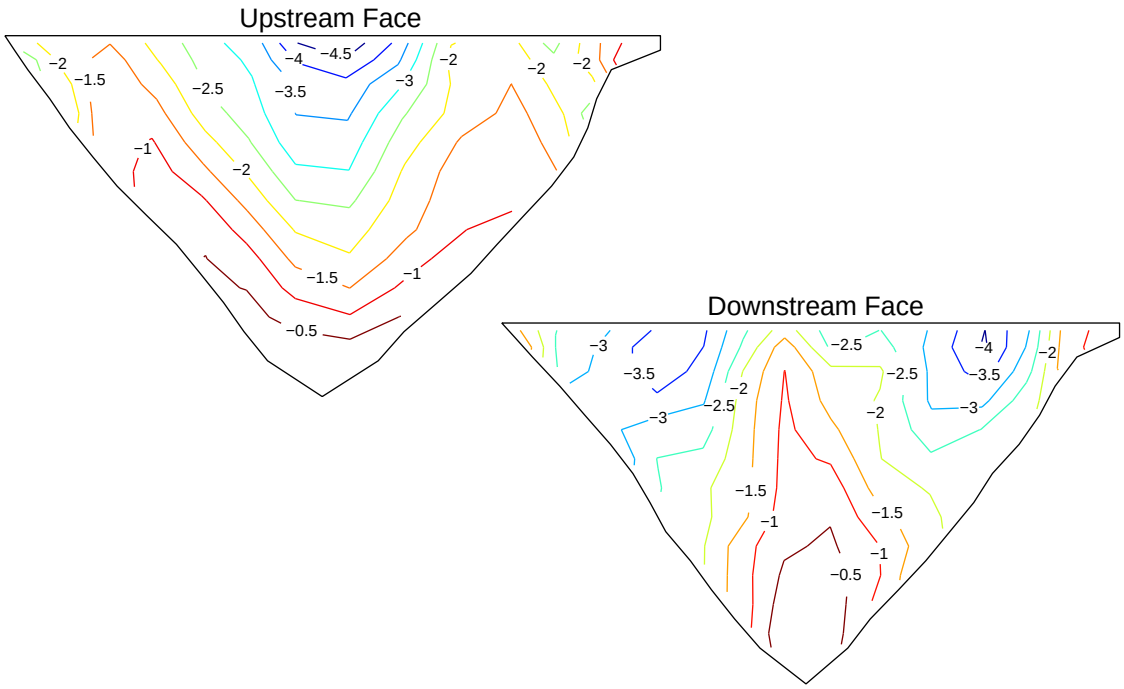

Figure C.81: Maximum compressive arch stresses (MPa) computed during a nonlinear analysis with uniform ground motion input (recorded base channels 9–11)

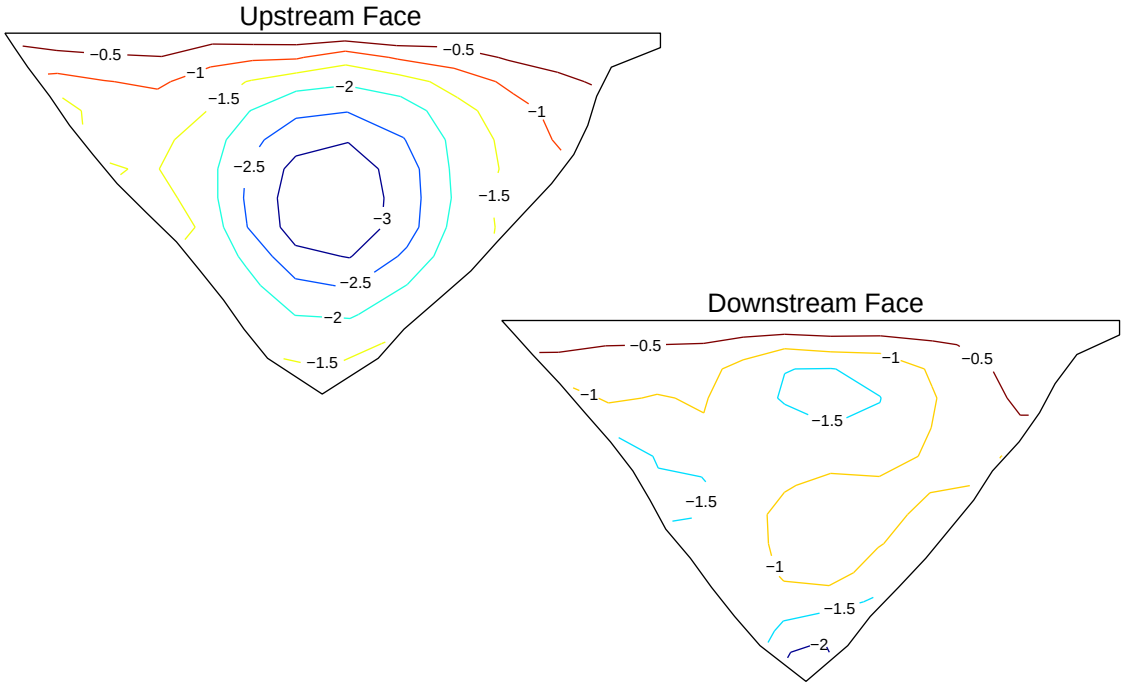

Figure C.82: Maximum compressive cantilever stresses (MPa) computed during a nonlinear analysis with uniform ground motion input (recorded base channels 9–11)

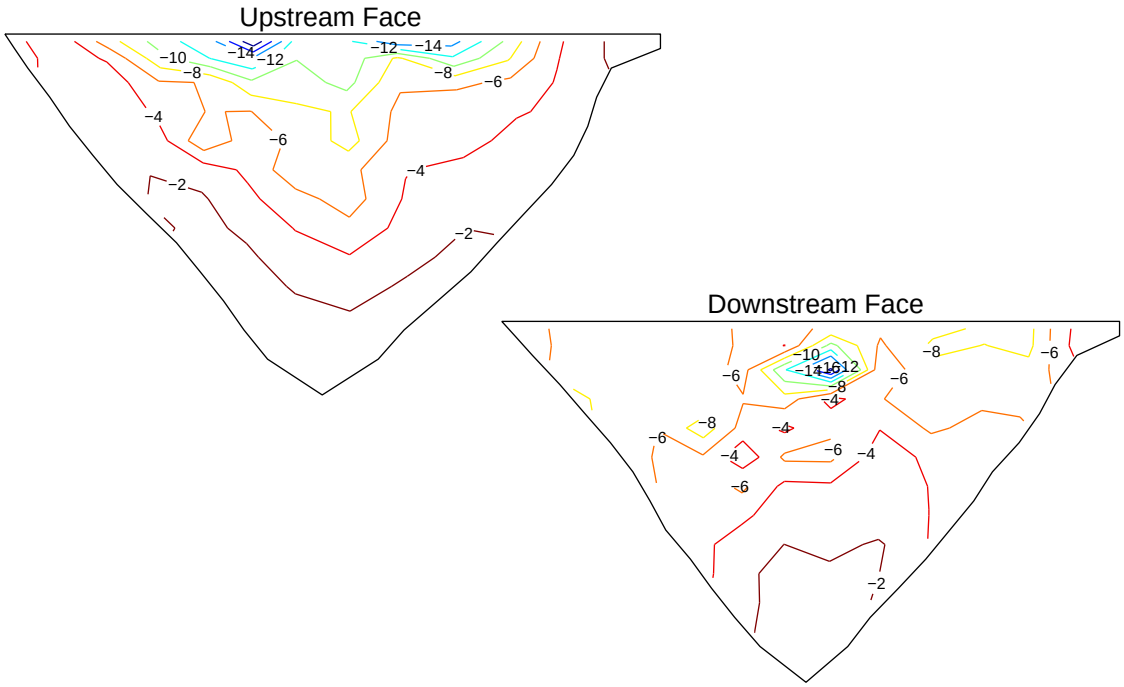

Figure C.83: Maximum compressive arch stresses (MPa) computed during a nonlinear analysis with uniform ground motion input (method 1 right abutment channels 12–14)

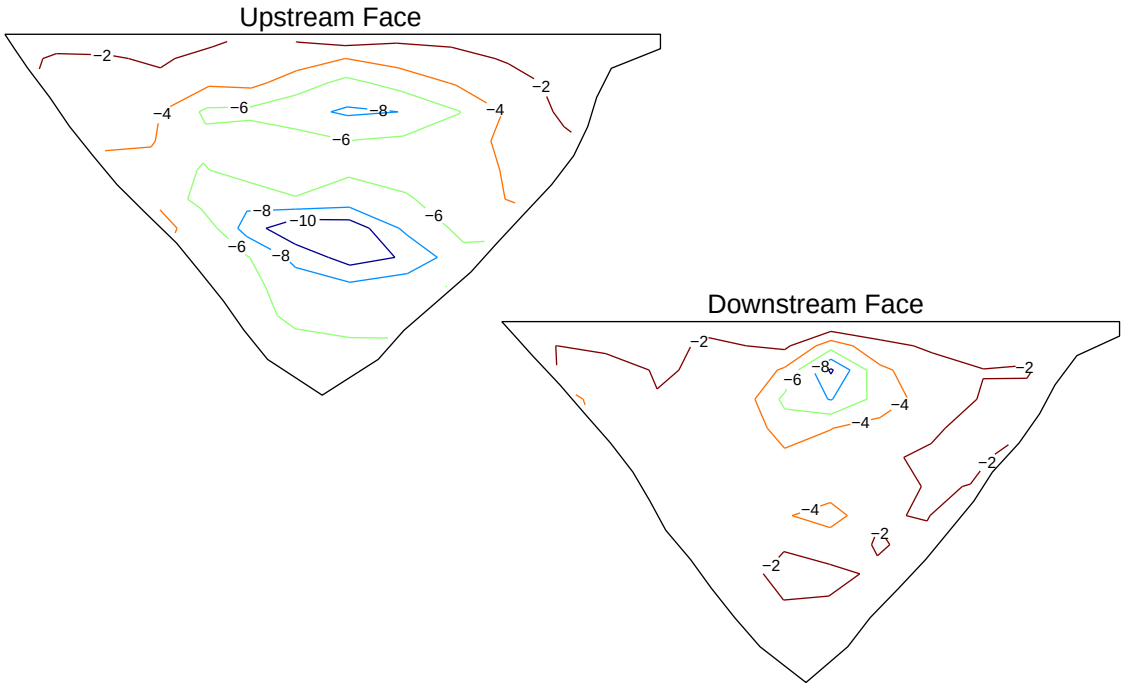

Figure C.84: Maximum compressive cantilever stresses (MPa) computed during a nonlinear analysis with uniform ground motion input (method 1 right abutment channels 12–14)

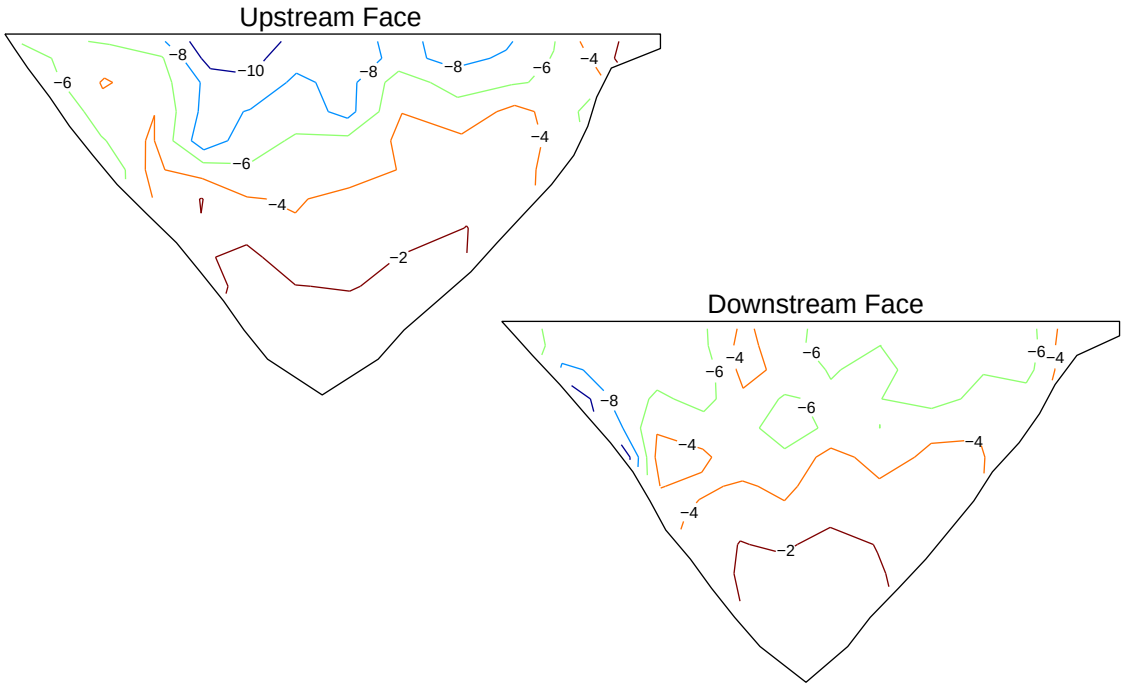

Figure C.85: Maximum compressive arch stresses (MPa) computed during a nonlinear analysis with uniform ground motion input (method 1 left abutment channels 15–17)

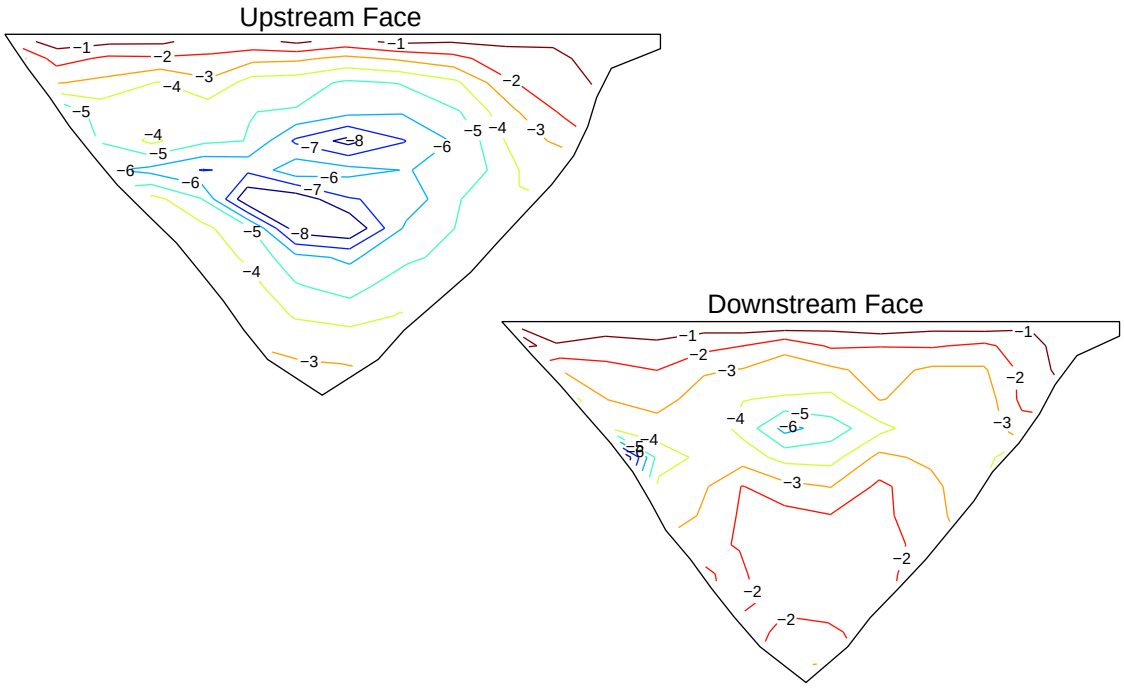

Figure C.86: Maximum compressive cantilever stresses (MPa) computed during a nonlinear analysis with uniform ground motion input (method 1 left abutment channels 15–17)

0.00	0.92	1.03	1.29	0.44	1.15	2.48	2.84	1.02	1.16	0.59	2.66	0.00	0.00
0.00	0.81	0.99	1.42	0.49	1.09	2.29	2.71	0.87	1.19	0.64	2.49	0.00	0.00
	0.58	1.01	1.58	0.76	0.94	2.10	2.45	0.60	1.02	0.91	2.23	0.00	
	0.24	0.91	1.54	1.00	0.70	1.88	2.10	0.47	1.24	1.24	1.63	0.00	
		0.86	1.28	1.22	0.49	1.35	1.64	0.41	1.37	1.19	1.04		
		0.47	1.08	1.32	0.64	0.59	1.11	0.38	1.25	0.94	0.45		
			1.18	1.02	0.25	0.40	1.04	0.31	1.00	0.85			
			0.49	0.61	0.15	0.50	0.95	0.58	0.68	0.30			
				0.48	0.27	0.28	0.79	0.95	0.53				
				0.19	0.24	0.23	0.94	0.50	0.17				
					0.20	0.14	0.81	0.36					
					0.06	0.08	0.49	0.11					
						0.03	0.15						

Figure C.87: Maximum joint opening (cm) computed during a nonlinear analysis with nonuniform ground motion input (method 1)

0.00	0.00	0.00	0.00	0.00	0.00	0.00	0.00	0.00	0.00	0.00	0.00	0.00	0.00
0.13	0.00	0.00	0.00	0.00	0.00	0.00	0.00	0.00	0.00	0.00	0.00	0.00	0.00
	0.00	0.00	0.00	0.00	0.00	0.00	0.00	0.00	0.00	0.00	0.00	0.00	
	0.00	0.00	0.00	0.00	0.00	0.00	0.00	0.00	0.00	0.00	0.00	0.26	
		0.00	0.00	0.00	0.00	0.00	0.00	0.00	0.00	0.00	0.00		
		0.29	0.00	0.00	0.00	0.00	0.00	0.00	0.00	0.00	0.00		
			0.00	0.00	0.72	0.90	0.38	0.00	0.00	0.00			
			0.49	0.37	0.00	0.46	0.82	0.55	0.00	0.00			
				0.00	0.00	0.00	0.00	0.00	0.00				
				0.27	0.00	0.00	0.00	0.00	0.00				
					0.00	0.00	0.00	0.00					
					0.00	0.00	0.00	0.00					
						0.00	0.00						

Figure C.88: Maximum crack opening (cm) computed during a nonlinear analysis with nonuniform ground motion input (method 1)

0.00	0.22	0.43	0.64	0.24	0.33	0.84	1.13	0.30	0.33	0.40	0.30	0.00	0.00
0.00	0.19	0.42	0.71	0.32	0.26	0.73	1.03	0.24	0.36	0.35	0.29	0.00	0.00
	0.15	0.40	0.73	0.39	0.19	0.59	0.83	0.15	0.36	0.26	0.28	0.00	
	0.08	0.33	0.68	0.41	0.18	0.43	0.59	0.14	0.37	0.27	0.23	0.00	
		0.22	0.60	0.40	0.19	0.24	0.36	0.10	0.34	0.29	0.20		
		0.08	0.41	0.33	0.15	0.10	0.14	0.07	0.28	0.22	0.10		
			0.20	0.21	0.08	0.04	0.04	0.08	0.20	0.15			
			0.05	0.12	0.03	0.02	0.04	0.07	0.16	0.05			
				0.06	0.02	0.02	0.04	0.04	0.09				
				0.02	0.02	0.02	0.04	0.04	0.03				
					0.02	0.02	0.06	0.03					
					0.01	0.02	0.05	0.01					
						0.01	0.02						

Figure C.89: Maximum joint opening (cm) computed during a nonlinear analysis with uniform ground motion input (recorded base channels 9–11)

0.00	0.00	0.00	0.00	0.00	0.00	0.00	0.00	0.00	0.00	0.00	0.00	0.00	0.00
0.00	0.00	0.00	0.00	0.00	0.00	0.00	0.00	0.00	0.00	0.00	0.00	0.00	0.00
	0.00	0.00	0.00	0.00	0.00	0.00	0.00	0.00	0.00	0.00	0.00	0.00	
	0.00	0.00	0.00	0.00	0.00	0.00	0.00	0.00	0.00	0.00	0.00	0.00	
		0.00	0.00	0.00	0.00	0.00	0.00	0.00	0.00	0.00	0.00		
		0.00	0.00	0.00	0.00	0.00	0.00	0.00	0.00	0.00	0.00		
			0.00	0.00	0.00	0.00	0.00	0.00	0.00	0.00			
			0.00	0.00	0.00	0.00	0.00	0.00	0.00	0.00			
				0.00	0.00	0.00	0.00	0.00	0.00				
				0.00	0.00	0.00	0.00	0.00	0.00				
					0.00	0.00	0.00	0.00					
					0.00	0.00	0.00	0.00					
						0.00	0.00						

Figure C.90: Maximum crack opening (cm) computed during a nonlinear analysis with uniform ground motion input (recorded base channels 9–11)

0.00	0.80	1.86	2.71	1.95	4.83	7.03	10.84	4.75	2.31	1.83	1.53	0.00	0.00
0.00	0.77	1.87	3.01	3.10	4.61	6.20	9.17	4.69	3.27	2.08	1.50	0.00	0.00
	0.69	1.75	3.29	5.10	3.76	4.29	5.23	3.44	3.72	2.45	1.46	0.00	
	0.36	1.33	3.06	4.20	2.42	2.96	1.52	1.62	2.35	2.40	1.22	0.00	
		1.02	2.67	2.98	1.06	2.56	1.40	0.60	2.14	1.98	0.85		
		0.42	1.81	2.38	0.29	1.44	1.18	0.36	2.13	1.32	0.36		
			1.01	1.59	0.94	0.59	0.82	0.29	1.82	0.97			
			0.31	1.23	0.44	0.19	0.43	0.27	1.42	0.34			
				0.79	0.31	0.12	0.30	0.38	0.92				
				0.26	0.37	0.08	0.14	0.29	0.30				
					0.38	0.05	0.14	0.34					
					0.16	0.03	0.11	0.13					
						0.04	0.04						

Figure C.91: Maximum joint opening (cm) computed during a nonlinear analysis with uniform ground motion input (method 1 right abutment channels 12–14)

0.00	0.00	0.00	0.00	0.00	0.00	0.00	0.00	0.00	0.00	0.00	0.00	0.00	0.00
0.00	0.00	0.00	0.00	0.00	0.00	0.00	0.00	0.00	0.00	0.00	0.00	0.00	0.00
	0.00	0.00	1.03	0.00	0.00	2.48	1.71	0.52	0.00	0.00	0.00	0.00	
	0.00	0.00	0.00	2.09	3.15	4.12	4.99	2.95	0.73	0.00	0.00	0.00	
		0.00	0.00	0.00	0.00	0.00	0.00	0.00	0.26	0.00	0.00		
		0.00	0.00	0.45	0.30	0.00	0.00	0.75	1.04	0.00	0.00		
			0.00	0.98	1.18	0.00	0.00	0.48	0.00	0.00			
			0.00	0.00	2.26	4.28	4.08	2.22	0.27	0.75			
				0.00	0.00	0.61	0.99	1.17	0.90				
				0.00	0.00	0.00	0.00	0.00	0.00				
					0.00	0.00	0.00	0.00					
					0.00	0.00	0.00	0.00					
						0.00	0.00						

Figure C.92: Maximum crack opening (cm) computed during a nonlinear analysis with uniform ground motion input (method 1 right abutment channels 12–14)

0.00	0.95	1.18	1.96	2.56	4.63	7.17	5.99	1.35	1.24	1.71	1.66	0.00	0.00
0.00	0.97	1.52	1.99	2.50	3.92	6.07	5.02	1.23	1.38	1.73	1.70	0.00	0.00
	1.06	1.79	1.81	2.16	3.01	4.63	3.20	1.10	1.39	1.98	1.61	0.00	
	0.62	1.82	1.65	1.80	2.18	2.92	1.43	1.02	1.66	1.99	1.36	0.00	
		2.25	2.08	0.99	1.29	0.87	0.65	0.58	1.23	1.66	1.08		
		1.45	1.29	0.68	0.49	0.48	0.21	0.51	1.07	0.94	0.51		
			0.60	0.99	0.44	0.25	0.13	0.49	1.00	0.75			
			0.20	0.59	0.32	0.18	0.13	0.44	0.80	0.27			
				0.46	0.17	0.16	0.08	0.42	0.52				
				0.15	0.21	0.18	0.09	0.32	0.18				
					0.24	0.15	0.12	0.25					
					0.10	0.09	0.10	0.11					
						0.03	0.05						

Figure C.93: Maximum joint opening (cm) computed during a nonlinear analysis with uniform ground motion input (method 1 left abutment channels 15–17)

0.00	0.00	0.00	0.00	0.00	0.00	0.00	0.00	0.00	0.00	0.00	0.00	0.00	0.00
0.00	0.00	0.00	0.00	0.00	0.00	0.00	0.00	0.00	0.00	0.00	0.00	0.00	0.00
	0.00	0.00	0.00	0.00	0.00	0.00	0.00	0.00	0.00	0.00	0.00	0.00	
	0.36	0.41	0.00	0.00	0.00	0.00	0.00	0.00	0.00	0.00	0.00	0.00	
		0.00	0.00	0.36	2.14	4.21	4.65	3.35	1.64	0.60	0.00		
		1.17	1.66	2.39	1.00	0.00	0.00	0.00	0.71	0.00	0.00		
			0.00	1.20	2.96	2.10	1.44	0.99	0.00	0.00			
			0.00	0.00	0.00	0.69	0.68	0.00	0.00	0.00			
				0.00	0.00	0.00	0.00	0.00	0.00				
				0.00	0.00	0.00	0.00	0.00	0.00				
					0.00	0.00	0.00	0.00					
					0.00	0.00	0.00	0.00					
						0.00	0.00						

Figure C.94: Maximum crack opening (cm) computed during a nonlinear analysis with uniform ground motion input (method 1 left abutment channels 15–17)

C.4 Pseudostatic Analysis

A nonlinear pseudostatic analysis with the nonuniform ground motion generated from the Northridge earthquake base records by method 1 was done. Hydrostatic pressure for water up to about 20 meters below the crest was applied for the static part of the analysis. The pseudostatic response is that which would occur if the input ground motion is applied very slowly so that inertial and damping effects are negligible. This is actually computed by removing the mass and damping from the model and running the "dynamic" part of the SCADA analysis. The reservoir is not present for this analysis. The displacements that are computed for this pseudostatic analysis at the locations corresponding to channels 1–17 are compared to the displacements computed by the full dynamic analysis, which does include the pseudostatic component. The contours of maximum pseudostatic compression on both faces of the dam computed in the arch and cantilever directions are shown; and the maximum joint opening and crack opening for each element of the dam model are also shown from the pseudostatic analysis.

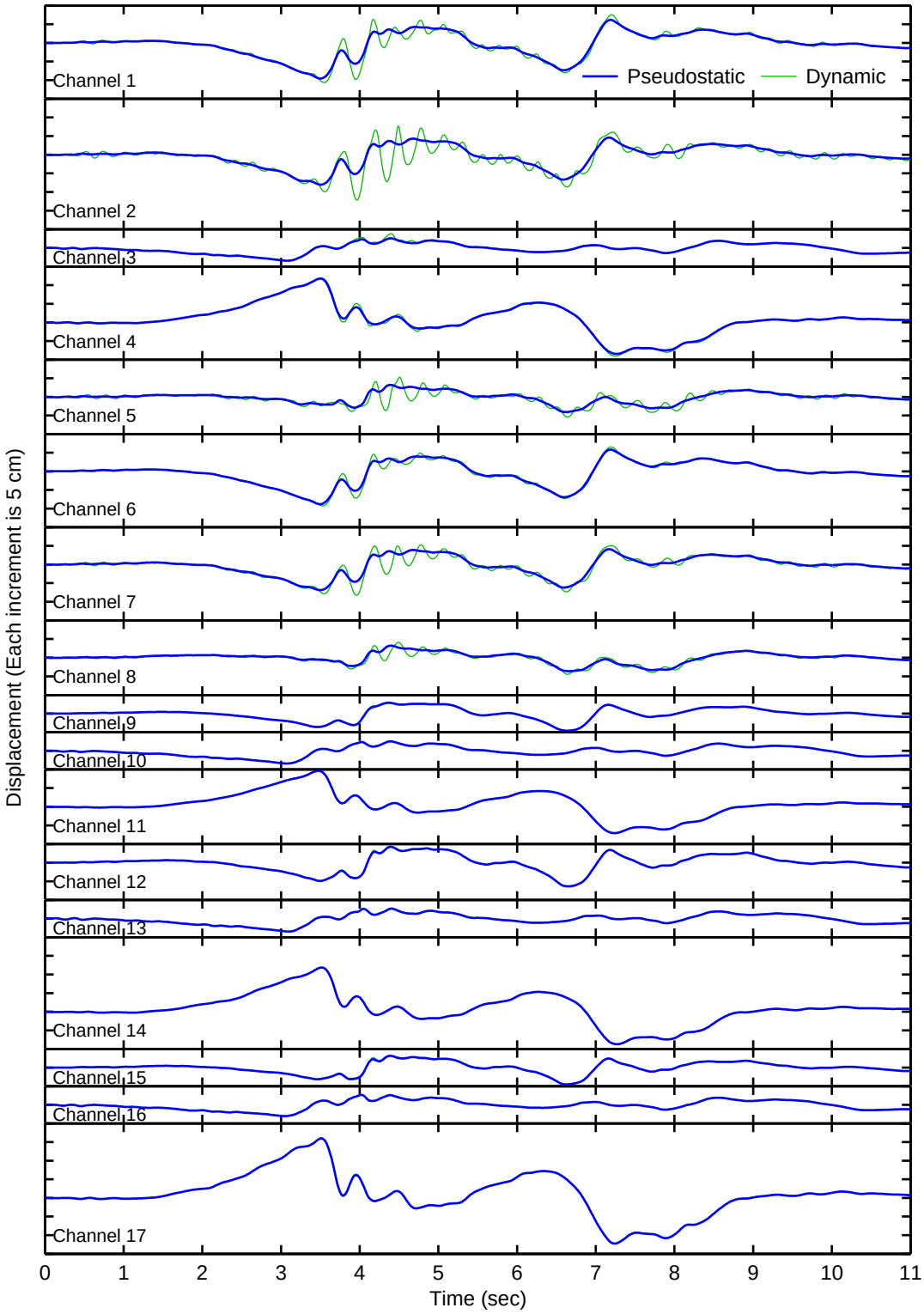

Figure C.95: Displacement time histories at locations corresponding to channels 1–17 computed from a nonlinear pseudostatic analysis compared to the time histories from a nonlinear dynamic analysis (method 1)

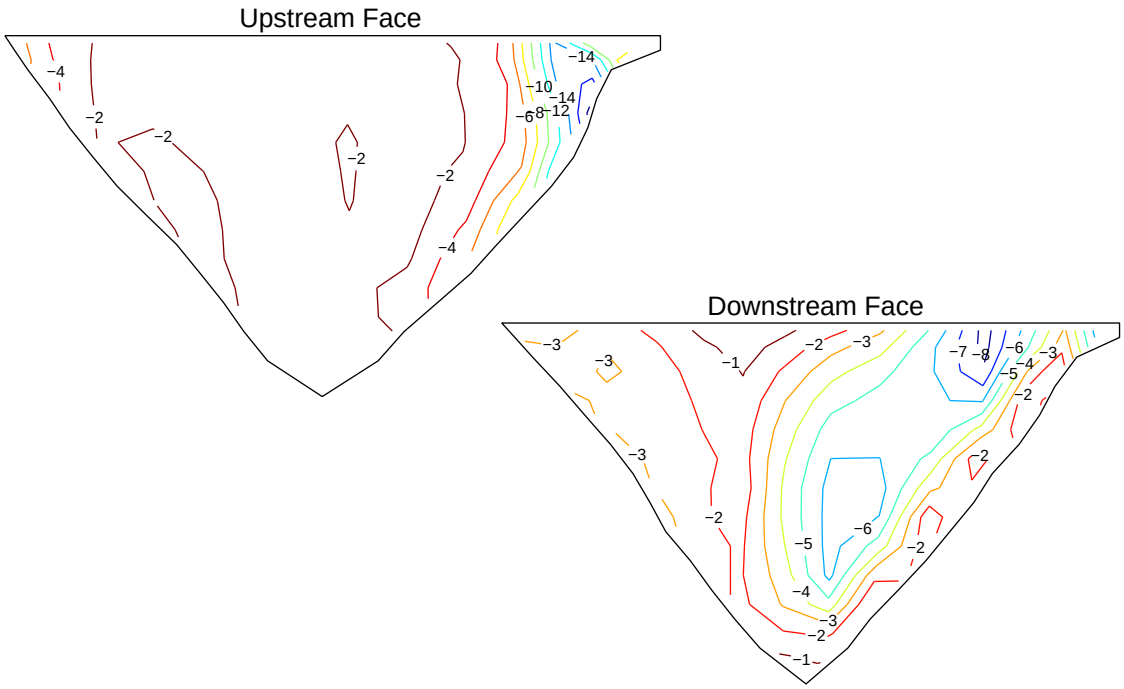

Figure C.96: Maximum compressive arch stresses (MPa) computed during a nonlinear pseudostatic analysis with nonuniform ground motion input (method 1)

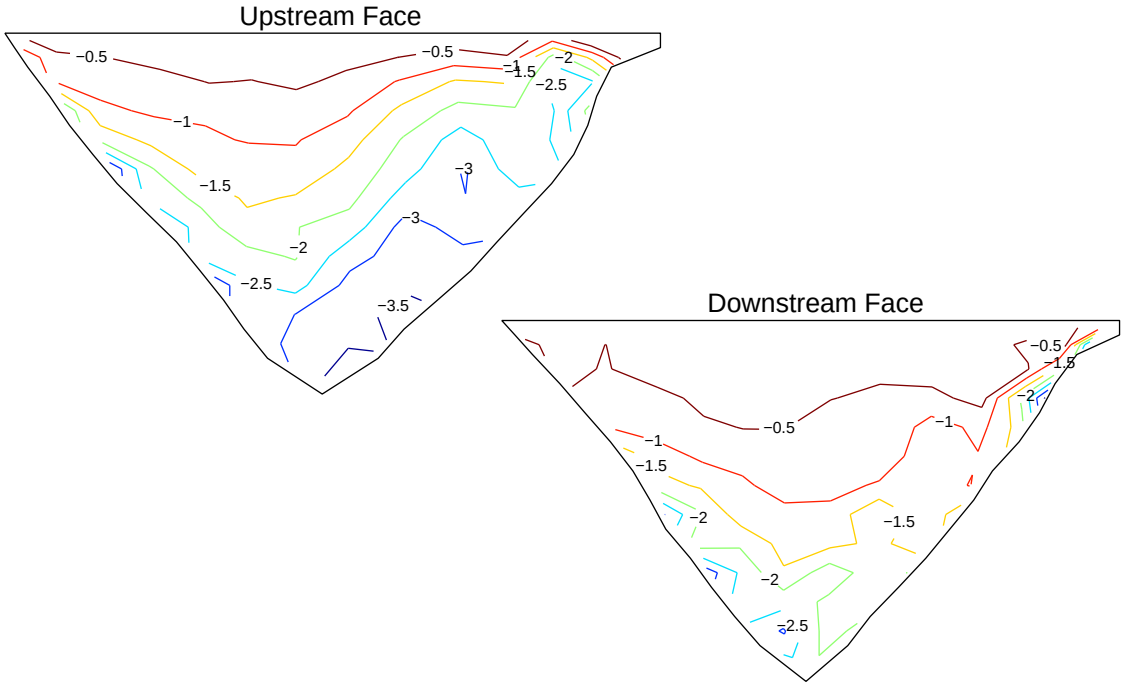

Figure C.97: Maximum compressive cantilever stresses (MPa) computed during a nonlinear pseudostatic analysis with nonuniform ground motion input (method 1)

0.00	0.89	0.56	0.11	0.01	0.05	0.08	0.24	0.08	0.34	0.03	3.02	0.00	0.00
0.00	0.81	0.72	0.07	0.06	0.06	0.09	0.30	0.15	0.22	0.26	2.86	0.00	0.00
	0.63	0.85	0.12	0.10	0.05	0.11	0.37	0.29	0.25	0.72	2.57	0.00	
	0.26	0.54	0.41	0.03	0.04	0.13	0.48	0.34	0.15	1.07	1.88	0.00	
		0.58	0.57	0.05	0.04	0.14	0.58	0.33	0.14	1.04	1.20		
		0.24	0.31	0.22	0.03	0.13	0.66	0.31	0.45	0.93	0.50		
			0.15	0.26	0.04	0.11	0.69	0.43	0.47	0.96			
			0.05	0.13	0.05	0.09	0.69	0.57	0.63	0.32			
				0.07	0.06	0.08	0.77	0.47	0.57				
				0.02	0.07	0.08	0.87	0.44	0.17				
					0.03	0.07	0.79	0.35					
					0.01	0.04	0.47	0.09					
						0.01	0.14						

Figure C.98: Maximum joint opening (cm) computed during a nonlinear pseudostatic analysis with nonuniform ground motion input (method 1)

0.00	0.00	0.00	0.00	0.00	0.00	0.00	0.00	0.00	0.00	0.00	0.00	0.00	0.00
0.00	0.00	0.00	0.00	0.00	0.00	0.00	0.00	0.00	0.00	0.00	0.00	0.00	0.00
	0.00	0.00	0.00	0.00	0.00	0.00	0.00	0.00	0.00	0.00	0.00	0.00	
	0.00	0.00	0.00	0.00	0.00	0.00	0.00	0.00	0.00	0.00	0.00	0.27	
		0.00	0.00	0.00	0.00	0.00	0.00	0.00	0.00	0.00	0.00		
		0.00	0.00	0.00	0.00	0.00	0.00	0.00	0.00	0.00	0.00		
			0.00	0.00	0.00	0.00	0.00	0.00	0.00	0.00			
			0.23	0.00	0.00	0.00	0.00	0.00	0.00	0.00			
				0.00	0.00	0.00	0.00	0.00	0.00				
				0.23	0.00	0.00	0.00	0.00	0.00				
					0.00	0.00	0.00	0.00					
					0.00	0.00	0.00	0.00					
						0.00	0.00						

Figure C.99: Maximum crack opening (cm) computed during a nonlinear pseudostatic analysis with nonuniform ground motion input (method 1)